Synthesis and Characterisation

of

Ruthenium(II) Tris(heteroleptic) Complexes

containing a Triazole Ligand

by Declan Mulhern

DCU

Dublin City University
Ollscoil Chathair Bhaile Átha Cliath

A Thesis presented to Dublin City University

for the

Degree of Doctor of Philosophy

under the supervision of Professor Johannes G. Vos

School of Chemical Sciences

Dublin City University

2003

Dedicated to my parents, Paddy and Ann
And my brother and sister, Niall and Emer.

I love deadlines.

I like the whooshing sound they make as they fly by.

Douglas Adams (1952 – 2001)

Authors Declaration

I hereby certify that this material, which I now submit for assessment on the programme of study leading to the award of Doctor of Philosophy by research and thesis, is entirely my own work and has not been taken from work of others, save and to the extent that such work has been cited within the text of my work.
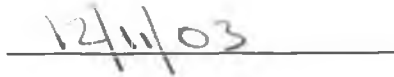
Signed:

Declan Mulhern

Student I.D. No.:   98970607

Date:

Abstract

The synthesis, spectroscopic and electrochemical characterisation of Ru(II) tris(heteroleptic) mononuclear and dinuclear complexes are described. Special attention is paid to the introduction of a triazole ligand to the metal sphere. Chapter 1 is an introductory chapter in that the basic concepts regarding Ru(II) polypyridyl chemistry are introduced and explained. The parent complex $[Ru(bpy)_3]^{2+}$ is examined along with its photochemical and photophysical properties. The replacement of a bpy ligand with that of a triazole is discussed as are the new properties associated with such a complex. Ultimately, this thesis focuses on the synthesis of Ru(II) complexes containing three different ligands and so previously reported synthetic routes to such Ru(II) tris(heteroleptic) complexes are discussed.

The next chapter introduces the synthetic and analytical methods used in the synthesis of tris(heteroleptic) complexes. The synthesis and purification of starting and reference materials used throughout the thesis are discussed.

Having introduced tris(heteroleptic) complexes in the opening chapter, Chapter 3 takes a practical look at the various synthetic strategies used to synthesise such complexes. Previously reported synthetic routes are explored for their suitability in allowing a triazole ligand to be incorporated into tris(heteroleptic) compounds. The methods have been subdivided into four categories, namely the $[Ru(bpy)Cl_3]$, $[Ru(bpy)(DMSO)Cl_2]$, decarbonylation and photosubstitution methods. The trial 1,2,4-triazole complex $[Ru(bpy)(Me_2bpy)(pytrz)]^+$ was best synthesised and purified by a synthetic route which included the photolysis of $[Ru(bpy)(CO)_2Cl_2]$ in MeCN to produce material that yielded the dichloride $[Ru(bpy)(Me_2bpy)Cl_2]$. This dichloride was successfully reacted with the 1,2,4-triazole ligand to produce the tris(heteroleptic) complex.

With a successful method of incorporating a triazole ligand, Chapter 4 describes the synthesises of a series of such complexes. Two more dichlorides, $[Ru(bpy)(phen)Cl_2]$ and $[Ru(bpy)(dpp)Cl_2]$ are prepared and together with $[Ru(bpy)(Me_2bpy)Cl_2]$ are successfully reacted with the bridging ligands Hbpt and Hbpzt to create mononuclear tris(heteroleptic) complexes. These complexes are characterised and crystal structures of both a bpt⁻ and bpzt⁻ complex are reported. The photochemical and photophysical properties of the complexes are investigated and compared to those of analogous bis(heteroleptic) complexes such as $[Ru(bpy)_2(bpt)]^{3+}$. The difference in Hbpt and Hbpzt bridging ligands is also discussed.

Chapter 5 follows on from Chapter 4 and investigates the possibility of creating dinuclear tris(heteroleptic) complexes. The dinuclear analogues of the Chapter 4 mononuclear complexes are prepared, along with a range of dpp dinuclear complexes. In some cases only one metal centre is tris(heteroleptic) while in others both are designed this way. The properties of these new complexes are explored and compared with the properties of the mononuclear compounds.

Finally, the results of the work undertaken are summarised with suggestions on further possible research directions.

Acknowledgements

Table of Contents

Abbreviations and Symbols

AIBN	2,2'-azobisisobutyronitrile	k_r	radiative decay
BuLi	butyllithium	λ	absorption wavelength
CH_2Cl_2	dichloromethane	λ_{em}	emission wavelength
$CHCl_3$	chloroform	L	ligand
CHN	carbon, hydrogen, nitrogen analysis	LC	ligand centred
COSY	correlated spectroscopy	LMCT	ligand to metal charge transfer
CT	charge transfer	LUMO	lowest occupied molecular orbital
CV	cyclic voltammetry		
δ	chemical shift (NMR)	MC	metal centred
DMF	dimethylformamide	Me_3NO	trimethylamine-N-oxide
DMSO	dimethylsulphoxide	MeCN	acetonitrile
DPV	differential pulse voltammetery	MeOH	methanol
		^{1}MLCT	singlet metal to ligand charge transfer
ε	extinction coefficient		
$E_{1/2}$	half-wave potential	^{3}MLCT	triplet metal to ligand charge transfer
EDTA	ethylenediaminetetraacetic acid		
		MS	mass spectrometry
ES	electrospray (MS)	M_w	molecular weight
Et_3N	triethylamine	m/z	mass to charge ratio (MS)
EtOAc	ethyl acetate	NBS	N-bromosuccinimide
EtOH	ethanol	NMR	nuclear magnetic spectroscopy
FAB	fast atom bombardment		
Fc/Fc$^+$	ferrocene/ferricinium redox couple	PET	petroleum ether
		PS	photosensitiser
GS	ground state	PTZ	phenothiazine
HOMO	highest occupied molecular orbital	PV	photovoltaic
		py	pyridine
HPLC	high performance liquid chromatography	SCE	standard calomel electrode
		τ	lifetime
ic	internal conversion	TLC	thin layer chromatography
IR	infrared	TMNO	trimethylamine-N-oxide
isc	intersystem crossing	UV/Vis	ultraviolet/visible
J	coupling constant (NMR)	ν	stretching vibration (IR)
k_{nr}	non-radiative decay		

Ligand Abbreviations and Structures

4,4'-bpy	4,4'-bipyridine
ambpy	4,4'-bis(phenylethylamido)-2,2'-bipyridine
biq	2,2'-biquinoline
bpm	2,2'-bipyrimidine
bi-naph	bi-1,8-naphthyridine
bpp	2,3-bis(pyridin-2-yl)pyrazine
bpy	2,2-bipyridine
bpyCH$_2$MV^{2+}	1-((4'-methyl-2,2'-bipyridin-4-yl)methyl-1'-methyl-4,4'-bipyridine
bpyCH$_2$PTZ	10-((4'-methyl-2,2'-bipyridin-4-yl)methyl)phenothiazine
bpz	2,2'-bipyrazine
dcb	4,4'-dicarboxy-2,2'-bipyridine
dpa	di(2-pyridylamine)
dpp	4,7-diphenyl-1,10'-phenanthroline
estbpy	4,4'-bis(phenylethyloxycarbonyl)-2,2'-bipyridine
H$_2$biim	2,2'-biimidazole
H$_2$bibzim	benzoimidazole
H$_3$przbzim	3,5-bis(benzoimidazole)-pyrazole
Hbpt	3,5-bis(pyridin-2-yl)-1,2,4-triazole
Hbpzt	3,5-bis(pyrazin-2-yl)-1,2,4-triazole
Hpyim	2-(pyridin-2-yl)-imidazole
Hpyprz	3-(pyridin-2-yl)-pyrazole
Hpytrz	3-(pyridin-2-yl)-1,2,4-triazole
Hpztrz	3-(pyrazin-2-yl)-1,2,4-triazole
Me$_2$bpy	4,4'-dimethyl-2,2'-bipyridine
Me$_2$phen	4,7-dimethyl-1,10'-phenanthroline
Me$_4$bpy	4,4',5,5'-tetramethyl-2,2'-bipyridine
Mepytrz	1-methyl-3-(pyridin-2-yl)-1,2,4-triazole
MV^{2+}	1,1'-dimethyl-4,4'-bipyridine (methyl viologen)
phen	1,10'-phenanthroline
qpy	2,2';3',2'';6'',2'''-quaterpyridine

R$_1$	R$_2$	
H	H	bpy
Me	Me	Me$_2$bpy
COOH	COOH	dcb
CONHC(CH$_3$)Ph	CONHC(CH$_3$)Ph	ambpy
COOC(CH$_3$)Ph	COOC(CH$_3$)Ph	estbpy
Me	CH$_2$MV^{2+}	bpyCH$_2$MV^{2+}
Me	CH$_2$PTZ	bpyCH$_2$PTZ

Me$_4$bpy

dpa

4,4'-bpy

bpp

qpy

R = H   phen
R = Ph   dpp

biq

bi-naph

Mepytrz

X = C   pytrz
X = N   pztrz

X = C   Hbpt
X = N   Hbpzt

bpm

bpz

Hpyim

H$_2$bzim

H$_2$biim

Hpyprz

H$_3$przbzim
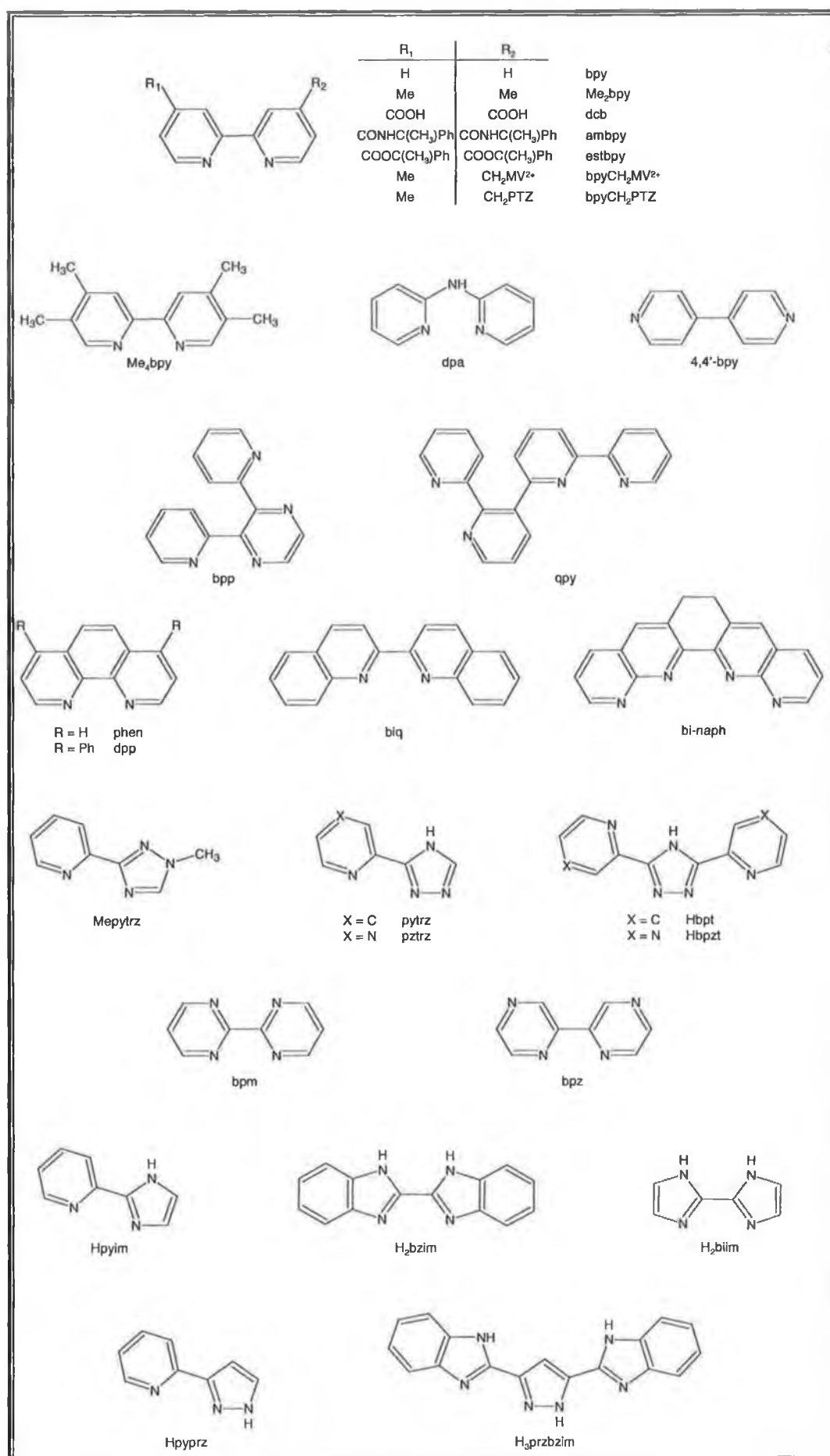
Chapter 1.

Introduction

The principles of photovoltaic electricity and photochemical production of H_2 are introduced, with special emphasis on the photosensitiser required. The archetypical photosensitiser, $[Ru(bpy)_3]^{2+}$, is introduced and its photochemical and photophysical properties discussed. The effect of replacing one bpy ligand with a triazole ligand is examined. Finally, the synthetic strategies employed to date in synthesising Ru(II) complexes with three different bidentate ligands are discussed.

1.1 Introduction

Much has been made of late about the limited supply of fossil fuels and of the global damage such fuels have caused and continue to cause to our environment. Although the effects of global warming continue to be debated [1] there is wide consensus that alternative, renewable fuels are required in the near future. Photovoltaic energy conversion and photochemical production of hydrogen are considered by many to be the renewable energy sources of choice for the next century [2,3,4,5]. Technological progress is constantly being made, and with the current political climate favouring a shift towards "greener" fuel sources, its economic progress looks assured. The recent Kyoto Protocol [6,7] brought the rise of greenhouse gases to the fore of political agendas and even if not yet ratified by all signatories, countries have clearly made a political commitment to meeting the targets they have accepted.

As an energy technology, photovoltaics can be used for almost anything that requires electricity – from small remote applications to large central power stations. Electricity produced from photovoltaics has a far smaller impact on the environment than traditional methods of electrical generation. During their operation, PV cells use no fuel other than sunlight and give off no atmospheric or water pollutants.

On the other hand, the photochemical generation of hydrogen from water is attractive in that the chemical energy produced (H_2) can be stored and transported in the same manner as conventional fossil fuels. In fact, the energy storage capacity of H_2 (119,000 $J.g^{-1}$) is three times higher than that of oil (40,000 $J.g^{-1}$) [8]. What's more, the raw materials (H_2O, sunlight) are cheap and plentiful and combustion of H_2 in air gives only water as a by-product, Eq. (1). Thus the whole process is cyclical and non polluting.

$$H_2 + \tfrac{1}{2}O_2 \longrightarrow energy + H_2O \qquad Eq.\ (1)$$

1.1.1 Photovoltaic Production of electricity

Fig. 1.1 shows a typical set up for a conventional silicon photovoltaic cell. When light with energy greater than the semiconductor bandgap is absorbed an electron-hole pair is produced. If the electron or hole diffuse to the depletion layer before they recombine, the depletion layer electric field drives electrons towards the n-type end and holes towards the p-type end. These electrons and holes may then be made do work by connecting a load across the junction potential.
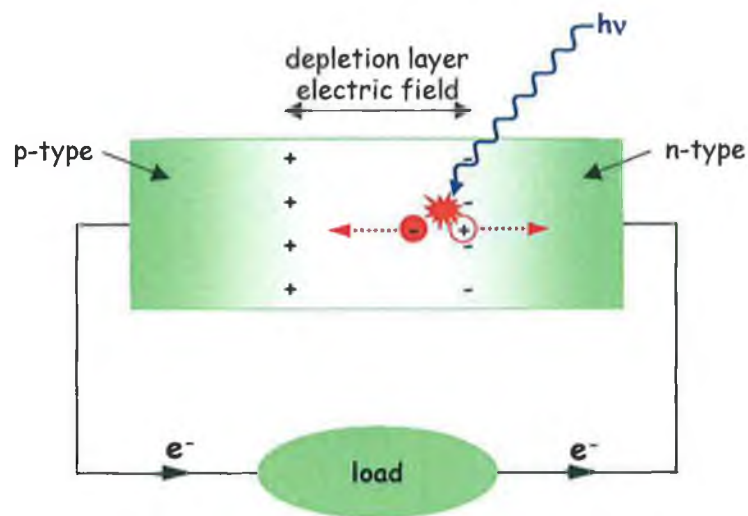
Figure 1.1. *Electron–hole pairs being driven apart by the depletion layer electric field upon absorption of a photon.*

A distinct disadvantage with conventional PV cells is their inability to utilise the full solar spectrum. Incident photons with energy lower than the bandgap do not produce electron–hole pairs. Photons with energy much greater than the bandgap, while still producing electron–hole pairs, lose most of their energy through heat dissipation. Only light at, or slightly above the bandgap produces efficient photon to electrical energy conversion. All these factors lead to a theoretical maximum yield of 33% for a single crystal Si cell. In reality performances of 24% have been measured under laboratory conditions while commercial cells produce efficiencies of 12–16% [9].

To make the cell shown in Fig. 1.1 more efficient, a dye can be adsorbed to the semiconductor which allows more sunlight to be absorbed and utilised by the cell [10]. A typical model of such a system is shown in Fig. 1.2. In this case, the photosensitiser (PS) absorbs a photon resulting in the excitation of an electron to a higher energy level (PS*), ①. The excited PS* may then relax back to PS with dissipation of energy or, under favourable conditions, be made to donate its electron to the semiconductor, ②. This results in the oxidation of PS* to PS$^+$, ③. This electron is passed through an external circuit to the counter electrode whereby an electron accepting species, R, is reduced ④. The reduced species R$^-$ diffuses away from the counter electrode ⑤ and reacts with PS$^+$ to regenerate the starting materials PS and R ⑥. Progress has already been made with such cells, the most notable being the Grätzel cell which uses TiO_2 as semiconductor, $[Ru(dcb)_2(NCS)_2]$ as PS and I/I$^-$ as the redox couple, R/R$^-$ [11]. Although the initial efficiencies were comparatively low (7%) they have continued to improve as alternative dyes and redox couples are explored [12,13].
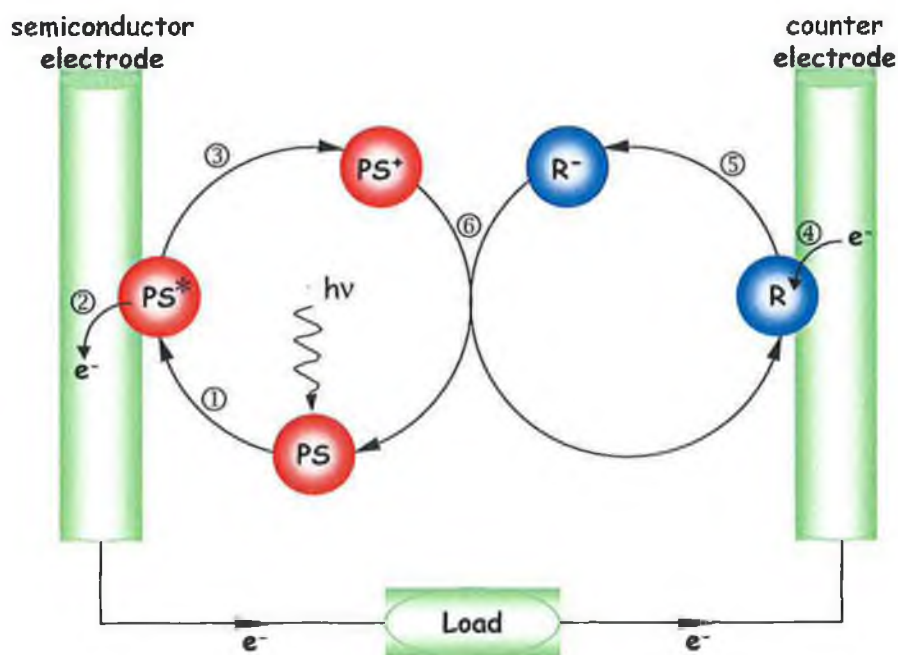
Figure 1.2. Schematic model of a dye-sensitised PV cell.

1.1.2 Photochemical generation of H_2

The free energy splitting of water in Eq. (2) is 237.2 kJ/mol or 2.46 eV/molecule of H_2O. The reduction of water to produce H_2 in Eq. (3) is a two-electron transfer process which therefore requires 1.23 eV per electron transferred.

$$H_2O \longrightarrow H_2 + \tfrac{1}{2}O_2 \qquad \textbf{Eq. (2)}$$

$$2H_2O + 2e^- \longrightarrow H_2 + 2OH^- \qquad \textbf{Eq. (3)}$$
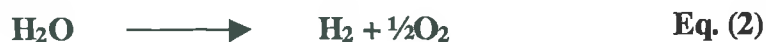
Therefore, photons with $\lambda < 1008$ nm (1.23 eV) can induce the cleavage of water. However, as water does not absorb light at this wavelength range, intermediates are required to achieve Eq. (3). One such photochemical generation of H_2 is summarised in Fig. 1.3.
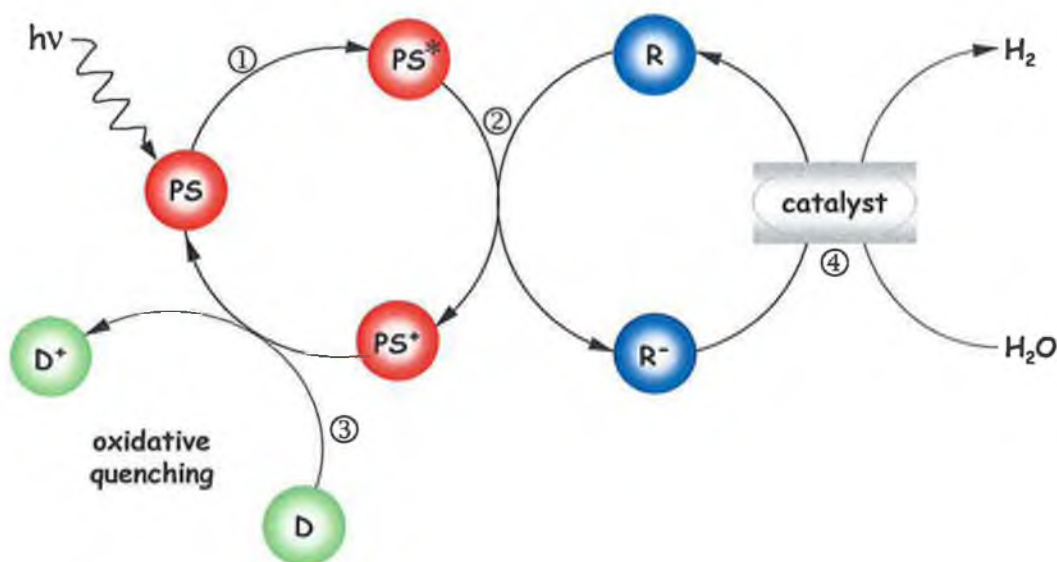
Figure 1.3. Schematic representation of the redox catalytic cycle in the photoreduction of H_2O to H_2 in a four-component model system [8].

The absorption of light generates the excited state PS* of the photosensitiser PS, ①. PS* may subsequently react with an electron acceptor R to generate the

reduced species R^- and oxidised species PS^+, ②. Before PS^+ and R^- recombine to produce PS and R, a PS^+ scavenger (D) is required to donate an electron to PS^+, ③. D is used up in the process (decomposes) and is said to be a sacrificial donor. The absence of PS^+ leaves R^- free to cleave H_2O at a suitable catalyst ④. The redox potential of R^- must be less than -0.41 V to take part in Eq. (3). In such systems, PS and R are regenerated with only D being consumed.

Different variations of the model in Fig. 1.3 have been investigated using a myriad of species for PS, R, D and the catalyst [8,14]. One such example proposed by Kalyanasundaram utilises $[Ru(bpy)_3]^{2+}$ as PS, MV^{2+} as R, EDTA as D and colloidal Pt as catalyst [15] with $\Phi(H_2)$ of 0.3. However, significant drawbacks include the degradation of $[Ru(bpy)_3]^{2+}$ and MV^{2+}.

1.1.3 Photosensitisers

The scope of this thesis does not allow for an exhaustive discussion on all the components mentioned in the PV cell and the photochemical generation of H_2. However, one important constituent of both systems is the presence of the photosensitiser (PS). Different types of PS have been used including transition metal complexes [16,17] and metalloporphyrins [18]. The ideal PS should have the following properties;

- ability to absorb light below a wavelength of about 1000 nm,
- inject electrons to the semiconductor (PV cell, Fig. 1.2) or R (fuel cell, Fig. 1.3) with a quantum yield of unity
- redox potential that is sufficiently high to accept electron from R^- (PV cell) or D (fuel cell)
- be able to sustain 10^8 turnover cycles (~20 years illumination).
- the PS for a PV cell also requires attachment groups (e.g. $-COOH^-$).

Transition metal complexes, specifically Ru(II) complexes, have been shown to exhibit all the properties outlined above. These complexes are ideal in that they

can be "tuned" to vary their electrochemical and photophysical properties as will be explained in later sections. One of the draw backs of Ru(II) systems is that the excited state can quickly relax back to its ground state before interacting with a second molecule. This problem is overcome by building large supramolecular structures made possible by the synthetic accessibility of Ru(II) complexes.

1.1.4   Supramolecular Systems

When a large molecular system contains a number of chemical entities that retain their own individual characteristics yet contribute to the formation of new features for the whole molecule then that molecule may be referred to as a supramolecular species. In practice, the distinction between a large molecule and a supramolecular species may be made by the degree of localisation of energy or charge that occurs within the system as shown for a donor–acceptor molecule (D~A) in Scheme 1.1 [19].
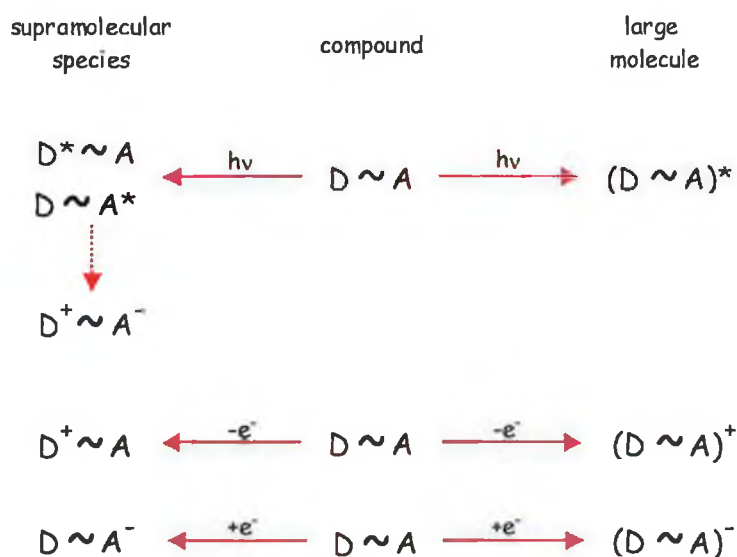
Scheme 1.1. Illustration of the photochemical and electrochemical criteria used to classify a complex as a supramolecular species or as a large molecule [19].

For a large molecule, charge and excitational energy are delocalised throughout the whole system. On the other hand, for a supramolecular species, charge and energy are localised on one of the molecular subunits [20]. For example, if D~A is radiated with light and one of its subunits (D or A) is excited rather than the whole molecule, it can be classed as a supramolecular species. For the system shown above, regardless of whether D or A is excited, the supramolecular system has two options. It may relax back to the ground state (energy dissipated as light/heat) or charge transfer may occur, in which case D^+~A^- is formed. Charge recombination usually occurs very quickly unless a quenching molecule is present to oxidise/reduce the charge separated species D^+~A^-. Section 1.2 revisits the energy and charge transfer processes for such a system.

Each component of a supramolecular species has its own individual properties but when coupled together produce new photophysical and photochemical processes accessible only to the species as a whole. Many types of supramolecular species, such as dendrimers, interlocked systems, catenanes, rotaxanes, knots [21,22] and supramolecular systems not containing metals [22], have been created and some even show remarkable self-assembly [23,24,25]. However, our interest lies with those whose components are covalently linked through bridging ligands and whose properties include charge-separation sometimes by use of the antenna effect.

1.1.5   Charge Separation

Absorption of a photon and creation of a long-lived charge-separated state is the most fundamental energy conversion for any process utilising a PS for electron donation. As illustrated in Scheme 1.1, absorption of a photon by a species forms the excited state D*~A or D~A* which then undergoes a series of electron transfer steps to form D^+~A^-. In reality systems containing three and more units are necessary for efficient charge separation. Fig. 1.4 illustrates two types of triads and the relative energies of the orbitals involved with electron transfer. Fig. 1.4a mimics natural reaction centres such as that found in photosynthetic centres,

whereas that of Fig. 1.4b has been used to achieve charge separation in artificial centres.
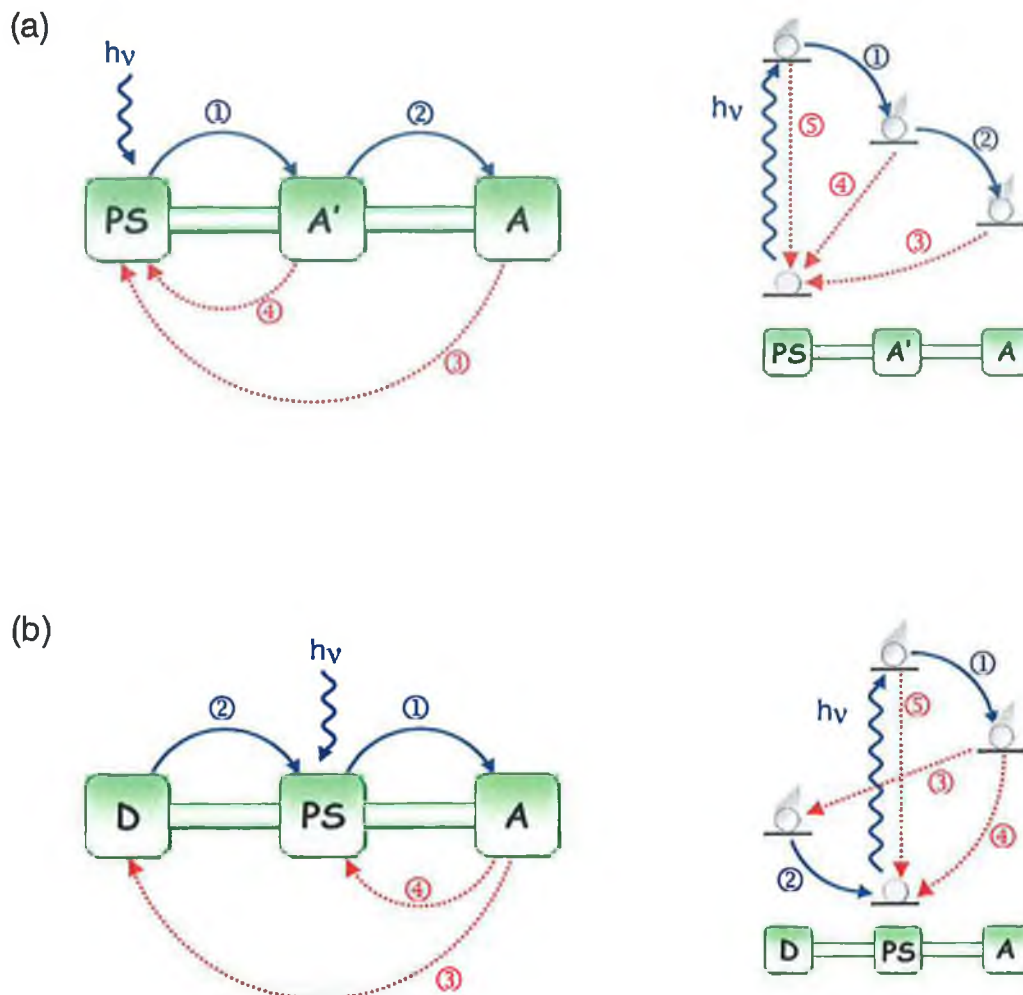
Figure 1.4. *The triads and their corresponding electronic energy levels for (a) natural charge separation centres and (b) artificial charge separation centres.*

In both cases a photosensitiser, PS, is excited and transfers an electron to a primary acceptor ①. Thermal electronic transfer then occurs to a secondary acceptor, ②. In the case of Fig. 1.4a, PS is the donor moiety but in Fig. 1.4b it becomes the secondary acceptor, receiving an electron from D. The efficiency of charge separation in a triad D–PS/A'–A depends on the indirect mixing of the HOMOs and LUMOs of D, A and PS/A' with the HOMOs and LUMOs of the bridge that connects them. Charge separation efficiency also depends critically on the competition between the secondary electron transfer step and the primary charge recombination step. That is, in Fig. 1.4 , process ① competes with

excited-state deactivation, ⑤, and process ② competes with primary charge recombination, ④. Eventual charge recombination between remote molecular components leads back to the original triad, ③.

Many complexes arising from this model have been synthesised and the relationships of the charge-separation to their size, geometry and individual substituents have been studied. Triad systems have been designed using Ru(II) polyimine complexes as chromophoric components, quaternarised bipyridines as acceptor units and phenothiazine or aromatic amines as donor components [26,27,28,29]. To increase the efficiency and lifetime of charge separation, more complicated systems such as tetrads and pentads have been constructed [28,30,31]. The synthesis of such complexes demand a highly ordered synthetic pathway especially if stereoisomers are to be separated. This can be avoided by the use of tris-chelating bridging ligands such as terpyridine that form achiral complexes and where introduction of substituents in the 4-position does not decrease the symmetry. However, because of its "bite-angle" the lifetimes of such complexes are short but recently some improvements have been achieved [32].
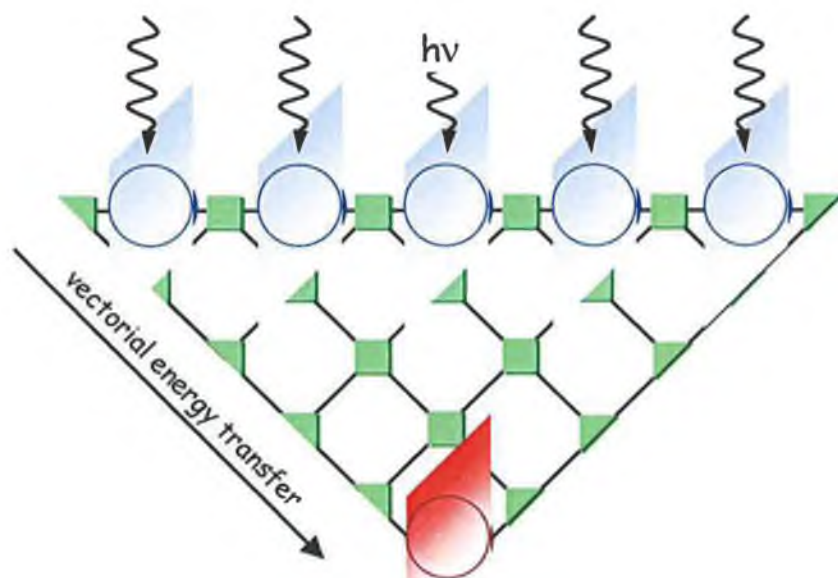
Figure 1.5. *Schematic model of a dendrimer. Light is harvested by an array of chromophores (blue) and this energy is transferred to a reaction centre (red).*

In Fig. 1.4, the photosensitiser is intimately linked to the electron transfer process. In reality, the PS does not always absorb enough photons and so large regularly branched macromolecules are used to harvest incident photons and channel that energy towards a reaction centre where charge separation can take place. Fig. 1.5 shows a schematic model of such a light harvesting system. Transition metal complexes have also been used as dendrimers and have been synthesised using either the electron poor 2,3- and 2,5-bis(2-pyridyl)pyrazine bridging ligands [33], anionic electron-rich ligands such as tris(triazole) [34] or with a mixture of both [35]. To increase light harvesting, a greater number of nuclear centres were included for greater absorption of the solar spectrum. These higher nuclearity dendrimers have been shown to direct energy transfer to a single central unit [36] or peripheral unit [37] when four metal units are used [33]. Upon greater nuclearity (10 [38], 13 [39] and 22 [40,41] centres) unidirectional energy migration to a single unit has been impossible with the use of only two different metals. Recently, Sommovigo *et al.* used three different metals [Ru(II), Os(II) and Pt(II)] to allow energy transfer to a single osmium unit at the centre of a decanuclear dendrimer [42]. A similar approach (the "complexes as metals and complexes as ligands" strategy) to that used in earlier studies was employed [38].

1.2   Principles of molecular photophysics

The whole photochemical process begins when a molecule absorbs a photon, Eq. (4). This gain in energy promotes an electron from the highest occupied molecular orbital (HOMO) to the lowest unoccupied molecular orbital (LUMO).

$$PS + h\nu \longrightarrow PS^* \qquad \textbf{Eq. (4)}$$

The excited molecule, now unstable, quickly decays to its original state, the ground state, by losing the energy acquired from the photon. This loss of energy may take different forms – radiative or non-radiative decay, as illustrated in Fig. 1.6.
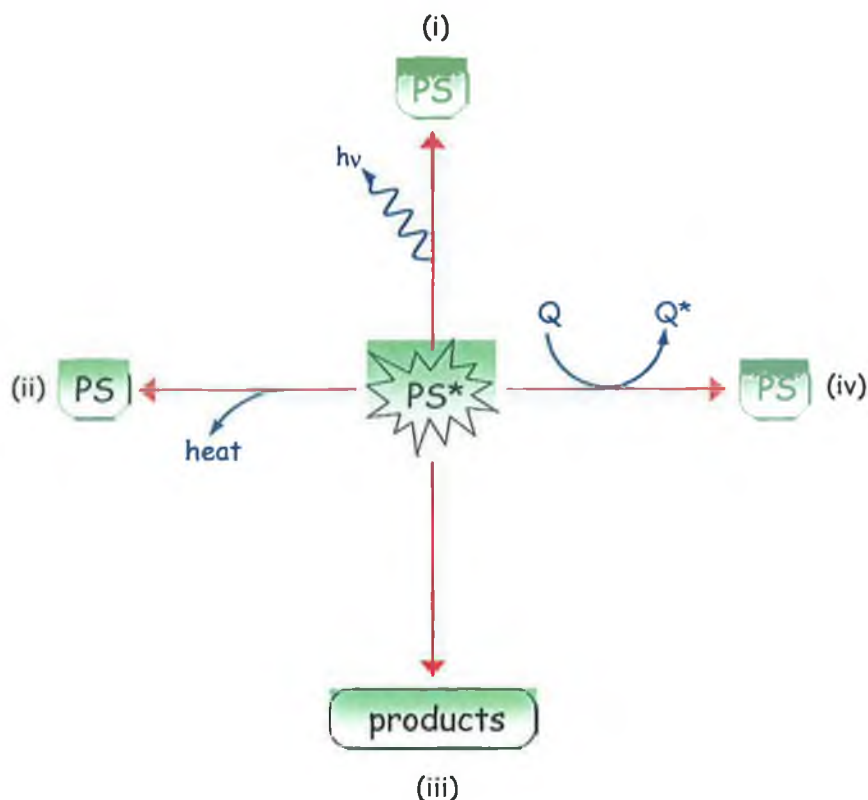
Figure 1.6. *Deactivation of PS* by radiative (i) and non-radiative (ii–iv) means. For details see text.*

The processes in Fig. 1.6 may be summarised as follows:

Radiative decay: (i)   return to the ground state with emission of a photon

Non-radiative decay: (ii)   deactivation with excess energy dissipated as heat

                        (iii)   formation of products

                        (iv)   quenching of the excited state by another molecule, Q.

In excited transition metal complexes both radiative and non-radiative decay processes compete with one another. As processes (i)–(iii) occur within the molecule they are said to be unimolecular. Process (iv) involves a second molecule so is termed bimolecular.

1.2.1 Radiative decay (luminescence)

The relative energies of the HOMO and LUMO and the different decay paths available to the excited species PS* are represented in Fig. 1.7.
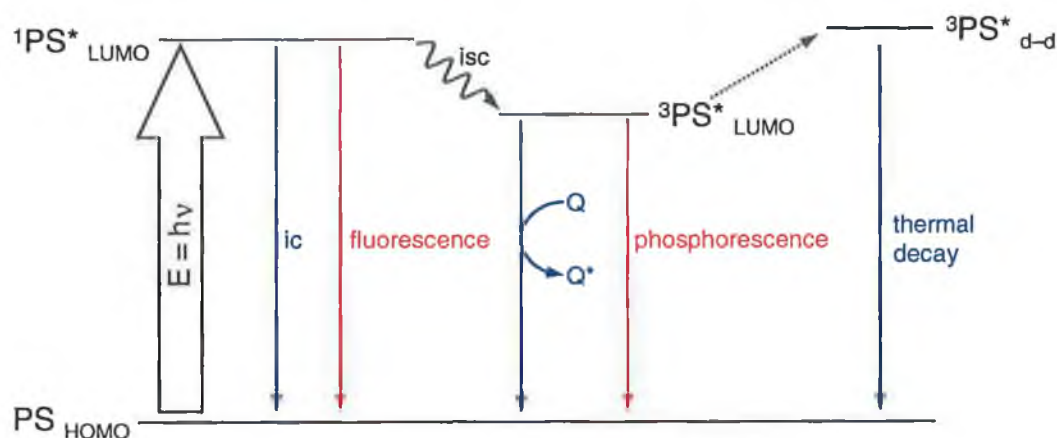
Figure 1.7. *Decay paths available to the excited species PS* where PS represents a metal complex. Decay paths in blue represent non-radiative decay whereas those in red represent radiative decay.*

Radiative decay occurs when an excited state relaxes to another lower lying state with the release of a photon. As the multiplicity of most molecules in their ground state is of a singlet nature, the absorption of hv excites an electron to a higher lying singlet state, ^{1}PS*. Emission which occurs from the decay of this state is spin-allowed (fluorescence), whereas that of the nearby triplet state, ^{3}PS*, involves a change in multiplicity so is spin-forbidden (phosphorescence). Normally, population of the triplet state is spin-forbidden but when a heavy atom, such as a transition metal, is present then spin–orbit coupling causes mixing of the upper degenerate states. This allows population of the triplet ^{3}PS* and is known as intersystem crossing (isc).

1.2.2   Non-radiative decay

Decay without the emission of light may occur as outlined in Fig. 1.7. The electron might simply decay to the ground state (from $^1PS^*$ or $^3PS^*$) and the excess energy dissipated as heat to the surrounding medium. As for radiative decay, deactivation between states of the same multiplicity is spin-allowed and is called internal conversion (ic), whereas that between different multiplicities (isc) is spin-forbidden. Population of the thermally accessible d–d metal orbitals may also occur as ic, leading to the degradation of the original species, thereby, forming new products. An alternative decay path to unimolecular decay is that offered by quenching. Quenching involves the bimolecular transfer of excitational energy to another species, Q, and as such is the most important decay path for the development of artificial photosynthesis. The quenching process can take the form of energy or electron transfer but requires a suitably long lived excited state. In general, photoinduced electron transfer is followed by a fast back electron transfer process, and energy transfer is followed by the radiative and radiationless deactivation of the excited state of the quencher. Both electron and energy transfer cause the quenching of the luminescence of the absorbing species.

1.2.2.1 Energy transfer

$$PS^* + Q \longrightarrow PS + Q^* \qquad\qquad Eq.\ (5)$$

Upon absorption of a photon, if PS* remains excited sufficiently long enough for it to interact with another molecule, Q, then Q may be excited which results in the quenching of the excited state PS*, Eq. (5). The quenching molecule is now sensitised (Q*) and may itself undergo unimolecular decay or photochemical reactions even though it did not, and possibly could not, absorb the original photon. Excitational energy transfer occurs only when Q has a lower excited state available than that of the PS* excited state.

In its simplest form, energy may be exchanged by the emission of a photon from PS* and the absorption of that photon by Q. The quenching molecule has no way

of influencing the emission of the excited species and merely intercepts the emitted photon. Otherwise, an exchange may occur *via* long-range resonance interaction (Förster mechanism [43,44]) or *via* contact–exchange interaction (Dexter mechanism [45]).

Förster long-range interaction occurs when PS* behaves as an oscillating dipole, thus, creating an electric field. When Q approaches this electric field it will enter in resonance and energy transfer will take place with the simultaneous relaxing of PS* and formation of Q* (Fig. 1.8).
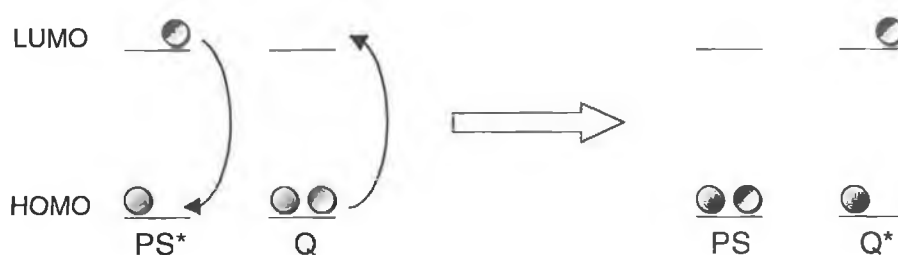
Figure 1.8. *Schematic representation of the Förster long range resonance interaction.*

This kind of energy exchange does not require spin conservation but is most effective when singlet excited states are involved and, thus, is seldom important for coordination compounds. The dipole–dipole coulombic interaction maximises when the transition moments of the donor and acceptor are parallel and vanish when they are orthogonal. Although not important for energy transfer between molecules in solution (mutual orientations are averaged), it is important between rigidly linked molecular components when designing supramolecular systems.

For the Dexter contact–exchange interaction (Fig. 1.9), the two species must be able to approach one another without either being sterically hindered so as to allow spatial overlap of their molecular orbitals. Transfer of energy may then only proceed between states of similar multiplicity.
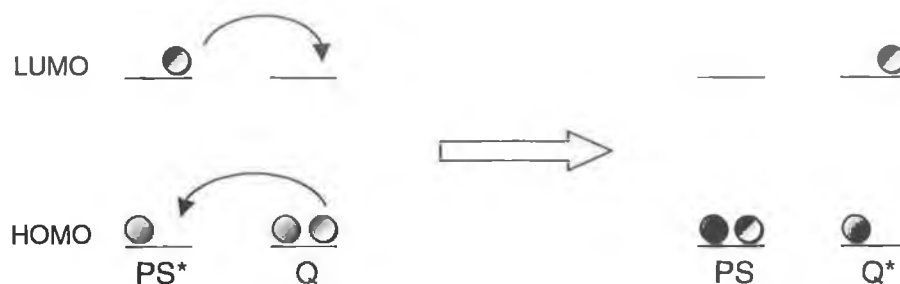
Figure 1.9. *Schematic representation of the Dexter contact–exchange interaction.*

Due to the exponential fall-off of donor–acceptor orbital overlap, the rate constant of exchange energy transfer is expected to fall off with distance exponentially. If the donor and acceptor are covalently linked together as in a supramolecular structure, the bridging group will be important in mediating electronic coupling and will have an exponential dependence on bridge length [46].

1.2.2.2 Electron Transfer

When an electron is promoted to produce an excited species, the new species is often a better oxidant and reductant than the original molecule. This is especially true of transition metal complexes where a d-electron is excited to an outer shell, thereby, leaving a "hole" in its place. If PS* donates this electron to form a new species, Q^-, then oxidative quenching is said to have occurred. Likewise, if PS* accepts an electron from Q to form PS^-, then reductive quenching has occurred, Eq. (6).

$$PS^+ + Q^- \longleftarrow PS^* + Q \longrightarrow PS^- + Q^+ \qquad \text{Eq. (6)}$$

oxidative quenching

reductive quenching
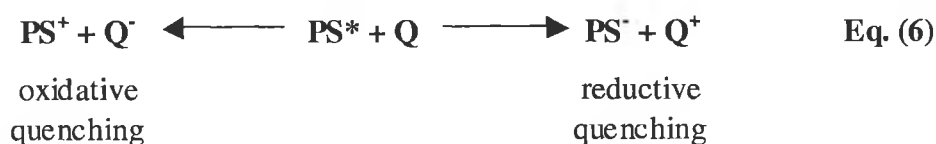
If two or more subunits are joined together in a supramolecular species, then electron transfer may take place without the need of a quencher. In this case light energy may be converted into chemical energy in the donor–acceptor molecule (D~A) from Scheme 1.1. For this to occur, the energy level of the photochemical products must lie between that of the initial ground state molecule and the excited

state molecule, Fig. 1.10. Scheme 1.1 previously illustrated the photochemical and electrochemical criteria that defines a supramolecule. Light absorption leads to the excited species D~A* or D*~A. In an electron transfer reaction the excited species decays to form the product D^+~A^-. This new charge separated product may revert back to the ground state by back-electron transfer or may be used to carry out some desired function. The rate at which electron transfer occurs is dependent on the bridge-length between the donor/acceptor moieties [47].
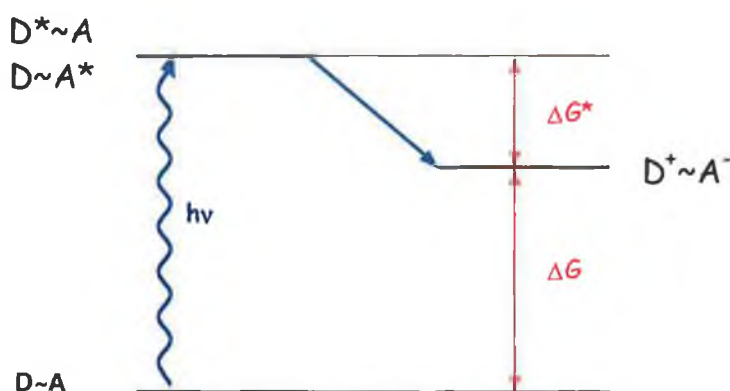
Figure 1.10. Schematic representation of energy levels for electron transfer in a D~A supramolecular species.

1.2.3   Decay kinetics of excited states

In transition metal complexes, the absorption of light may excite a number of electrons to a number of different orbitals. The most common of these excitations are those that are metal centred (MC), ligand centred (LC) and those that involve the promotion of an electron from one part of the molecule to another, i.e., charge transfer (CT). This transfer may promote an electron from a metal d-orbital to an unoccupied ligand orbital, i.e., metal to ligand charge transfer (MLCT) or *vice versa*, i.e., ligand to metal charge transfer (LMTC).

For Ru(II) systems absorption of a photon promotes an electron from the ground state (GS) to the spin-allowed ^{1}MLCT level. Intersystem crossing then allows for population of the ^{3}MLCT level. The electron then returns to the GS without

emission (non-radiative decay), with emission (phosphorescence) or populates the ^{3}MC level (formation of products or non-radiative decay). These processes are illustrated in Fig. 1.11.
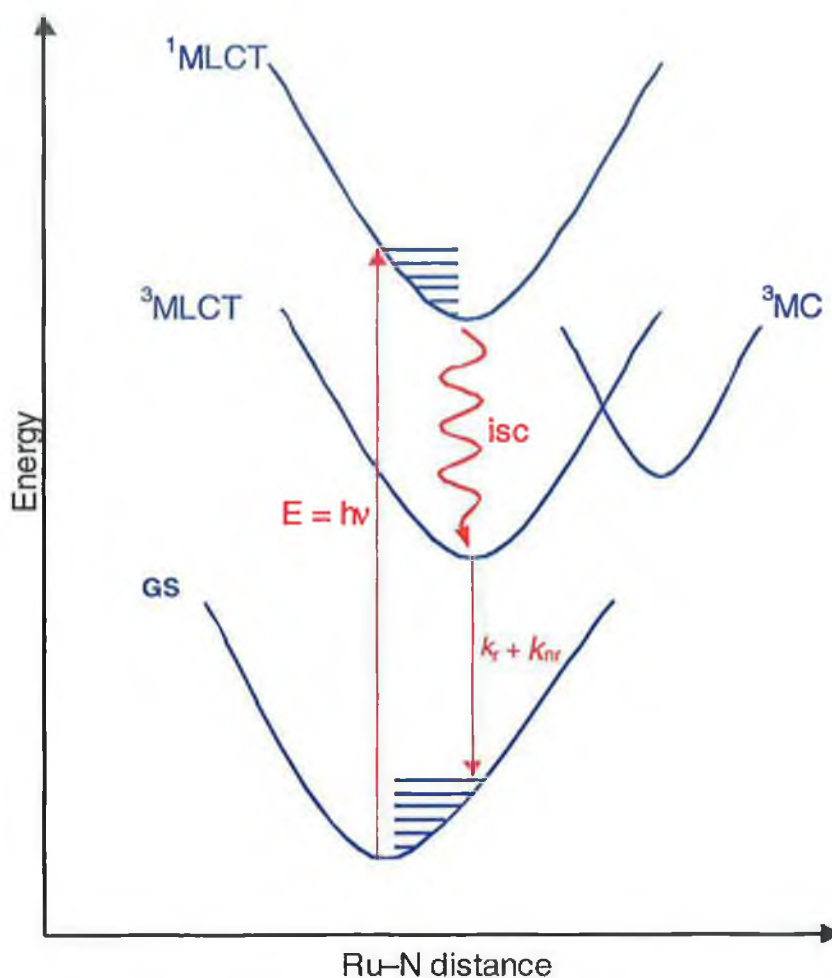
Figure 1.11 Decay paths in a typical Ru(II) polypyridyl complex.

To quantify these processes we denote each decay pathway by a rate constant, k, and each population of an excited state by a lifetime, τ, where

$$\tau = \frac{1}{\sum_i k_i}$$

Eq. (7)

and k_i is the first order rate constant for a generic process that causes the decay of the excited state. This process can take the form of radiative decay, non-radiative decay, inter-system crossing, etc. For the decay pathways shown for a Ru(II) polypyridyl complex in Fig. 1.11, the lifetime τ is represented by

$$\tau = \frac{1}{\left(k_r + k_{nr}\right)} \qquad \text{Eq. (8)}$$

where k_r and k_{nr} are the rate constants for radiative and non-radiative decay, respectively. The extent at which a level "x" is populated is defined as the quantum yield, Φ, and can be expressed as

$$\Phi_x = \eta_x k_x \tau_x \qquad \text{Eq. (9)}$$

for a species which spends τ_x in an excited state and has a decay constant of k_x. For the emission observed in Fig. 1.7 (phosphorescence), Φ_{em}, this equates to

$$\Phi_{em} = \eta_{isc} k_{em} \tau_{3_{MLCT}} \qquad \text{Eq. (10)}$$

where k_{em} is the rate at which the electron returns to the GS, $\tau_{3_{MLCT}}$ is the lifetime of the emitting ^{3}MLCT state and η_{isc} is the efficiency at which the ^{3}MLCT state is populated.

1.3   [Ru(bpy)₃]²⁺

Ever since Paris and Brandt reported the emission of light by the ruthenium(II) polypyridyl complex [Ru(bpy)₃]²⁺ in 1959 [48], a great deal of interest has been generated by these types of complexes [17,19,23,29,33,49]. Indeed, [Ru(bpy)₃]²⁺ (considered as the model compound) has been extensively studied and its photophysical and photochemical properties are well documented [50,51,52]. As it is readily synthesised and purified and the fact that its properties are well

understood, it has become the standard reference for comparing other Ru(II) polypyridyl systems.

$[Ru(bpy)_3]^{2+}$ was first reported by Burstall [53] and is easily synthesised by reacting excess bpy with $[RuCl_3].xH_2O$ in aqueous EtOH. The Ru(II) centre is a stable low-spin d^6 species and forms octahedral coordination complexes with a diamagnetic t_{2g}^6 electronic configuration [50]. Two enantiomers are present (Fig. 1.12 shows the Λ-enantiomer) and have been separated by Rutherford *et al.* [54].
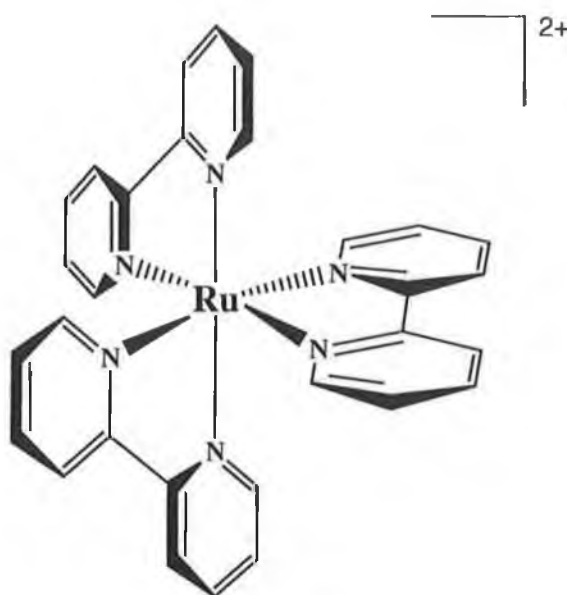
Figure 1.12. Octahedral structure of Λ–[Ru(bpy)$_3$]$^{2+}$.

1.3.1 Photophysical properties

In $[Ru(bpy)_3]^{2+}$, the three bipyridyl ligands contain σ-donor orbitals localised on the nitrogen atoms and π-donor and π^*-acceptor orbitals delocalised on the aromatic rings. The ligand-centred π^*-orbitals are lower in energy than the metal-centred σ^*-(e$_g$)-orbitals. Therefore, upon excitation of $[Ru(bpy)_3]^{2+}$, an electron from the ground state orbital (π_M) of ruthenium is promoted to a ligand orbital (π^*_L) localised on one of the bipyridyl rings. This promotion of an electron is known as a metal to ligand charge transfer (MLCT) and in the case of

$[Ru(bpy)_3]^{2+}$ is assigned as a ^{1}MLCT. The excited molecule has a large dipole moment and so the absorption of a photon can effectively be written as Eq. (11).

$$[Ru^{II}(bpy)_3]^{2+} + h\nu \longrightarrow [Ru^{III}(bpy)_2(bpy^{\bullet-})]^{2+} \qquad \text{Eq. (11)}$$

Fast intersystem crossing from the singlet to the triplet state occurs with an efficiency of unity. The excited state molecule then relaxes to the ground state with the emission of a photon or by radiationless deactivation. Fig. 1.13 shows the absorption and emission spectra for $[Ru(bpy)_3]^{2+}$ in MeCN. Another deactivation pathway is available (population of the ^{3}MC state) which can lead to photodecomposition of the complex. Such photodecomposition can be controlled by altering the ligand structures around the metal centre as is discussed in Section 1.4.
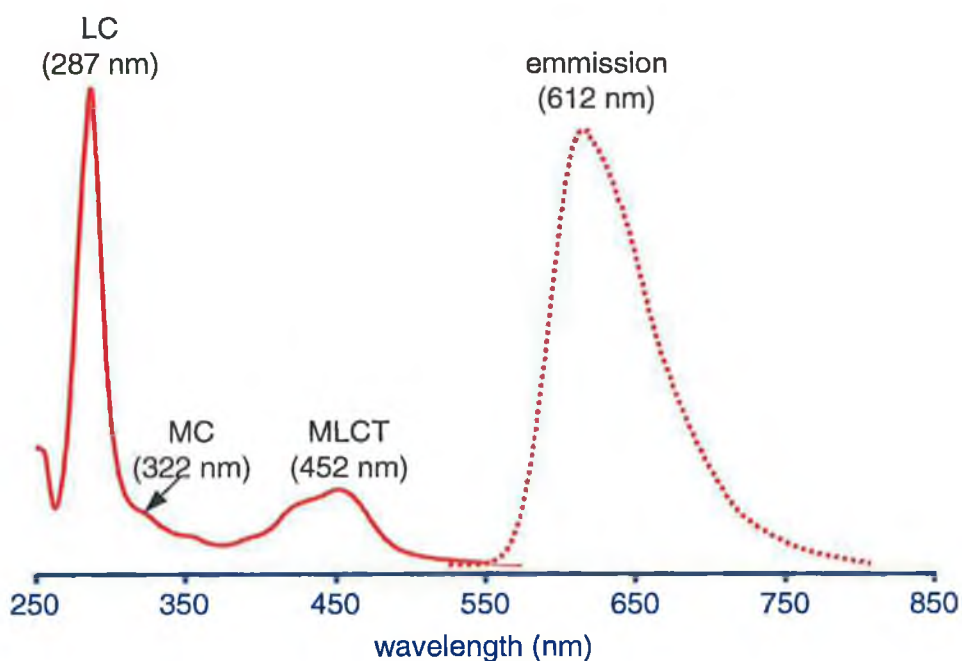
Figure 1.13. The absorption and emission spectra for $[Ru(bpy)_3]^{2+}$ in MeCN at 298 K.

1.3.2 Electrochemical properties

$[Ru(bpy)_3]^{2+}$ is attractive as a photosensitiser because of its favourable redox properties. It exhibits a metal based oxidation at 1.26 V (SCE) and a ligand based first reduction at −1.35 V (SCE). Fig. 1.14 shows the cyclic voltamogram of $[Ru(bpy)_3]^{2+}$ in MeCN with TBABF$_4$. The oxidised and reduced complex is relatively inert to ligand labilisation as shown by the reversible nature of the CV waves.
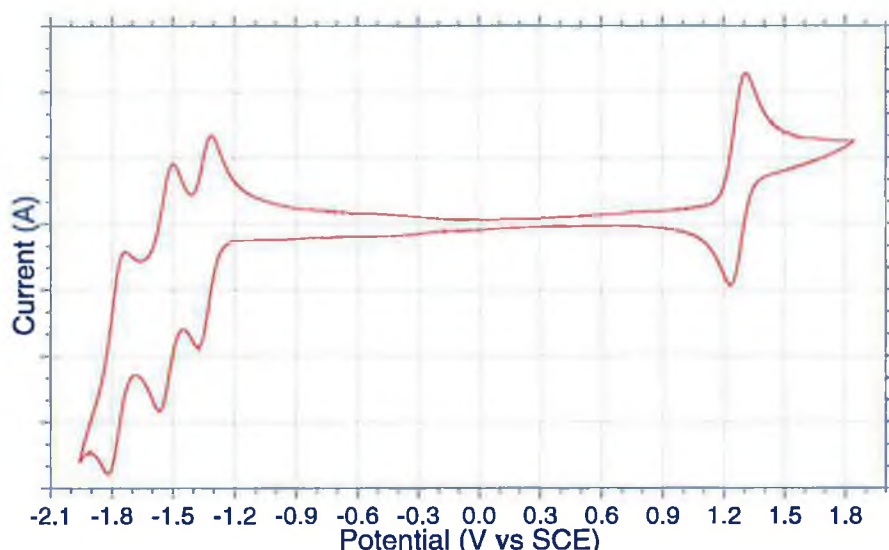
Figure 1.14. Electrochemical data obtained for $[Ru(bpy)_3]^{2+}$ in deaerated MeCN with 0.1 M TBABF$_4$.

Excitation of an electron to a peripheral bpy ligand means that the excited complex is both a better oxidant and reductant than when in its ground state configuration. This can be explained by the fact that an electron localised on a ligand is less strongly bound than that on the metal and so is more readily removed. Conversely, the excitation of the electron leaves an electron "hole" on the metal to which another electron is more easily introduced. The relationship between the ground and excited state redox properties are summarised in Fig. 1.15.
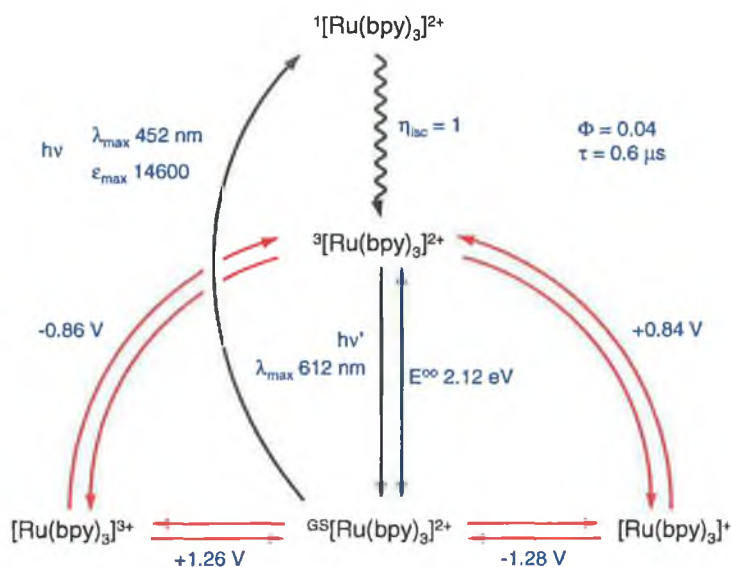
Figure 1.15. *Latimer-type diagram showing the photophysical and redox properties of [Ru(bpy)$_3$]$^{2+}$.*

1.4   Bis(heteroleptic) Ru(II) Complexes

In [Ru(bpy)$_3$]$^{2+}$, at elevated temperatures, the ^{3}MC state is readily thermally populated from the ^{3}MLCT level which causes the complex to undergo photosubstitution, thus, rendering it unsuitable as a photocatalyst. One solution to the photo-instability of [Ru(bpy)$_3$]$^{2+}$ is the introduction of different ligands to the ruthenium centre. If these ligands are designed carefully, then the relative energies of the excited states can be manipulated so as to achieve a complex capable of matching the photophysical properties of [Ru(bpy)$_3$]$^{2+}$ but increasing the ^{3}MLCT– ^{3}MC energy gap. Many complexes now exist with the general structure [Ru$^{(II)}$(bpy)$_2$(L)]$^{n+}$ and, depending on the electronic nature of the ligand L, the photophysical and photochemical properties of the complexes can been altered [55]. The types of ligands used can be categorised into two main groups depending on their relative electron donating/accepting abilities as compared with bpy. Class A are defined as those ligands with weaker σ-donating but stronger π-accepting abilities than bpy. Class B are defined as ligands with stronger σ-donating but weaker π-accepting abilities.

1.4.1 Class A ligand examples – weak σ-donor, strong π-acceptor abilities
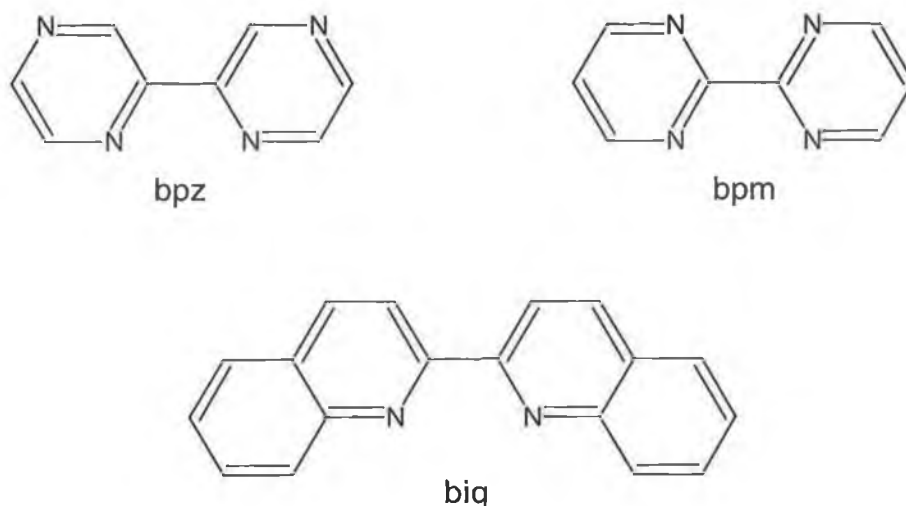
Figure 1.16. Examples of Class A ligands.

These ligands (Fig. 1.16) – which include 2,2'-bipyrazine (bpz) [56], 2,2'-bipyrimidine (bpm) [56,57] and 2,2'-biquinoline (biq) [58] – cause less ligand-field splitting of their respective Ru(II) complexes, and thus the ^{3}MC state becomes more readily populated. This leads to a reduction in the photostability of these complexes. Complexes of the type $[Ru^{(II)}(bpy)_2L]^{n+}$, where L is a Class A ligand, have reduced electron density around the metal centre compared to $[Ru(bpy)_3]^{2+}$ and so show higher corresponding metal-based oxidation potentials. On the other hand, as they are strong π-acceptors, the first reduction is L based and as such all emission properties are located on the L ligand.

1.4.2 Class B ligand examples – strong σ-donor, weak π-acceptor abilities

Ligands which possess strong σ-donor abilities, such as those shown in Fig. 1.17, increase the ligand-field splitting and, thereby, diminish the likelihood of ^{3}MC population.
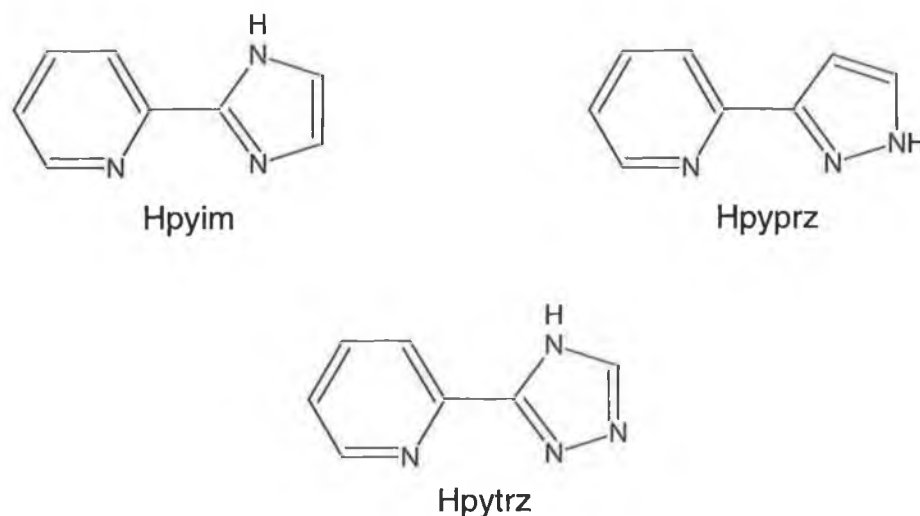
Figure 1.17. *Examples of Class B ligands.*

Examples of such ligands are 2-(pyridin-2-yl)-imidazole (Hpyim) [59], 3-(pyridin-2-yl)-pyrazole (Hpyprz) [60,61] and 3-(pyridin-2-yl)-1,2,4-triazole [62,63]. They are, however, weak π-acceptor ligands and so the energy difference between the metal d–d orbital and the π^*-accepting orbital of the ligand is greater. The overall effect is greater photostability but lower emission yields. $[Ru^{(II)}(bpy)_2L]^{n+}$ type complexes where L is a Class B ligand tend to have lower oxidation potentials (due to the increased electron density around the metal centre). The first two reduction waves are bpy based with the reduction of the L ligand at a far more negative potential.

$[Ru(bpy)_3]^{2+}$ is prone to photo-substitution but by replacing a bpy ligand with one of the class B ligands, population of the ^3MC state is reduced due to the now greater ligand-field splitting caused by the stronger σ-donating ligand. This has been observed for complexes such as $[Ru(bpy)_2(pytrz)]^+$, $[Ru(bpy)_2(Hbii)]^+$ and $[Ru(bpy)_2(HBzim)]^+$ (for ligand structures and abbreviations see pages x and xi). Thermal activation of the upper ^3MC excited state in $[Ru(bpy)_2(bpt)]^+$ is found to be absent [64].

The σ-donating ligand raises the ground state energy thus causing a reduction in the ^{3}MLCT transition energy and as a result a red shift in the absorption ([Ru(bpy)$_2$(bpt)]$^+$, λ_{max} 475 nm) and emission ([Ru(bpy)$_2$(bpt)]$^+$, λ_{em} 678 nm) spectra is observed. The π*-levels of the poor π-accepting ligand lie at much higher energies as compared to the bpy ligands and in complexes of this type the LUMO is on the auxiliary bpy ligands and so the excited state is always bpy-based [65,66].

The extent to which some of these ligands are poor π-acceptors can be seen by the reduction potentials of their homoleptic complexes [67]. Rillema *et al.* found that both [Ru(H$_2$bii)$_3$]$^{2+}$ and [Ru(H$_2$Bzim)$_3$]$^{2+}$ do not exhibit reduction waves between 0 and –2 V (SCE), whereas substitution by a bpy ligand caused a reduction at approximately –1.4 V (SCE), similar to that of [Ru(bpy)$_3$]$^{2+}$ [68]. In fact, all bpy-mixed ligand complexes of bii^{2-}, Bzim^{2-}, bpt$^-$ and pzbzim^{3-} exhibit first reduction potentials of about –1.4 V (SCE), indicating that the first reduction is bpy-based [49]. Indeed, resonance Raman studies on the mononuclear [Ru(bpy)$_2$(bpt)]$^+$ suggest that the lowest-energy MLCT absorption is bpy-based [66].

The oxidation potential of a metal centre is lowered with increasing number of σ-donor ligands. Rillema *et al.* found that these potentials decreased from 1.26 V (SCE) for [Ru(bpy)$_3$]$^{2+}$ to 0.54 V (SCE) for [Ru(H$_2$bii)$_3$]$^{2+}$ [67]. Likewise, although not carried out systematically, Hage found that the oxidation potential for a triazole derivative [Ru(bpy)$_2$(3Mepytr)]$^{2+}$ to be 1.20 V (SCE) and that of [Ru(3Mepytr)$_3$]$^{2+}$ to be 1.10 V (SCE) [69].

1.4.3 1,2,4-Triazole containing ligands

The interesting properties of triazole complexes have resulted in them being the focus of many research projects and one with which this thesis will focus. The first report of ruthenium triazole complexes was by Vos *et al.* [70]. Since then a great deal of knowledge has been acquired on the photochemistry and

photophysics of such complexes [64,69,71]. An interesting feature of 1,2,4-triazoles as ligands is the position of the nitrogen atoms as shown in Fig. 1.18. Such positioning allows the triazole ligands to form structural isomers depending on whether the metal centre is bound through N2 or N4. If a large substituent R is present on the triazole ring, metal coordination through N2 is almost entirely preferred over that of N4. Without a substituent both isomers are formed in equal measure. Differences in the photophysical characteristics of the different isomers have been reported because the N2 site has been shown to be a stronger σ-donor than that of N4 [71,72].
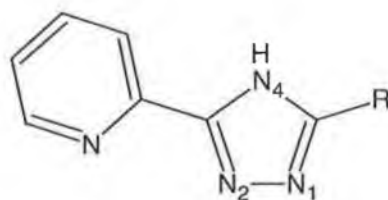
Figure 1.18. *Numbering scheme used throughout this thesis for nitrogens on the 1,2,4-triazole ligand.*

Triazole containing complexes feature an interesting pH dependent photochemistry [73]. When bound to a metal centre the triazole becomes a much stronger acid (pK_a 4.0±0.1) than the free ligand (pK_a 8.4±0.1), Eq. (12). This suggests substantial electron donation from the ligand to the metal centre.

$$[\text{Ru(bpy)}_2\text{bpt}]^+ \xrightleftharpoons{\;\;H^+\;\;} [\text{Ru(bpy)}_2\text{Hbpt}]^{2+} \qquad \text{Eq. (12)}$$

When the complexed triazole is protonated the σ-donating abilities of the ligand decrease, lowering the ground state energy of the complex. This causes an increase in the observed MLCT transition energies. Consequently, a blue shift in the absorption and emission spectra is observed. Similar behaviour has been observed for a series of compounds containing imidazole, pyrazole and 1,2,4-triazole ligands [74,75].

In order to combine the characteristics of Class A and Class B ligands, Hage *et al.* synthesised a series of pyrazyl-triazoles. Hage *et al.* found that these ligands were still strong σ-donors although not quite as strong as their pyridyl analogues. On the other hand the reduction potentials of the free ligands proved to be less negative than bpy or the pyridine-triazoles making them better π-acceptors. Thus complexes containing a pyrazyl-triazole show different properties to those outlined for pyridyl-triazoles. As for bpt⁻ systems, the emitting state for $[Ru(bpy)_2(bpzt)]^+$ is bpy-based. However, upon protonation, resonance Raman studies show both bpy and Hbpzt vibrations. This suggests that when protonated, a significant lowering of the π*-orbital takes place leading to a Hbpzt-based MLCT transition of $[Ru(bpy)_2(Hbpzt)]^{2+}$. This is in agreement with the red-shift of the absorption and emission spectra observed by O'Connor [76].

1.4.4 Bridging ligands

Ligands that join two or more metal centres together in a polynuclear complex are called bridging ligands. The resulting electronic and redox properties of such complexes are strongly influenced by the nature of the bridging ligand mediating the metal–metal interactions. To be effective the molecular orbitals of the bridging ligand should be symmetry- and energy-matched to interact with the donor and acceptor orbitals of the metal centres. As was previously discussed for auxiliary ligands, both π-accepting and σ-donating bridging ligands exist. As this thesis deals mainly with the triazole bridging ligand, σ-donating ligands will be discussed in more detail. For a list of the most common bridging ligands and their electronic and redox properties see Ref. [77].

1.4.4.1 π-Accepting bridging ligands

These ligands form the majority of bridging ligands and are generally neutral derivatives of pyridine, pyrazine and pyrimidine, Fig 1.19. They include compounds such as 2,2';3',2'';6'',2'''-quaterpyridine (qpy) [78,79], 2,3-bis(pyridin-2-yl)-pyrazine (bpp) [80,81] and 2,2'-bipyrimidine [80]. They mediate

intermetallic interactions through low-lying π*-orbitals (LUMOs) by invoking an electron transfer super-exchange mechanism.
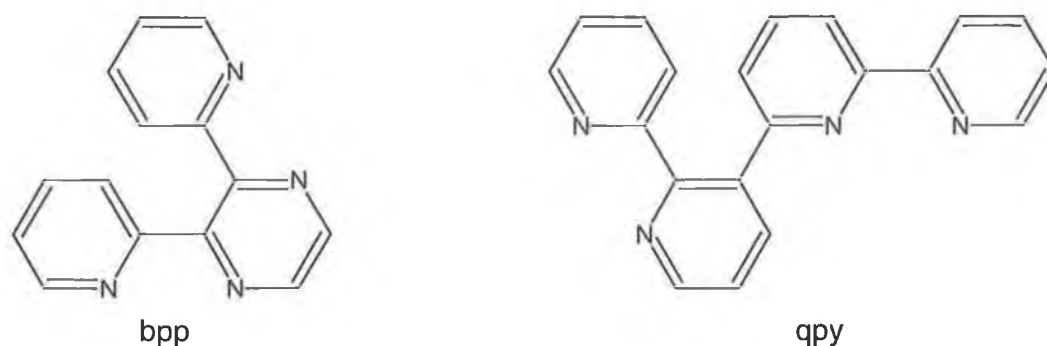
Figure 1.19. Examples of π-accepting bridging ligands.

Due to this low-lying π*-orbital, the lowest MLCT transition is bridge based and it is here that luminescence originates. Likewise, the first reduction wave of these complexes is found on the bridge with the first reduction potential being less negative in dinuclear as opposed to mononuclear complexes. This is due to stabilisation of the energy of the π*-levels on the bridge upon coordination of the second metal centre. Stabilisation of the π*-levels causes a red shift in the absorption and emission spectra, and lifetimes of excited dinuclear species are often significantly shorter than their mononuclear analogues.

1.4.4.2 σ-Donating bridging ligands

Bridging ligands with σ-donating abilities form their anionic analogues when complexed to a metal centre by deprotonation of their free nitrogen. Ligands such as 3,5-bis(pyridin-2-yl)-1,2,4-triazole (Hbpt) [82,63], 2,2-biimidazole/2,2'-bibenzoimidazole (H$_2$bii/H$_2$Bzim) [67] and 3,5-bis(benzoimidazole)-pyrazole (H$_3$pzbzim) [83,84] assist metal–metal coupling via hole-transfer mechanisms by taking advantage of relatively high-lying filled molecular orbitals (HOMOs). Fig. 1.20 shows the structures of some σ-donating ligands.
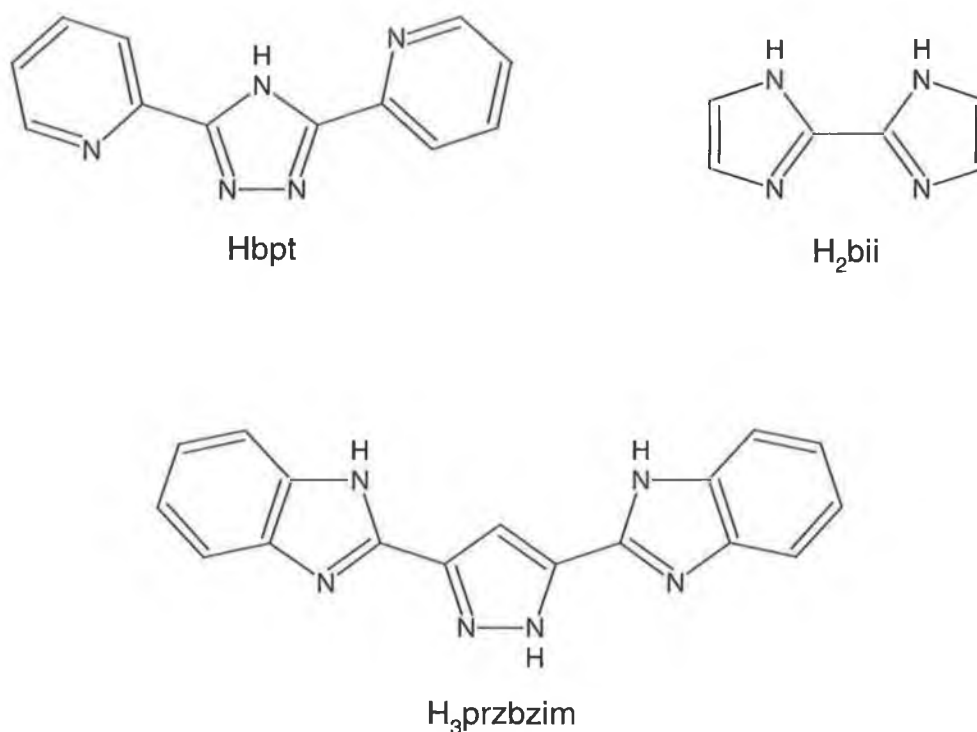
Figure 1.20. Examples of σ-donating bridging ligands.

With the coordination of a second metal centre, the ligand-field strength is much reduced due to the sharing of the σ-donating bridge. This is reflected in the blue shift of the absorption and emission bands and a correspondingly higher first oxidation potential. This is in sharp contrast to the π-accepting bridges described above which display a red shift due to their LUMO stabilisation. Because of the reduction in ligand-field strength, population of the ^{3}MC state is possible with dinuclear complexes and their photo-instability has been observed.

An interesting aspect of 1,2,4-triazoles as bridging ligands is the position of the donor atoms. When two different metals complex to the bridge, structural isomers are formed depending on whether each metal centre is bound through N2 or N4. As already outlined for the mononuclear species, differences in the photophysical characteristics of the different isomers exist because N2 is a stronger σ-donor site than that of N4. Photochemical experiments suggest that the ^{3}MC level of the N2-bound ruthenium is at a lower energy than that of the N4-bound centre and indeed photosubstitution has been observed at this position [85].

Hughes *et al.* investigated complexes of the form $[Ru(L_1)_2\text{-}bpt\text{-}Ru(L_2)_2]^{3+}$ where L_1 and L_2 were bpy or phen [86,87]. These complexes showed the usual metal-based oxidations and bpy/phen reductions. Resonance Raman studies show that the lowest excited state is bpy-based irrespective of the binding site (N2 or N4) at the triazole ligand, which confirmed earlier results by Chang *et al.* [88]. The excited state was only found on phen when $L_1=L_2=$phen. In the mixed valence species of the type $M^{II}M^{III}$, it was found that for both geometrical isomers the centre attached to the N2 position of the triazole ring was oxidised first, thus confirming the superior donating ability of N2.

In bimetallic complexes of bpt⁻, different oxidation potentials have been found for RuOs (Ru bound *via* N2, Os bound *via* N2) and OsRu (Os bound *via* N2, Ru bound *via* N4) [69,82]. Furthermore, the RuRu complex shows an unusually large separation of oxidation potentials, and as such, results suggest that significant electronic communication between the metal centres exists. To probe this communication, a RuRu complex with a bpzt⁻ bridging ligand was investigated. Although the lowest π^*-orbital (LUMO) of bpzt⁻ is much lower in energy than that of bpt⁻, the coupling between the metal centres is approximately the same for both complexes. This suggests that coupling *via* the LUMO is of minor importance for bpt⁻/bpzt⁻ complexes. It is most likely that metal–metal interaction involves the HOMO of the bridging ligand. The interaction between the first M^{III} and the electron rich HOMO of the bridging ligand reduces the electron density present on the second coordination centre and thus forces a higher oxidation potential. Van Diemen *et al.* further verified this type of interaction by studying a range of bimetallic complexes containing Ru, Rh and Ir [89].

1.5   Tris(heteroleptic) complexes

1.5.1   Introduction

While many examples of bis(heteroleptic) Ru(II) complexes exist, only a few tris(heteroleptic) Ru(II) species are known. Since Black *et al.* first reported a

tris(heteroleptic) Ru(II) complex, a few different routes to these complexes have been developed. As the primary interest of this thesis is to synthesise these types of molecules, particular detail has been paid to the synthesis rather than the properties of the complexes reported. For the purpose of this thesis, all the different routes to tris(heteroleptic) Ru(II) complexes have been categorised into four sections;

(a)   **[Ru(bpy)Cl₃] Method** :   Starting with [Ru(bpy)Cl₃], ligands are added sequentially in a one-pot reaction.

(b)   **[Ru(DMSO)₄Cl₂] Method**:   Similar to the method above but starting with [Ru(DMSO)₄Cl₂]. This reaction method generally utilises "softer" reaction conditions.

(c)   **Decarbonylation Method**:   This category has been further subdivided into two sections; chemical decarbonylation using TMNO and photochemical decarbonylation. Both methods involve the removal of CO ligands at some point during the synthesis.

(d)   **Photosubstitution Method**:   This method includes those synthetic routes that use light at some stage to substitute one ligand for another.

The following section serves as an introduction to the methods employed to this date by researchers in the field. Chapter 3 details the subsequent exploration of these routes as a viable method of incorporating a triazole to the metal sphere.

1.5.2 [Ru(bpy)Cl₃] Method

[RuCl$_3$].xH$_2$O will react with bpy or Me$_2$bpy in HCl to yield the monosubstituted complex [Ru(L)Cl$_3$] where L is bpy or Me$_2$bpy [90]. Thummel *et al.* synthesised a tris(heteroleptic) complex by the stepwise addition of bidentate ligands to [Ru(bpy)Cl$_3$]$_n$ in aqueous ethanol [91]. The intermediate complex [Ru(bpy)(biq)]X$_2$, where X represents a chloride, solvent or mixture of the two, was not isolated or characterised but instead reacted directly with one equivalent of bi-naph to yield the desired product as purple crystals (57%). The complex was characterized by MS, CHN and ^{1}H NMR. As expected, 26 aromatic protons were observed since each ring is chemically inequivalent.

Recently, Hesek *et al.* devised a synthesis whereby they prepare a compound similar to [Ru(L)Cl$_3$] by gently heating [RuCl$_3$].xH$_2$O with bpy in DMF [92]. This intermediate complex was isolated and the structure confirmed as [Ru(bpy)(sol)Cl$_3$] by X-ray diffraction analysis (sol = MeCN). However, when synthesising their tris(heteroleptic) complex they began by first heating [RuCl$_3$] with ambpy. After some time estbpy was added and the temperature of the reaction increased. Removal of solvent and addition of Me$_2$bpy under standard aqueous alcoholic conditions afforded the desired complex (44%). The selectivity of this method is based upon variation of the reaction temperature and stoichiometries of the reagents. As Maxwell *et al.* had discovered earlier [94], the order in which the ligands were added was of prime importance. In this case, it was found that the least reactive ligand, i.e., the ambpy, should be added first, followed by estbpy and finally Me$_2$bpy. The reason behind this is that as the ligand architecture increases in complexity, the bipyridyls with withdrawing groups attached will require longer reaction times under the harsher conditions. This will add to the number of by-products, side chain racemizations (in this instance) and scrambling of the ligands around the central ruthenium. Both [Ru(Me$_2$bpy)(S-estbpy)(R-ambpy)]Cl$_2$ and [Ru(Me$_2$bpy)(R-estbpy)(R-ambpy)]Cl$_2$ were prepared and separated into their respective Δ/Λ-diasterioisomers by preparative chiral HPLC.
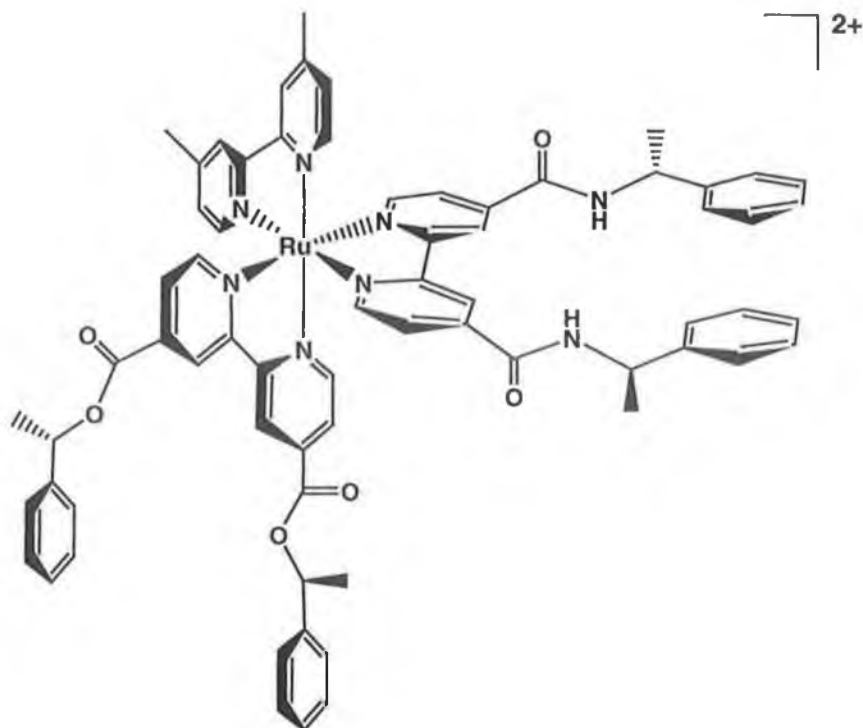
Figure 1.21. *The tris(heteroleptic) complex synthesised by Hesek et al. in a one-pot reaction [92].*

1.5.3 [Ru(DMSO)₄Cl₂] Method

The need for a "softer" approach to incorporate oxidation sensitive ligands to the coordination sphere led Zakeeruddin *et al.* to develop a new synthetic strategy utilising [Ru(DMSO)$_4$Cl$_2$] as starting material [93]. Although the complex reported was tris(heteroleptic) in nature, one of the three ligands was a dithiocarbamate and not a polypyridyl ligand as has been featured throughout this thesis. Nevertheless, this reaction pathway was one that could be explored as a possible route to our desired complex.

The synthesis of a tris(heteroleptic) species using [Ru(DMSO)$_4$Cl$_2$] as starting material is attractive because it does not require the use of TMNO. Reacting [Ru(DMSO)$_4$Cl$_2$] with a bidentate ligand, L, results in the complex [Ru(L)(DMSO)$_2$Cl$_2$]. Zakeeruddin *et al.* then attached a dicarboxy-bipyridine to the metal centre by refluxing in DMF. They were able to isolate their product as

the dichloride [Ru(bpy)(dcb)Cl₂] (75%) which they characterised by UV and CHN analysis.
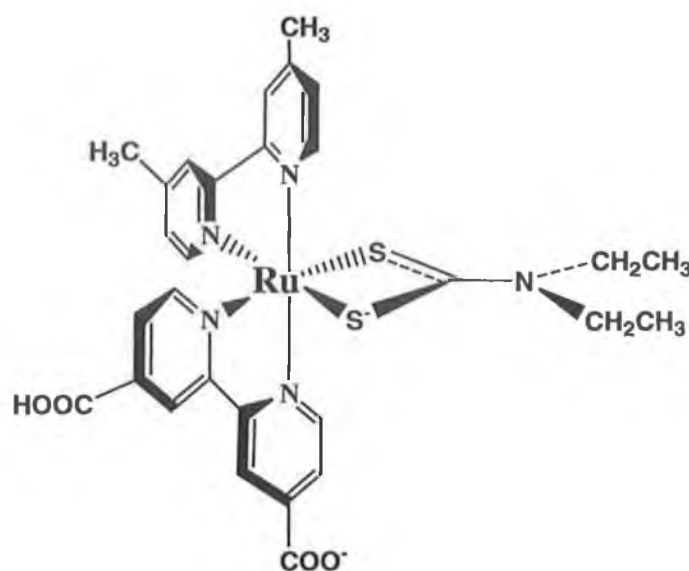
Figure 1.22. *A tris(heteroleptic) complex synthesised by Zakeeruddin et al. [93].*
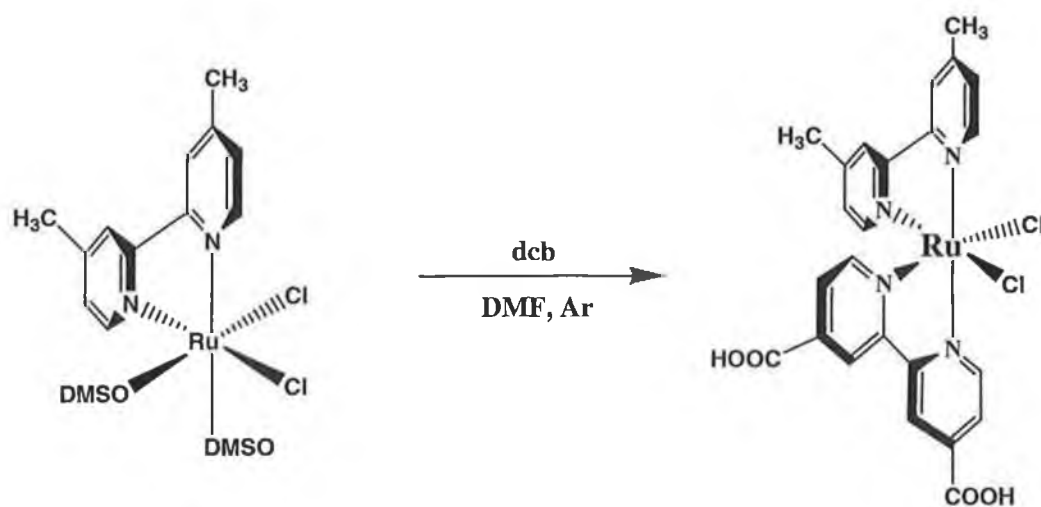
Scheme 1.2 *Formation of the dicarboxypyridine dichloride.*

Recently, Maxwell *et al.* reported a one-pot synthesis of a tris-heteroleptic donor–acceptor assembly in which the bis-intermediate was not isolated [94]. This

involved the sequential addition of the ligands dcb, bpyCH₂MV²⁺ and bpyCH₂PTZ to [Ru(DMSO)₄Cl₂].
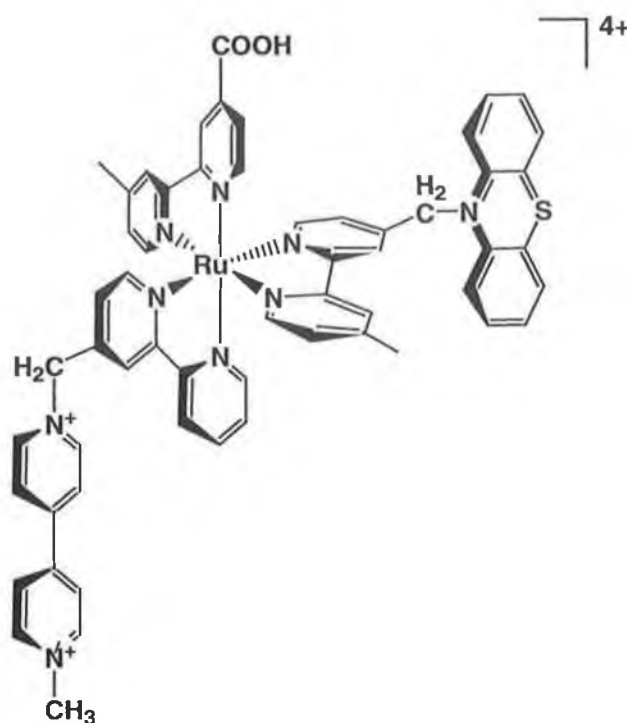
Figure 1.23. A donor-quencher complex synthesised by Maxwell et al. [94].

The tris(heteroleptic) complex was isolated in low yield (19%) by cation-exchange chromatography. The order in which the ligands were introduced was found to be crucial to the formation of the tris-complex. If the basic bpyCH₂PTZ was added first, then the tris-homoleptic complex [Ru(bpyCH₂PTZ)₃]²⁺ was formed. Therefore dcb and bpyCH₂MV²⁺ were added simultaneously to an ethanolic solution of [Ru(DMSO)₄Cl₂] and allowed react for 35 min. Finally, bpyCH₂PTZ was added and the reaction followed by UV–Vis to optimise the yield of the desired complex and minimise losses due to ligand scrambling. Although the desired complex was isolated, a great number of complexes could be formed under such conditions. Before bpyCH₂PTZ is even added a mixture of [Ru(dcb)₂(sol)(Cl)]⁺, [Ru(bpyCH₂MV²⁺)₂(sol)(Cl)]⁵⁺ and [Ru(dcb)(bpyCH₂MV²⁺)(sol)(Cl)]³⁺ might be present. Separation was achieved by utilising the differences in charge of the possible side products formed. Under the

chromatographic conditions employed, dcb exists as bpyCOO⁻ and thus each possible product exists with a different total charge.

1.5.4 Decarbonylation Method

The first reports of a tris(heteroleptic) Ru(II) complex were back in 1982 when Black *et al.* decarbonylated a Ru(II) carbonyl compound using trimethylamine-N-oxide (TMNO), Scheme 1.3. In the presence of dpa or biq they produced a complex in which the three bidentate ligands around the metal centre were different [95].

[Ru(bpy)(phen)(CO)₂]²⁺
+
dpa

$\xrightarrow{\text{Me}_3\text{NO}}{\text{methoxyethanol}}$
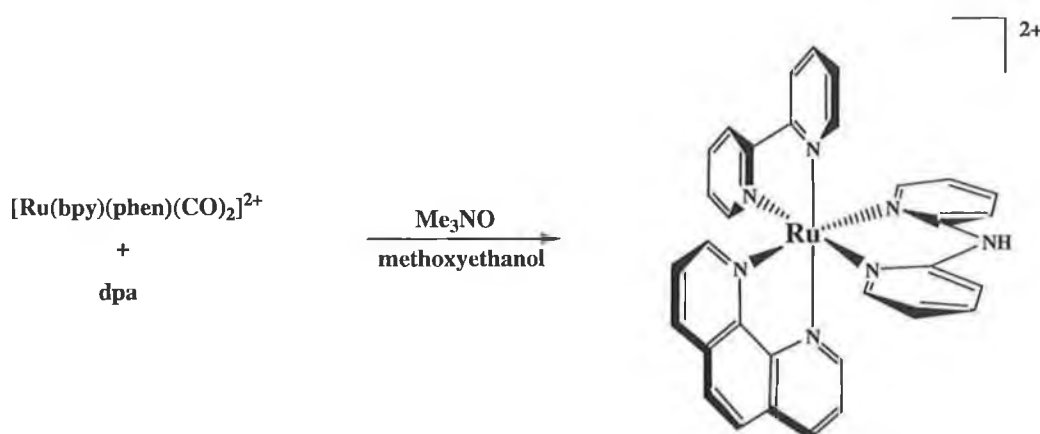
Scheme 1.3. The strategy employed by Black et al. [95] and the first reported tris(heteroleptic) complex.

A pure product (HPLC) in 70% yield was obtained and X-ray crystallography was used to confirm the presence of the three bidentate ligands. A number of such tris(heteroleptic) complexes as studied by FAB mass spec. are reported [96]. Black *et al.* claim that the reaction proceeds through the slow formation of a mono-carbonylated species after studying analogous bis(heteroleptic) reactions [97]. Such a species was never isolated however. They found that [Ru(bpy)(CO)₂Cl₂] only underwent monodecarbonylation in pyridine to form [Ru(bpy)(py)(CO)Cl₂]. TMNO assisted decarbonylation is generally restricted to carbonyls with v(CO) > 2000 cm⁻¹ [98]. As monocarbonyls show stronger Ru–

carbonyl bonding (1940 cm^{-1}) than di-carbonyls (2100–2000 cm^{-1}) the disubstitutions with pyridine were not successful. However, in the presence of a bidentate ligand in refluxing methoxyethanol the desired complexes were produced.

As discussed earlier in Section 1.4, altering the ligands around the metal centre can vary the properties of the excited states of these complexes. It was with this intention that Strouse *et al.* modified the earlier decarbonylation reaction so that they could incorporate different functionalised ligands into the coordination sphere [99,100]. The starting material [Ru(bpy)(CO)$_2$Cl$_2$] was converted to the corresponding triflato species by heating in triflouromethansulfonic acid [101,102]. This triflato species was reacted with a second ligand Me$_4$bpy to produce the carbonyl complex [Ru(bpy)(Me$_4$bpy)(CO)$_2$]$^{2+}$. By heating this complex with TMNO in the presence of a third ligand Strouse *et al.* produced three new tris(heteroleptic) complexes [99].

[Ru(Me$_2$bpy)(Me$_4$bpy)(CO)$_2$]$^{2+}$

+

(EtCO$_2$)$_2$bpy

$\xrightarrow{\text{Me}_3\text{NO}}_{\text{methoxyethanol}}$
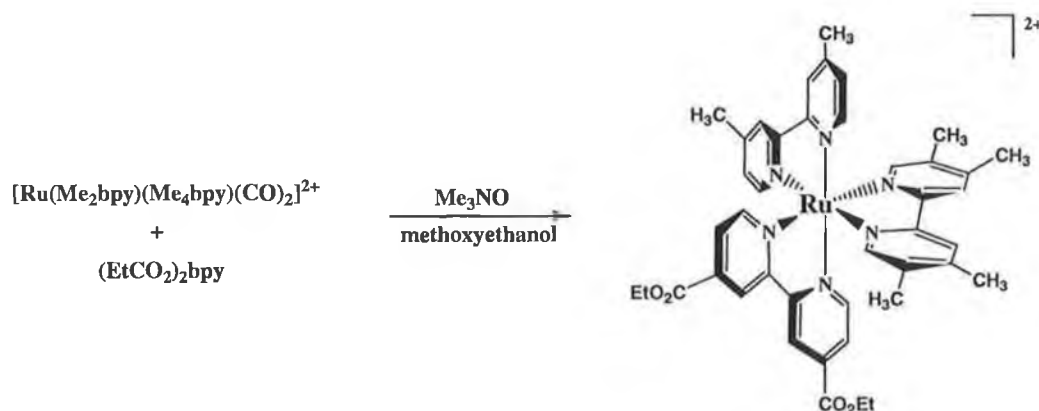
Scheme 1.4. Complex prepared by Strouse et al. [99] using TMNO as decarbonylating agent.

The complexes showed satisfactory elemental analysis and were pure as observed by HPLC. Mass spectrometry confirmed the presence of the desired complexes. No yields were reported for the final two synthetic steps.

The seminal publication for the decarbonylation reaction by Anderson *et al.* introduces a wide variety of tris(heteroleptic) Ru(II) complexes with ligands containing various functional groups and in some cases bridging ligands themselves [103]. This is the first detailed account of the synthetic procedures used to prepare the complexes mentioned previously. As reported by Black *et al.* [102], Anderson *et al.* reacted a series of $[Ru(L)(CO)_2Cl_2]$ with triflouromethanesulfonic acid to yield the triflato complexes $[Ru(L)(CO)_2(CF_3SO_3)_2]$. As $CF_3SO_3^-$ ligands are far more labile than Cl^- ligands they are readily interchangeable with a second polypyridyl ligand [104]. This exchange was carried out in 1,2-dichlorobenzene and temperatures were kept at 100°C as the authors found that higher temperatures led to degradation of the species.

Anderson *et al.* followed the previous method by Strouse *et al.* [99] and used TMNO to decarbonylate the $[Ru(L)(L)(CO)_2]$ complex. Anderson *et al.* found that the rate of decarbonylation depended on the two ligands already attached to the Ru(II) centre. The more electron-withdrawing the ligands, the more rapid the rate of decarbonylation. This can be explained when one considers the nature of the metal–carbonyl bond, Fig. 1.24.

The bond that forms between the Ru centre and the carbonyl ligand is a synergic process involving a mixing of the metal d-orbitals with the σ and π^* orbitals of the CO moiety. As the CO ligand approaches the metal centre, the mixing of the Ru d_{z^2} and the CO 3σ orbital causes accumulation of electron density on the metal atom. This extra electron density is dissipated by delocalisation of electrons from the full metal t_{2g} orbitals to the carbonyls LUMO, i.e., the $2\pi^*$ orbital. Thus, any withdrawing groups on the ligands already present in the metal coordination sphere will reduce this π-backbonding, leading to a weaker metal-carbon bond.
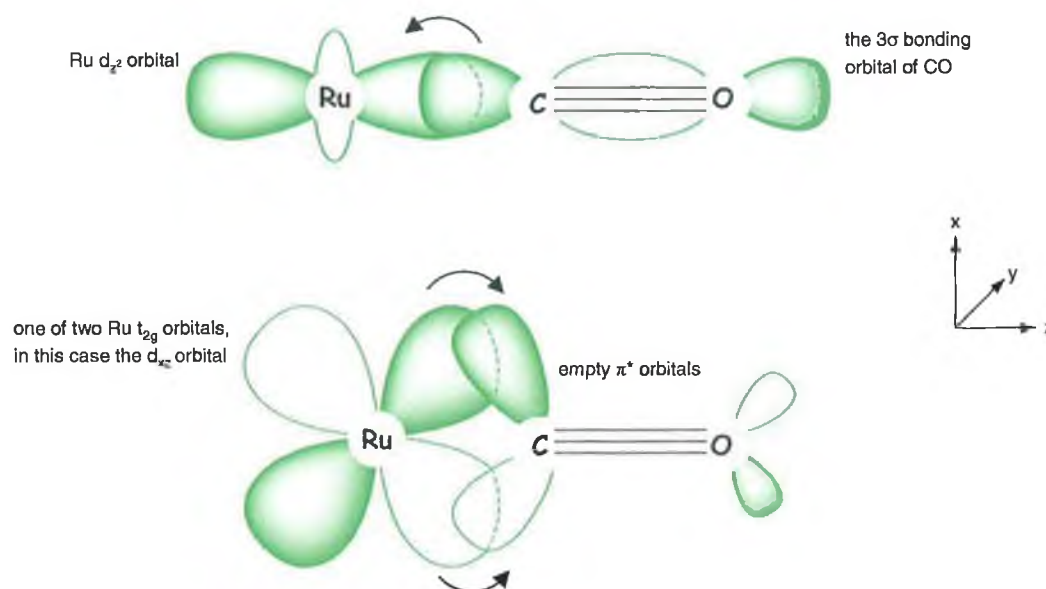
Figure 1.24. The synergic π-backbonding between Ru and CO.

Although they prepare a great range of tris(heteroleptic) complexes, the conditions involved with the use of TMNO may prove too harsh for other oxidisable ligands. TMNO is a strong oxidizing agent and ligands incorporating groups such as phenothiazine would be susceptible to attack. Rutherford *et al.* avoided this problem by reacting $[Ru(Me_2bpy)(bpy-MV^{2+})(CO)_2]^{4+}$ with pyridine to form the intermediate $[Ru(Me_2bpy)(bpy-MV^{2+})(py)_2]^{4+}$. This could then be reacted with the phenothiazine derivative under milder conditions to yield the tris(heteroleptic) species [105,106]. This strategy has also been adopted by Treadway and Meyer [107] although they use it to synthesise highly asymmetrical complexes of the structure $[Ru(L)(L')(X)(Y)]^{n+}$ where L and L' are non-identical bidentate ligands and X and Y are non-identical monodentate ligands respectively. Such complexes, although synthetically interesting are outside the scope of this thesis.

1.5.5 Photosubstitution method

Von Zelewsky and Gremaud utilised the intermediary $[Ru(bpy)(biq)(MeCN)_2]^{2+}$ to prepare a series of tris(heteroleptic) complexes [108]. They state that some of their complexes were prepared using $[Ru(bpy)(biq)Cl_2]$ as an intermediate but do not give an account of how they obtained such a compound. $[Ru(bpy)(biq)(MeCN)_2]^{2+}$ was prepared by the photolysis of $[Ru(bpy)(biq)_2]^{2+}$ in MeCN and was isolated as the PF_6^- salt.
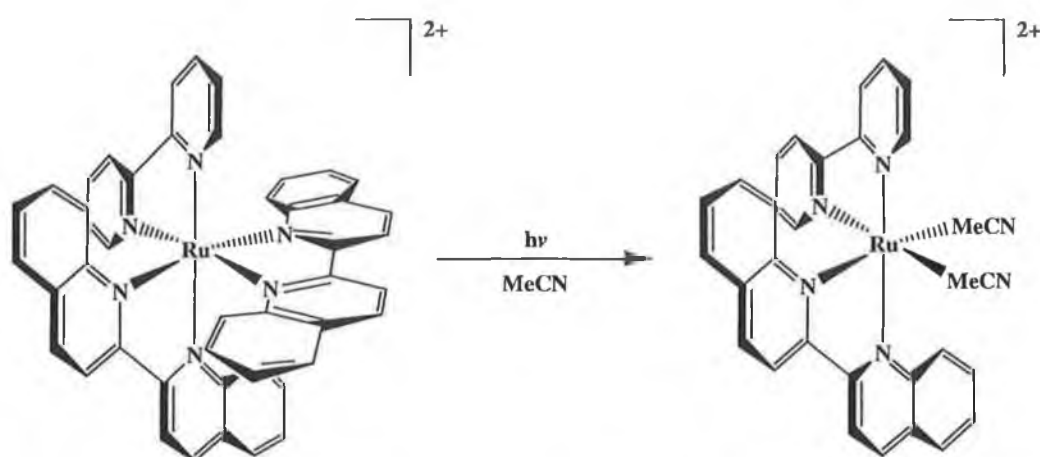
Scheme 1.5. *The photolabilisation of biq in MeCN as prepared by Von Zelewsky and Gremaud [108].*

^{1}H NMR suggests that the MeCN ligands have a *cis*-conformation. It then reacts at relatively low temperatures with a third ligand, L, to form the tris(heteroleptic) complex. If the tris(heteroleptic) complex was itself irradiated in MeCN, Von Zelewsky and Gremaud found that the second biq ligand could be replaced by two acetonitrile molecules although none of these complexes were isolated.

Ross *et al.* also synthesised a complex using an acetonitrile intermediate containing the ligands bpy, bpm and bpz [109]. They irradiate a $[Ru(bpm)_2(bpy)]^{2+}$ sample in MeCN in the presence of tetraethylammonium chloride to yield $[Ru(bpm)(bpy)(MeCN)Cl]^+$. This was then reacted with bpz to yield the tris(heteroleptic) complex $[Ru(bpz)(bpm)(bpy)]^{2+}$.

41

The most recent publication reporting the synthesis of a tris(heteroleptic) complex was by Freedman *et al.* who prepared the two complexes $[Ru(Me_2bpy)(phen)(Me_2phen)]^{2+}$ and $[Ru(bpy)(Me_2bpy)(phen)]^{2+}$ by a new method [110].
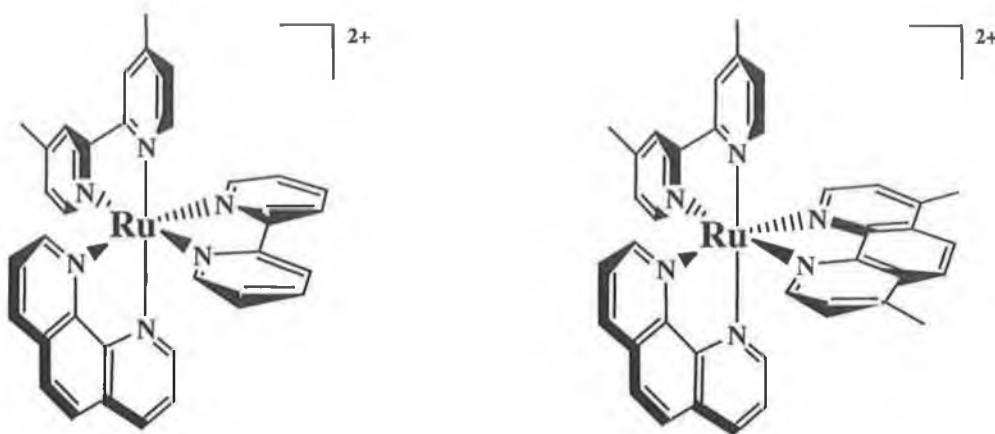
Figure 1.25. The two complexes synthesised by Freedman et al. [110].

This involved starting from the dimeric material $[BzRuCl_2]_2$ [111] which was reacted with bpy or Me_2bpy to produce $[BzRu(L)Cl]Cl$ in yields of about 80%. The second step involves the removal of the η^6-benzene and as the authors found that thermal displacement of η^6-benzene does not occur, $[BzRu(L)Cl]Cl$ was photolysed in MeCN. This produced the mixture of acetonitrile complexes, $[Ru(L)(CH_3CN)_3Cl]Cl$ and $[Ru(L)(CH_3CN)_2Cl_2]$ which yielded the dichloride $[Ru(L)(L')Cl_2]$ when reacted with L' in acetone. The final addition of L'' was carried out in aqueous EtOH as for the bis(heteroleptic) complexes.

1.6 Scope of Thesis

The research carried out for this thesis is focused primarily on the synthesis of tris(heteroleptic) complexes. To date, only a handful of synthetic methodologies exist to synthesise such species. This work centres on whether previously reported synthetic strategies would be viable when a triazole was incorporated into the

synthetic design. The previous synthetic methods were categorised depending on their synthetic approach and each method was then explored. Ultimately a new approach to such systems was required as is reported in Chapter 3. The successful synthesis of a tris(heteroleptic) complex containing a simple triazole ligand is reported. The knowledge acquired in Chapter 3 allowed the synthesis of more complicated systems as reported in Chapters 4 and 5. Chapter 4 deals with a series of mononuclear complexes where the ligands around the metal centre are systematically altered. Both pyridine- and pyrazine-triazole bridging ligands are employed. The characterisation of these complexes is addressed by using different analytical techniques such as ^{1}H NMR, MS, HPLC and X-ray crystallography to confirm the successful synthesis of the target complexes. Chapter 5 is a natural progression of the synthetic work completed in Chapter 4. The dinuclear analogues of the complexes are synthesised and their photophysical properties measured. A range of bpt⁻ dinuclear complexes containing dpp are synthesised and any differences that dpp exerts on N2- and N4-bound metal centres is examined.

1.7   Bibliography

[1]   Kessel D.G., *J. Pet. Sci. Eng.*, **2000**, *26*, 157–168.

[2]   Lodhi M.A.K., *Energy Convers. Manage.*, **1997**, *38*, 1881–1893.

[3]   Bolton J.R., *Solar Energy*, **1996**, *57*, 37–50.

[4]   Nicoletti G., *Int., J., Hydrogen Energy*, **1995**, *20*, 759–765.

[5]   Harvey L.D.D., *Int., J., Hydrogen Energy*, **1996**, *21*, 583–595.

[6]   Kyoto Protocol to the United Nations Framework Convention on Climate Change, **1997.**

[7]   Leggett J., *Renew. Sustain. Energy Rev.*, **1998**, *2*, 345–351.

[8]   Amouyal E., *Sol. Energy Mater., Sol. Cells*, **1995**, *38*, 249–276.

[9]   McConnell R.D., *Renew. Sustain. Energy Rev.*, 2002, 6, 273–295.

[10]   Grätzel M., *J. Photochem. Photobiol. C*, **2003**, *in press.*

[11]   O'Regan B., Grätzel M, *Nature*, **1991**, *335*, 737–740.

[12]   Nazeeruddin M., Kay A., Rodicio I., Humphry-Baker R., Muller E., Liska P., Vlachopoulos N., Grätzel M., *J. Amer. Chem. Soc.*, **1993**, *115*, 6382–6390.

[13]   Nusbaumer H., Zakeeruddin S.M., Moser J.-E., Grätzel M., *Chem. Eur. J.*, **2003**, *9*, 3756–3763.

[14]   Bard A.J., Fox M.A., *Acc. Chem., Res.*, **1995**, *28*, 141–145.

[15]   Kalyanasundaram K., *Coord. Chem., Rev.*, **1982**, *46*, 159–244.

[16]   Barigelletii F., DeCola L., Balzani V., Hage R., Haasnoot J.G., Reedijk J., Vos J.G., *Inorg. Chem.*, **1991**, *30*, 641–645.

[17]   Kalyanasundaram K., Photochemistry of Polypyridine and Porphyrin Complexes, Academic Press, London, **1992**.

[18]   Kalyanasundaram K., Vlachopoulos N., Krishnan V., Monnier A., Grätzel M., *J. Phys. Chem.*, **1987**, *91*, 2342–2347.

[19]   Balzani V., Scanola F., Photochemical and photophysical devices, in: Reinhoudt D.N., Atwood J.L., Davies J.E.D., MacNicol D.D., Vögtle F. (Eds.), Comprehensive Supramolecular Chemistry, Pergamon Press, Oxford, **1996**, *Vol. 10*, pp. 687–746.

[20]   Balzani V., *Tetrahedron*, 1992, **48**, 10443–10514.

[21] Schill G., Catenanes, Rotaxanes, and Knots, Academic Press, New York, **1971**.

[22] Atwood J.L., Davies J.E.D., MacNicol D.D., Vögtle F. (Eds.), Comprehensive Supramolecular Chemistry, *Vol. 9*, Pergamon, Oxford, **1996**.

[23] Sauvage J.-P., Collin J.-P., Chambron J.-C., Guillerez S., Coudret C., *Chem. Rev.*, 1994, **94**, 993–1019.

[24] Lehn J.-M., *Angew. Chem. Int. Ed. Engl.*, **1988**, *27*, 90–112.

[25] Lehn J.-M., *Angew. Chem. Int. Ed. Engl.*, **1990**, *29*, 1304–1319.

[26] Mecklenburg S.L., Peek B.M., Erickson B.W., Meyer T.J., *J. Am. Chem. Soc.*, **1991**, *113*, 8540–8542.

[27] Mecklenburg S.L., Peek B.M., Schoonover J.R., McCafferty D.G., Wall C.G., Erickson B.W., Meyer T.J., *J. Am. Chem. Soc.*, **1993**, *115*, 5479–5495.

[28] Collin J.-P., Guillerez S., Sauvage J.-P., Barigelletti F., DeCola L., Flamigni L., Balzani V., *Inorg. Chem.*, **1991**, *30*, 4230–4238.

[29] Sauvage J.-P., Collin J.-P., Chambron J.-C., Guillerez S., Coudret C., Balzani V., Barigelletti F., DeCola L., Flamigni L., *Chem. Rev.*, **1994**, *94*, 993–1019.

[30] Gust D., Moore T.A., Moore A.L., *Acc. Chem. Res.*, **1993**, *26*, 198–205.

[31] Gust D., Moore T.A., Moore A.L., Macpherson A.N., Lopez A., DeGraziano J.M., Govni I., Bittersmann E., Seely G.R., Gao F., Nieman R.A., Ma X.C., Demanche L.J., Hung S.-C., Luttrull D.K., Lee S.-J., Kerrigan P.K., *J. Am. Chem. Soc.*, **1993**, *115*, 11141–11152.

[32] Duati M., Fanni S., Vos J.G., *Chem. Commun.*, **2000**, *3*, 68–70.

[33] Denti G., Serroni S., Campagna S., Ricevuto V., Balzani V., *Coord. Chem. Rev.*, **1991**, *111*, 227–236.

[34] De Wolf J.M., Hage R., Haasnoot J.G., Reedijk J., Vos J.G., *New J. Chem.*, **1991**, *15*, 501–507.

[35] Serroni S., Campagna S., Denti G., Keyes T.E., Vos J.G., *Inorg. Chem.*, **1996**, *35*, 4513–4518.

[36] Campagna S., Denti G., Sabatino L., Serroni S., Ciano M., Balzani V., *J. Chem. Soc. Chem. Commun.*, **1989**, 1500–1501.

[37] Denti G., Serroni S., Campagna S., Ricevuto V., Balzani V., *Inorg. Chim. Acta*, **1991**, *182*, 127–129.

[38] Denti G., Campagna S., Serroni S., Ciano M., Balzani V., *J. Am. Chem. Soc.*, **1992**, *114*, 2944–2950.

[39] Campagna S., Denti G., Serroni S., Ciano M., Juris A., Balzani V., *Inorg. Chem.*, **1992**, *31*, 2982–2984.

[40] Serroni S., Denti G., Campagna S., Juris A., Ciano M., Balzani V., *Angew. Chem. Int. Ed. Engl.*, **1992**, *31*, 1493–1495.

[41] Campagna S., Denti G., Serroni S., Juris A., Venturi M., Ricevuto V., Balzani V., *Chem. Eur. J.*, **1995**, *1*, 211–221.

[42] Sommovigo M., Denti G., Serroni S., Campagna S., Mingazzini C., Mariotti C., Juris A., *Inorg. Chem.*, **2001**, *40*, 3318–3323.

[43] Förster T., *Discuss. Faraday Soc.*, **1959**, *27*, 7–17.

[44] Förster T., Kasper K., *Z. Phys. Chem. Neue Folge*, **1954**, *1*, 275–277.

[45] Dexter D.L., *J. Chem. Phys.*, **1953**, *21*, 836–850.

[46] Scholes G.D., Ghiggino K.P., Oliver A.M., Paddon-Row M.N., *J. Phys. Chem.*, **1993**, *97*, 11871–11876.

[47] Yonoemoto E.H., Saupe G.B., Schmehl R.H., Hubig S.M., Riley R.L., Iverson B.L., Mallouk T.E., *J. Am. Chem. Soc.*, **1994**, *116*, 4786–4795.

[48] Paris J.P., Brandt W.W., *J. Am. Chem. Soc.*, **1959**, *81*, 5001–5002.

[49] Hage R., Haasnoot J.G., Reedijk J., Vos J.G., *Chemtracts (Inorg. Chem.)*, **1992**, *4*, 75–93.

[50] Seddon E.A., Seddon K.R., The Chemistry of Ruthenium, Elsevier, Amsterdam, The Netherlands, **1984**, Chapter 9, pp. 341–890.

[51] Casper J.V., Meyer T.J., *J. Am. Chem. Soc.*, 1983, **105**, 5583–5590.

[52] Watts R. J., *J. Chem. Ed.*, **1983**, *60*, 834–842.

[53] Burstall F.H., *J. Chem. Soc.*, **1936**, 173.

[54] Rutherford T.J., Pellegrini P.A., Aldrich-Wright J., Junk P.C., Keene F.R., *Eur. J. Inorg. Chem.*, **1998**, 1677–1688.

[55] Caspar J.V., Meyer T.J., *Inorg. Chem.*, **1983**, 22, 2444–2453.

[56] Allen G.H., White R.P., Rillema D.P., Meyer T.J., *J. Am. Chem. Soc.*, **1984**, *106*, 2613–2620.

[57] Ross H.B., Boldaji M., Rillema D.P., Blanton C.B., White R.P., *Inorg. Chem.*, **1989**, *28*, 1013–1021.

[58] Juris A., Campagna S., Balzani V., Gremaud G., Von Zelewski A., *Inorg. Chem.*, **1988**, *27*, 3652–3655.

[59] Rau S., Büttner T., Temme C., Ruben M., Görls H., Walther D., Duati M., Fanni S., Vos J.G., *Inorg. Chem.*, **2000**, *39*, 1621–1624.

[60] Downard A.J., Honey G.E., Steel P.J., *Inorg. Chem.*, **1991**, *30*, 3733–3737.

[61] Steel P.J., Lahousse F., Lerner D., Marzin C., *Inorg. Chem.*, **1983**, *22*, 1488–1493.

[62] Fanni S., Di Petro C., Serroni S., Campagna S., Vos J.G., *Inorg. Chem. Commun.*, **2000**, *3*, 42–44.

[63] Haasnoot, J.G., *Coord. Chem. Rev.*, **2000**, *200–202*, 131–185.

[64] Barigelletti F., DeCola L., Balzani V., Hage R., Haasnoot J., Reedijk J., Vos J.G., *Inorg. Chem.*, **1989**, *28*, 4344–4350.

[65] Nieuwenhuis H.A., Haasnoot J.G., Hage R., Reedijk J., Snoeck T.L., Stufkens D.J., Vos J.G., *Inorg. Chem.*, **1991**, *30*, 48–54.

[66] Hage R., Haasnoot J.G., Stufkens D., Snoeck T.L., Vos J.G., Reedijk J., *Inorg. Chem.*, **1989**, *28*, 1413–1414.

[67] Rillema D.P., Sahai R., Matthews P., Edwards A.K., Shaver R.J., Morgan L., *Inorg. Chem.*, **1990**, *29*, 167–175.

[68] Durham B., Casper J.V., Nagle J.K., Meyer T.J., *J. Am. Chem. Soc.*, **1982**, *104*, 4803–4810.

[69] Hage R., Ruthenium and osmium complexes containing triazole ligands: syntheses, structures, electrochemical and photophysical properties, Ph.D. Dissertation, Leiden University, The Netherlands, **1991**.

[70] Vos J.G., Haasnoot J.G., Vos G, *Inorg. Chim. Acta*, **1983**, *71*, 155–162.

[71] Hage R., Haasnoot J.G., Nieuwenhuis H.A., Reedijk J., DeRidder D.J.A., Vos J.G., *J. Am. Chem. Soc.*, **1990**, *112*, 9245–9251.

[72] Hage R., Haasnoot J.G., Nieuwenhuis H.A., Reedijk J., Wang R., Vos J.G., *J. Chem. Soc. Dalton Trans.*, **1991**, 3271–3275.

[73] Wang R., Vos J.G., Schmehl R.H., Hage R., *J. Am. Chem. Soc.*, **1992**, *114*, 1964–1970.

[74] Hage R., Prins R., Haasnoot J.G., Reedijk J., Vos J.G., *J. Chem. Soc. Dalton Trans.*, **1987**, 1389–1395.

[75] Steel P.J., Lahousse F., Lerner D., Marzin C., *Inorg. Chem.*, **1983**, *22*, 1488–1493.

[76] O'Connor C.M., Synthesis and characterisation of novel Ru(II) complexes with selective deuteration, Ph.D. Dissertation, Dublin City University, **1999**.

[77] Balzani V., Juris A., Venturi M., *Chem. Rev.*, **1996**, *96*, 759–833.

[78] Ward M.D., *J. Chem. Soc. Dalton Trans.*, **1993**, 1321–1325.

[79] Balzani V., Bardwell D.A., Barigelletti F., Cleary F.L., Guardigli M., Jeffery J.C., Sovrani T., Ward M.D., *J. Chem. Soc. Dalton Trans.*, **1995**, 3601–3608.

[80] Kalyanasundaram K., Nazeeruddin Md.K., *Inorg. Chem.*, **1990**, *29*, 1888–1897.

[81] Denti G., Serroni S., Campagna S., Ricevuto V., Balzani V., *Coord. Chem. Rev.*, **1991**, *111*, 227–236.

[82] Hage R., Dijkhuis A.H.J., Haasnoot J.G., Prins R., Reedijk J., Buchanan B.E., Vos J.G., *Inorg. Chem.*, **1988**, *27*, 2185–2189.

[83] Baitalik S., Flörke U., Nag K., *Inorg. Chem.*, **1999**, *38*, 3296–3308.

[84] Baitalik S., Flörke U., Nag K., *J. Chem. Soc. Dalton Trans.*, **1999**, 719–727.

[85] Hughes H.P., Vos J.G., *Inorg. Chem.*, **1995**, *34*, 4001–4003.

[86] Hughes H.P., The synthesis, characterisation, photochemical and photophysical properties of ruthenium(II) and osmium(II) polypyridyl complexes containing triazole ligands, Ph.D. Dissertation, Dublin City University, Ireland, **1993**.

[87] Hughes H.P., Martin D., Bell S., McGarvey J.J., Vos J.G., *Inorg. Chem.*, **1993**, *32*, 4402–4408.

[88] Chang Y.J., Xu X., Yabe T., Yu S.-C., Anderson D.R., Orman L.K., Hopkins J.B., *J. Phys. Chem.*, **1990**, *94*, 729–736.

[89] Van Diemen J.H., Hage R., Haasnoot J.G., Lempers H.E.B., Reedijk J., Vos J.G., DeCola L., Barigelletti F., Balzani V., *Inorg. Chem.*, **1992**, *31*, 3518–3522.

[90] Krause R.A., *Inorg. Chim. Acta*, **1977**, *22*, 209–213.

[91] Thummel R.P., Lefoulon F., Chirayil S., *Inorg. Chem.*, **1987**, *26*, 3072–3074.

[92] Hesek D., Inoue Y., Everitt S.R.L., Ishida H., Kunieda M., Drew M.G., *Inorg. Chem.*, **2000**, *39*, 308–316.

[93] Zakeeruddin S.M., Nazeeruddin Md.K., Humphry-Baker R., Grätzel M., Shklover V., *Inorg. Chem.*, **1998**, *37*, 5251–5259.

[94] Maxwell K.A., Sykora M., DeSimone J.M., Meyer T.J., *Inorg. Chem.*, **2000**, *39*, 71–75.

[95] Black D.St.C., Deacon G.B., Thomas N.C., *Inorg. Chim. Acta*, **1982**, *65*, L75–L76.

[96] Miller J.M., Balasanmugam K., Nye J., Deacon G.B., *Inorg. Chem.*, **1987**, *26*, 560–562.

[97] Black D.St.C., Deacon G.B., Thomas N.C., Inorg. Chim. Acta, **1981**, *54*, L143–L144.

[98] Blumer D.J., Barnett K.W., Brown T.L., J. Organometal. Chem., **1979**, *173*, 71–76.

[99] Strouse G.F., Anderson P.A., Schoonover J.R., Meyer T.J., Keene F.R., *Inorg. Chem.*, **1992**, *31*, 3004–3006.

[100] Anderson P.A., Strouse G.F., Treadway J.A., Keene F.R., Meyer T.J., *Inorg. Chem.*, **1994**, *33*, 3863–3864.

[101] Black D.St.C., Deacon G.B., Thomas N.C., *Aust. J. Chem.*, **1982**, *35*, 2445–2453.

[102] Black D.St.C., Deacon G.B., Thomas N.C., *Polyhedron*, **1983**, *2*, 409–412.

[103] Anderson P.A., Deacon G.B., Haarmaan K.H., Keene F.R., Meyer T.J., Reitsma D.A., Skelton B.W., Strouse G.F., Thomas N.C., Treadway J.A., White A.H., *Inorg. Chem.*, **1995**, *34*, 6145–6157.

[104] Lawrance G.A., *Chem. Rev.*, **1986**, *86*, 17–33

[105] Rutherford T.J., Keene F.R., *Inorg. Chem.*, **1997**, *36*, 2872–2878.

[106] Treadway J.A., Chen P., Rutherford T.J., Keene F.R., Meyer T.J., *J. Phys. Chem. A*, **1997**, *101*, 6824–6826.

[107] Treadway J.A., Meyer T.J., *Inorg. Chem.*, **1999**, *38*, 2267–2278.

[108] Von Zelewsky A., Gremaud G., *Helv. Chim. Acta*, **1988**, *71*, 1108–1115.

[109]Ross H.B., Boldaji M., Rillema D.P., Blanton C.B., White R.P., *Inorg. Chem.*, **1989**, *28*, 1013–1021.

[110]Freedman D.A., Evju J.K., Pomije M.K., Mann K.R., *Inorg. Chem.*, **2001**, *40*, 5711–5715.

[111]Zelonka R.A., Baird M.C., Can. J. Chem., **1972**, *50*, 3063–3072.

Chapter 2.

Synthetic and Instrumental Methods

An introduction to the synthetic and instrumental methods used throughout this thesis. Special attention is paid to the synthesis and purification of starting materials required in later chapters. Reference materials are also addressed as these are used later to confirm the success of various synthetic strategies.

2.1   Synthetic Methods

2.1.1   General

The synthetic materials and reagents used throughout this thesis were of reagent grade or better. The compounds 2,2'-bipyridine (bpy), 4,4'-bipyridine, 1,10-phenanthroline (phen), 4,7-diphenyl-1,10-phenanthroline (dpp) and phenothiazine (PTZ) were purchased from Aldrich and used without further purification. The ligand 4,4'-dimethyl-2,2'-bipyridine (Me$_2$bpy) was purchased from Fluka and recrystallised from EtOH before use. [RuCl$_3$].xH$_2$O was purchased from Avocado and used without further purification.

All solvents were used as purchased except acetone (dried and distilled over anhydrous CaSO$_4$), 1,4-dioxane (filtered through activated aluminum oxide to remove peroxides), CHCl$_3$ (dried over anhydrous CaCl$_2$) and THF (dried and distilled over Na) [1].

Column chromatography was performed using neutral activated aluminum oxide (150 mesh) or silicon oxide (35–70 μm). In some cases deactivated silicon oxide was used. Columns were deactivated by two methods, both giving identical results. In the first [2], 40% w/w of H$_2$O was added to the silica. This was mechanically shaken for 24 h before use, stored in an airtight container and then used effectively over a period of months. The second method involved the *in situ* deactivation of the columns [3]. The column was initially made up in a 10% triethylamine (Et$_3$N) in hexane solution. The excess Et$_3$N was then removed by washing the column with hexane before the solvent system was gradually altered to that of the required solvent ratios. Silica TLC plates were also deactivated using a 10% Et$_3$N in hexane solution. TLC plates were simply allowed to dry before use.

Bulk photolysis was carried out in a specifically designed reaction flask. The lamp employed is a 400 W medium pressure Hg Lamp, Model 3040 (Photochemical Reactors Ltd., UK) in a quartz immersion well, Model 3230. Tap A allows the reaction to be sampled at different intervals without having to disturb the N_2 atmosphere. After the reaction is complete, the solvent may be filtered and removed through Tap B.
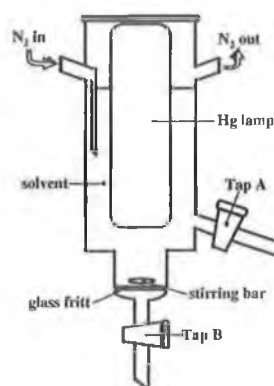
2.1.2 Synthesis of starting materials

The ligands Hpytrz, Hbpt and Hbpzt were prepared as previously reported by Hage [4]. The complexes *cis*-[Ru(DMSO)$_4$Cl$_2$] [5], *cis*-[Ru(bpy)$_2$Cl$_2$].xH$_2$O [6], *cis*-[Ru(Me$_2$bpy)$_2$Cl$_2$].xH$_2$O [7], *cis*-[Ru(dpp)$_2$Cl$_2$].xH$_2$O [8], [Ru(CO)$_2$Cl$_2$]$_n$ [9], [Ru(bpy)(CO)$_2$Cl$_2$] [9], [Ru(Me$_2$bpy)(CO)$_2$Cl$_2$] [9] ,[Ru(phen)(CO)$_2$Cl$_2$] [10] and [Ru(bpy)Cl$_3$] [11] were also prepared with the synthesis and any modifications to previous procedures detailed below;

3-(Pyridin-2-yl)-1,2,4-triazole (Hpytrz)

A mixture of 2-cyanopyridine (10.00 g, 96 mmol) and hydrazine hydrate (4.80 g, 96 mmol) were heated for 20 h at 50°C in EtOH (100 ml). The precipitate was filtered and washed with ethanol. The amidrazone was added to formic acid (50 ml) at 0°C. This solution was stirred for 3 h and then the acid was removed using rotary evaporation. The remaining oil was heated on a sand bath at 150°C for 30 min. The triazole was recrystallised twice from acetone to yield a fine white powder. Yield 7.11 g, 49 mmol, 51%. ^{1}H NMR (d$_6$-DMSO, 298 K) δ 8.71 (d), 8.27 (s), 8.10 (d), 8.00 (t), 7.52 (t). M.p. 161–163°C.
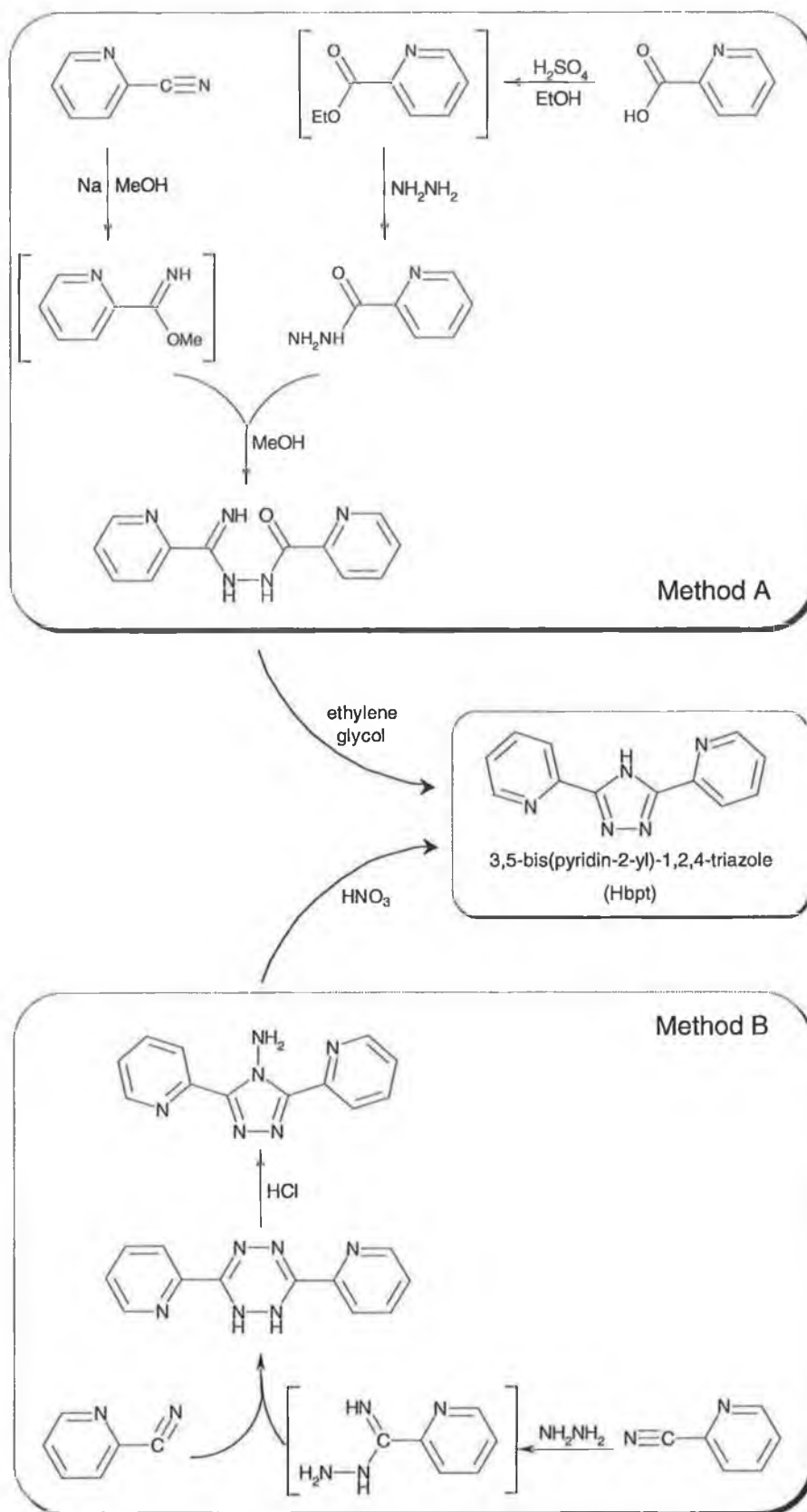
Scheme 2.1. *Two synthetic routes used to synthesise 3,5-bis(pyridin-2-yl)-1,2,4-triazole.*

3,5-Bis(pyridin-2-yl)-1,2,4-triazole (Hbpt) – Method A

2-Pyridinecarboxylic acid (10.5 g, 85 mmol) and conc. H_2SO_4 (2 ml) were heated at reflux in EtOH for 3 h. Sodium carbonate was added to neutralize the H_2SO_4 after which excess hydrazine hydrate (6.0 g, 120 mmol) was added. The solution was stirred at 0°C for 3 h. The precipitate was filtered and washed with cold EtOH. 2-Cyanopyridine (6.2 g, 60 mmol) was converted to 2-pyridylmethylimidate by heating it at reflux with Na metal in MeOH for 3 h. The hydrazide from above was added and the solution heated for an additional 2 h. The yellow precipitate was filtered, washed with cold EtOH and dried *in vacuo*. 3,5-Bis(pyridin-2-yl)-1,2,4-triazole was obtained by heating the hydrazide at reflux in ethylene glycol for 1 h. Yield 10.3 g, 46 mmol, 54%. ^{1}H NMR (d$_6$-DMSO, 298 K) δ 8.67 (d), 8.16 (d), 8.01 (t), 7.52 (t). M.p. 213–215°C.

–Method B

3,5-bis(pyridin-2-yl)-4-amino-1,2,4-triazole

A mixture of 2-cyanopyridine (20.0 g, 0.19 mol) and hydrazine hydrate (20.0 g, 0.40 mol) were heated at 100°C for 3 h. The orange precipitate that formed was filtered, washed with cold EtOH (10 ml) and diethyl ether (100 ml). The orange 3,5-bis(pyridin-2-yl)-4-amino-1,2,4-triazole was dissolved in 2 M HCl (120 ml) and boiled for 10 min. The solution was allowed cool to room temperature and then made alkaline by addition of ammonia. The solution was cooled to –4°C for 1 h and then filtered. The tan precipitate was washed with alkaline H_2O and recrystallised from EtOH. Yield: 21.4 g, 0.09 mol, 47%. ^{1}H NMR (d$_6$-DMSO, 298 K) δ 8.79 (d), 8.20 (d), 8.02 (t), 7.88 (s), 7.43 (t).

3,5-Bis(pyridin-2-yl)-1,2,4-triazole

The tan 3,5-bis(pyridin-2-yl)-4-amino-1,2,4-triazole (10.0 g, 42 mmol) was dissolved in boiling 5 M nitric acid (50 ml). The solution was cooled to 0°C and an aqueous sodium nitrite solution (30 g in 50 ml) was slowly added drop wise with stirring until no further brown fumes were released. This solution was then boiled for 5 min and cooled to room temperature. The solution was made alkaline by addition of ammonia and the precipitate filtered. The white product was

washed with alkaline H_2O and cold EtOH. The product was then recrystallised from EtOH. Yield: 8.1 g, 36 mmol, 86%. ^1H NMR and M.p. data are similar to those reported for Method A.

3,5-Bis(pyrazin-2-yl)-1,2,4-triazole (Hbpzt)

The synthesis of Hbpzt was achieved using Method A as for Hbpt above. 2-Pyrazinecarboxylic acid (8.0 g, 65 mmol) and conc. H_2SO_4 (2 ml) were heated at reflux in EtOH for 3 h. Sodium carbonate was added to neutralize the H_2SO_4 after which excess hydrazine hydrate (5.05 g, 101 mmol) was added. The solution was stirred at 0°C for 3 h. The precipitate was filtered and washed with cold EtOH. 2-Cyanopyrazine (4.2 g, 40 mmol) was converted to 2-pyrazylmethylimidate by heating it at reflux with Na metal in MeOH for 3 h. The hydrazide from above was added and the solution heated for an additional 1 h. The yellow precipitate was filtered and washed with cold EtOH. 3,5-Bis(pyrazin-2-yl)-1,2,4-triazole was obtained by heating the pyrazine-2-carboxylic acid N'-(imino-pyrazin-2-yl-methyl)-hydrazide at reflux in ethylene glycol for 1 h. Yield 6.1 g, 27 mmol, 42%. ^1H NMR (d_6-DMSO, 298 K) δ 9.35 (s), 8.81 (d), 8.78 (d). M.p. 271°C.

cis-[Ru(bpy)$_2$Cl$_2$].2H$_2$O

[RuCl$_3$].xH$_2$O (5.0 g, 21 mmol) and LiCl (1.0 g) were stirred in hot deaerated DMF for 20 min. Bpy (6.5 g, 44 mmol) was added and the reaction mixture was heated at reflux for 8 h under an Ar atmosphere . The reaction was cooled to room temperature, added to acetone (250 ml) and stored at −4°C overnight. The precipitate formed was filtered, washed with acetone (100 ml) and then washed with H_2O until the filtrate became colourless. The resulting dark purple microcrystalline product was dried *in vacuo*. Yield 7.87 g, 15 mmol, 72%. ^1H NMR (d_6-DMSO, 298 K) δ 9.93 (d), 8.60 (d), 8.46 (d), 8.03 (t), 7.72 (t), 7.65 (t), 7.48 (d), 7.07 (t).

cis-[Ru(dpp)$_2$Cl$_2$].2H$_2$O

As for *cis*-[Ru(bpy)$_2$Cl$_2$].2H$_2$O except [RuCl$_3$].xH$_2$O (1.0 g, 4.1 mmol), LiCl (1.0 g), dpp (2.33 g, 7 mmol) and DMF (40 ml). Reaction was refluxed for 14 h. Yield 2.3 g, 2.6 mmol, 64%. ^{1}H NMR (d$_6$-DMSO, 298 K) δ 10.42 (d), 8.25 (d), 8.25 (d), 8.10 (d), 8.04 (d), 7.88 (d), 7.73(t), 7.71 (d), 7.57 (m), 7.40 (d).

cis-[Ru(DMSO)$_4$Cl$_2$]

[RuCl$_3$].xH$_2$O (1.0 g, 4 mmol) was dissolved in 5 ml DMSO and refluxed for 5 min. The solution was reduced in half by vacuum pump and acetone was added (20 ml). The yellow precipitate that fell out was filtered and washed with acetone. Yield 1.74 g, 3.6 mmol, 90%. The product was recrystallised from an acetone/DMSO (20:1) solution left standing for 1 week. ^{1}H NMR (d$_6$-DMSO, 298 K) δ 3.43 (s), 3.37 (s), 3.25 (s), 2.67 (s).

[Ru(CO)$_2$Cl$_2$]$_n$

[RuCl$_3$].xH$_2$O (5.0 g, 20.5 mmol) and paraformaldehyde (1.5 g) were added to a 90% solution of formic acid. The solution was heated at reflux for 5 h. The colour of the solution changed from red to dark green to orange. When the orange colour was obtained the reaction was cooled in an ice bath and stored in the freezer overnight (−4°C). The solvent was removed by rotary evaporation to leave a yellow solid. This was washed with hexane and dried *in vacuo*. Yield 4.6 g, 20.2 mmol, 98%. IR (KBr): 2074 and 2020 cm^{-1}.

[Ru(bpy)(CO)$_2$Cl$_2$]

[Ru(CO)$_2$Cl$_2$]$_n$ (1.0 g, 4.4 mmol) was dissolved in 50 ml Ar sparged MeOH with a little heating. After dissolution, bpy (1.0 g, 6.4 mmol) was added in one portion. The red solution was heated at reflux for 30 min whereupon a yellow precipitate fell out. The precipitate was filtered and washed with cold MeOH and allowed to air dry. Yield 1.3 g, 3.4 mmol, 77%. ^{1}H NMR (d$_6$-DMSO, 298 K); δ 9.25 (d), 8.82 (d), 8.39 (t), 7.87 (t). IR (MeCN): 2064 and 2001 cm^{-1}.

[Ru(Me₂bpy)(CO)₂Cl₂]

[Ru(CO)₂Cl₂]$_n$ (1.0 g, 4.4 mmol) and Me₂bpy (1.5 g, 8.2 mmol) were used as in the procedure above. Yield 1.1 g, 2.6 mmol, 60%. ^{1}H NMR (d₆-DMSO, 298 K); δ 9.03 (d), 8.65 (s), 7.66 (d), 2.59 (s). IR (MeCN): 2062 and 1998 cm^{-1}.

[Ru(phen)(CO)₂Cl₂]

As above but with [Ru(CO)₂Cl₂]$_n$ (1.0 g, 4.4 mmol) and phen (1.26 g, 7.0 mmol). Yield 1.0 g, 2.42 mmol, 55%. ^{1}H NMR (d₆-DMSO, 298 K); δ 9.64 (d), 9.00 (d), 8.36 (s), 8.17 (dd). IR (KBr): 2065 and 2005 cm^{-1}.

[Ru(bpy)Cl₃].xH₂O

Bpy (2.76g, 15 mmol) was dissolved in a 30ml of 1 N HCl solution (30 ml). [RuCl₃].xH₂O (3.65 g, 15 mmol) was added. The mixture was stirred for 3 h and let stand for 4 weeks. After standing, the solution was filtered and the dark green crystalline powder washed with H₂O and diethyl ether. Yield 1.96 g, 4.9 mmol, 33%.

2.1.3   Synthesis of reference materials

[Ru(bpy)₃](PF₆)₂

[Ru(bpy)₂Cl₂].xH₂O (1.5 g, 2.9 mmol) and bpy (0.5 g, 3 mmol) were heated at reflux in EtOH/H₂O (80/20, 50 ml) for 6 h. The solution was then reduced to dryness, redissolved in minimum MeCN and purified by column chromatography on silica using a 0.1 M KNO₃ in MeCN/H₂O mobile phase. The main band (2nd) was collected, reduced and the product redissolved in water. An aqueous NH₄PF₆ solution was added and the precipitate collected and dried *in vacuo*. Yield 1.74 g, 2.0 mmol, 70 %. ^{1}H NMR (d₃-MeCN, 298 K) δ 8.42 (d), 7.98 (dd), 6.51 (d), 7.33 (dd).

[Ru(bpy)$_2$(Me$_2$bpy)](PF$_6$)$_2$

cis-[Ru(bpy)$_2$Cl$_2$].2H$_2$O (1.0g, 1.9 mmol) and Me$_2$bpy (0.40 g, 2.2 mmol) were heated at reflux in EtOH/H$_2$O (80/20, 30 ml) for 3 h. The product was isolated and purified in a similar manner to [Ru(bpy)$_3$](PF$_6$)$_2$ above. Yield 1.40 g, 1.6 mmol, 83%. ^{1}H NMR (d$_3$-MeCN, 298 K) δ 8.50 (d), 8.39 (s), 8.04 (t), 7.77 (d), 7.56 (d), 7.40 (t), 7.22 (d), 2.50 (s).

2.1.4   Discussion of synthetic procedures

cis-[Ru(L)$_2$Cl$_2$].2H$_2$O complexes where L represents a polypyridyl ligand were prepared by previous reported methods [6,7]. Yields were typically consistent at about 70% for all dichlorides. After precipitation from acetone, the precipitate was washed with copious H$_2$O to remove various carbonyl complexes formed during the reaction due to the decomposition of DMF. *cis*-[Ru(dpp)$_2$Cl$_2$].2H$_2$O was prepared in larger volumes of DMF to increase solubility and a slight excess of [RuCl$_3$].xH$_2$O was employed to reduce the presence of unreacted dpp. In no case were any *trans*-dichlorides observed.

The synthesis of the precursor [Ru(DMSO)$_4$Cl$_2$] is relatively straight forward and is a useful alternate starting material to [RuCl$_3$].xH$_2$O. The reflux is short, but if not stopped in time the product obtained has a brownish green colour and will not react with bpy to form [Ru(bpy)(DMSO)$_2$Cl$_2$]. [Ru(DMSO)$_4$Cl$_2$] shows four methyl peaks in its ^{1}H NMR due to the fact that three of the four DMSO molecules are S-bonded to the metal centre in a facial configuration, while the last one is O-bonded [12,13]. This can be seen in the crystal structure in Fig. 2.1. [Ru(bpy)(DMSO)$_2$Cl$_2$] is reported to have various crystal structures depending on the method of recrystallisation. Mercer and Trotter obtained monoclinic cubic crystals from methanol [12], Attia and Calligaris studied orthorhombic crystals from DMSO [14] and later Alessio *et al.* obtained monoclinic prisms from an acetone/DMSO solution [13]. Alessio *et al.* produced their crystals from hot acetone/DMSO solution. Crystals were obtained in our laboratory by letting a mainly acetone (DMSO/acetone 1:20) solution sit for 1 week but no X-ray crystallography was performed.
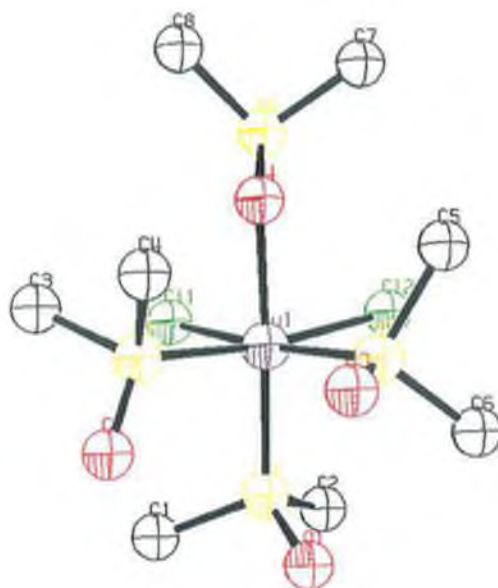
Figure 2.1. *Crystal structure of [Ru(DMSO)$_4$Cl$_2$] obtained from Alessio et al. [13]. Data for crystal was supplied by Cambridge Crystallographic Data Centre and modelled using CCDC supplied Mercury 1.1.2 software. H atoms are omitted for reasons of clarity.*

Preparation of the oligomer was performed as outlined in Scheme 2.2 [9,15]. This method is an improvement over a previously reported method involving the use of both HCl and formic acid [16]. For the purpose of these studies, [Ru(CO)$_2$Cl$_2$]$_n$ was formed by heating [RuCl$_3$].xH$_2$O in formic acid without the presence of HCl. The reaction was stopped once [RuCl$_4$(CO)$_2$]$^{2-}$ was formed and stored below 0°C overnight. If the reaction is allowed to proceed too far the [RuCl$_2$(CO)$_3$]$_n$ will be present as an impurity. The presence of such impurity can be determined by IR, Fig. 2.2.

$[RuCl_3] \cdot xH_2O + HCO_2H$

$\downarrow$ 1 h

$[RuCl_5(CO)]^{2-}$
(deep red)

$\downarrow$ 1 h

$[RuCl_4(CO)(H_2O)]^{2-}$
(green)

$\downarrow$ 4 h

$[RuCl_4(CO)_2]^{2-}$ $\xrightarrow[\text{12 h}]{-4°C}$ $[RuCl_2(CO)_2]_n$
(orange)   (yellow)

$\downarrow$ 2 h

$[RuCl_3(CO)_3]^{-}$ $\xrightarrow[\text{12 h}]{-4°C}$ $[RuCl_2(CO)_3]_n$
(yellow)   (yellow)
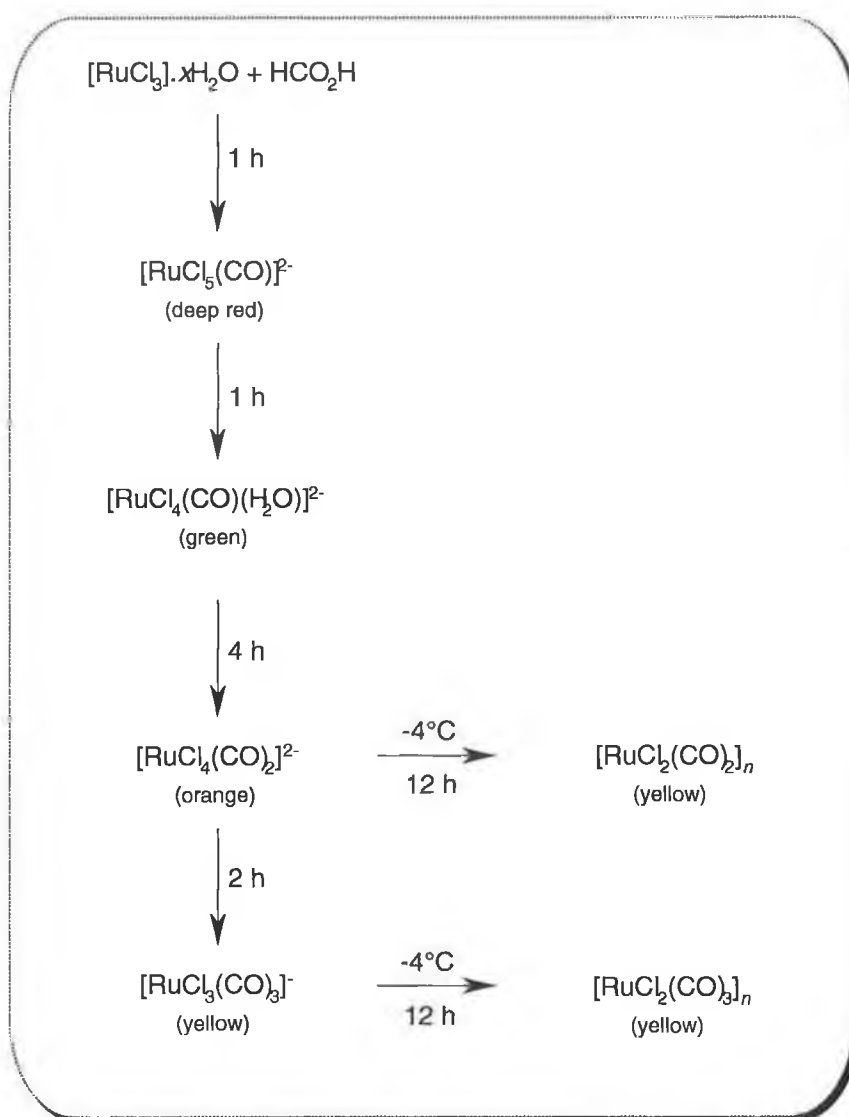
Scheme 2.2. Synthetic pathway to [Ru(CO)₂Cl₂]ₙ and [Ru(CO)₃Cl₂]ₙ.

The two $v_{(CO)}$ stretching bands at 2074 and 2020 cm^{-1} correspond to the oligomer whereas the extra band at 2140 cm^{-1} is caused by the extra CO ligand in $[RuCl_2(CO)_3]$ [17]. This impurity can be removed by successive recrystallisations from acetone and diethyl ether. However, if the reaction is stopped just before the orange colour becomes dominant, the oligomer is obtained in a pure state as confirmed by IR, Fig. 2.2. The presence of formaldehyde favours the formation of the oligomer and is added as paraformaldehyde to reduce the yield of $[RuCl_2(CO)_3]_n$ still further. $[RuCl_2(CO)_3]_n$ forms as a result of HCl produced during the reaction. Anderson *et al.* found that addition of HCl to the reaction mixture increases the yield of $[RuCl_2(CO)_3]_n$ substantially [9]. Thus, it is not

surprising that Colton and Farthing reported three carbonyl $v_{(CO)}$ stretching bands as they used both HCl and formic acid in the original synthesis [16].
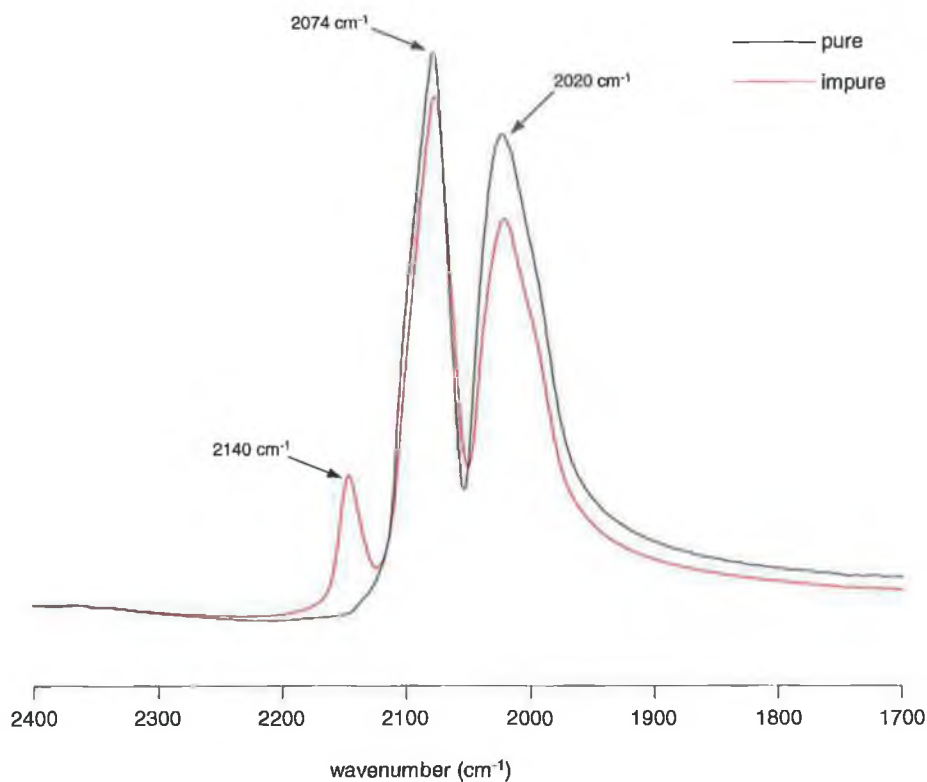
Figure 2.2. *IR of two different samples of [Ru(CO)₂Cl₂]ₙ in KBr.*

The oligomer reacts with bidentate ligands in MeOH to form complexes of the general structure [Ru(L)(CO)$_2$Cl$_2$] in good yields. ^{1}H NMR spectra of these complexes show that the two rings of the bidentate ligand are equivalent which suggests either a *cis*-(Cl),*trans*-(CO) or *trans*-(Cl),*cis*-(CO) geometry. An example of the equivalency of the two rings is shown by the ^{1}H NMR of [Ru(bpy)(CO)$_2$Cl$_2$] in Fig. 2.3.
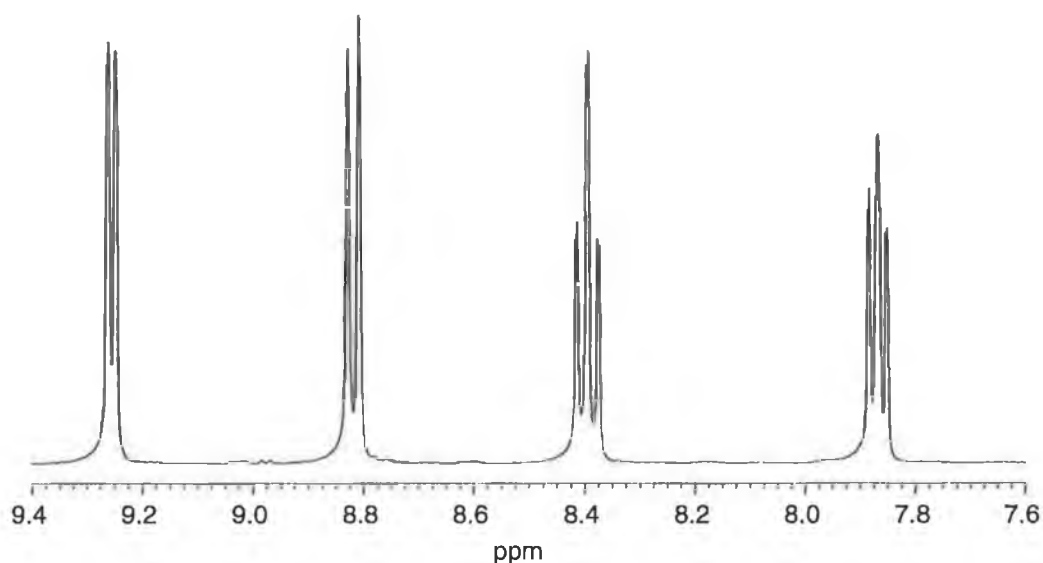
Figure 2.3. *^{1}H NMR of [Ru(bpy)(CO)$_2$Cl$_2$] in d$_6$-DMSO.*

The two v_{CO} stretching bands at 2064 and 2001 cm^{-1} in MeCN are consistent with either geometry. However, the carbonyl ligands would be expected to favour a *cis*-formation due to competition for π-back-bonding from the metal d-orbitals as is in agreement with previous studies [18,19]. It was found that complexes of bpy formed in greater yields than that of Me$_2$bpy or phen.

[Ru(bpy)Cl$_3$] is probably not monomeric but best represented by [Ru(bpy)Cl$_3$]$_n$ [11,20]. It is difficult to characterize this complex as NMR becomes redundant due to its paramagnetic nature. The compound was reacted with excess bpy and excess Me$_2$bpy and the successful synthesis of [Ru(bpy)$_3$]$^{2+}$ and [Ru(bpy)(Me$_2$bpy)$_2$]$^{2+}$ as described in Section 3.7.1 suggests that [Ru(bpy)Cl$_3$].xH$_2$O had indeed been synthesized.

2.2 Instrumental Methods

2.2.1 Structural Characterisation

Nuclear Magnetic Resonance (NMR) Spectroscopy

^{1}H NMR (400 MHz) and ^{13}C NMR (100 MHz) spectra were obtained on a Bruker Avance 400 NMR Spectrometer in deuterated solvents with either TMS or residual solvent peaks as reference. Free induction decay (FID) profiles were processed using an XWIN-NMR software package. The 2-D correlated spectroscopy (COSY) experiments involved the accumulation of 128 FIDs of 16 scans. Digital filtering was sine-bell squared and the FID was zero filled in the F1 dimension. Acquisition parameters were F1 = ±500 Hz, F2 = 1000 Hz and $t_{1/2}$ = 0.001 s. The cycle time delay was 1.5 s. Residual solvent traces and common contaminants (water, solvents, oils) were accounted for using a table of these contaminants in various deuterated solvents [21].

High Performance Liquid Chromatography (HPLC)

HPLC measurements were performed on a JVA analytical HPLC system consisting of a Varian Prostar HPLC pump using a Partisil P10SCX-3095 cation exchange column (HiChrom) and a Varian Prostar photodiode array detector. A 20 μl injection loop delivered the sample to the column using typically 0.08 M $LiClO_4$ in MeCN/H_2O (80/20) mobile phase at a flow rate of 1.8 ml min^{-1}. The chromatogram was monitored at 280 nm and analysed using Varian Star software.

Elemental Analysis

Carbon, hydrogen and nitrogen (CHN) elemental analyses were carried out on an Exador Analytical CE440 by the Microanalytical Department, University College Dublin.

Infrared Spectroscopy (IR)

Infrared spectra of compounds were measured in $CHCl_3$ or as a KBr disc on a Perkin Elmer 2000 FTIR spectrometer.

Ultra Violet/Visible Spectroscopy (UV/Vis)

UV–vis absorption spectra were recorded on a Shimadzu 3100 UV-Vis/NIR instrument with 1-cm quartz cells.

Mass Spectrometry

Mass spectra were recorded with a Bruker-EsquireLC_00050 electrospray ionisation mass spectrometer at positive polarity with cap-exit voltage of 167 V. Each spectrum was recorded by summation of 20 scans.

X-Ray Crystallography

Crystals were analysed by Dr. John Gallagher, Dublin City University, Dr. Sven Rau, Friedrich-Schiller Universität, Jena, Germany and Dr. Sally Brooker, Otago University, New Zealand.

2.2.2 Photophysical and Electrochemical Characterisation

Emission spectra

Emission spectra at various temperatures were obtained in UVASOL grade solvents (Merck) on a Perkin-Elmer LS50B luminescence spectrometer equipped with a red sensitive Hamamatsu R928 detector. Emission and excitation slit widths were typically 3, 5 or 10 nm depending on individual circumstances. Measurements at room temperature were carried out in 1-cm quartz cells.

Electrochemistry

Cyclic voltammetry and DPV experiments were carried out using a CH Instruments CHI Version 2.07 software controlled potentiostat (CH Instruments Memphis 660) [22]. Solutions of the complex to be tested were typically made up in a 0.1 M solution of TBABF$_4$ (Aldrich) in dry MeCN. The solution was purged with Ar (10 min) and an Ar atmosphere was maintained throughout the experiment. The three electrodes employed consisted of a platinum disc (working, 2 mm diameter), platinum wire (counter) and a Ag/Ag$^+$ (acetonitrile + 10 mM AgNO$_3$ + 0.1 M TBABF$_4$) half-cell (reference). The pH of

the solutions was adjusted using perchloric acid or triethylamine. The instruments were calibrated using the Fc/Fc$^+$ couple at an equivalent molarity to the sample being tested. The results obtained were compared with previous studies on similar complexes using different electrodes by using conversion values obtained from the literature [23].

Luminescent Lifetime Measurements

Lifetime measurements were performed on an Edinburgh Analytical Instruments single photon counter with a T setting, using a lamp (nF900, in a nitrogen setting), monochromators (J-yA models), with a single photon photomultiplier detection system (model S 300), an MCA card (Norland N5000) and PC interface (Cd900 serial). Data correlation and manipulation was carried out using the program F900, Version 5.13. The pH of the samples being tested was altered using trifluoroacetic acid and triethylamine. The samples were excited using 337 nm as excitation wavelength and the lifetimes were collected in the maxima of the emission. Lifetime errors are estimated to be less than 8%.

Resonance Raman Measurements

Resonance Raman Measurements were carried out by Dr. Wesley Browne and Ms. Kate Ronayne in Queens University, Belfast. The measurements were obtained in CD_2Cl_2 at room temperature and 457.9 nm excitation using a 350 mW laser source.

2.3   Bibliography

[1]   Armarego W.L.F., Perrin D.D., Purification of Laboratory Chemicals, 4th Edition, Butterworth Heinemann, Oxford; Boston, **1996**.

[2]   Vogle A.I., Vogel's Textbook of Practical Organic Chemistry, 5th Edition, Longman Scientific & Technical, London; Wiley, New York, **1989**, pp. 212.

[3]   Savage S.A., Smith A.P., Fraser C.L., *J. Org. Chem.*, **1998**, *63*, 10048–10051.

[4]   Hage R., Ruthenium and osmium complexes containing triazole ligands: syntheses, structures, electrochemical and photophysical properties, Ph.D. Dissertation, Leiden University, The Netherlands, 1991.

[5]   Evans I.P., Spencer A., Wilkinson G., *J. Chem. Soc. Dalton Trans.*, 1973, 204–209.

[6]   Sullivan B. P., Salmon D. J., Meyer T. J., *Inorg. Chem.*, **1978**, *17*, 3334–3341.

[7]   Jones W.E., Smith R.A., Abramo M., Williams M.D. Van Houten J., *Inorg. Chem.*, **1989**, *28*, 2281–2285.

[8]   Browne W.R., Probing ground and excited state properties of Ruthenium(II) and Osmium(II) polypyridyl complexes, Ph.D. Dissertation, Dublin City University, 2002.

[9]   Anderson P.A., Deacon G.B., Haarmaan K.H., Keene F.R., Meyer T.J., Reitsma D.A., Skelton B.W., Strouse G.F., Thomas N.C., Treadway J.A., White A.H., *Inorg. Chem.*, **1995**, *34*, 6145–6157.

[10] Black D.S., Deacon G.B., Thomas N.C., *Aust. J. Chem.*, **1982**, *35*, 2445–2453.

[11] Krause R.A., *Inorg. Chim. Acta*, **1977**, *22*, 209–213.

[12] Mercer A., Trotter J., *J. Chem. Soc., Dalton Trans.*, **1975**, 2480–2483.

[13] Alessio E., Mestroni G., Nardin G., Attia W.M., Calligaris M., Sava G., Zorzet S., *Inorg. Chem.*, **1988**, *27*, 4099–4106.

[14] Attia W.M., Calligaris M., *Acta Crystallogr., Sect. C: Cryst. Struct. Commun.*, **1987**, *C43*, 1426.

[15] Bruce M.I., Ruthenium carbonyls and related compounds, in: Wilkinson G., Stone F.G.A., Abel E.W., Comprehensive Organometallic Chemistry, Pergamon Press, Oxford, **1982**, *Vol. 4*, pp. 661–690.

[16] Colton R., Farthing R.H., *Aust. J. Chem.*, **1967**, *20*, 1283–1286.

[17] Benedetti E., Braca G., Sbrana G., Salvetti F., Grassi B., *J. Organometal. Chem.*, **1972**, *37*, 361–373.

[18] Kelly J.M., O'Connell C.M., Vos J.G., *Inorg. Chim. Acta*, **1982**, *64*, L75–L76.

[19] Black D.S., Deacon G.B., Thomas N.C., *Polyhedron*, **1983**, *2*, 409–412.

[20] Thummel R.P., Lefoulon F., Chirayil S., *Inorg. Chem.*, **1987**, *26*, 3072–3074.

[21] Gottlieb H.E., Kotlyar V., Nudelman, *J. Org. Chem.*, **1997**, *62*, 7512–7515.

[22] Kaifer A.E., Gomez-Kaifer M., Supramolecular Electrochemistry, Wiley-VCH, Weinheim, Germany, 1999.

[23] Pavlishchuk V.V., Addison A.W., *Inorg. Chim. Acta*, **2000**, *298*, 97–102.

Chapter 3.

Synthetic Routes to Tris(heteroleptic) Triazole Complexes

This chapter examines the synthetic strategies previously reported in the literature and outlined in Chapter 1. Each method is explored and tested for its suitability in allowing a triazole ligand to be incorporated. The synthesis of a tris(heteroleptic) complex containing the ligand Hpytrz is reported by two separate procedures. One of these procedures shows potential of being a generic route to such complexes.

3.1   Introduction

As described in Chapter 1, polypyridyl complexes of Ru(II) have been extensively studied for their interesting MLCT excited states [1,2,3,4]. The photoinduced electron and energy transfer properties of these complexes can be altered by methodically varying the ligands in the coordination sphere. Adding electron withdrawing or donating substituents to the ligands increases or decreases the metal t_{2g} levels respectively. Thus, with a prudent choice of ligands, new complexes with specifically designed excited state properties can be explored. To create tris(heteroleptic) complexes such as $[Ru(L)(L')(L'')]^{2+}$, only a few synthetic methodologies have been reported in the literature. Of the handful of synthetic routes devised, few are general enough to incorporate a wide variety of ligands. Thus it was the aim of this project to test these different synthetic methods with the goal of incorporating the pyridyl-triazole ligand 3-(pyridin-2-yl)-1,2,4-triazole (Hpytrz) to the metal sphere. If this could not be done, then a new synthetic method would need to be developed.
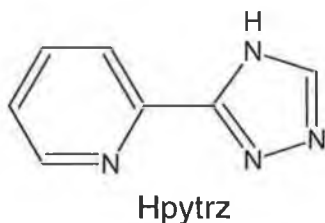
Hpytrz

Figure 3.1. Struture of the triazole ligand Hpytrz used throughout this chapter.

The synthetic routes to tris(heteroleptic) Ru(II) complexes have been discussed in Chapter 1 and are divided into subcategories for the purpose of these investigations.

(a)   **[Ru(bpy)Cl₃] Method**

This method, possibly the most rudimentary approach, involves the sequential addition of bidentate ligands to [RuCl₃] or [Ru(bpy)Cl₃]. This method was used by Thummel *et al.* [5] to synthesise

$[Ru(bpy)(biq)(bi-naph)]^{2+}$ and Hesek *et al.* [6] to synthesise a complex which retained the stereoisomeric properties of the ligands involved.

(b)   **[Ru(DMSO)₄Cl₂] Method**

Similar to the method above, this technique involves the sequential addition of ligands to the precursor $[Ru(DMSO)_4Cl_2]$. Zakeeruddin *et al.* [7] developed this technique and it was also used by Maxwell *et al.* [8] who synthesised a donor-acceptor tris(heteroleptic) complex in a one-pot reaction.

(c)   **Decarbonylation Method**

This method primarily relies on the chemical removal of two carbonyl ligands as the final step in yielding the desired complexes. Typically, $[Ru(L)(L')(CO)_2]^{2+}$ is treated with a third ligand, L'', in the presence of the decarbonylating agent TMNO. This technique is the most widely reported, with Anderson *et al.* [9,10] being among its most ardent advocates.

(d)   **Photosubstitution Method**

The photosubstitution method includes those methods that use light as a means of replacing one ligand with another. The use of light in the synthesis of tris(heteroleptic) complexes was first reported by Von Zelewsky and Gremaud [11]. The most recent publication of a tris(heteroleptic) complex was by Freedman *et al.* [12] who prepared the two complexes $[Ru(Me_2bpy)(phen)(Me_2phen)]^{2+}$ and $[Ru(bpy)(Me_2bpy)(phen)]^{2+}$ using light to photolyse a [BzRu(bpy)Cl]Cl starting material.

All of these methods have been explored, but ultimately a new synthetic route was designed. The new route involves the removal of carbonyl ligands using light. Although this is technically a decarbonylation technique, it has been included in the photosubstitution section as no chemical decarbonylation takes place.

For a synthetic method to be deemed suitable, the following requirements were considered necessary;

- Reaction conditions: It is imperative that all ligands used in the synthesis of a tris(heteroleptic) complex can withstand the conditions being used.
- Triazole compatibility: Any strategy worth pursuing must allow the introduction of a triazole moiety to the metal sphere.
- Dichloride isolation: The isolation of a dichloride ([Ru(L)(L')Cl$_2$]) would allow the relatively simple task of adding a third ligand in aqueous EtOH.
- Yields: Due to the cost of starting materials and the fact that these synthetic methods require a number of steps, it is important that each step has a sufficiently high yield to allow further investigations.

Each synthetic route investigated was analysed with the above requirements in mind.

3.2   [Ru(bpy)Cl$_3$] Method

The most basic approach to creating a tris(heteroleptic) complex would be to simply add three ligands to a [RuCl$_3$].xH$_2$O solution and heat at reflux for an appropriate period of time. However, with such an uncontrolled reaction, 10 possible complexes may form (three homoleptic, six bis(heteroleptic) and one tris(heteroleptic)). Thus the yield of the desired complex would be very small, and if unfavourable ligand scrambling were to occur, the yield may reduce to zero. It is therefore sensible to begin such a reaction one step further on and use [Ru(bpy)Cl$_3$].xH$_2$O as the starting point. A one-pot reaction with two different ligands now results in only three complexes (two bis(heteroleptic) and one tris(heteroleptic)). Such a step was taken by Thummel *et al.* [5] whereas Hesek *et al.* [6] preferred to start with the initial [RuCl$_3$].xH$_2$O salt.

72

[Ru(bpy)Cl$_3$].xH$_2$O was synthesised in 1 N HCl as described by Krause [13]. As the metal centre exists in the Ru(III) oxidation state, the ^{1}H NMR is not very well defined and so characterisation is difficult but HPLC showed only one species to be present. A series of reactions were carried out in which typically 1 mmol of Me$_2$bpy and Hpytrz were added 1 h apart to a solution of 1 mmol [Ru(bpy)Cl$_3$].xH$_2$O in 30 ml EtOH/H$_2$O or DMF.
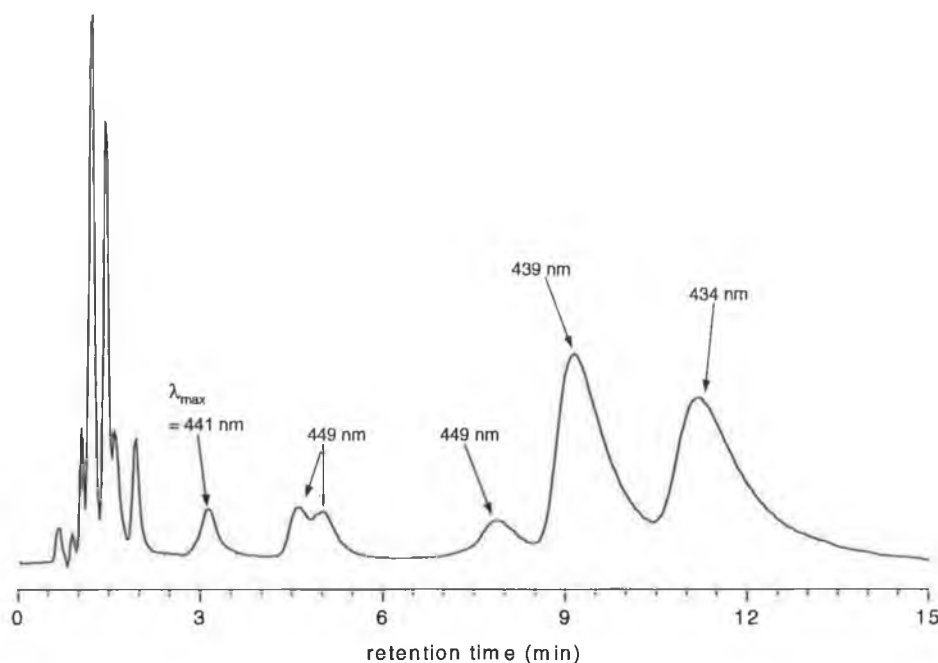
Figure 3.2. HPLC trace of [Ru(bpy)Cl$_3$] reaction with Me$_2$bpy and Hpytrz. Mobile phase: 0.08 M LiClO$_4$ in 80/20 MeCN/H$_2$O using P10SCX-3095 cation exchange column and flow rate 1.5 ml min^{-1}.

The reaction was also monitored by TLC but the number of products formed were too great to be successfully separable by column chromatography. A HPLC analysis showed the number of products formed in more detail. The wavelengths for each of the peaks in Fig. 3.2 represent λ_{max} for the species attributable to that peak. The integrations can be found in Table 3.1 (pg. 79) where they are compared with those of an alternative synthetic strategy. The initial peaks, i.e. those eluting below 3 min, do not show any significant visible absorption bands and so are most likely free ligand or solvent peaks. Larger volumes of solvent and longer time periods between the addition of the two ligands did not show any

substantial difference in the product ratios. As well as not being able to separate the materials formed, this reaction method has a distinct disadvantage in that no intermediates can be isolated. Thus, it is difficult to determine in what way any tris(heteroleptic) complex (if any) is formed.

$[Ru(bpy)Cl_3].xH_2O$ was successfully reacted with two molar equivalents of Me_2bpy to form the bis(heteroleptic) complex $[Ru(bpy)(Me_2bpy)_2]^{2+}$, albeit in small yields. As such, this reaction method seems to work but with Hpytrz the method was deemed to be impractical.

3.3 $[Ru(DMSO)_4Cl_2]$ Method

$[Ru(DMSO)_4Cl_2]$ can be used as the starting point to tris(heteroleptic) complexes and analogous to the $[Ru(bpy)Cl_3]$ method, it too has been used in one-pot synthetic reactions [8]. However, using $[Ru(DMSO)_4Cl_2]$ as a starting point in a one-pot reaction strategy poses the same problems as discussed for the $[Ru(bpy)Cl_3]$ method. Specifically, the number of final products formed and hence the reaction outcome are difficult to control and as such, $[Ru(bpy)(DMSO)_2Cl_2]$ and $[Ru(Me_2bpy)(DMSO)_2Cl_2]$ were used as starting materials. These complexes appeared interesting in that Zakeeruddin *et al.* isolated a dichloride precursor by reacting $[Ru(Me_2bpy)(DMSO)_2Cl_2]$ with dcb to form $[Ru(Me_2bpy)(dcb)Cl_2]$ [7]. As stated previously, a key characteristic of any successful tris(heteroleptic) method would be one in which the immediate precursor (e.g. a dichloride) could be isolated. Additionally, due to the more labile nature of the DMSO ligands, the reaction of $[Ru(bpy)(DMSO)_2Cl_2]$ and $[Ru(Me_2bpy)(DMSO)_2Cl_2]$ with additional bidentate ligands can be achieved at milder, more favourable conditions than with $[Ru(bpy)Cl_3]$.

Both $[Ru(bpy)(DMSO)_2Cl_2]$ and $[Ru(Me_2bpy)(DMSO)_2Cl_2]$ were synthesised by reacting the precursor $[Ru(DMSO)_4Cl_2]$ with bpy or Me_2bpy respectively in $CHCl_3$. Yields in the range of 40–60% were obtained. Unfortunately, $[Ru(bpy)(DMSO)_2Cl_2]$ could not be isolated satisfactorily pure. The difficulty in

isolating $[Ru(bpy)(DMSO)_2Cl_2]$ in a pure manner is probably why Zakeeruddin *et al.* preferred to work with $[Ru(Me_2bpy)(DMSO)_2Cl_2]$ [7].

Zakeeruddin *et al.* found that reacting $[Ru(DMSO)_4Cl_2]$ with Me_2bpy in CH_2Cl_2 resulted in poor yields whereas carrying out the reaction in protic solvents led to the formation of disubstituted products [7]. No studies on reaction solvent dependency were carried out during the course of this research. However, variations in reaction time and temperature failed to improve yields or purity to any considerable extent. Gently heating the reactants over long periods (2–24 h) resulted in a mixture of $[Ru(L)(DMSO)_2Cl_2]$ and starting materials. Heating at reflux for similar time periods did not improve yields by any appreciable amount.

The isolation of $[Ru(L)(DMSO)_2Cl_2]$ proved more troublesome than reported in the literature. After the initial reaction, upon removal of the $CHCl_3$, a black wax was recovered as opposed to the brown solid found by Zakeeruddin *et al.* This was dissolved in acetone and re-precipitated from ether to yield a light brown powder. This powder was subsequently filtered and dried under an N_2 atmosphere. Any attempts at redissolving or washing with possible coordinating solvents such as H_2O and MeCN yielded new impurities as observed by ^{1}H NMR. In fact, just dissolving in D_2O for ^{1}H NMR at least doubled the number of peaks observed in the aromatic region. As such, no further purification methods were developed.

Although impure, the presence of $[Ru(bpy)(DMSO)_2Cl_2]$ is clearly evident with ^{1}H NMR showing the presence of eight resonances, each integrating to a value of 1, Fig. 3.3a. There are also two sets of four resonances integrating to values of 0.35 and 0.6. This suggests the presence of at least three different species. In contrast, the ^{1}H NMR of $[Ru(Me_2bpy)(DMSO)_2Cl_2]$ shows it to be relatively pure, Fig. 3.3b. As expected, six resonances appear in the aromatic region with the two singlets at 8.00 and 7.96 ppm indicative of the 4,4-disubstituted Me_2bpy. In Fig. 3.3b below, the residual solvent peak at 7.27 ppm slightly obscures the doublet at 7.26 ppm.
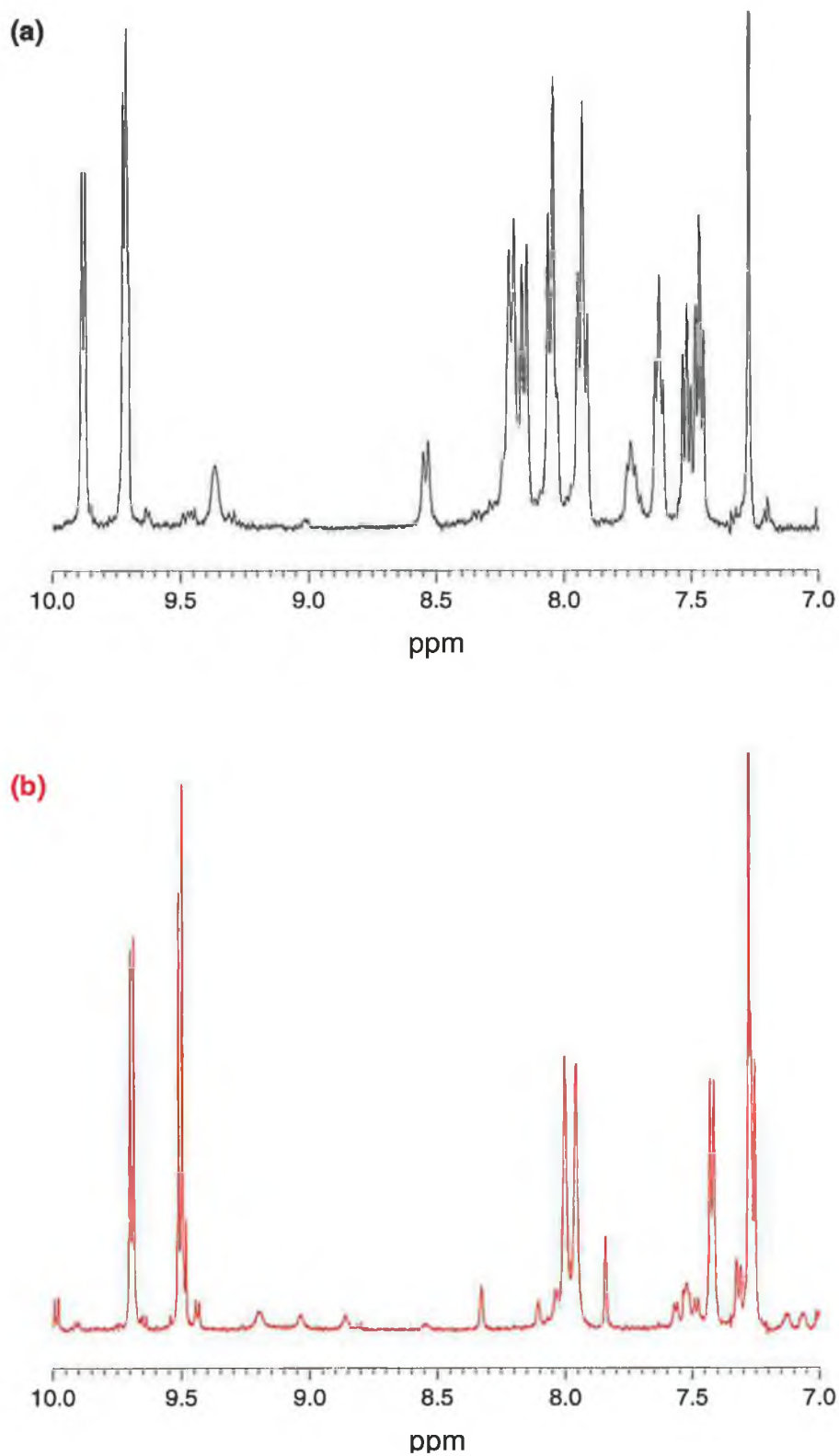
Figure 3.3. ^1H *NMR spectra of aromatic region of (a) [Ru(bpy)(DMSO)$_2$Cl$_2$] and (b) [Ru(Me$_2$bpy)(DMSO)$_2$Cl$_2$] in CDCl$_3$.*

The appearance of protons for each ring in the ^{1}H NMR of [Ru(bpy)(DMSO)$_2$Cl$_2$] and [Ru(Me$_2$bpy)(DMSO)$_2$Cl$_2$] indicates that the rings of the polypyridyl ligands are inequivalent. This suggests that the complexes take up the configuration whereby each ring is *trans-* to a different monodentate ligand. Thus, the configuration of these complexes is shown by the structure of [Ru(Me$_2$bpy)(DMSO)$_2$Cl$_2$] in Fig. 3.4.
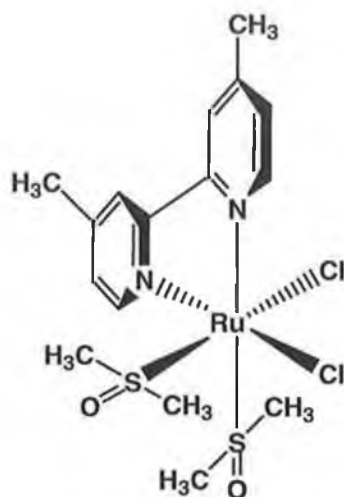
Figure 3.4. *Structure of [Ru(Me$_2$bpy)(DMSO)$_2$Cl$_2$] [7].*

Both the impure [Ru(bpy)(DMSO)$_2$Cl$_2$] and pure [Ru(Me$_2$bpy)(DMSO)$_2$Cl$_2$] were reacted with Me$_2$bpy and bpy respectively in DMF in an attempt to synthesise the [Ru(L)(L')Cl$_2$] dichloride. No dichloride was isolated using either of the two starting materials. However, the reaction of [Ru(Me$_2$bpy)(DMSO)$_2$Cl$_2$] with bpy did result in the reaction solvent taking on a slight purple tinge. A UV of this reaction showed the familiar MLCT transitions at 480 and 550 nm for a dichloride species. In an attempt to isolate a dichloride the volume of DMF was varied (10–100 ml) as well as the length of time the reaction solution (mixed with acetone) was allowed to stand (–4°C for 1–7 days). In all cases the second ligand was added in three or four portions so as to minimise the formation of a tris-complex.

Unfortunately the isolation of the dichloride proved elusive, and so several one-pot reactions, similar to the [Ru(bpy)Cl$_3$] method, were attempted. The

reaction of bpy with [Ru(Me₂bpy)(DMSO)₂Cl₂] was deemed to be the most promising as a dichloride had been observed, albeit only *in situ*. Thus bpy was added stepwise to [Ru(Me₂bpy)(DMSO)₂Cl₂] under N_2 in DMF solution at reflux. The reaction was monitored by HPLC and UV cross-sections of the HPLC trace at 3 h showed peaks with the characteristic absorption of [Ru(L)₂Cl₂] and [Ru(L)₃]²⁺ species. The reaction was further monitored and at 6 h the presence of the [Ru(L)₂Cl₂] species was deemed to have reached its maximum. Hpytrz was added at this point, along with a few drops of H_2O to aid in Cl labilisation. HPLC of the reaction mixture showed the presence of charged ruthenium complexes but recovery from the DMF solution proved troublesome. Without proper separation it was not possible to determine whether they were tris-heteroleptic in nature, whether ligand scrambling may have occurred or whether the chlorine atoms were simply displaced by neutral monodentate ligands such as H_2O, CO or solvent.
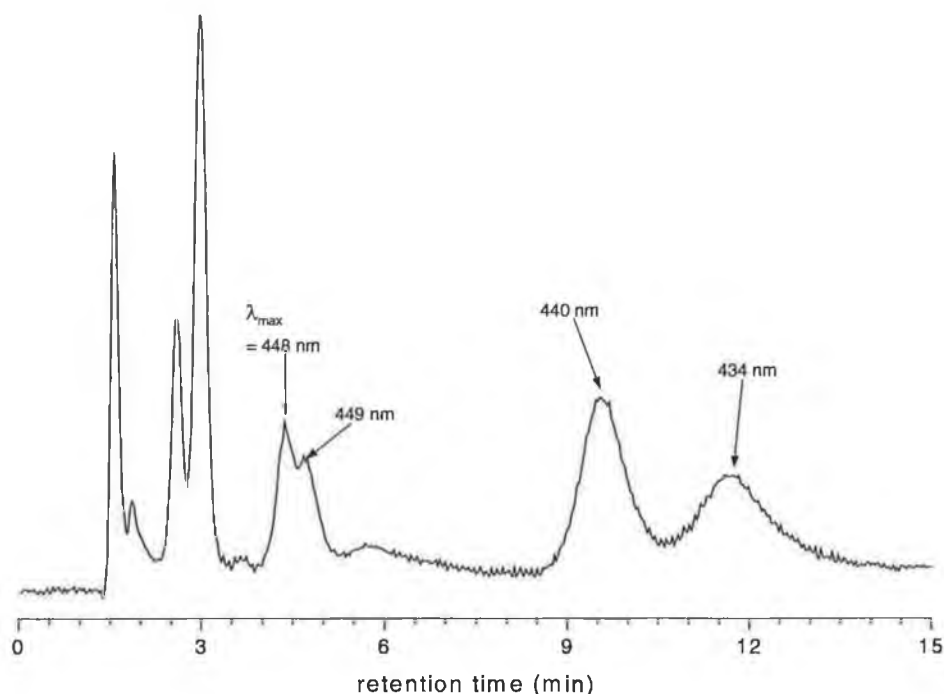
Figure 3.5. *HPLC trace of [Ru(Me₂bpy)(DMSO)₂Cl₂] reaction with bpy and Hpytrz. Mobile phase: 0.08 M LiClO₄ in 80/20 MeCN/H₂O using P10SCX-3095 cation exchange column and flow rate 1.8 ml min⁻¹.*

The HPLC analysis of the reaction mixture is remarkably similar to the analogous reaction of [Ru(bpy)Cl$_3$] with Me$_2$bpy and Hpytrz. The detector employed used a photodiode array as explained in Chapter 2. Thus, it was possible to take UV cross sections of the various species separated on the column. In both Fig. 3.2 and Fig. 3.5 it can be seen that several peaks elute before 3 min has elapsed. The quick elution time and lack of absorption in the visible spectrum suggest that these are unreacted ligands or solvent peaks. Unfortunately the peak integrations cannot be accurately used to determine the percentage of unreacted ligand due to different absorption coefficients of ligands and complexes. The products that elute from the HPLC column are monitored at 280 nm. Any species with a large absorption coefficient at 280 nm would therefore appear larger than an equivalent amount of another species with a lower coefficient value. The integrations can be used to compare ligands with ligands or compare complexes with complexes as these tend to have similar 280 nm coefficient values. The results are tabulated in Table 3.1 below.

Table 3.1. Retention time, relative area and λ_{max} for the two one-pot reactions. Those peaks which did not exhibit a MLCT λ_{max} are not included.

[Ru(bpy)Cl$_3$] reaction			[Ru(Me$_2$bpy)(DMSO)$_2$Cl$_2$] reaction		
Time (min)	λ_{max} (nm)	area (%)	Time (min)	λ_{max} (nm)	area (%)
1.07	–	1.8	1.56	–	7.4
1.23	–	10.5	1.87	–	2.1
1.43	–	7.5	2.58	–	5.9
1.60	–	3.0	2.97	–	16.7
1.93	–	2.9	4.37	448	9.5
3.11	441	2.4	4.69	449	5.3
4.60	449	2.8	9.54	440	28.6
5.01	449	3.2	11.70	434	23.1
7.86	449	4.0			
9.15	439	30.9			
11.18	434	29.8			

Both traces show a mixture of species that show MLCT transitions. These are marked with their respective λ_{max} in each case. As both traces were obtained using slightly different operating conditions (1.5 ml min^{-1} for [Ru(bpy)Cl$_3$] reaction and 1.8 ml min^{-1} for [Ru(Me$_2$bpy)(DMSO)$_2$Cl$_2$] reaction) the early eluting species show different retention times. The longer a species remained on the column, i.e. the more it interacted with the column, the less significant the flow rate seems to have been. Thus the last two peaks to elute in either case have similar retention times. The fact that both these sets of peaks also have similar λ_{max}'s suggests that they are the same compounds.

The reaction solvent was reduced and separation was attempted using Sephadex columns and varying concentrations of aqueous NaCl solutions. With an initial 0% NaCl solution no coloured band was seen to elute, suggesting that no neutral [Ru(bpy)(pytrz)$_2$] complex was formed during the reaction. Increasing the NaCl concentration to elute singly charged complexes led to a faint red band. Taking into account the possibility of ligand scrambling, potential structures are [Ru(bpy)$_2$(pytrz)]$^+$, [Ru(Me$_2$bpy)$_2$(pytrz)]$^+$ and [Ru(bpy)(Me$_2$bpy)(pytrz)]$^+$ based on the fact that all have similar charges and will elute together on a cation-exchange column. On increasing NaCl concentration the remaining coloured band eluted from the Sephadex column. This band is likely to be a mixture of the bis(heteroleptic) complexes [Ru(bpy)$_2$(Me$_2$bpy)]$^{2+}$ and [Ru(Me$_2$bpy)$_2$(bpy)]$^{2+}$ and the homoleptic species [Ru(bpy)$_3$]$^{2+}$ and [Ru(Me$_2$bpy)$_3$]$^{2+}$.

In any case this reaction method did not produce a tris(heteroleptic) complex which could be isolated. The failure to isolate a dichloride is most likely the reason the one-pot attempt also failed. Heating DMF at reflux is often problematic as carbonyl complexes can form, leading to reduced yields of the desired Ru(II) complex. The same problems were encountered for the synthesis of the dichlorides in Chapter 2.

3.4   Decarbonylation Method

The decarbonylation of a bipyridyl complex of the type $[Ru(L)(L')(CO)_2]^{2+}$ is by far the most widely reported strategy in synthesising tris(heteroleptic) Ru(II) complexes. The route to such carbonyl complexes is difficult as demanding reagents are required. Triflouromethanesulfonic acid needs to be fresh and TMNO needs to be freshly sublimed. Nevertheless the procedures utilised by various research groups including Anderson *et al.* were explored for their compatibility at incorporating the triazole, Hpytrz, to the coordinating sphere [14,15,16,17]. The reactions, both successful and unsuccessful are summarised in Scheme 3.1.

A series of complexes $[Ru(L)(CO)_2Cl_2]$ where L represents a triazole ligand were synthesised and are reported in Appendix A. However, as these carbonyl–triazole complexes failed to react in subsequent steps this section will deal only with $[Ru(bpy)(CO)_2Cl_2]$ and $[Ru(Me_2bpy)(CO)_2Cl_2]$ and their subsequent reactions. The synthesis and characterisation of the triazole carbonyls are discussed in Appendix A.

Initially, the oligomer $[Ru(CO)_2Cl_2]_n$ was reacted with the bidentate ligands bpy or Me$_2$bpy in MeOH to form complexes of the general structure $[Ru(L)(CO)_2Cl_2]$. The addition of a second bidentate ligand involves removal of the chlorine ligands. When $[Ru(bpy)(CO)_2Cl_2]$ was reacted with Me$_2$bpy or bpy in aqueous EtOH, the complexes $[Ru(bpy)(Me_2bpy)(CO)_2]^{2+}$ or $[Ru(bpy)_2(CO)_2]^{2+}$ respectively were isolated as the PF_6^- salts. However, these were the only instances where a second ligand could be introduced simply by heating at reflux in EtOH. When Hpytrz or indeed Hbpt was used, the triazole was returned quantitatively from the reaction. TLC of the reaction mixture showed no signs of a new complex. Alternately, the reaction of $[Ru(trz)(CO)_2Cl_2]$ (trz = any triazole) with bpy or Me$_2$bpy produced no $[Ru(trz)(L)(CO)_2]^{2+}$ species where L represents bpy or Me$_2$bpy.
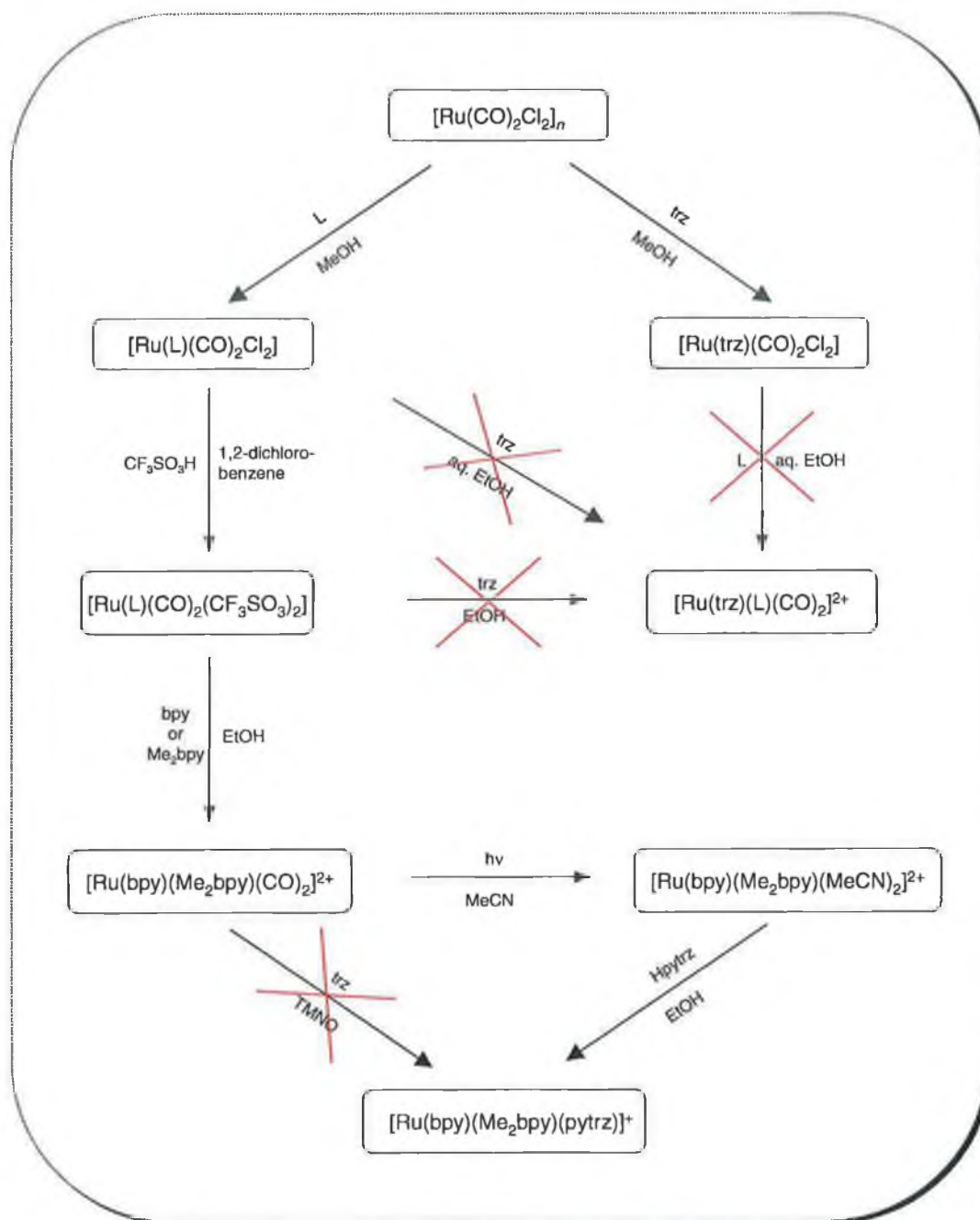
Scheme 3.1. *Different routes explored in the synthesis of a tris(heteroleptic) complex containing the triazole ligand Hpytrz. Those marked with 'X' were unsuccessful. L represents either bpy or Me$_2$bpy and trz represents any triazole ligand.*

The unreactivity of the [Ru(L)(CO)$_2$Cl$_2$] species was overcome by first replacing the chlorine ligands with a more labile species. In a typical experiment, [Ru(bpy)(CO)$_2$Cl$_2$] or [Ru(Me$_2$bpy)(CO)$_2$Cl$_2$] was treated with triflouromethanesulfonic acid in 1,2-dichlorobenzene [18,19].

Triflouromethanesulfonic acid is a highly reactive substance and needs to be handled with great care. In both cases the triflato-species were isolated and the ^{1}H NMR data were consistent with the literature reports [9]. In both [Ru(bpy)(CO)$_2$(CF$_3$SO$_3$)$_2$] and [Ru(Me$_2$bpy)(CO)$_2$(CF$_3$SO$_3$)$_2$] the complex assumes a *cis*-(CO),*cis*-(CF$_3$SO$_3^-$) configuration. This is confirmed by the appearance of two $v_{(CO)}$ stretching bands at 2102 and 2026 cm^{-1} for [Ru(bpy)(CO)$_2$(CF$_3$SO$_3$)$_2$] and 2101 and 2025 cm^{-1} for [Ru(Me$_2$bpy)(CO)$_2$(CF$_3$SO$_3$)$_2$]. The inequivalence of the two rings of the polypyridine ligand is also apparent in the ^{1}H and ^{19}F NMR.
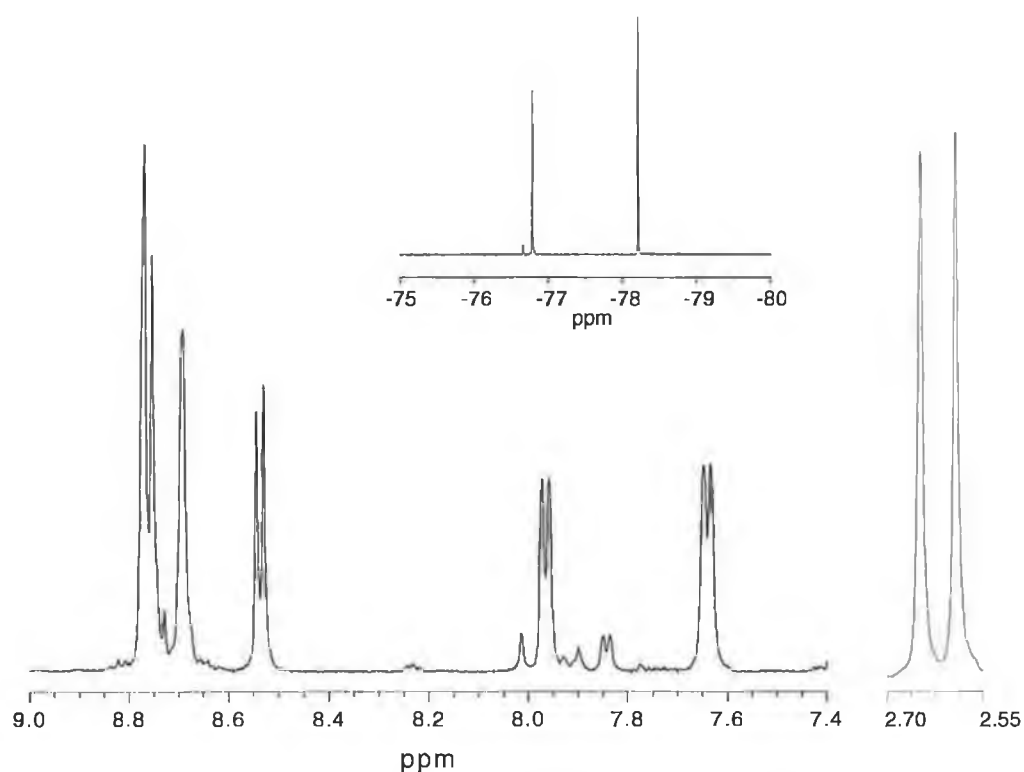
Figure 3.6. *^{1}H NMR spectra of aromatic and aliphatic regions for [Ru(Me$_2$bpy)(CO)$_2$(CF$_3$SO$_3$)$_2$] in d$_6$-DMSO with ^{19}F NMR spectra (inset).*

In the example shown in Fig. 3.6, all six aromatic protons on the coordinated Me$_2$bpy are clearly visible. The two methyl peaks at 2.65 and 2.59 ppm are evidence of ring inequivalency, as too are the two fluorine peaks obtained by ^{19}F NMR at –76.78 and –78.22 ppm. It is clear then that the ligand orientation

changes as [Ru(bpy)(CO)$_2$Cl$_2$] has the initial configuration of *cis*-(CO),*trans*-(Cl) as explained in Chapter 2.

Addition of the second bidentate ligand proved straightforward when that ligand was bpy or Me$_2$bpy. Addition of the second ligand conserves the symmetry in that the CO ligands retain their *cis*-conformation. Again this is evident by two $v_{(CO)}$ stretching bands at 2100 and 2051 cm^{-1} for [Ru(bpy)$_2$(CO)$_2$]$^{2+}$ and 2099 and 2047 cm^{-1} for [Ru(bpy)(Me$_2$bpy)(CO)$_2$]$^{2+}$. The ^{1}H NMR spectra in Fig. 3.7 also show resonances for each individual ring. In the case of [Ru(bpy)(Me$_2$bpy)(CO)$_2$]$^{2+}$, the two singlets at 8.79 and 8.68 ppm are indicative of the 4,4'-disubstitued Me$_2$bpy, as too are the two methyl peaks at 2.69 and 2.47 ppm. The absence of any ^{19}F resonance confirms the complete substitution of the acid moieties.
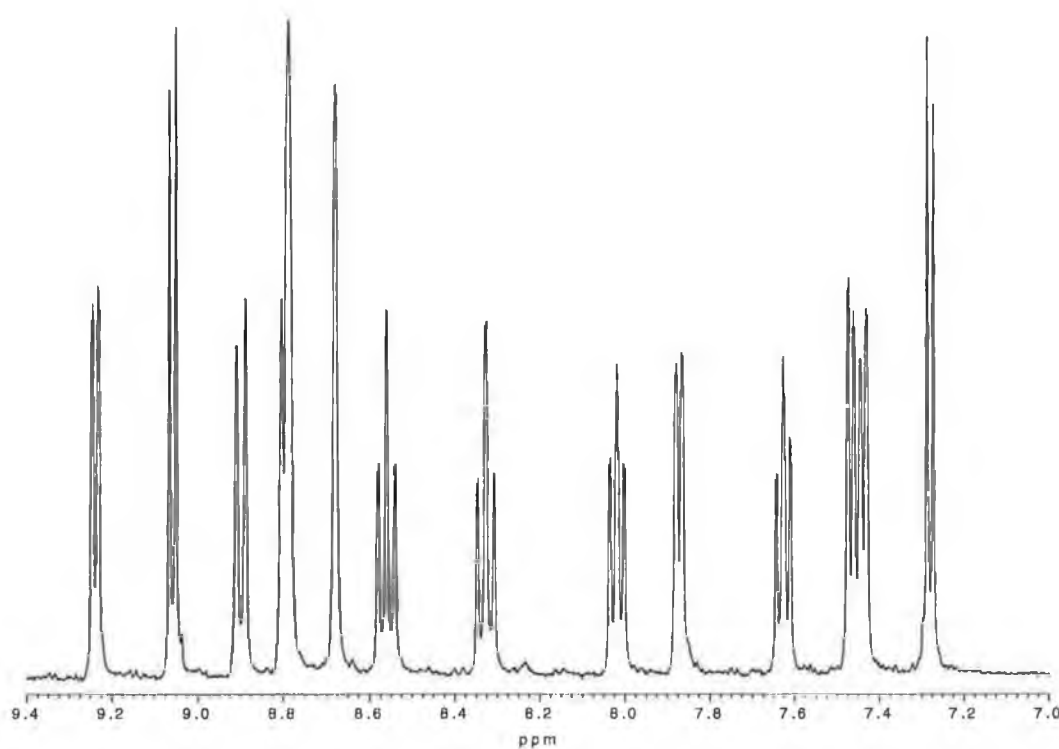
Figure 3.7. *^{1}H NMR of aromatic region of [Ru(bpy)(Me$_2$bpy)(CO)$_2$]$^{2+}$ in d$_6$-DMSO.*

84

As mentioned above, attempts at synthesising these complexes without the use of triflouromethanesulfonic acid proved only partly successful. The reaction of [Ru(bpy)(CO)$_2$Cl$_2$] with Me$_2$bpy in EtOH/H$_2$O yielded a compound with identical spectroscopic data to [Ru(bpy)(Me$_2$bpy)(CO)$_2$]$^{2+}$ formed by the procedure above.

Addition of a third bidentate ligand requires the removal of the CO ligands. This can be achieved chemically with the use of TMNO or photochemically by irradiating the carbonyl with light in the presence of a chelating ligand such as MeCN. To chemically remove the carbonyls, [Ru(bpy)(Me$_2$bpy)(CO)$_2$]$^{2+}$ was dissolved in EtOH. Freshly sublimed TMNO and the third ligand Hpytrz were added. The solution was refluxed and stirred for 2–5 h. The reaction was followed by TLC but no tris(heteroleptic) complex was observed.

3.5   Photosubstitution Method

3.5.1   Photolysis of [Ru(L)(L')(CO)$_2$]$^{2+}$

[Ru(bpy)$_2$(CO)$_2$]$^{2+}$ was dissolved in MeCN and placed in the pholoysis well depicted in Chapter Two. The solution was purged with Ar before irradiation commenced. Even before the lamp was switched on, a new vibrational stretch at 2016 cm^{-1} was seen to appear, Fig. 3.8. As the solution was to be irradiated anyway, no care was taken to eliminate daylight from the solution. Although the solution was only briefly exposed to daylight, the immediate formation of this new band highlights the ease at which CO removal can be attained in MeCN.

[Ru(bpy)$_2$(CO)$_2$]$^{2+}$ was irradiated with UV light from a Hg lamp and the reaction followed by IR. Once the lamp was switched on, samples were taken at regular intervals from the well, and the process followed by IR as shown in Fig. 3.8. This figure shows both initial bands at 2100 and 2051 cm^{-1} gradually disappearing and being replaced by a single band at 2016 cm^{-1}. After 30 min only residual traces of the initial complex remained. The reaction was completed after 120 min but faster reaction times were observed when a more dilute solution of [Ru(bpy)$_2$(CO)$_2$]$^{2+}$ was initially used. After removal of the solvent, the ^{1}H NMR spectra of the

product was consistent with that of $[Ru(bpy)_2(MeCN)_2]^{2+}$ which was synthesised using traditional methods, namely refluxing $[Ru(bpy)_2Cl_2]$ with excess MeCN in aqueous EtOH.
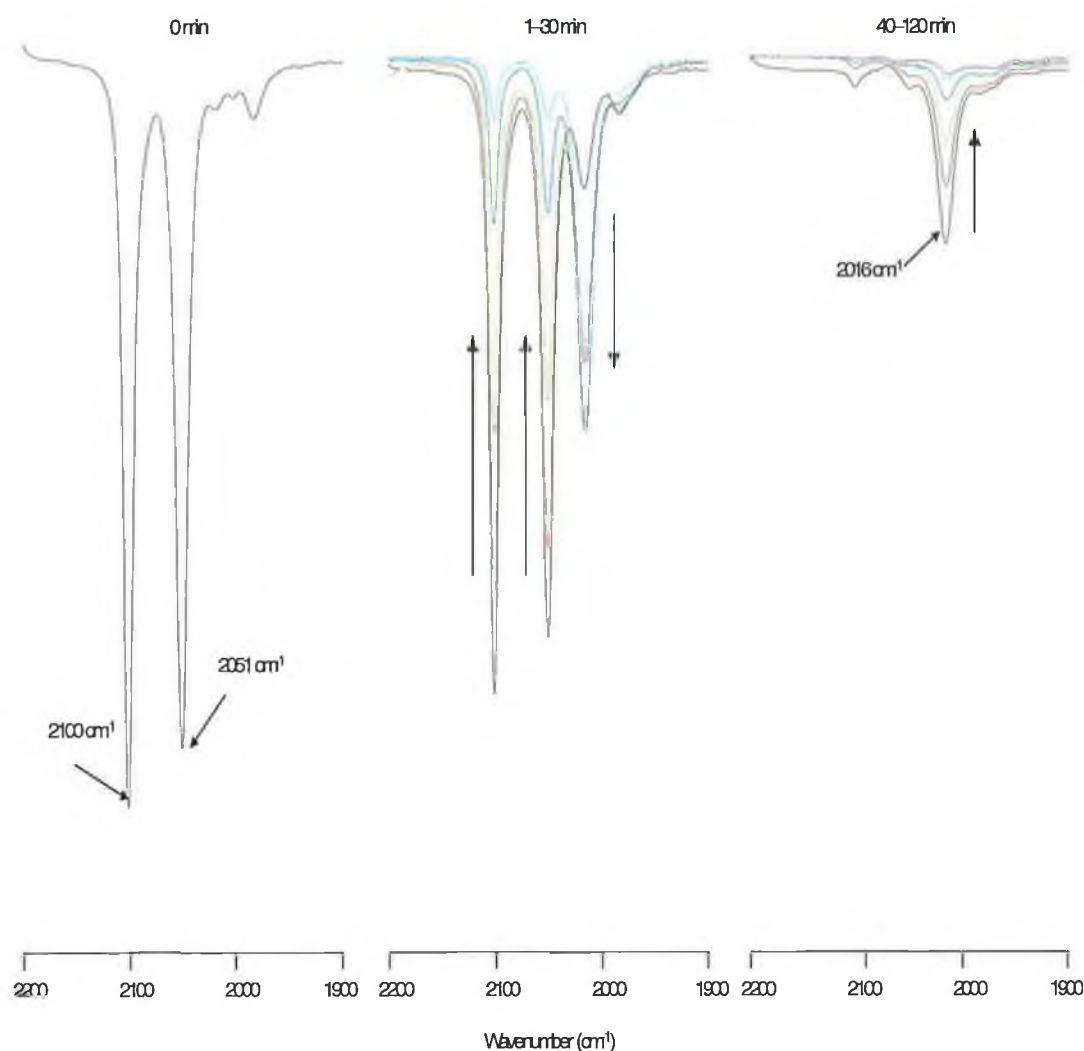
Figure 3.8. IR spectra taken from the photolysis reaction of $[Ru(bpy)_2(CO)_2]^{2+}$ in MeCN over 120 min.

As the decarbonylation of $[Ru(bpy)_2(CO)_2]^{2+}$ by UV light proved successful, the procedure was repeated with $[Ru(bpy)(Me_2bpy)(CO)_2]^{2+}$. A similar procedure to the photolysis of $[Ru(bpy)_2(CO)_2]^{2+}$ was followed and the results, as monitored by IR, are shown in Fig. 3.9. As was found for the $[Ru(bpy)_2(CO)_2]^{2+}$ photolysis, a brief exposure of the complex in MeCN to daylight results in a new band at

2012 cm^{-1} beginning to form. As before the two initial bands, $(2099 \text{ and } 2047 \text{ cm}^{-1})$ are replaced by a single band at 2012 cm^{-1}, which over time gradually disappears. After photolysis was complete, HPLC showed the presence of only one species. Both $[Ru(bpy)_2(MeCN)_2]^{2+}$ and $[Ru(Me_2bpy)(bpy)(MeCN)_2]^{2+}$ show similar retention times on the cationic column with elution times of 2.48 and 2.68 min respectively.
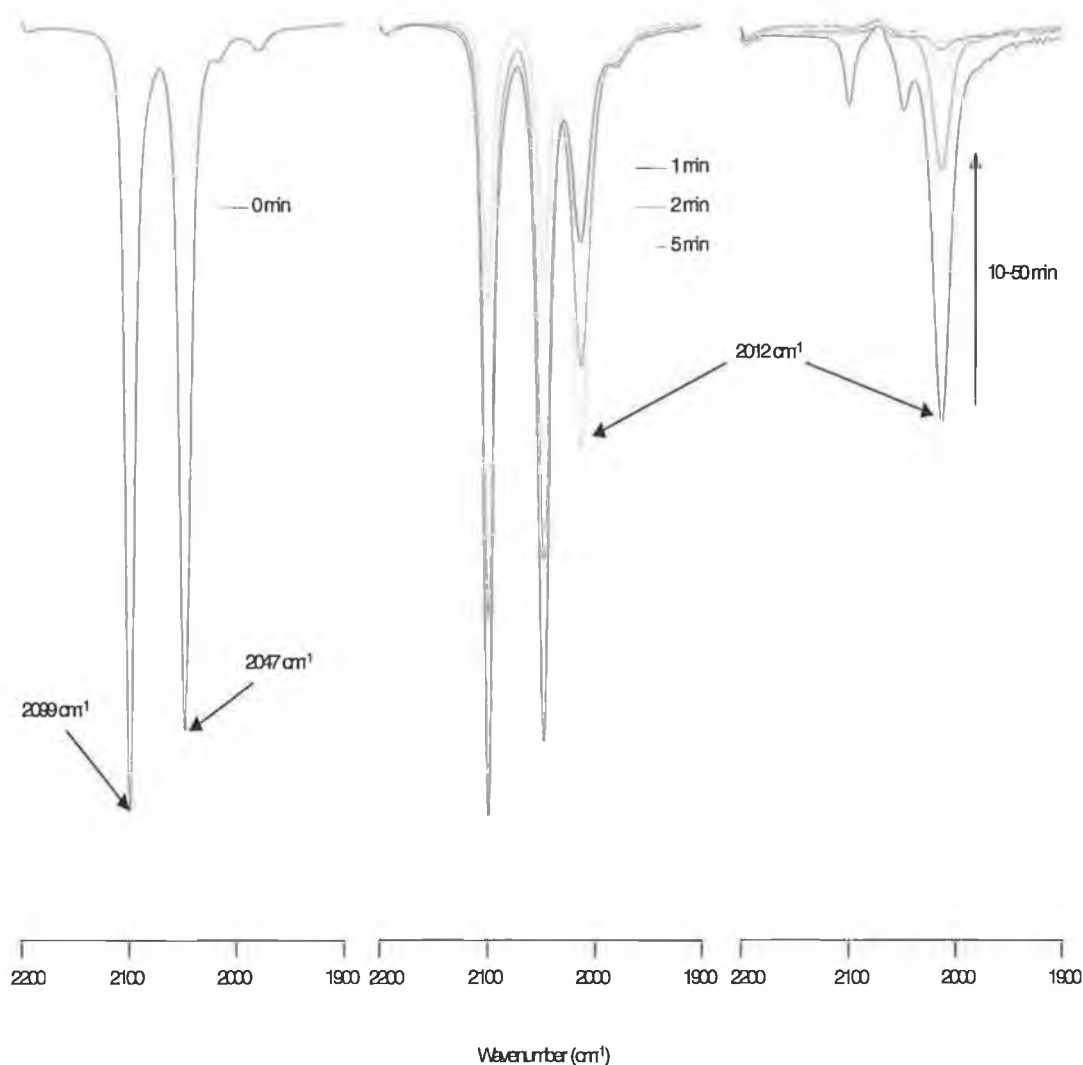
Figure 3.9. *IR spectra taken from the photolysis reaction of $[Ru(Me_2bpy)(bpy)(CO)_2]^{2+}$ in MeCN over 60 min.*

Upon removal of the solvent, the product $[Ru(Me_2bpy)(bpy)(MeCN)_2]^{2+}$ was confirmed by ^{1}H NMR and CHN. The experiment was repeated with

[Ru(bpy)(Me$_2$bpy)(CO)$_2$]$^{2+}$ from earlier triflato experiments and as expected the same results were obtained. The disparity between the individual rings of the polypyridyl ligands by ^{1}H NMR (Fig. 3.10) confirms that the ligand orientation around the molecule has been maintained throughout the photolysis procedure (Scheme 3.2). The presence of 14 individual peaks as well as the two indicative singlets at 8.72 and 8.58 confirm that both rings are still coordinated to the metal centre. As expected four peaks integrating to a value of 3 each are found at 2.69, 2.48, 2.47 and 2.44 ppm.
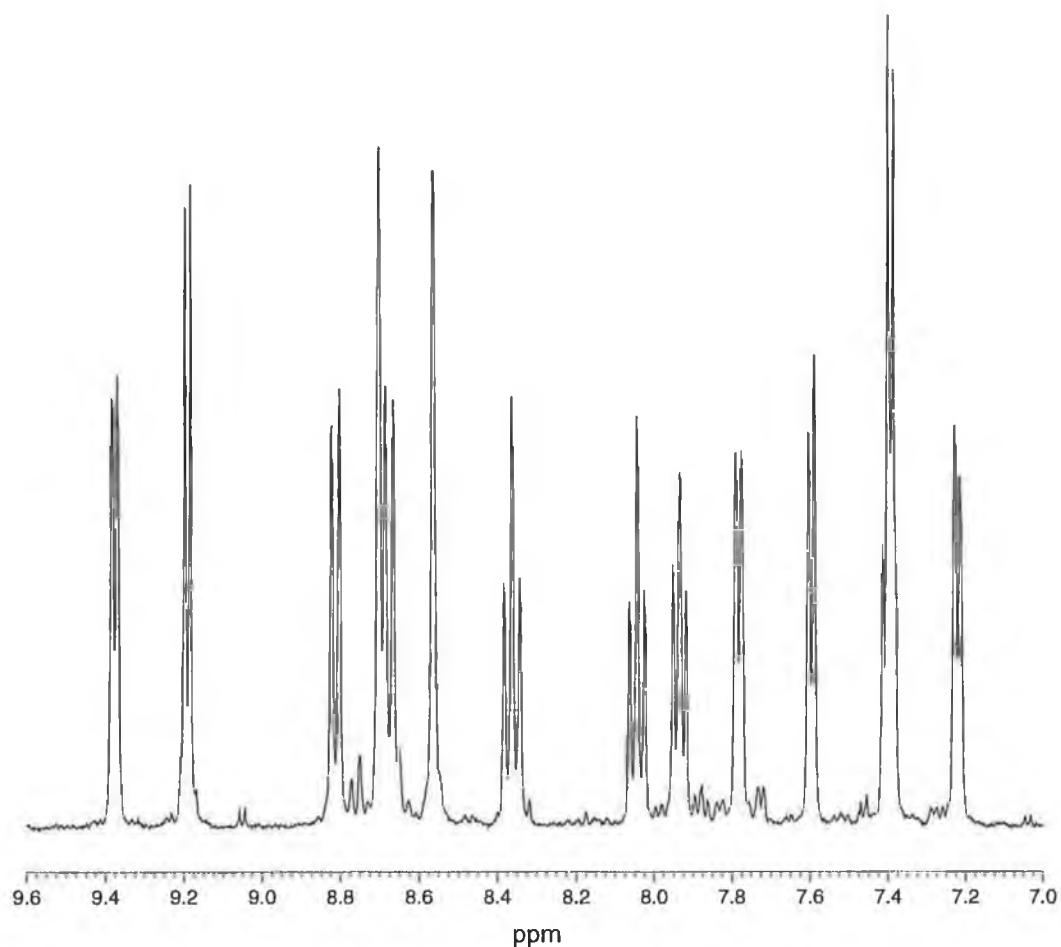
Figure 3.10. *^{1}H NMR of aromatic region of [Ru(bpy)(Me$_2$bpy)(MeCN)$_2$]$^{2+}$ in d$_6$-DMSO.*
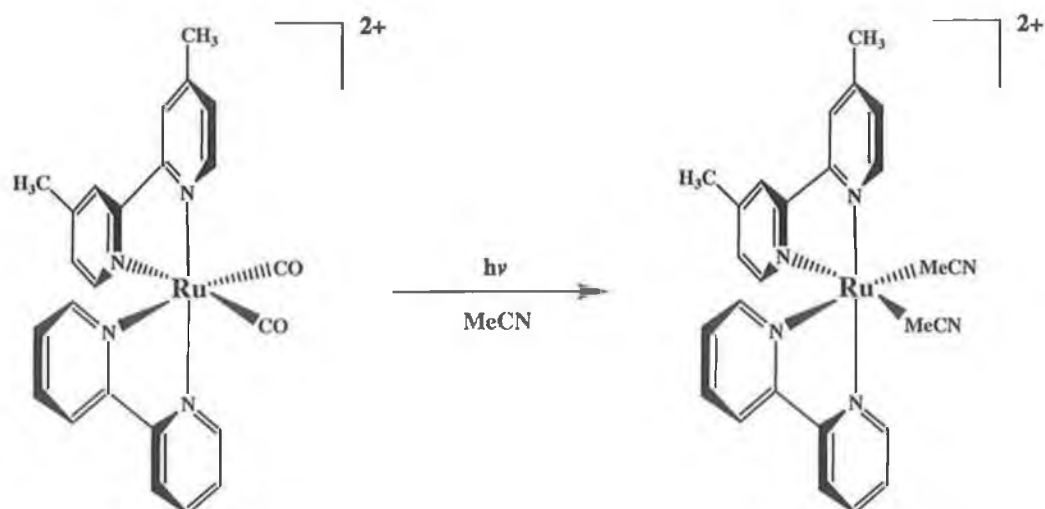
Scheme 3.2. *Formation of the acetonitrile complex [Ru(bpy)(Me₂bpy)(MeCN)₂]²⁺ showing retention of ligand orientation.*

Crystals of $[Ru(Me_2bpy)(bpy)(MeCN)_2](PF_6)_2$ were grown by allowing diethyl ether to slowly diffuse into an MeCN solution of the complex. X-ray crystallography experiments carried out by Dr. Sven Rau at the Friedrich–Schiller Universität, Jena, Germany, confirmed earlier ¹H NMR data as can be seen in Fig. 3.11. Full crystallographic data are presented in Table D9 in Appendix D.
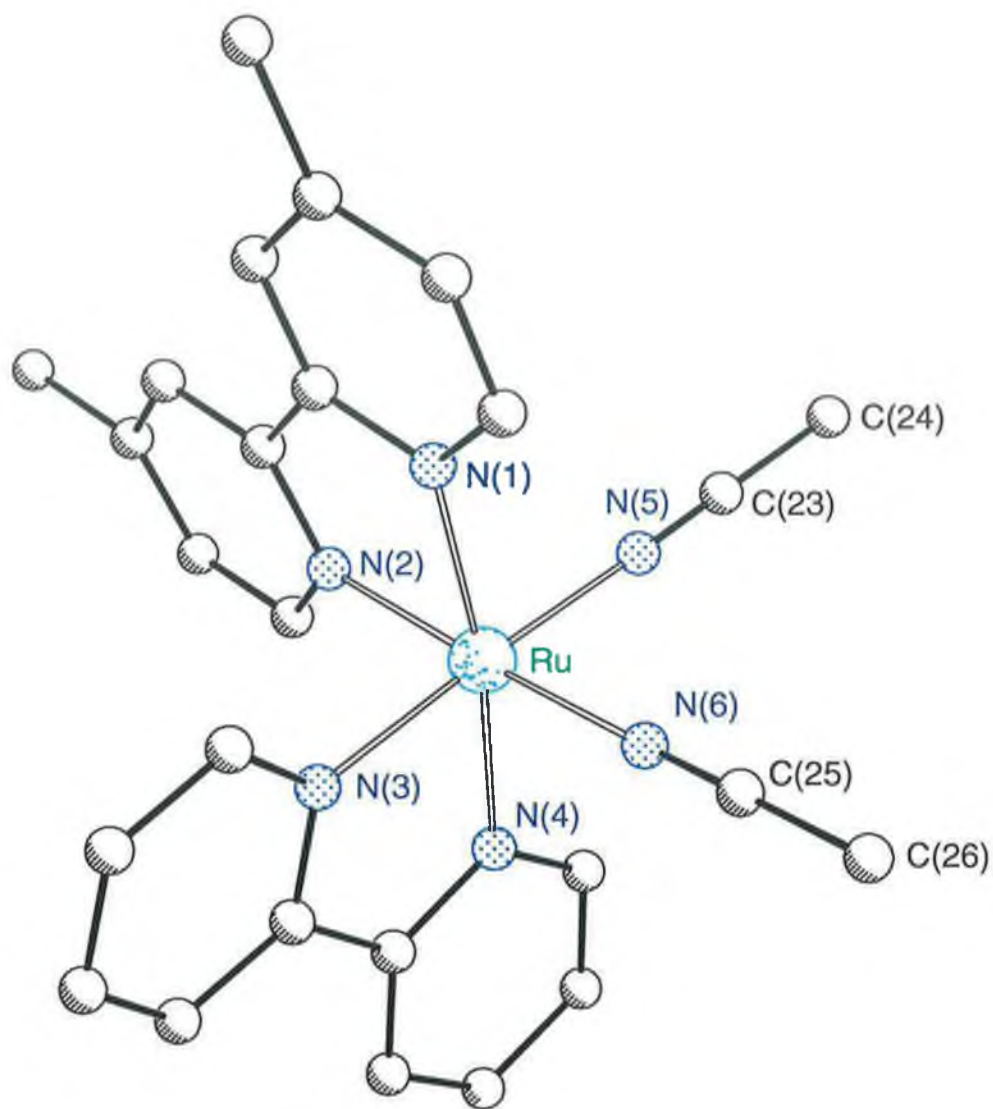
Figure 3.11. *Crystal structure of the [Ru(bpy)(Me₂bpy)(MeCN)₂]²⁺ cation. Hydrogen atoms, diethyl ether and PF₆⁻ molecules are omitted for reasons of clarity.*

Table 3.2. Bond distances and bond angles for $[Ru(bpy)(Me_2bpy)(MeCN)_2]^{2+}$. The corresponding distances and angles for $[Ru(bpy)_2(MeCN)_2]^{2+}$ are also included for comparison [20].

	$[Ru(bpy)_2(MeCN)_2]^{2+}$	$[Ru(bpy)(Me_2bpy)(MeCN)_2]^{2+}$
	Bond distances (Å)	
Ru-N(1)	2.063(5)	2.067(3)
Ru-N(2)	2.040(5)	2.046(3)
Ru-N(3)	2.045(6)	2.043(3)
Ru-N(4)	2.067(6)	2.067(3)
Ru-N(5)	2.033(7)	2.032(4)
Ru-N(6)	2.033(6)	2.037(4)
N(5)-C(23)	1.11(1)	1.134(5)
N(6)-C(25)	1.14(1)	1.145(5)
C(23)-C(24)	1.49(2)	1.468(6)
C(25)-C(26)	1.49(1)	1.451(6)
	Bond angles (deg.)	
N(1)-Ru-N(4)	172.5(2)	171.14(13)
N(2)-Ru-N(6)	174.9(2)	175.34(14)
N(3)-Ru-N(5)	174.4(2)	176.04(14)
N(1)-Ru-N(2)	79.4(2)	78.70(14)
N(1)-Ru-N(3)	95.1(2)	94.26(13)
N(1)-Ru-N(5)	90.1(2)	89.67(13)
N(1)-Ru-N(6)	95.5(2)	96.65(14)
N(2)-Ru-N(3)	86.2(2)	90.43(13)
N(2)-Ru-N(4)	95.9(2)	95.79(14)
N(2)-Ru-N(5)	92.4(2)	89.88(13)
N(3)-Ru-N(4)	78.7(2)	78.74(14)
N(3)-Ru-N(6)	94.0(2)	89.66(13)
N(4)-Ru-N(5)	96.1(2)	97.30(14)
N(4)-Ru-N(6)	89.1(2)	88.80(13)
N(5)-Ru-N(6)	87.8(3)	90.35(13)
Ru-N(5)-C(23)	175.1(6)	177.4(4)
Ru-N(6)-C(25)	174.9(7)	177.8(4)
N(5)-C(23)-C(24)	179.4(7)	178.4(5)
N(6)-C(25)-C(26)	178(1)	179.3(5)

It can be seen from the data in Table 3.2 that the crystal of $[Ru(bpy)(Me_2bpy)(MeCN)_2](PF_6)_2$ is virtually identical to the results reported by Heeg *et al.* for $[Ru(bpy)_2(MeCN)_2](PF_6)_2$ [20]. In both cases an octahedral coordination mode is observed with the bipyridine ligands exhibiting acute bite-angles, in this case 78.7° for the Me_2bpy ligand and 78.74° for the bpy ligand of $[Ru(bpy)(Me_2bpy)(MeCN)_2](PF_6)_2$. The presence of methyl groups on one of the bipyridine ligands has little effect on the Ru–N bond lengths of that ligand.

Three separate bond lengths are apparent for both complexes. The shortest of these are the Ru–N bond lengths of the MeCN ligand (approx. 2.033 Å). The next set of bond-lengths are the Ru–N (bpy/Me$_2$bpy) where that ring is *trans* to a MeCN ligand. These bonds average at about 2.044 Å and are shorter to those of Ru–N (bpy/Me$_2$bpy) where the ring is *trans* to another pyridyl ring (average bond length of 2.067 Å). The bipyridyl ligands are stronger π-acids than the MeCN ligands and so the rings *trans* to MeCN exhibit shorter Ru–N bonds. On the other hand, the Ru–N (MeCN) bond-lengths are shortest of all because of the smaller radius of the N(sp) orbital in MeCN than that of N(sp^2) of the bipyridyl ligands [20].

The last step in the formation of the tris(heteroleptic) complex involved reacting the acetonitrile complex [Ru(Me$_2$bpy)(bpy)(MeCN)$_2$]$^{2+}$ with the triazole ligand Hpytrz. The reaction was carried out in aqueous EtOH at reflux for 6 h. The triazole has two possible binding sites as discussed in Chapter 1, through either the N2 or N4 triazole nitrogen. As the metal binds, the triazole becomes deprotonated and so care is needed when isolating the complex as a salt. Aqueous NH$_3$ is added prior to precipitation, in order to isolate the deprotonated complex. This allows easier characterisation than would be possible if a mixture of protonated and deprotonated samples were isolated. The N2 and N4 isomers were separated on a silica column, isolated as a PF$_6$ salt and then further purified on an alumina column. The full characterisation of this complex is carried out in Section 3.6.

3.5.2   Photolysis of [Ru(L)(CO)$_2$Cl$_2$]

Although the tris(heteroleptic) complex [Ru(bpy)(Me$_2$bpy)(pytrz)]$^{2+}$ was isolated by the previous method, several large problems still exist. The chemical decarbonylation of [Ru(L)(L')(CO)$_2$]$^{2+}$ with TMNO in the presence of the triazole was not successful. However, the photolysis of the two carbonyl complexes [Ru(bpy)$_2$(CO)$_2$]$^{2+}$ and [Ru(bpy)(Me$_2$bpy)(CO)$_2$]$^{2+}$ proved very efficient and present viable alternatives in decarbonylating these types of molecules. Despite

this fact, the main drawback is in synthesising $[Ru(L)(L')(CO)_2]^{2+}$ species in the first place.

Against this background it was decided to investigate photochemically induced decarbonylation of $[Ru(L)(CO)_2Cl_2]$ to produce synthetically useful intermediates. This would circumvent the necessity to synthesise the $[Ru(L)(L')(CO)_2]^{2+}$ complexes. It was anticipated that the species $[Ru(L)(MeCN)_2Cl_2]$ might then be attainable which would then yield a dichloride of the form $[Ru(L)(L'')Cl_2]$. The photolysis of $[Ru(bpy)(CO)_2Cl_2]$ and $[Ru(Me_2bpy)(CO)_2Cl_2]$ were carried out as described in Chapter 2. The complex to be photolysed was dissolved in MeCN and purged with Ar for 15 min. A sample of the reaction mixture was taken for IR and the lamp switched on. The solution colour changed from yellow to red over the course of a few minutes and was periodically monitored over the course of 2 h, Fig. 3.12.

The removal of CO is confirmed by the disappearance of the $\nu_{(CO)}$ stretching bands. The initial bands at 2064 and 2001 cm^{-1} disappear rapidly and are replaced by one band at 1969 cm^{-1}. This band is indicative of a monocarbonyl or a *trans*-CO symmetrical species. Previous work by Eskelinen *et al.* suggests that it is a monocarbonyl species [21]. It is clear from Fig. 3.12 that one carbonyl ligand is replaced within 5 min. The carbonyl attributed to the 1969 cm^{-1} band gradually disappears until no trace of any carbonyl complex remains.
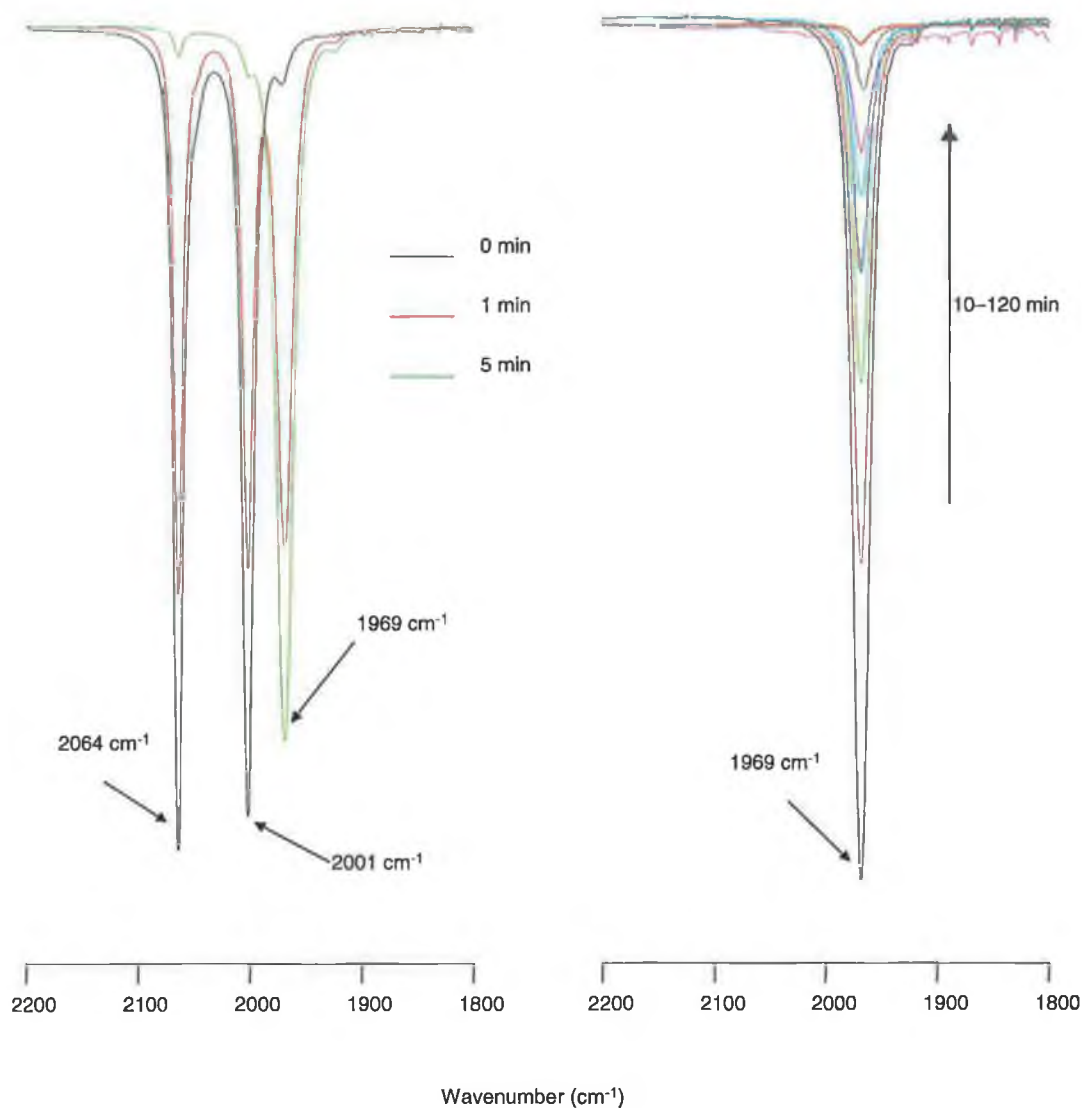
Figure 3.12. *IR spectra taken from the photoylsis reaction of [Ru(bpy)(CO)₂Cl₂]²⁺ in MeCN over 120 min.*

HPLC studies were carried out over a longer time period than that shown in Fig. 3.12. These results are shown in Fig. 3.13 and it can be seen that after 1 h, the starting material (retention time 1.39 min) is replaced by two species (retention times of 2.25 and 2.94 min). When the reaction was completed (after 2 h as observed by IR), the main product (retention time 2.25 min) was present with an 80% yield. Over the course of 6 h, no new species developed but the relative abundances of the two compounds was observed to shift to the compound with a retention time of 2.94 min.
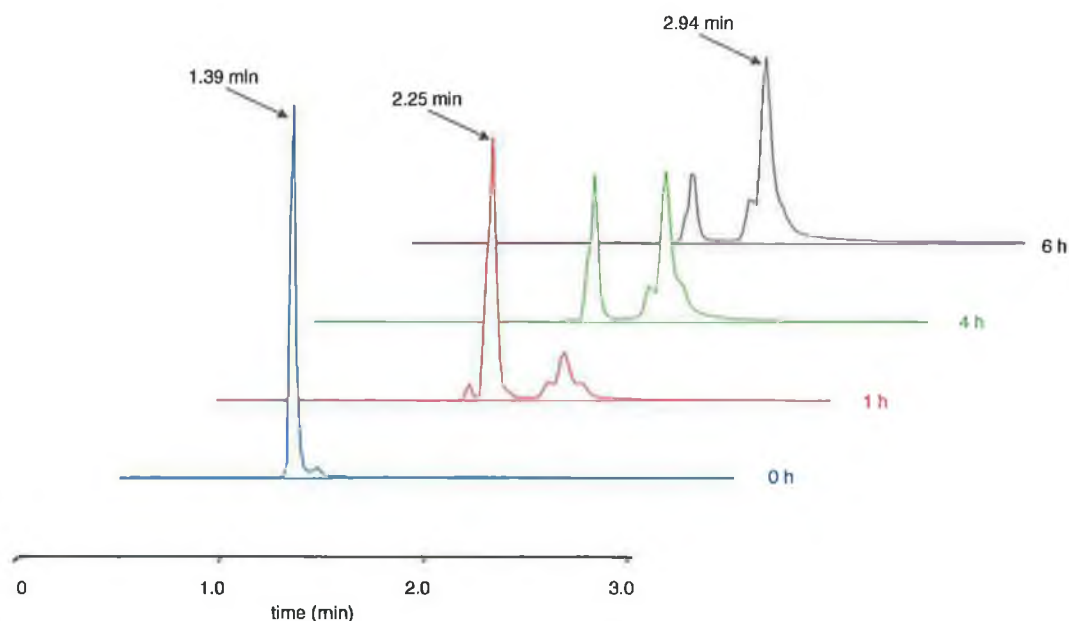
Figure 3.13. *HPLC trace of [Ru(bpy)(CO)₂Cl₂] photolysis reaction in MeCN. Mobile phase: 0.08 M LiClO₄ in 80/20 MeCN/H₂O using P10SCX-3095 cation exchange column and flow rate 1.8 ml min⁻¹.*

After photolysis, the MeCN was reduced by rotary evaporation and the product precipitated by dropping into diethyl ether. The ^{1}H NMR of this product suggests the presence of two species, Fig. 3.14. In this figure, eight resonances, which integrate to one proton each, are clearly visible. A further four resonances which integrate to 0.5 are also present and are marked by arrows. In some cases these are hidden by overlapping peaks, but are clearly noticeable in the peak integrations.

Separating the two products obtained from the photolysis reaction proved to be difficult. Chromatography on alumina with MeCN removed trace amounts of starting material but the main products remained on the column. Washing the crude product repeatedly with CH_2Cl_2 slowly separated the products but yields were detrimentally affected. However, the ^{1}H NMR of one of the separated products shows eight aromatic resonances and two methyl resonances. All aromatic resonances integrate to 1 and the two methyl resonances at 2.80 and 2.35 integrate to 3 and 6 respectively. The only possible arrangement of MeCN ligands around the metal centre that will lead to these integrations is that in Fig. 3.15a.
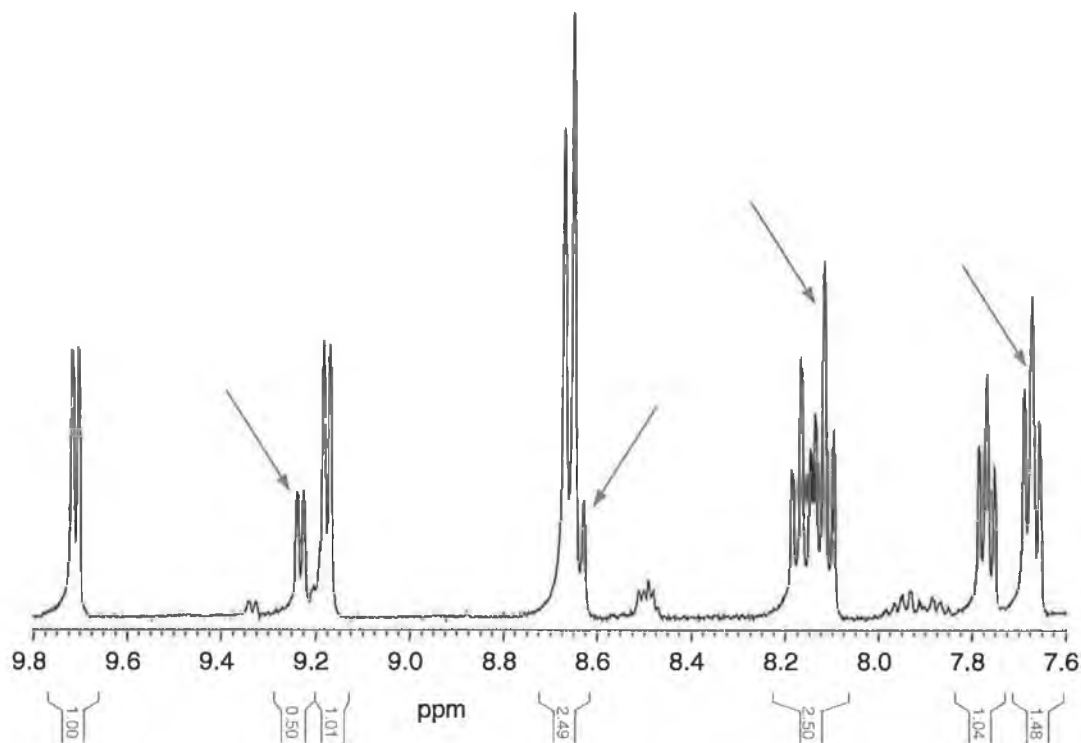
Figure 3.14. *^1H NMR of aromatic region of photolysis product in d_3-MeCN. The arrows point to peaks (some hidden) integrating to 0.5 units.*
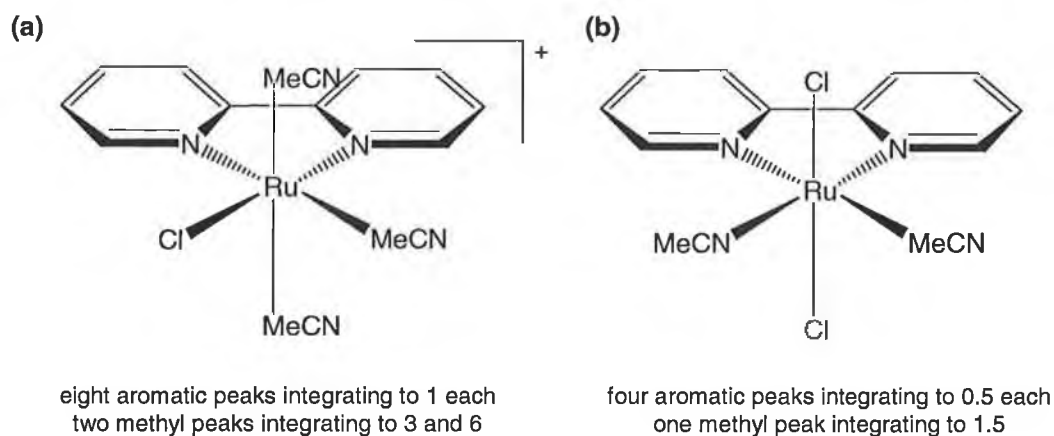
Figure 3.15. *Possible structures of the major (a) and minor (b) products obtained by photolysis of [Ru(bpy)(CO)$_2$Cl$_2$] in MeCN for 2 h.*

Assuming that the species with aromatic resonances integrating to 1 is that of Fig. 3.15a, then the lesser species contributes 4×0.5 to the aromatic integrations.

Since there are only four aromatic peaks relating to this product, each with an integration of 0.5, it can be assumed that each individual aromatic proton contributes 0.25 to the integrations (both rings are in a symmetrical environment). The ^{1}H NMR of the mixed product shown in Fig. 3.14 above shows two methyl peaks at 2.80 and 2.34 ppm. integrating to 4.5 and 6.2 respectively. As the major product contributes 3 and 6 to these integrations, the minor product must contribute 1.5 to the peak at 2.80 ppm. Four aromatic peaks and one methyl peak suggests a symmetrical complex with eight aromatic protons and two MeCN ligands. The only possible structure fulfilling all these requirements is that of Fig. 3.15b.

Electrochemical analysis of the product mixture was carried out as shown in Fig. 3.16. These results are in agreement with ^{1}H NMR and HPLC data in that two products are clearly visible. The DPV scan in MeCN shows two peaks with an integration ratio of 1:4 with oxidation potentials of 0.14 and 0.74 V (Ag/Ag$^+$) respectively.

Earlier work by Collomb-Dunand-Sauthier *et al.* found a similar reaction mixture to be that of [Ru(bpy)(MeCN)$_2$Cl$_2$] and [Ru(bpy)(MeCN)$_3$Cl]$^+$ [22]. In their experiments, they irradiated a sample of [Ru(bpy)(CO)$_2$Cl$_2$] in MeCN at 366 nm using a 250 W Hg lamp. Electrochemical and mass spectrometry studies show the initial formation of [Ru(bpy)(CO)(MeCN)Cl$_2$]. Further irradiation leads to [Ru(bpy)(MeCN)$_3$Cl]Cl through the intermediary [Ru(bpy)(MeCN)$_2$Cl$_2$]. Although they were not able to isolate the dichloride intermediate, they did observe a reversible oxidation E$_{1/2}$ at 0.10 V (Ag/Ag$^+$). Fig. 3.16 is in agreement with these findings. It is expected that replacement of a Cl$^-$ with a weaker donor ligand such as MeCN would shift the oxidation potential of the metal centre to a more positive value. This is indeed found to be the case with [Ru(bpy)(MeCN)$_3$Cl]Cl exhibiting an E$_{1/2}$ at 0.74 V (Ag/Ag$^+$).
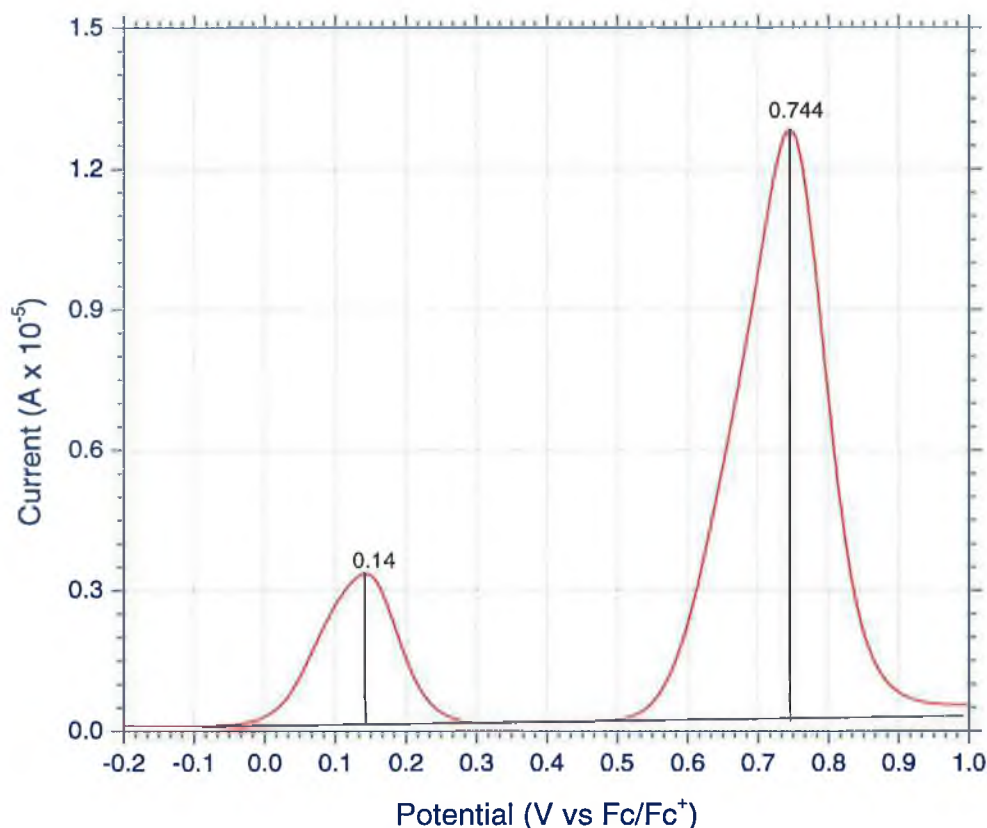
Figure 3.16. *DPV scan of photolysis mixture in MeCN (Ag/Ag$^+$).*

As separation of the photolysis mixture proved troublesome, the [Ru(bpy)(MeCN)$_3$Cl]Cl and [Ru(bpy)(MeCN)$_4$]Cl$_2$ mixture was refluxed with an equimolar amount of bpy in CHCl$_3$ overnight. The solution turned from a murky red colour to the familiar deep purple colour of dichloride solutions. A UV analysis of the final solution showed the presence of two bands at 481 and 542 nm, a characteristic of these dichloride complexes. After allowing the reaction to cool, the purple precipitate was filtered and ^{1}H NMR showed it to be pure [Ru(bpy)$_2$Cl$_2$]. The procedure was repeated using Me$_2$bpy and the product [Ru(bpy)(Me$_2$bpy)Cl$_2$] was isolated as confirmed by ^{1}H NMR, MS and CHN. Fig. 3.17 shows a comparison of the two ^{1}H NMR spectra obtained. It is clear from these spectra that methylating one of the bpy ligands reduces the symmetry of the molecule.
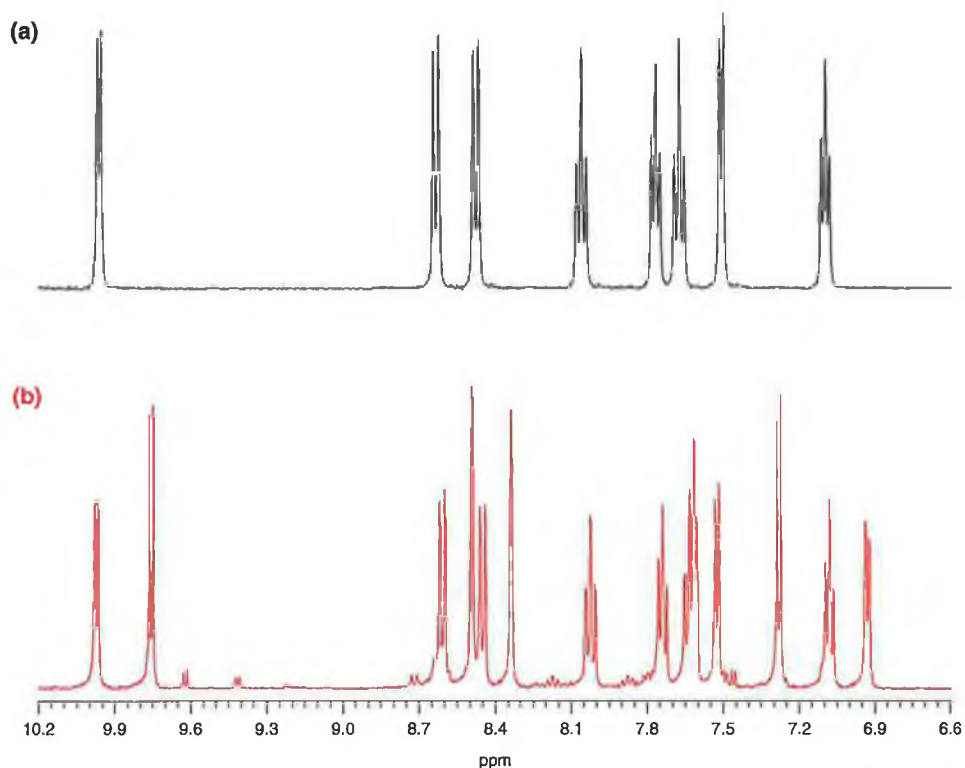
Figure 3.17. *^1H NMR of the aromatic regions of (a) [Ru(bpy)$_2$Cl$_2$] and (b) [Ru(bpy)(Me$_2$bpy)Cl$_2$] in d$_6$-DMSO obtained from reacting bpy and Me$_2$bpy respectively with the photolysis mixture.*

The reaction was carried out in CH$_2$Cl$_2$ and CCl$_4$ but no improvements in yield were obtained. In fact, in CH$_2$Cl$_2$ the yields obtained were diminished, most likely due to the lower boiling point of this solvent. The reaction was also carried out in acetone, the solvent used by Freedman *et al.* in introducing a second ligand [12]. Yields were somewhat increased but no observable increases in purity were observed. A 2D COSY experiment in d$_6$-DMSO for [Ru(bpy)(Me$_2$bpy)Cl$_2$] was carried out and gave the spectra in Fig. 3.18. This allowed the complete characterisation of the aromatic protons for the different bpy and Me$_2$bpy rings. For a fuller explanation of the characterisation of [Ru(bpy)(Me$_2$bpy)Cl$_2$] see Appendix B.
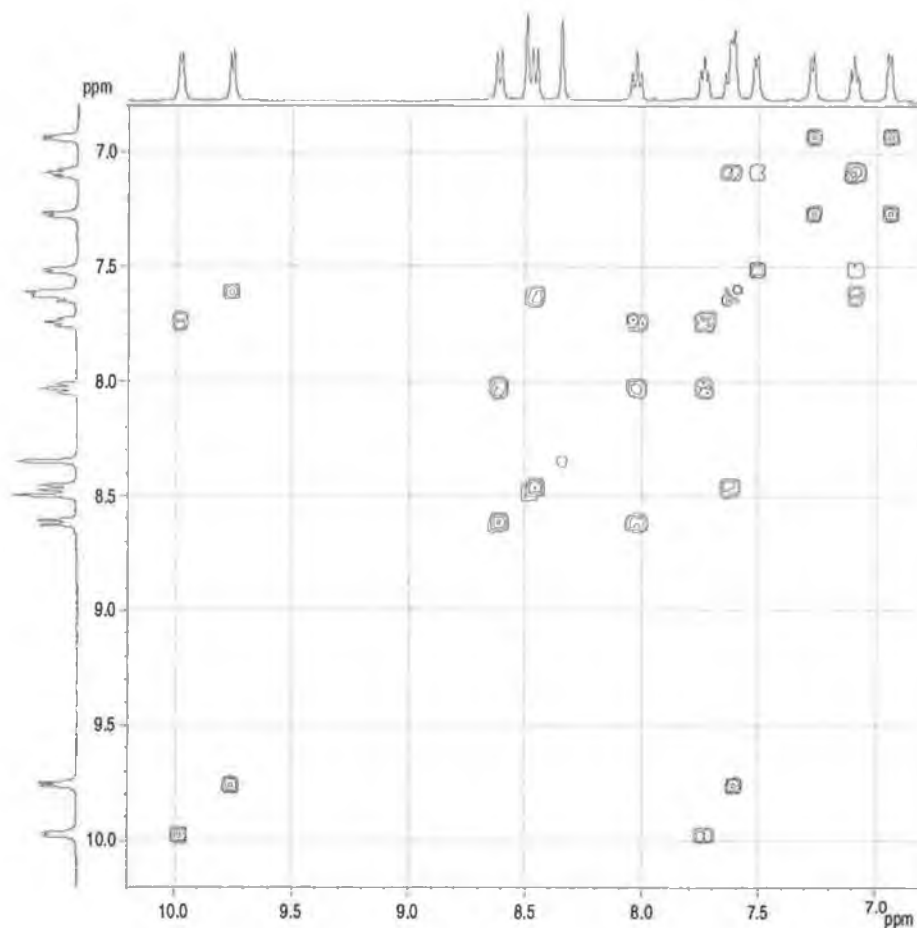
Figure 3.18. 2D COSY ^1H NMR of the [Ru(bpy)(Me$_2$bpy)Cl$_2$] complex in d_6-DMSO.

As the dichloride could be isolated in adequate yields and was satisfactorily pure, it was further reacted with Hpytrz in aqueous EtOH. The solution turned from the characteristic purple of dichlorides to a deep red over the course of the reaction and after 4 h the complex was isolated as described in Section 3.5.1. The synthetic route for the photolysis of [Ru(bpy)(CO)$_2$Cl$_2$] and successful isolation of [Ru(bpy)(Me$_2$bpy)(pytrz)]$^+$ is given in Scheme 3.3.

$[Ru(CO)_2Cl_2]_n$

MeOH | bpy

$[Ru(bpy)(CO)_2Cl_2]$ 77%

MeCN | hν

$[Ru(bpy)(MeCN)_3Cl]Cl$ + $[Ru(bpy)(MeCN)_2Cl_2]$

CHCl$_3$ or acetone | Me$_2$bpy

$[Ru(bpy)(Me_2bpy)Cl_2]$

aq. EtOH | Hpytrz

$[Ru(bpy)(Me_2bpy)(pytrz)]^+$ 80%
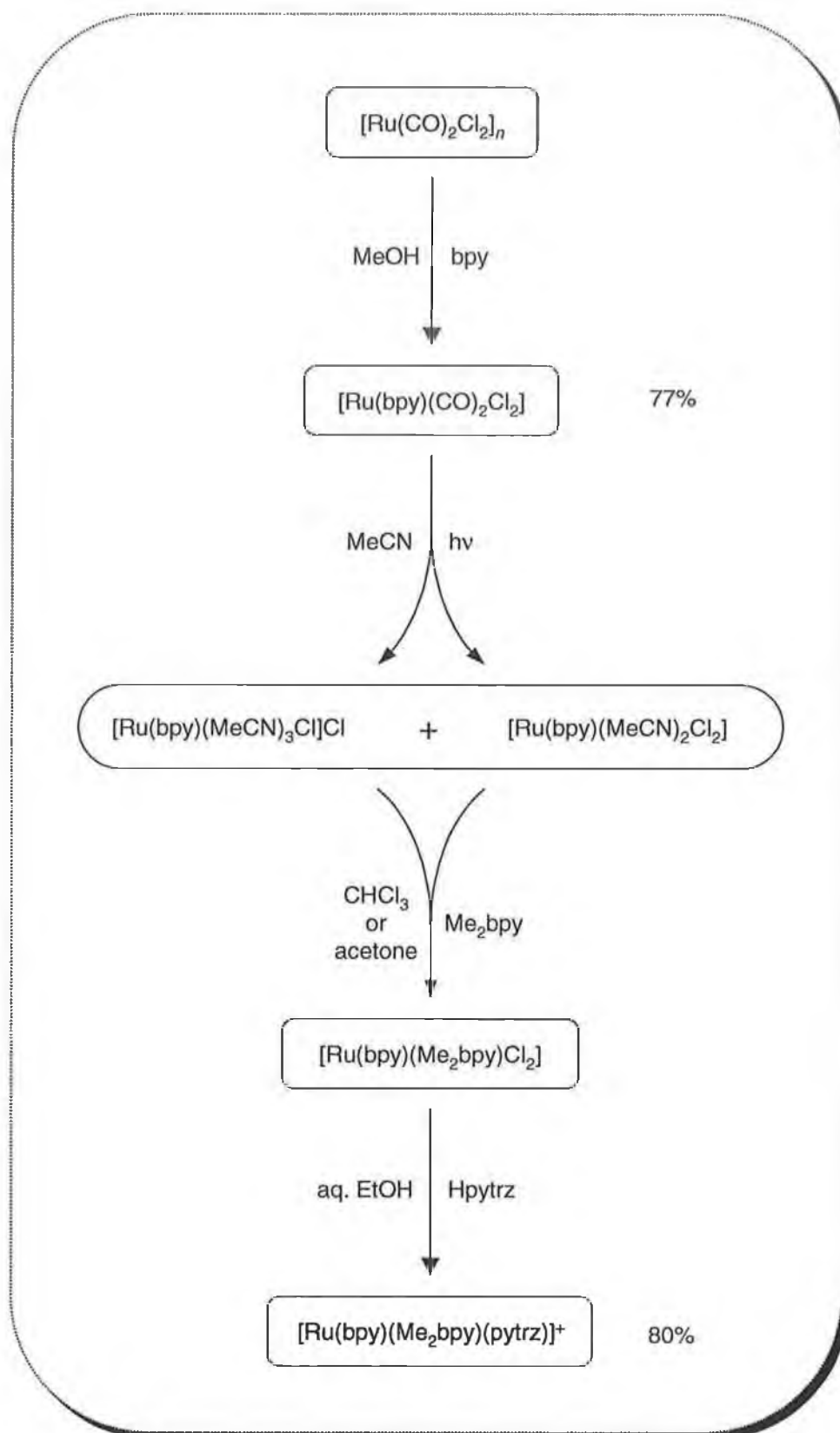
Scheme 3.3. *Successful reaction scheme leading to the isolation of a triazole tris(heteroleptic) Ru(II) complex.*

3.6 Characterisation of [Ru(bpy)(Me₂bpy)(pytrz)]⁺

When dealing with tris(heteroleptic) complexes containing a triazole ring, consideration must me taken of the geometrical arrangement of the ligands around the metal centre. In the first instance, the triazole may bind in either of two modes, i.e. through the N2 or N4 of the triazole ring. Because the triazole is asymmetric a further two possible isomers of each N2 and N4 coordination mode may be formed. Fig. 3.19 below depicts the isomers that may be present. Appendix C gives a fuller account of how the names for the tris(heteroleptic) complexes were assigned.

(a)   N2 bound *trans*(trz, bpy)

(b)   N2 bound *trans*(trz, Me₂bpy)

(c)   N4 bound *trans*(trz, bpy)

(d)   N4 bound *trans*(trz, Me₂bpy)
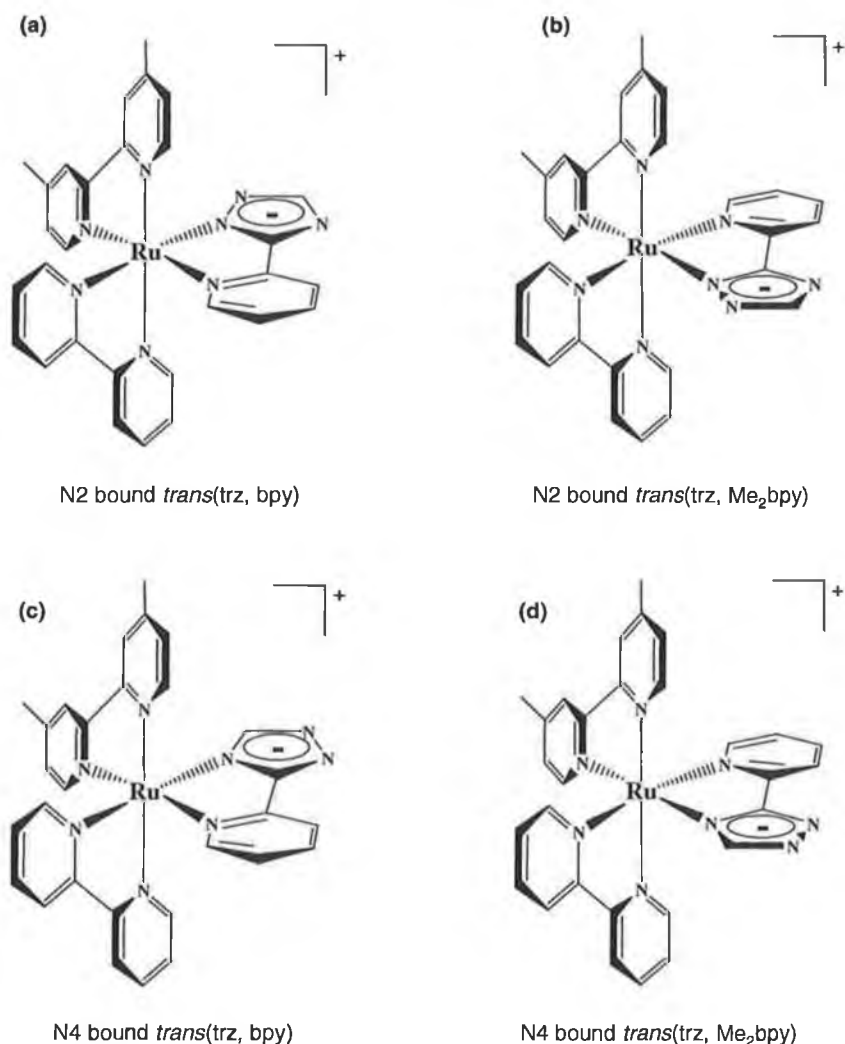
Figure 3.19. Possible isomers obtained by reacting [Ru(bpy)(Me₂bpy)Cl₂] with pytrz. (a) N2 trans(trz, bpy); (b) N2 trans(trz, Me₂bpy); (c) N4 trans(trz, bpy) and (d) N4 trans(trz, Me₂bpy).

Additionally, each of the isomers (a)–(d) shown in Fig. 3.19 has an optical isomer. The complexes in Fig. 3.19 are all shown in their Λ configuration, but each also has a corresponding Δ isomer. For the characterisation techniques employed, both the Λ and Δ isomers will behave identically to each other and will not be distinguishable. As the current interest of these studies is in the synthesis of these complexes and not their optical isomer resolution, no further remarks on Λ and Δ optical isomers will be made.

The complexes could not be separated into four separate species. Instead, only a separation of N2 bound and N4 bound was achieved. This was made possible by their different affinities to alumina in MeCN solution. After isolating the mixed N2/N4 species, the product is placed on an alumina column. MeCN causes N2 to elute while leaving N4 on the column. Gradual solvent shift to MeOH then causes N4 to elute [23]. While N2 was obtained satisfactorily pure, the N4 isomer always contained some N2 traces as visible by ^{1}H NMR.

Each binding mode can have two different isomers as shown in Fig. 3.19. The ^{1}H NMR spectra of each binding mode in Fig. 3.20 is therefore a mixture of two isomers and so is rather complicated. The most immediate differences between the two spectra is in the aliphatic region. The N2 isomers produce three peaks at 2.55, 2.51 and 2.47 ppm, each of which integrate to 3. In fact the peak at 2.55 ppm is split slightly and probably represents the two methyl groups of one of the isomers. In this case, the isomers would appear to be present in a ratio of 1:2. Determining which isomers correspond to which methyl peaks is more difficult and would only be possible if both isomers could be isolated. However, it is likely that the complex in Fig. 3.19b is the major isomer. The σ-donating ability of the triazole ring would have little effect on the Me$_2$bpy rings for complex (a) and so both Me peaks would encounter a similar chemical environment. Complex (b) has the triazole ring *trans* to one Me$_2$bpy ring thus causing a slight difference in chemical environment resulting in two separate Me peaks.

103

(a)

(b)
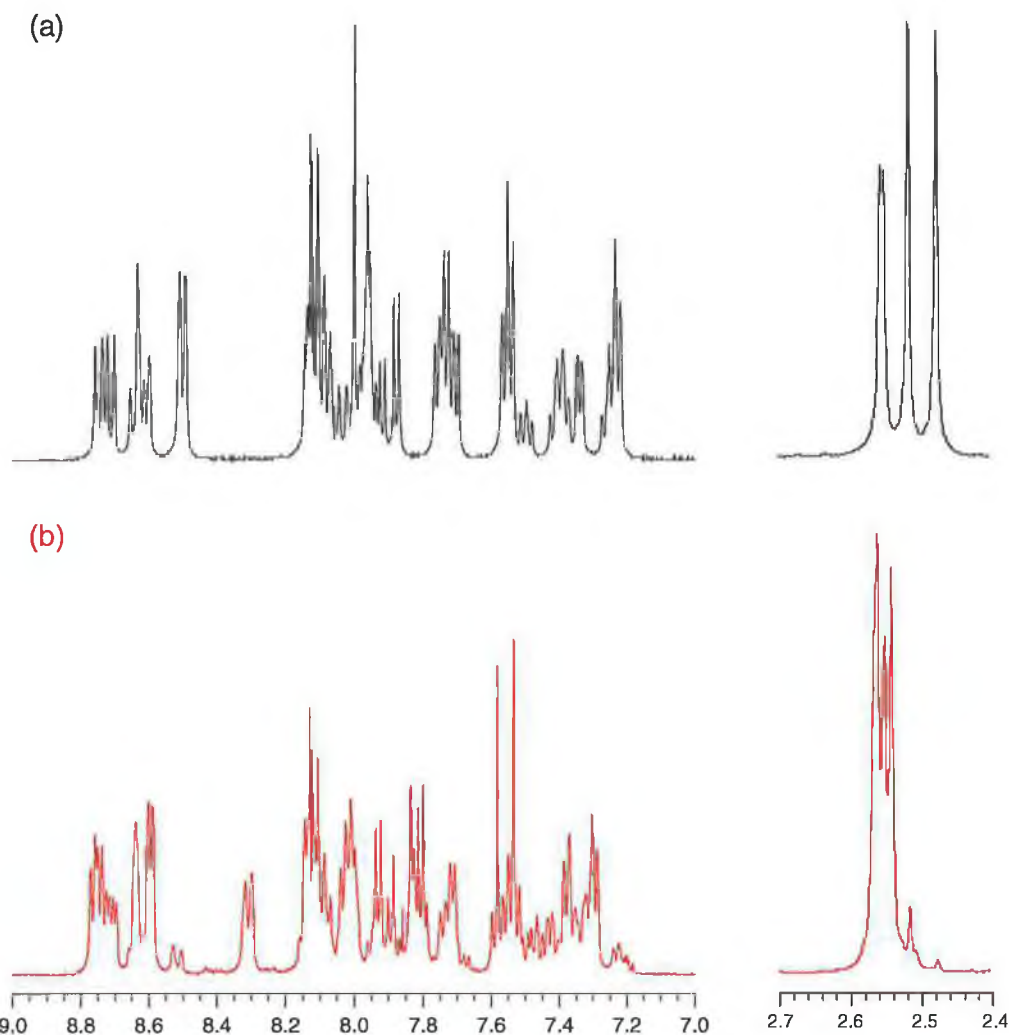
Figure 3.20. $^1H\,NMR$ spectra of N2 (a) and N4 (b) isomers of [Ru(bpy)(Me$_2$bpy)(pytrz)]$^+$ in d$_6$-acetone.

The ^{1}H NMR of the N4 isomer also shows three Me peaks but with similar chemical shifts. N4 bound triazoles do not posses as strong a σ-donating ability as N2. Therefore the position of the pytrz⁻ ligand in Fig. 3.19c and d will not have as much effect on the Me shifts as the N2-bound isomers. The total integration of the Me peaks is 13. There is a slight N2 impurity visible at 2.51 ppm which might account for the integration being 13 rather than 12. It is interesting that the N4-bound isomers seem to be present in a 1:1 ratio whereas the N2-bound isomers are present in a 1:2 ratio.

Another distinguishing feature of the two spectra is the position of H5 of the triazole ring. In the N2 isomer, the H5 sits in free space and so is relatively unaffected upon complexation to the metal centre, Fig. 3.21. In this case it can be seen as a singlet at 8.00 ppm. However, in the case of the N4 isomer, this proton sits on top of one of the methyl rings and anisotropic effects cause it to shift further upfield to 7.53 and 7.57 ppm. Hage noticed this for the similar bis(heteroleptic) complex $[Ru(bpy)_2(pytrz)]^+$ [24]. In the case of the bis(heteroleptic) complex, the triazole H5 was observed to shift upfield by 0.73 ppm from 8.27 (free) to 7.54 ppm (complexed) when N4 bound. The N2 bound H5 only shifted upfield by 0.28 ppm to 7.99 ppm. The appearance of two singlets in Fig. 3.20b further suggests the ratio of N4-bound isomers to be 1:1. Only one singlet is observed for the N2-bound isomer, the other probably obscured by the rest of the spectrum.

H5 unaffected by
ring anisotropy

N2 bound *trans*(trz, bpy)

H5 sitting over
Me₂bpy ring

N4 bound *trans*(trz, bpy)
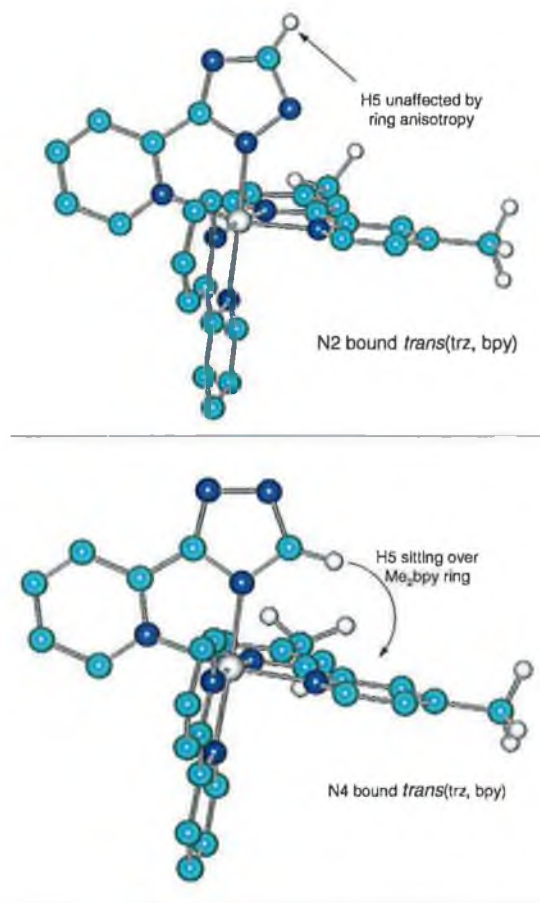
Figure 3.21. *Different orientations of the triazole H5 for N2 and N4 bound isomers.*

Mass spectrometry has been used previously to characterise Ru(II) polypyridyl complexes [25,26,27]. Miller *et al.* have used FAB mass spectrometry to compare $[RuLL'L'']^{2+}/[RuLL'L'']^{+}$ intensity ratios and thus utilising MS as a powerful characterisation tool [25].
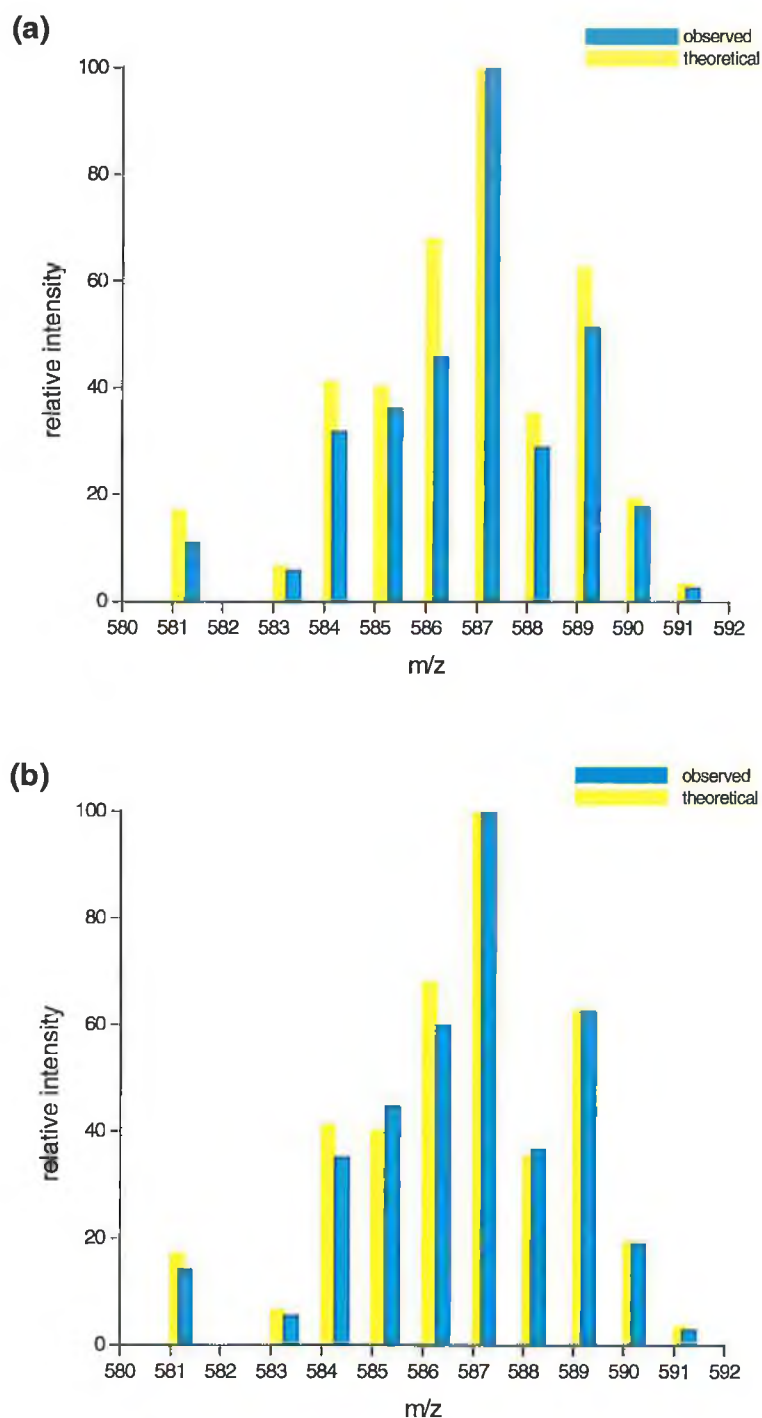
Figure 3.22. The isotopic distributions of the molecular ions for (a) the N2 bound isomers and (b) the N4 bound isomers.

For the triazole tris(heteroleptic) in this chapter, electrospray mass spectrometry was used [28]. This is a soft ionisation technique and so no strong fragmentation patterns are observed. Instead, the molecular ion and its isotopic distribution can be studied. Fig. 3.22 shows such a pattern for the N2 and N4 isomers. The two spectra are virtually identical, the only difference being their relative intensities. This is expected as both complexes have identical molecular masses. Both peaks are accountable by the loss of the single PF_6^- counter-ion from the overall complex. This ion at 587 m/z is the base ion in each case, and the only significant ion observed.

With the results of the analytical methods described above, it is likely that a tris(heteroleptic) complex containing the ligand pytrz⁻ has been synthesised and isolated. The method used produces a dichloride precursor which should react with most polypyridyl ligands to produce tris(heteroleptic) species. The following chapter will report the synthesis of a series of such complexes containing both pyridine- and pyrazine-triazole ligands.

3.7 Experimental

3.7.1 [Ru(bpy)Cl₃] Method

Ultimately, no tris(heteroleptic) products were isolated using this method. However, the bis(heteroleptic) complex $[Ru(bpy)(Me_2bpy)_2]^{2+}$ was isolated by the method followed below. This method was attempted for the tris(heteroleptic) complex but with the addition of equal molar equivalents of Me_2bpy and Hpytrz. The synthesis of the tris(heteroleptic) complex failed and so only the bis(heteroleptic) synthesis are described here. For more information see Section 3.2. All molecular weights and hence moles used are estimated by using the bis-aqua complex $[Ru(bpy)Cl_3].2H_2O$.

$[Ru(bpy)_3](PF_6)_2$

$[Ru(bpy)Cl_3].xH_2O$ (0.2 g, 0.5 mmol) and bpy (0.16 g, 1 mmol) were dissolved in DMF (20 ml). The reaction was heated at reflux for 4 h after which the solution was reduced on a rotary evaporator. After redissolving in minimum H_2O a concentrated aqueous NH_4PF_6 solution was added. The orange precipitate was filtered, dried *in vacuo* and purified on an alumina column using MeCN as mobile phase. Yield 0.33 g, 0.38 mmol, 75%. ^{1}H NMR (d₃-MeCN, 298 K) δ 8.40 (d), 7.99 (dd), 6.51 (d), 7.32 (dd).

$[Ru(bpy)(Me_2bpy)_2](PF_6)_2$

$[Ru(bpy)Cl_3].xH_2O$ (1.0 g, 2.5 mmol) was dissolved in DMF (40 ml). The solution was heated under Ar and Me_2bpy (0.92 g, 5 mmol) was added in two portions over 1 h. The reaction was allowed continue for an additional 4 h. The reaction solution was reduced to dryness. The red compound was dissolved in 10 ml H_2O and a concentrated aqueous NH_4PF_6 solution added. The orange precipitate was filtered, dried *in vacuo* and purified on an alumina column using MeCN as mobile phase. Yield 1.63 g, 1.78 mmol, 71%.

3.7.2   [Ru(DMSO)₄Cl₂] Method

[Ru(bpy)(DMSO)₂Cl₂]

[Ru(DMSO)$_4$Cl$_2$] (0.48 g, 1.0 mmol) was dissolved in CHCl$_3$ (100 ml). Bpy (0.16 g, 1.0 mmol) was added and the solution was heated at reflux for 1 h under N$_2$ and in reduced light. The solution was filtered through a sintered glass crucible. The filtrate was evaporated to dryness to yield a black waxy solid. This was dissolved in acetone (5 ml) to which diethyl ether (20 ml) was added. The resulting precipitate was filtered under N$_2$ to yield a light brown solid. The solid was washed several times with diethyl ether. Yield 0.3 g, 0.62 mmol, 62%. ^{1}H NMR (CDCl$_3$, 298 K) δ 9.88 (d), 9.71 (d), 8.20 (d), 8.05 (d), 7.92 (t), 7.63 (t), 7.52 (t), 7.47 (t), 3.58 (s, 3H), 3.56 (s, 3H), 3.53 (s, 3H), 3.22 (s, 3H).

[Ru(Me₂bpy)(DMSO)₂Cl₂]

The same procedure as above was followed. [Ru(DMSO)$_4$Cl$_2$] (0.48 g, 1.0 mmol) reacted with Me$_2$bpy (0.18 g, 1.0 mmol) to yield [Ru(Me$_2$bpy)(DMSO)$_2$Cl$_2$]. Yield 0.21 g, 0.4 mmol, 40%. ^{1}H NMR (CDCl$_3$, 298 K) δ 9.69 (d), 9.50 (d), 8.00 (s), 7.96 (s), 7.42 (d), 7.26 (d), 3.57 (s, 3H), 3.55 (s, 3H), 3.52 (s, 3H), 3.21 (s, 3H), 2.58 (s, 3H), 2.53 (s, 3H).

[Ru(bpy)(Me₂bpy)Cl₂]

It should be noted that this complex was only observed by UV and not isolated. [Ru(Me$_2$bpy)(DMSO)$_2$Cl$_2$] and bpy were dissolved in DMF (30 ml) and heated at reflux for 6 h under Ar. A UV of the reaction solvent showed the presence of two bands at 480 and 547 nm after 2 h. After 6 h the reaction was allowed cool, filtered and poured into acetone (200 ml). This mixture was allowed stand overnight at −4°C. No precipitate was observed after this time.

[Ru(bpy)(Me₂bpy)₂](PF₆)₂

[Ru(bpy)(DMSO)$_2$Cl$_2$] (0.2 g, 0.4 mmol) and Me$_2$bpy (0.18 g, 1 mmol) were refluxed in EtOH/H$_2$O (1/1, 40 ml) for 4 h under reduced light. The red solution was then reduced by rotary evaporation. The remaining solid was dissolved in minimum H$_2$O and filtered into a saturated aqueous NH$_4$PF$_6$ solution. The resulting precipitate was filtered and recrystallised from acetone/water to yield red

crystals. These crystals were further recrystallised from MeCN/diethyl ether to yield red micro-crystals. Yield 0.28 g, 0.3 mmol, 75%.

3.7.3 Decarbonylation Method

[Ru(bpy)(CO)$_2$(CF$_3$SO$_3$)$_2$]

[Ru(bpy)(CO)$_2$Cl$_2$] (0.85 g, 2.2 mmol) in 200 ml 1,2-dichlorobenzene was purged with Ar for 20 min. A 0.5-ml aliquot of freshly opened CF$_3$SO$_3$H was added through a septum. The solution was heated at 100°C for 1.5 h. The solution was then cooled to 0°C and 200 ml diethyl ether was added. The milky white solution was placed in a fridge for 1 h and then filtered under N$_2$ leaving a creamy white solid. This was washed with diethyl ether, water and finally diethyl ether. Yield 0.79 g, 1.3 mmol, 59%. ^{1}H NMR (d$_6$-DMSO, 298 K); δ 8.97 (d), 8.79 (t), 8.65 (t), 8.62 (d), 8.59 (t), 8.41 (t), 8.01 (d), 7.80 (d).

[Ru(Me$_2$bpy)(CO)$_2$(CF$_3$SO$_3$)$_2$]

[Ru(Me$_2$bpy)(CO)$_2$Cl$_2$] (0.73 g, 1.8 mmol) in 200 ml 1,2-dichlorobenzene was sparged with Ar for 30 min. A 0.5-ml aliquot of freshly opened CF$_3$SO$_3$H was added through a septum. The solution was heated at 100°C for 1.5 h. The solution was then cooled to 0°C and 200 ml diethyl ether was added. The milky white solution was placed in a fridge for 1 h and then filtered under N$_2$ leaving a creamy white solid. This was washed with diethyl ether, water and finally diethyl ether. Yield 0.70 g, 1.1 mmol, 62%. ^{1}H NMR (d$_6$-DMSO, 298 K); δ 8.77 (d), 8.75 (s), 8.69 (s), 8.54 (d), 7.96 (d), 7.64 (d), 2.65 (s, 3H), 2.59 (s, 3H).

[Ru(bpy)$_2$(CO)$_2$](PF$_6$)$_2$

Method 1:

[Ru(bpy)(CO)$_2$(CF$_3$SO$_3$)$_2$] (0.2 g, 0.33 mmol) and bpy (0.06 g, 0.38 mmol) were dissolved in EtOH (50 ml). The solution was heated at reflux under N$_2$ and a colour change from colourless to yellow occurred. After 2 h the solvent was removed by rotary evaporation. The remaining solid was dissolved in H$_2$O,

filtered and added to a saturated aqueous solution of NH_4PF_6. The slightly yellow precipitate was filtered, washed with H_2O and allowed dry under vacuum. Yield 0.18 g, 0.24 mmol, 72%. ^1H NMR (d_6-DMSO, 298 K); δ 9.48 (d), 9.02 (d), 8.84 (d), 8.79 (d), 8.48 (t), 8.34 (t), 8.02 (t), 7.70 (t). IR (MeCN): 2100 and 2051 cm^{-1}.

Method 2:

[Ru(bpy)(CO)$_2$Cl$_2$] (1.0 g, 2.6 mmol) and bpy (0.5 g, 3.2 mmol) were heated at reflux in EtOH/H$_2$O (2:1, 50 ml) solution under N$_2$ for 5 h. The yellow solution was then reduced by rotary evaporation and the remaining solid dissolved in H$_2$O, filtered and added to a saturated aqueous solution of NH$_4$PF$_6$. The slightly yellow precipitate was filtered, washed with H$_2$O and allowed dry under vacuum. Yield 1.59 g, 2.1 mmol, 80%. ^1H NMR (d_6-DMSO, 298 K); δ same as above. IR data same as above.

[Ru(Me₂bpy)(bpy)(CO)₂](PF₆)₂

Method 1:

[Ru(Me$_2$bpy)(CO)$_2$(CF$_3$SO$_3$)$_2$] (0.2 g, 0.31 mmol) and bpy (0.05 g, 0.35 mmol) were dissolved in EtOH (50 ml). The solution was heated at reflux under N$_2$ and a colour change from colourless to yellow occured. After 2 h the solvent was removed by rotary evaporation. The remaining solid was dissolved in H$_2$O, filtered and added to a saturated aqueous solution of NH$_4$PF$_6$. The slightly yellow precipitate was filtered, washed with H$_2$O and allowed dry under vacuum. Yield 0.17 g, 0.2 mmol, 67%. ^1H NMR (d_3-acetone, 298 K); δ 9.50 (d), 9.29 (d), 8.95 (d), 8.82 (d), 8.81 (s), 8.65 (s), 8.62 (t), 8.39 (t), 8.12 (t), 7.95 (d), 7.82 (d), 7.70 (t), 7.65 (d), 7.50 (d), 2.76 (s, 3H), 2.54 (s, 3H). IR (MeCN): 2099 and 2047 cm^{-1}.

Method 2:

[Ru(Me$_2$bpy)(CO)$_2$Cl$_2$] (1.0 g, 2.4 mmol) and bpy (0.57 g, 3.7 mmol) were heated at reflux in EtOH/H$_2$O (2:1, 50 ml) solution under N$_2$ for 5 h. The yellow solution was then reduced by rotary evaporation and the remaining solid dissolved in H$_2$O,

filtered and added to a saturated aqueous solution of NH$_4$PF$_6$. The slightly yellow precipitate was filtered, washed with H$_2$O and allowed dry under vacuum. Yield 1.55 g, 1.97 mmol, 82%. ^{1}H NMR (d$_6$-DMSO, 298 K); δ same as above. IR data same as above.

[Ru(bpy)(phen)(CO)$_2$](PF$_6$)$_2$

[Ru(bpy)(CO)$_2$Cl$_2$] (1.0 g, 2.6 mmol) and phen (0.72 g, 4.0 mmol) were heated at reflux in 50 ml of a EtOH/H$_2$O (2:1) solution under N$_2$ for 5 h. The yellow solution was then reduced by rotary evaporation and the remaining solid dissolved in H$_2$O, filtered and added to a saturated aqueous solution of NH$_4$PF$_6$. The slightly yellow precipitate was filtered, washed with H$_2$O and allowed dry under vacuum. Yield 0.78 g, 1 mmol, 40%. ^{1}H NMR (d$_3$-acetone, 298 K); δ 9.94 (d), 9.63 (d), 9.28 (d), 9.01 (t), 8.83 (d), 8.70 (t), 8.54 (d), 8.49 (t), 8.48 (d), 8.30 (t), 8.26 (d), 8.19 (t), 8.02 (dd), 7.74 (d), 7.48 (t).

3.7.4   Photosubstitution Method

[Ru(Me$_2$bpy)(bpy)(CH$_3$CN)$_2$](PF$_6$)$_2$

[Ru(Me$_2$bpy)(bpy)(CO)$_2$](PF$_6$)$_2$ (0.5 g, 0.64 mmol) was dissolved in HPLC grade MeCN (Ar purged) and placed in a photolysis cell. The solution was irradiated with light using a 400 W medium pressure Hg lamp with continous stirring and with a constant stream of N$_2$ through the solution. After 3 h HPLC confirmed the presence of only one species. The solution was removed by rotary evaporation to leave a red glassy solid. Yield 0.49 g, 0.6 mmol, 94%. ^{1}H NMR (d$_3$-MeCN, 298 K); δ 9.32 (d), 9.12 (d), 8.51 (d), 8.39 (s), 8.37 (d), 8.27 (t), 8.25 (s), 7.95 (t), 7.85 (t), 7.70 (d), 7.60 (d), 7.41 (d), 7.28 (t), 7.10 (d). Elemental Analysis for C$_{26}$H$_{26}$F$_{12}$N$_6$P$_2$Ru: Calc.   C 38.39,   H 3.22,   N 10.33,   Found   C   38.18, H 2.91, N 9.90.

[Ru(bpy)(MeCN)$_2$Cl$_2$]/[Ru(bpy)(MeCN)$_3$Cl]Cl

[Ru(bpy)(CO)$_2$Cl$_2$] (0.5 g, 1.3 mmol) was dissolved in 250 ml MeCN and placed in an immersion well with a stirring bar. The solution was sparged with Ar for 15

min before photolysis commenced. After 1 h the solution was reduced *in vacuo* yielding a dark red product. Yield (0.42 g).

[Ru(bpy)$_2$Cl$_2$]

[Ru(bpy)(MeCN)$_2$Cl$_2$]/[Ru(bpy)(MeCN)$_3$Cl]Cl, (0.2 g) and bpy (0.1 g, 0.64 mmol) were refluxed in CHCl$_3$ for 3 h. The purple red solution was reduced to 5 ml and 50 ml acetone was added. The solution was place in a freezer overnight and the precipitate was then filtered and washed with acetone. Yield 0.83 g, 1.7 mmol. ^{1}H NMR (d$_6$-DMSO, 298 K); δ 9.98 (d), 8.36 (d), 8.47 (d), 8.07 (t), 7.78 (t), 7.68 (t), 7.52 (d), 7.11 (t).

[Ru(bpy)(Me$_2$bpy)Cl$_2$]

[Ru(bpy)(MeCN)$_2$Cl$_2$]/[Ru(bpy)(MeCN)$_3$Cl]Cl, (0.4 g) and Me$_2$bpy (0.2 g, 1.1 mmol) were refluxed in CHCl$_3$ for 3 h. The solution was worked up as for above. Yield 0.16 g, 0.3 mmol. ^{1}H NMR (d$_6$-DMSO, 298 K); δ 9.99 (d), 9.76 (d), 8.61 (d), 8.50 (s), 8.45 (d), 8.35 (s), 8.03 (t), 7.76 (t), 7.63 (t), 7.61 (d), 7.54 (d), 7.29 (d), 7.10 (t), 6.94 (d), 2.62 (s), 2.34 (s). Elemental Analysis for C$_{22}$H$_{20}$Cl$_2$N$_4$Ru: Calc. C 51.57, H 3.93, N 10.93, Found C 51.90, H 3.90, N 10.99.

[Ru(Me$_2$bpy)(bpy)(pytrz)](PF$_6$)

[Ru(Me$_2$bpy)(bpy)Cl$_2$] (0.13 g, 0.25 mmol) and Hpytrz (44 mg, 0.3 mmol) were refluxed in 30 ml EtOH/H$_2$O (4:1) for 3 h. The solution was then allowed cool, filtered and reduced by rotary evaporation. The remaining solid was dissolved in 5 ml H$_2$O and filtered into a saturated aqueous NH$_4$PF$_6$ solution. The precipitate was filtered. The product was purified by column chromatography using alumina and a MeCN/H$_2$O/KNO$_3$ mobile phase (80:19:1). One product eluted with MeCN and the other with MeOH. Yield (total) 0.15 g, 0.2 mmol, 80%). Elemental Analysis for C$_{29}$H$_{25}$F$_6$N$_8$PRu: Calc. C 47.61, H 3.44, N 15.32, Found C 47.71, H 3.37, N 15.48.

3.8   Bibliography

[1]   Juris A., Balzani V., Barigelletti F., Campagna S., Belser P., von Zelewsky A., *Coord. Chem. Rev.*, **1988**, *84*, 85–277.

[2]   Kalayanasundaram K., *Coord. Chem. Rev.*, **1982**, *46*, 159-244.

[3]   Balzani V., Scandola F., Supramolecular Photochemistry; Ellis Horwood: Chichester, England, **1991**.

[4]   Balzani V., Juris A., Venturi M., *Chem. Rev.*, **1996**, *96*, 759–833.

[5]   Thummel R.P., Lefoulon F., Chirayil S., *Inorg. Chem.*, **1987**, *26*, 3072–3074.

[6]   Hesek D., Inoue Y., Everitt S.R.L., Ishida H., Kunieda M., Drew M.G., *Inorg. Chem.*, **2000**, *39*, 308–316.

[7]   Zakeeruddin S.M., Nazeeruddin Md.K., Humphry-Baker R., Grätzel M., Shklover V., *Inorg. Chem.*, **1998**, *37*, 5251–5259.

[8]   Maxwell K.A., Sykora M., DeSimone J.M., Meyer T.J., *Inorg. Chem.*, **2000**, *39*, 71–75.

[9]   Anderson P.A., Strouse G.F., Treadway J.A., Keene F.R., Meyer T.J., *Inorg. Chem.*, **1994**, *33*, 3863–3864.

[10]   Anderson P.A., Deacon G.B., Haarmaan K.H., Keene F.R., Meyer T.J., Reitsma D.A., Skelton B.W., Strouse G.F., Thomas N.C., Treadway J.A., White A.H., *Inorg. Chem.*, **1995**, *34*, 6145–6157.

[11]   Von Zelewsky A., Gremaud G., *Helv. Chim. Acta*, **1988**, *71*, 1108–1115.

[12]   Freedman D.A., Evju J.K., Pomije M.K., Mann K.R., *Inorg. Chem.*, **2001**, *40*, 5711–5715.

[13]   Krause R.A., *Inorg. Chim. Acta*, **1977**, *22*, 209–213.

[14]   Black D.St.C., Deacon G.B., Thomas N.C., *Inorg. Chim. Acta*, **1982**, *65*, L75–L76.

[15]   Black D.St.C., Deacon G.B., Thomas N.C., *Inorg. Chim. Acta*, **1981**, *54*, L143–L144.

[16]   Strouse G.F., Anderson P.A., Schoonover J.R., Meyer T.J., Keene F.R., *Inorg. Chem.*, **1992**, *31*, 3004–3006.

[17]   Anderson P.A., Strouse G.F., Treadway J.A., Keene F.R., Meyer T.J., *Inorg. Chem.*, **1994**, *33*, 3863–3864.

[18]   Black D.St.C., Deacon G.B., Thomas N.C., *Aust. J. Chem.*, **1982**, *35*, 2445–2453.

[19]   Black D.St.C., Deacon G.B., Thomas N.C., *Polyhedron*, **1983**, *2*, 409–412.

[20]   Heeg M.J., Kroener R., Deutsch E., *Acta Cryst.*, **1985**, *C41*, 684–686.

[21]   Eskelinen E., Haukka M., Venäläinen T., Pakkanen T.A., Wasberg M., Chardon-Noblat S., Deronzier A., *Organometallics*, **2000**, *19*, 163–169.

[22]   Collomb-Dunard-Sauthier M.-N., Deronzier A., Ziessel R., *J. Organometal. Chem.*, **1993**, *444*, 191–198.

[23]   O'Connor C.M., Synthesis and characterisation of novel Ru(II) complexes with selective deuteration, Ph.D. Dissertation, Dublin City University, **1999**.

[24]   Hage R., Ruthenium and osmium complexes containing triazole ligands: syntheses, structures, electrochemical and photophysical properties, Ph.D. Dissertation, Leiden University, The Netherlands, **1991**.

[25]   Miller J.M., Balasanmugam K., Nye J., Deacon G.B., *Inorg. Chem.*, **1987**, *26*, 560–562.

[26]   Liang X., Suwanrumpha S., Freas R.B., *Inorg. Chem.*, **1991**, *30*, 652–658.

[27]   Cerny R.L., Sullivan B.P., Bursey M.M., Meyer T.J., *Inorg. Chem.*, **1985**, *24*, 397–401.

[28]   Bignozzi C.A., Bortolini O., Curcuruto O., Hamdan M., *Inorg. Chim. Acta*, **1995**, *233*, 113–118.

Chapter 4.

Mononuclear Tris(heteroleptic) Complexes

Using the successful synthetic method of Chapter 3, a series of mononuclear complexes are synthesised using both pyridyl- and pyrazyl-triazole ligands. All the complexes are characterised and examined for their photophysical and electrochemical properties. The different properties of bpt⁻ and bpzt⁻ ruthenium complexes are examined.

4.1 Introduction

Chapter 3 described a successful synthetic method which incorporated a triazole ligand into a Ru(II) tris(heteroleptic) complex. The following chapter develops this strategy to synthesise a number of mononuclear complexes using the ligands illustrated in Fig. 4.1. In each case bpy and a triazole are used, together with either Me_2bpy, phen or dpp. The two types of triazole ligands discussed in Chapter 1, pyridine triazole and pyrazine triazole, are used so the differences between these ligands can be further investigated. The structures and abbreviations for the ligands cited in this chapter are shown in Fig. 4.1.

2,2'-dipyridyl

(bpy)

4,4'-dimethyl-2,2'-dipyridyl

(Me2bpy)

1,10'-phenanthroline

(phen)

4,7'-diphenyl-1,10'-phenanthroline

(dpp)

3,5-di(pyridin-2-yl)-1,2,4-triazole

(Hbpt)

3,5-di(pyrizin-2-yl)-1,2,4-triazole

(Hbpzt)
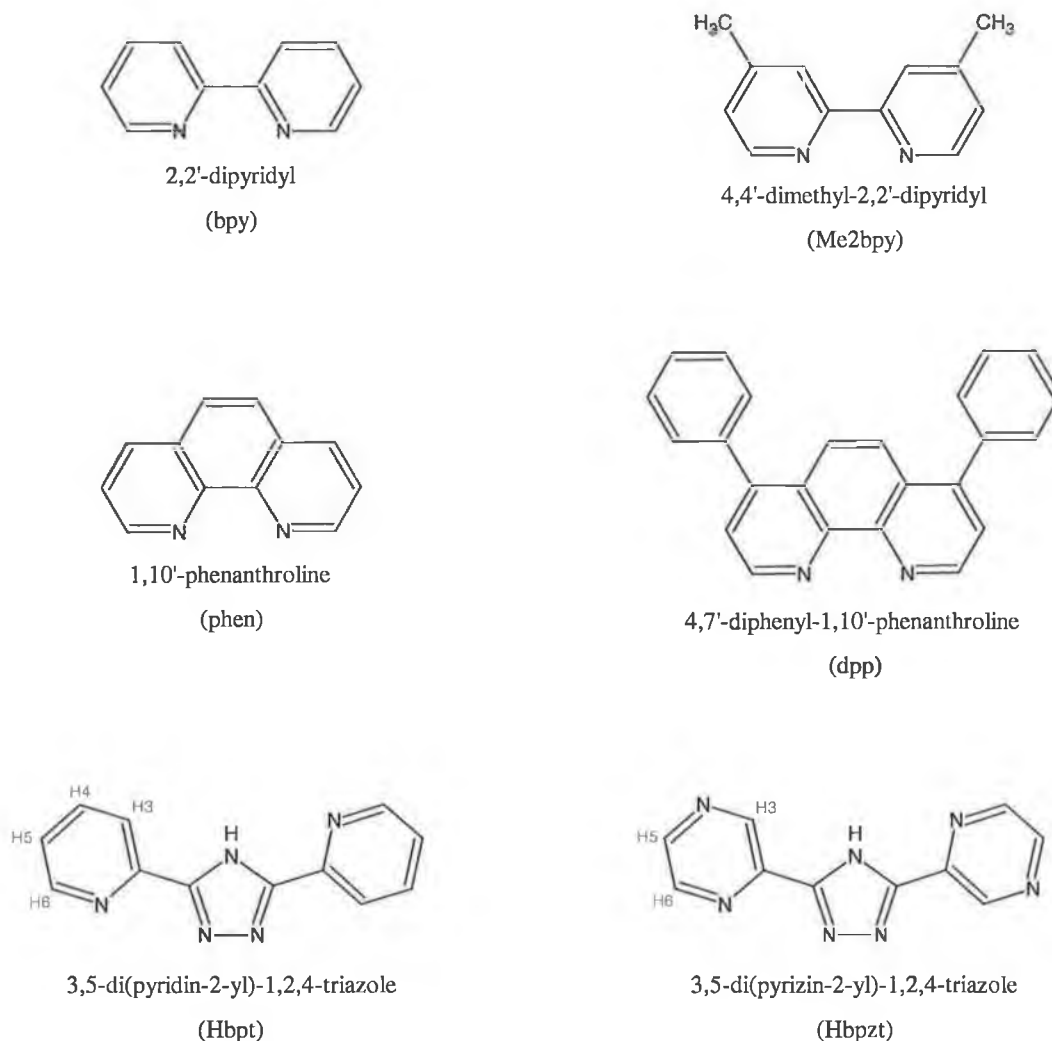
Figure 4.1. Structures of ligands and their abbreviations as cited throughout this chapter. For full names see ligand abbreviations on page x.

4.2   Synthesis of Ru(II) dichlorides

The synthetic method employed in the successful preparation and isolation of [Ru(bpy)(Me$_2$bpy)Cl$_2$] in Chapter 3 also yielded [Ru(bpy)(phen)Cl$_2$] and [Ru(bpy)(dpp)Cl$_2$]. Both of these complexes were obtained by heating the photolysis mixture [Ru(bpy)(MeCN)$_3$Cl]Cl and [Ru(bpy)(MeCN)$_2$Cl$_2$] from Chapter 3 with the respective second ligands. These dichlorides were prepared in dry acetone and no further purification was usually necessary other than washing with cold acetone after filtering. On occasion, the dichlorides were not isolated adequately pure as was observed by ^{1}H NMR. This was simply remedied by stirring the complex in a little cold DMF and filtering. Although, the complexes are quite soluble in DMF, the impurities were found to be more so and could thus be removed. The dichlorides were never isolated in the dark purple microcrystalline form of [Ru(bpy)$_2$Cl$_2$] but as a purple powder.
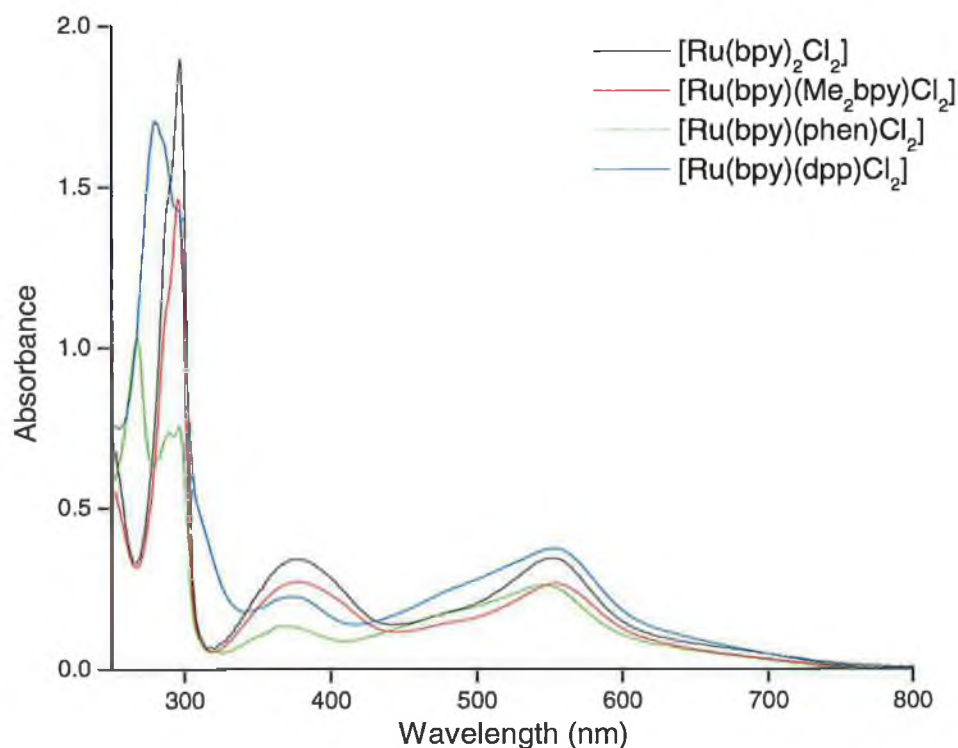
***Figure 4.2.** UV spectra of the dichloride precursors in MeCN.*

118

Fig. 4.2 shows the UV spectra obtained in MeCN for the three dichloride precursors to be used in this chapter. [Ru(bpy)$_2$Cl$_2$] has been included for comparison. Table 4.1 shows the λ_{max} values for the various peaks obtained.

Table 4.1. The λ_{max} in MeCN for dichloride precursors.

λ_{max} (nm)			
[Ru(bpy)$_2$Cl$_2$]	[Ru(bpy)(Me$_2$bpy)Cl$_2$]	[Ru(bpy)(phen)Cl$_2$]	[Ru(bpy)(dpp)Cl$_2$]
552	554	545	554
378	378	369	375
297	296	296	281
		291	
		268	

It is clear that both [Ru(bpy)$_2$Cl$_2$] and [Ru(bpy)(Me$_2$bpy)Cl$_2$] exhibit similar electronic transitions as both give similar spectra with comparable λ_{max} values. The phenanthroline based complexes [Ru(bpy)(phen)Cl$_2$] and [Ru(bpy)(dpp)Cl$_2$] show a much broader MLCT transition at 545 and 554 nm respectively. At higher energy a new π–π^* transition is visible. This is attributable to phen (π–π^*) at 268 nm and dpp (π–π^*) at 281 nm. In both cases the bpy (π–π^*) is still visible albeit just as a shoulder for [Ru(bpy)(dpp)Cl$_2$].

^{1}H NMR spectra of the two complexes [Ru(bpy)(phen)Cl$_2$] and [Ru(bpy)(dpp)Cl$_2$] are shown in Fig. 4.3. As was shown in Fig. 3.17b, two sets of resonances are observed between 10.0 and 10.4 ppm. Unlike [Ru(bpy)$_2$Cl$_2$] (Fig. 3.17a), the two new dichlorides, [Ru(bpy)(phen)Cl$_2$] and [Ru(bpy)(dpp)Cl$_2$], have two different ligands sitting over a Cl atom. This causes a large downfield shift for one of the H6 protons on each polypyridyl ligand. This is illustrated in the ^{1}H NMR of [Ru(bpy)(Me$_2$bpy)Cl$_2$] in Fig. B3, Appendix B. When assigning the peaks of the ^{1}H NMR it is important to distinguish between the two rings of each polypyridyl ligand. For further discussion on this matter see Appendix B. As the spectra are more complicated than that of [Ru(bpy)$_2$Cl$_2$], 2D COSY experiments in d$_6$-DMSO were carried out and the results illustrated in Fig. B.4 and Fig. B.5.

(a)

(b)
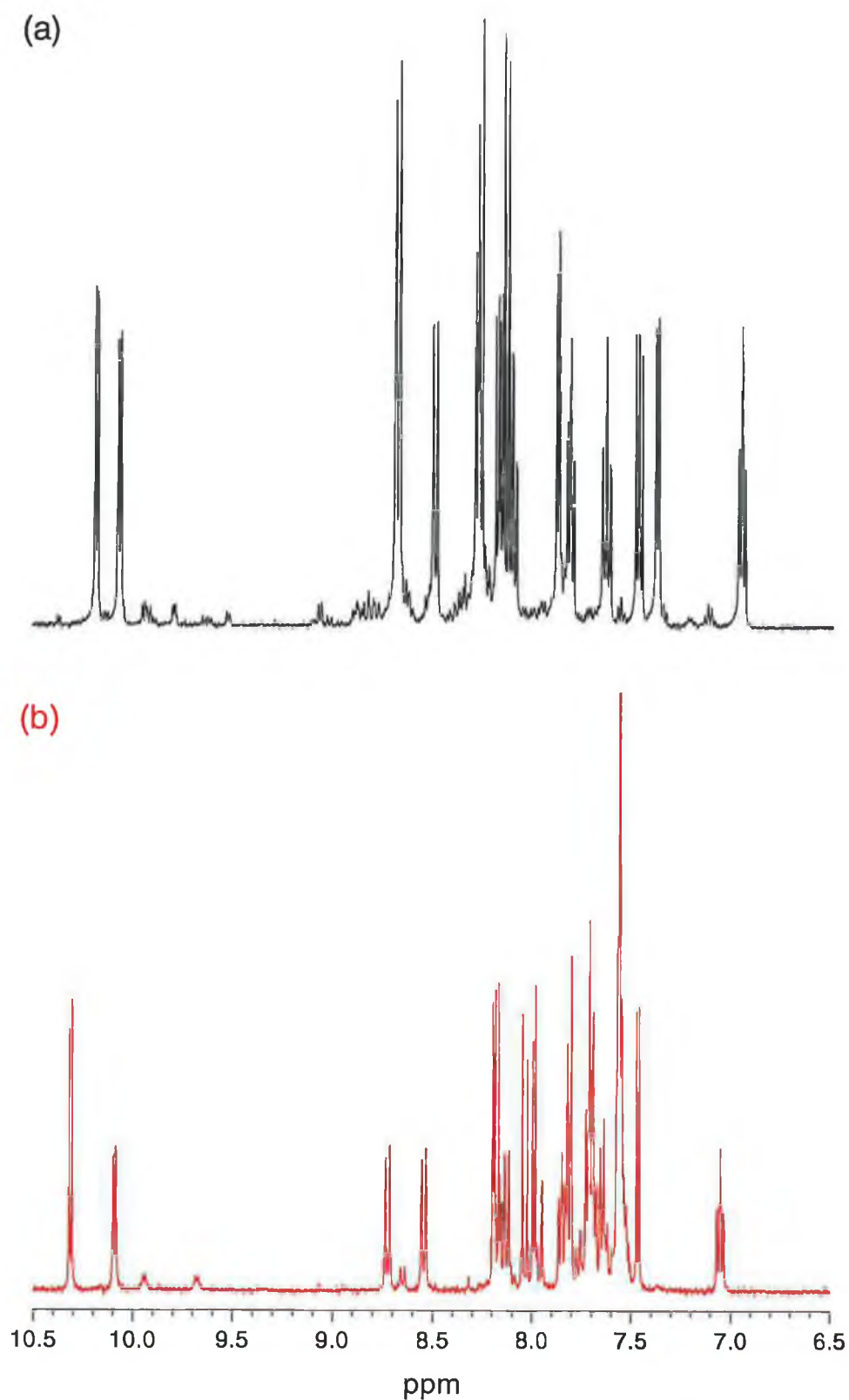
Figure 4.3. *^1H NMR spectra of aromatic region of (a) [Ru(bpy)(phen)Cl$_2$] and (b) [Ru(bpy)(dpp)Cl$_2$] in d$_6$-DMSO.*

4.3 Synthesis of tris(heteroleptic) mononuclear complexes

The three dichlorides [Ru(bpy)(Me$_2$bpy)Cl$_2$], [Ru(bpy)(phen)Cl$_2$] and [Ru(bpy)(dpp)Cl$_2$] were reacted with the two bridging ligands Hbpt and Hbpzt to form six new tris(heteroleptic) complexes. The procedure used was similar to that previously described by Hage [1]. In each case the dichloride was reacted with excess bridging ligand to reduce the possibility of dinuclear complexes forming. The reaction times were sufficient to allow the complete reaction of the dichloride (as monitored by TLC and HPLC). Column chromatography allowed the removal of excess ligand and purification of the desired complex. After removal of the reaction solvent, the product was columned on a silica column using MeCN/H$_2$O (80:20) with 0.05 M KNO$_3$ mobile phase. The product was easily identifiable as the main band on the column. It eluted usually as the first band, although sometimes a fainter red band was seen to elute first. After removal of the mobile phase the complexes were dissolved in minimum H$_2$O, a drop of ammonia solution added, followed by the addition of saturated aqueous NH$_4$PF$_6$ solution. Occasionally it was found that some product was difficult to redissolve in H$_2$O. In these cases, a drop of acetone was added. Addition of NH$_3$ ensures that the complex is isolated as the deprotonated species. After adding to an aqueous solution of NH$_4$PF$_6$, the precipitate is filtered, washed with copious H$_2$O to remove excess NH$_4$PF$_6$ and then dried *in vacuo*. If further purification was required, the complex was passed down a second alumina column using MeCN as mobile phase. The product was recovered as the first fraction in these cases.

The alumina column was found to work best in separating mononuclear complexes, dimers and free ligand. TLC analysis shows that the free ligand (triazole) remains unmoved at the top of the column whereas mononuclear complexes and dimers elute relatively easily (in that order). However, if any unreacted dichloride species was present, the MeCN/H$_2$O with KNO$_3$ on silica system worked best for separations. As this system was found to work best for chloride salts, it was used on the product obtained directly from the reaction. After purification the complex was isolated as the PF$_6$ salt, which could then be columned on alumina. This order is important as changing a PF$_6$ to a chloride salt, while possible, is more laborious than the other way round.

4.3.1   HPLC of mononuclear complexes

The purities of the complexes prepared were analysed using cation-exchange chromatography and the results for all the mononuclear complexes are illustrated in Fig. 4.4. All complexes were isolated as their deprotonated species and thus posses a single positive charge. As cation-exchange chromatography discriminates primarily on charge, it is expected that the complexes will have similar retention times.
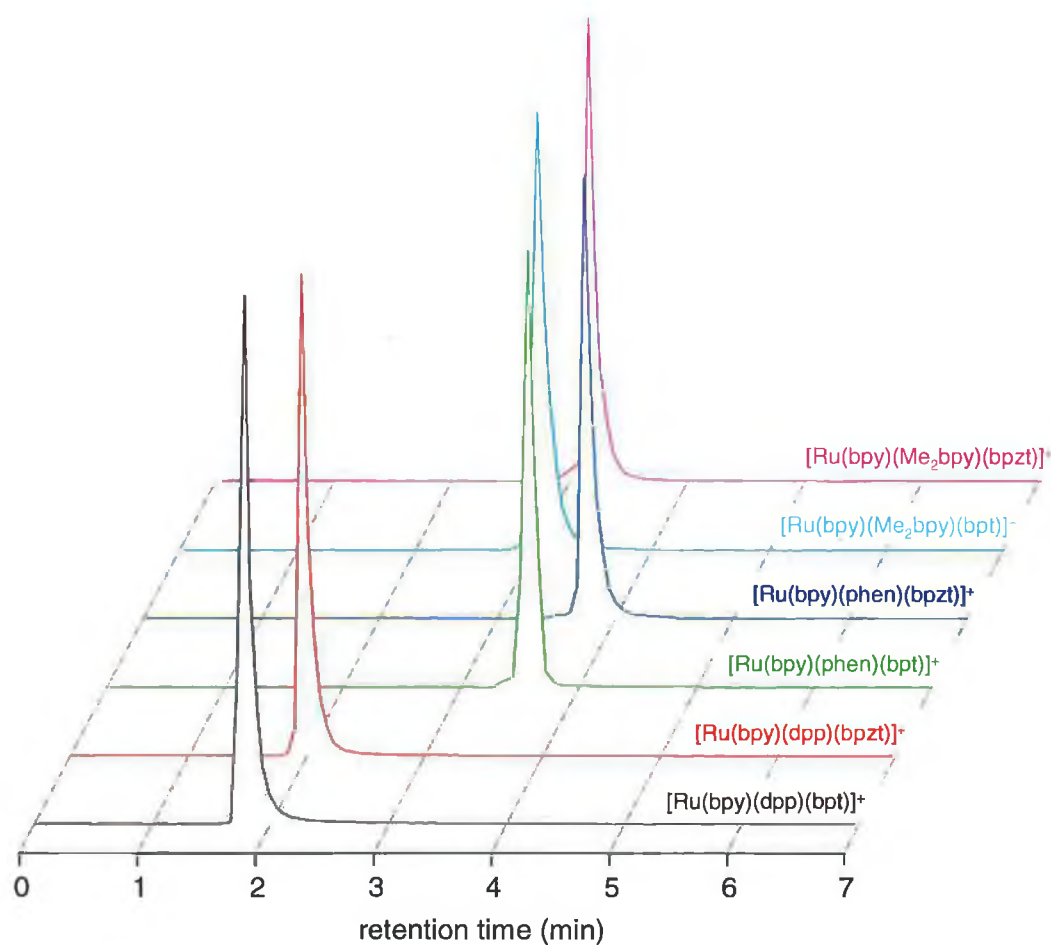
Figure 4.4. *HPLC trace of the tris(heteroleptic) mononuclear complexes. Mobile phase: 0.08 M LiClO₄ in 80/20 MeCN/H₂O using P10SCX-3095 cation exchange column and flow rate 1.5 ml min⁻¹.*

At fast flow rates (2 ml min⁻¹) the complexes elute at similar times but if the flow rate is reduced (1.5 ml min⁻¹), some differences in retention time are observed.

The retention times are tabulated in Table 4.2 below. The biggest difference is with the $[Ru(bpy)(dpp)(bpt)]^+$ and $[Ru(bpy)(dpp)(bpzt)]^+$ complexes. These complexes elute at 1.77 and 1.99 min respectively and elute earliest because they interact least with the column. This is attributed to the phenyl rings, which have a two-fold effect on the complex. Firstly they donate electron density to the metal centre and thus help delocalise the charge of the complex. Secondly, the bulky nature of these groups shields the metal centres from the column and counter-ions in solution. The result is an elution time 1 min shorter than for the other complexes. As expected, the Me_2bpy and phen ligands on the other complexes do not effect the elution times as drastically as the dpp ligand. However a reasonable separation still remains, with $[Ru(bpy)(Me_2bpy)(bpt)]^+$ and $[Ru(bpy)(Me_2bpy)(bpzt)]^+$ eluting at 2.98 and 3.11 min respectively whereas $[Ru(bpy)(phen)(bpt)]^+$ and $[Ru(bpy)(phen)(bpzt)]^+$ remain slightly longer on the column and elute at 3.55 and 3.71 min respectively.

The HPLC was coupled to a UV photodiode array detector that records a UV spectrum every 400 ms. This allows the UV spectrum of each eluting species to be analysed. Using this technique, a cross section of the eluting peak is examined. The peak purity, i.e. if the peak observed constitutes one or more eluting species, can be tested. A UV cross section is taken at different intervals throughout the peak in question and the UV spectra are examined. In all cases, the UV spectra of the peaks in Fig. 4.4 gave identical UV spectra throughout the peak cross section.

Table 4. 2. Retention time and λ_{max} of the absorption spectrum associated with that peak.

Complex	Retention time (min)	λ_{max} of peak (nm)
$[Ru(bpy)(Me_2bpy)(bpt)]^+$	2.98	476
$[Ru(bpy)(Me_2bpy)(bpzt)]^+$	3.11	445
$[Ru(bpy)(phen)(bpt)]^+$	3.55	452
$[Ru(bpy)(phen)(bpzt)]^+$	3.71	455
$[Ru(bpy)(dpp)(bpt)]^+$	1.77	482
$[Ru(bpy)(dpp)(bpzt)]^+$	1.99	460

A UV–visible spectrum could be obtained for each of the complexes studied by HPLC. It should be noted that these spectra are obtained in the HPLC mobile phase and so are useful only as a guide to the species present. Section 4.5 presents a more detailed analysis of the absorption properties for these complexes. The λ_{max} obtained by the HPLC studies suggest that these complexes are indeed mononuclear triazole complexes and not substituted variants of the dichloride precursors.

4.3.2   Mass spectrometry of mononuclear complexes

The complexes were examined using electrospray mass spectrometry. This involves analysing an ionised aerosol of the complex in question. The aerosol is achieved by passing the complex in solution (MeCN) through a fine needle held at 80 eV at 300°C. This is a soft ionisation technique and so fragmentation patterns are not observed for the complexes. Instead the complex remains intact and its molecular weight may be determined. This is in contrast to other techniques used such as fast atom bombardment (FAB) [2] and field desorption (FD) [3] where fragmentation occurs and many peaks are observed for the break up of the complexes.

For the purpose of these discussions the molecular ion will refer to the complex minus one PF_6^- counterion. Fig. 4.5 shows a typical spectrum obtained for the tris(heteroleptic) complexes. The molecular ion (M^+) for $[Ru(bpy)(Me_2bpy)(bpt)]^+$ is clearly visible at 812.4 m/z with the isotopic abundances also shown. Table 4.3 lists the observed and theoretical molecular ions for each complex. Electrospray mass spectrometry normally works by protonating the species being examined and thus the MH^+ peak is observed. Such was the case for the dichloride complexes examined. No such protonation was observed for any of the mononuclear tris(heteroleptic) complexes [4].
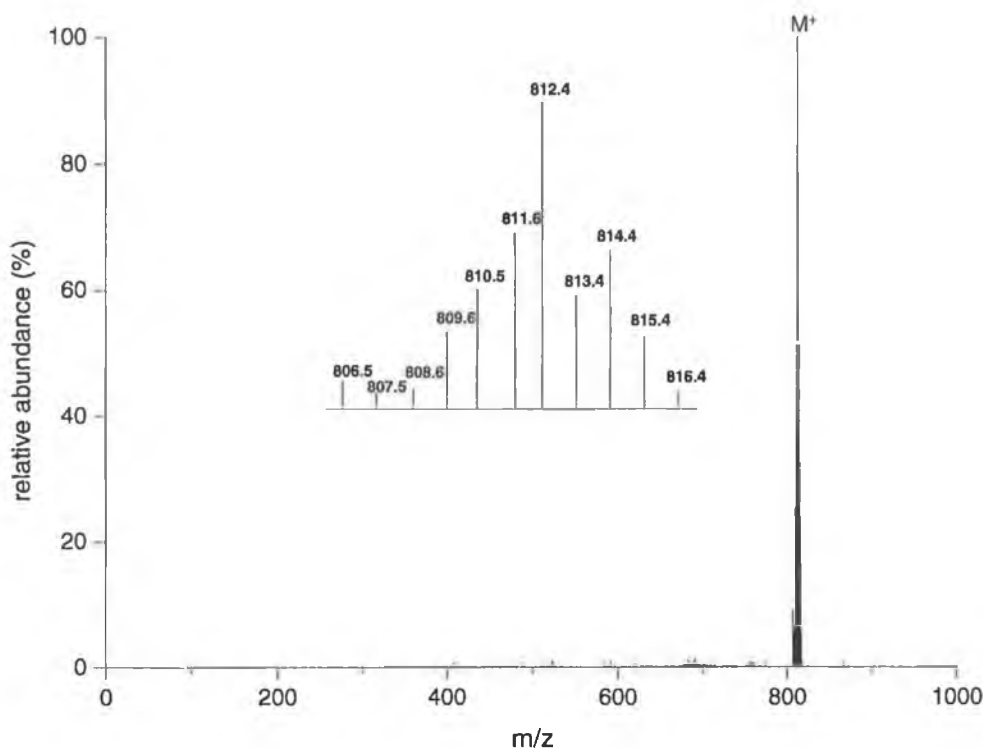
Figure 4.5. *Mass spectrum of [Ru(bpy)(Me₂bpy)(bpt)](PF₆) in MeCN. The isotopic distribution pattern in shown as inset.*

Table 4.3. Observed and theoretical m/z values for the dichloride [Ru(L)(L')Cl₂] and mononuclear tris(heteroleptic) complexes.

Complex	Observed (m/z)	Theoretical (m/z)
[Ru(bpy)(Me₂bpy)Cl₂]H⁺	513	513
[Ru(bpy)(phen)Cl₂]H⁺	509	509
[Ru(bpy)(dpp)Cl₂]H⁺	661	661
[Ru(bpy)(Me₂bpy)(bpt)]⁺	664.4	664.2
[Ru(bpy)(Me₂bpy)(bpzt)]⁺	666.5	666.1
[Ru(bpy)(phen)(bpt)]⁺	660.3	660.1
[Ru(bpy)(phen)(bpzt)]⁺	662.4	662.1
[Ru(bpy)(dpp)(bpt)]⁺	812.4	812.2
[Ru(bpy)(dpp)(bpzt)]⁺	814.4	814.2

As the complexes being examined were synthesised in their deprotonated form, they contained only one PF_6^- counter-ion. The loss of this counter-ion would leave

125

the complex with the required positive charge to enable it to be examined. Any further protonation would yield an electronically unfavourable M^{2+} species. As such, no peaks were observed for any doubly charged complex. In all cases the base peak was also the molecular ion peak. As the experiment progressed the molecular ion was seen to jump in intensity in an irregular fashion. In some cases it vanished altogether. This can be attributed to ion current fluctuations due to irregular bursts of ions through the apparatus. To get an accurate overall reading, an average of 50 scans was taken in each case.

Table 4.4. The seven stable isotopes of Ru and their corresponding relative abundancies.

Ru isotope	Relative abundance (%)
95.9	18
97.9	6
98.9	40
99.9	40
101.9	100
100.9	54
103.9	59

Ruthenium has seven stable isotopes ranging in atomic mass from 95.9 to 103.9 as shown in Table 4.4. The relative abundances of each isotope are also included. These isotopes, coupled with the isotopes present in C and N produce molecular ions with a unique fingerprint for each mononuclear complex. The measured and theoretical values for the isotope patterns for each mononuclear complex are illustrated in Fig. 4.6.
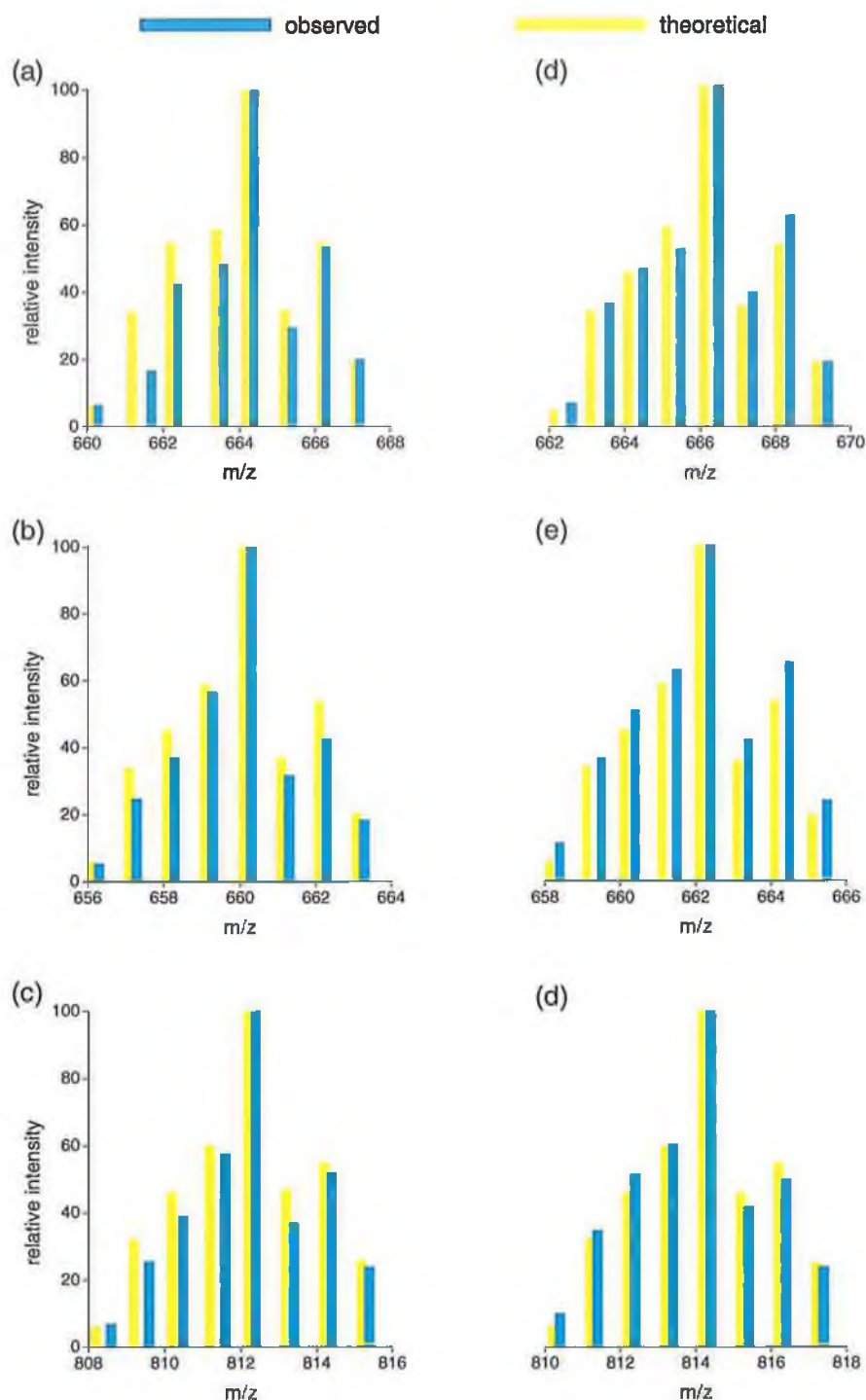
Figure 4.6. *Observed and theoretical isotopic distribution for the bpt⁻ and bpzt⁻ mononuclear tris(heteroleptic) complexes [Ru(bpy)(Me₂bpy)(bpt)]⁺ (a), [Ru(bpy)(phen)(bpt)]⁺ (b), [Ru(bpy)(dpp)(bpt)]⁺ (c) [Ru(bpy)(Me₂bpy)(bpzt)]⁺ (d), [Ru(bpy)(phen)(bpzt)]⁺ (e) and [Ru(bpy)(dpp)(bpzt)]⁺ (f).*

4.3.3 ^{1}H NMR of mononuclear complexes.

The HPLC and mass spectrometry analysis coupled with the CHN results obtained suggest that in each case the complexes have indeed been prepared. The ^{1}H NMR proves to be slightly more difficult to assign as each mononuclear complex has two positional isomers. In one instance, the triazole is opposite a pyridine ring of the bpy. In the other, the triazole is opposite a pyridine ring of the Me$_2$bpy, phen or dpp ligand. Both these isomers are inseparable under the HPLC conditions employed. CHN and mass spectrometry analysis also fail to distinguish the isomers as each gives identical results. However, their NMRs are expected to be different due to the different chemical environments experienced by the protons. An illustration of the two isomers is shown in Fig. 4.7. In each case the triazole ring is *trans* to a different polypyridyl ring, i.e. bpy or Me$_2$bpy.

[Ru(bpy)(Me$_2$bpy)(bpt)]$^+$ *trans*(trz, Me$_2$bpy)   [Ru(bpy)(Me$_2$bpy)(bpt)]$^+$ *trans*(trz, bpy)
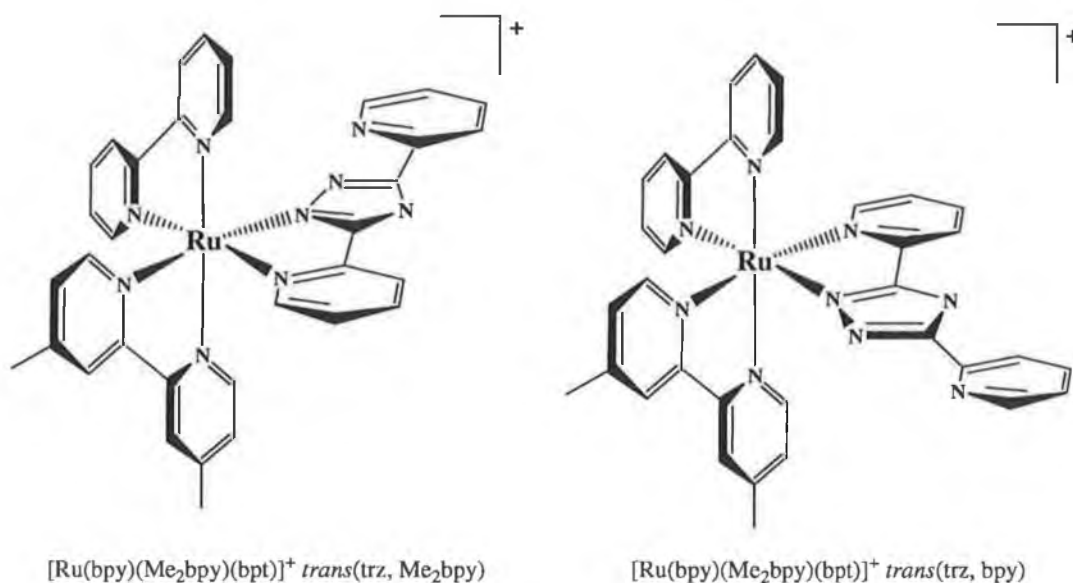
Figure 4.7. The two possible N2 isomers for [Ru(bpy)(Me$_2$bpy)(bpt)]$^+$. For explanation of naming system see Appendix C.

It can be seen that the ^{1}H NMR distinguishes somewhat between the two isomers as shown by Fig. 4.8a. The sample used for this ^{1}H NMR is that used to obtain the HPLC, CHN and mass spectrometry results. Four methyl peaks at 2.46, 2.44 (two

overlapping peaks) and 2.42 ppm are observed. The integrations of the peaks are 1.1, 4.2 and 3.1 respectively. This suggests that the isomers exist in a 1:3 ratio.
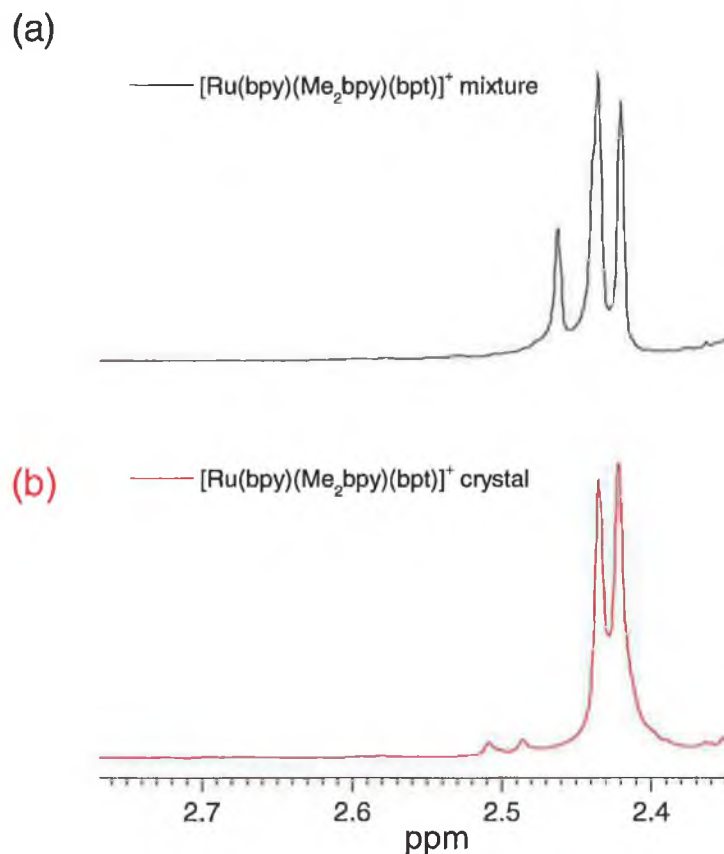
Figure 4.8. *^{1}H NMR of aliphatic region of two samples of [Ru(bpy)(Me$_2$bpy)(bpt)]$^+$ in d$_3$-MeCN. Sample (a) is that of the product after column chromatography. Sample (b) is a recrystallised sample.*

Crystals of this sample were grown from an MeCN/diethyl ether solution. ^{1}H NMR of these crystals gave the spectra shown in Fig. 4.8b and Fig. 4.9. Now only two peaks at 2.44 and 2.42 ppm are observed. Due to the presence of three different bidentate ligands, the aromatic spectrum is still quite complicated. The total integration of the aromatic region is 22, as expected for [Ru(bpy)(Me$_2$bpy)(bpt)]$^+$. The ^{1}H NMR results suggest that the major isomer crystallises more readily under the conditions employed. The structure was

deduced as the *trans*(trz, bpy) isomer from X-ray crystal studies. This will be discussed further in Section 4.3.4.
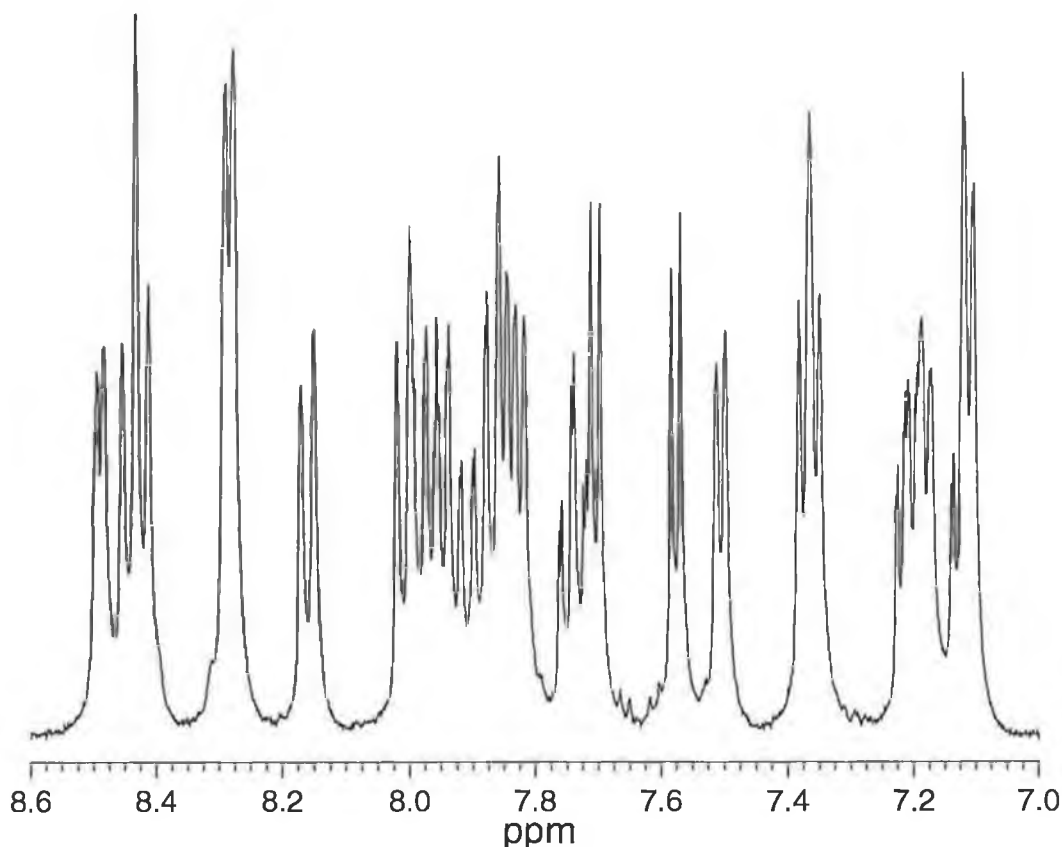
Figure 4.9. *^{1}H NMR of the aromatic region of the crystal sample of [Ru(bpy)(Me$_2$bpy)(bpt)]$^+$ in d$_3$-MeCN.*

The advantage of having a Me$_2$bpy ligand included in the coordination sphere is the presence of the two Me peaks in the ^{1}H NMR spectra. As shown above, the ratio of isomers can be determined and when used in conjunction with crystallographic studies, the actual isomers can be assigned. When phen or dpp is used instead of Me$_2$bpy, the absence of Me peaks makes the ratio determination far more difficult. This was not the case with the bpzt$^-$ mononuclear complexes. Fig. 4.10 below shows the aromatic region of [Ru(bpy)(phen)(bpzt)]$^+$. The most striking difference between the ^{1}H NMR of bpt- and bpzt-type complexes is the large downfield shift of H3 on both the coordinating and noncoordinating pyrazine rings. The presence of the metal centre causes a slightly greater

130

downfield shift of the bound pyrazine (9.30 ppm) than the free pyrazine ring (9.21 ppm). Closer inspection reveals the presence of an additional two smaller peaks alongside the main bpzt⁻ H3 peaks. As the complex was found to be pure by previous studies, these are most likely due to the fact that, like the bpt⁻ analogues, [Ru(bpy)(phen)(bpzt)]⁺ has two isomers. In fact, these peaks allow the ratio determination to be estimated in the same manner as the Me peaks did for [Ru(bpy)(Me₂bpy)(bpt)]⁺ and [Ru(bpy)(Me₂bpy)(bpzt)]⁺. It turns out that the ratio is once again close to 1:3. Unfortunately, no crystals could be grown for this complex to determine which isomer is most abundant.
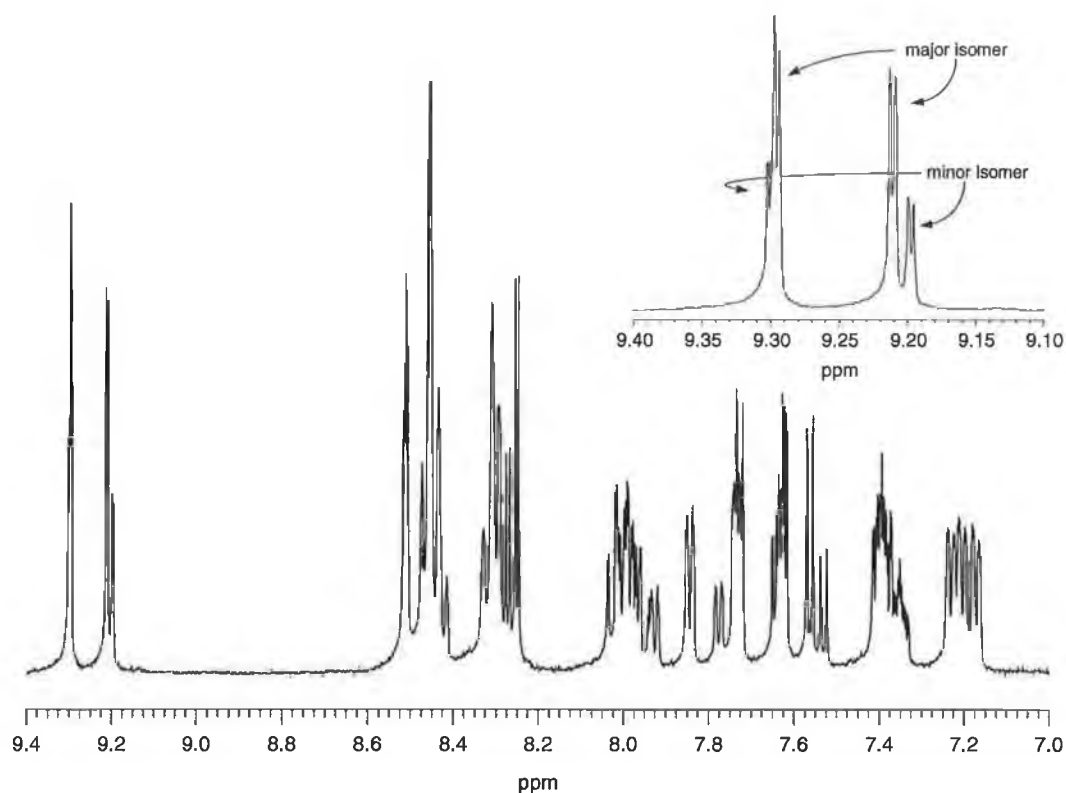
Figure 4.10. *¹H NMR of aromatic region of [Ru(bpy)(phen)(bpzt)]⁺ in d₃-MeCN. The inset shows a close up of the two pyrazine H3 protons.*

131

4.3.4 X-ray crystallography of [Ru(bpy)(Me₂bpy)(bpt)]⁺ and [Ru(bpy)(Me₂bpy)(bpzt)]⁺

Crystals of both bpt⁻ and bpzt⁻ mononuclear complexes were successfully grown by allowing diethyl ether to slowly diffuse with a MeCN solution of the complex. The structure of [Ru(bpy)(Me₂bpy)(bpt)](PF₆).½(C₄H₁₀O) (Fig. 4.11) and [Ru(bpy)(Me₂bpy)(bpzt)](PF₆) (Fig. 4.12) are shown below. The crystallographic parameters and relevant bond angles and distances are included in Tables 4.5 and 4.6. It is clear from these structures that the ruthenium centre binds to the three ligands in an octahedral fashion and *via* N2 of the triazole ring. One PF₆⁻ cation is present in each case, confirming that the triazole deprotonates upon coordination and that the overall charge of the complex +1. It is worth noting that in each case a pyridine ring rather than a Me-pyridine ring is *trans* to the triazole ring. In the case of [Ru(bpy)(Me₂bpy)(bpt)]⁺, the ¹H NMR of the crystals show *trans*(trz, bpy) to be the major isomer in the initial mixed isomer product. However, this cannot be confirmed for [Ru(bpy)(Me₂bpy)(bpzt)]⁺ as only a few crystals were isolated and no ¹H NMR could be carried out. However, with the evidence available for [Ru(bpy)(Me₂bpy)(bpt)]⁺ and the fact that the [Ru(bpy)(Me₂bpy)(bpzt)]⁺ mixed product also showed a ratio of approximately 1:3, it is quite likely that the structure shown in Fig. 4.12 is the major isomer. It must be emphasised that this evidence is not definitive and further ¹H NMR and HPLC studies are required to resolve the matter.

It is not absolutely clear why one isomer would be more favourable than another in these cases. A possible reason is the poorer π-back bonding properties of the Me₂bpy ligand. As the Me groups are electron donating the Me₂bpy ligand has slightly stronger σ-donor and hence weaker π-accepting capabilities. This is observed by the difference of reduction potentials for [Ru(bpy)₃]²⁺ (−1.65 V) and [Ru(Me₂bpy)₃]²⁺ (−1.76 V) versus SCE [5]. Although the difference is small, it might explain why the Me₂bpy orientates itself to be away (i.e. not *trans*) from the electron rich triazole ring.
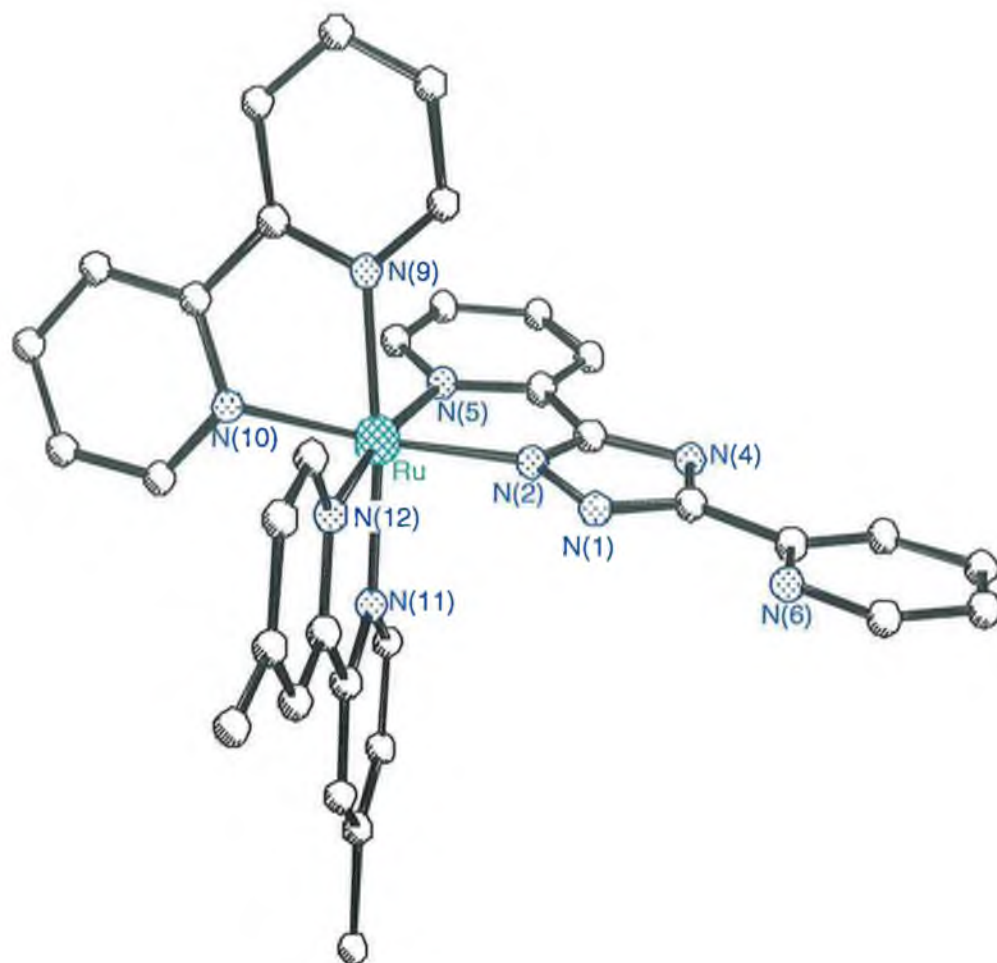
Figure 4.11. *Crystal structure for [Ru(bpy)(Me₂bpy()bpt)]⁺. The PF₆⁻ group, diethyl ether molecule and hydrogen atoms are omitted for reasons of clarity.*

The bond lengths and angles for the structures in Figs. 4.11 and 4.12 are typical of those found for other Ru(II) polypyridyl complexes containing triazoles [1,6,7] and are given in Tables 4.5 and 4.6. The Ru–bpy and Me₂bpy bond lengths are typically in the range of 2.55–2.70 ppm. The Ru–Me₂bpy bonds are generally slightly shorter than the Ru–bpy bonds. These shorter bonds confirm the slightly larger σ-donating capacity of Me₂bpy as discussed above.

133
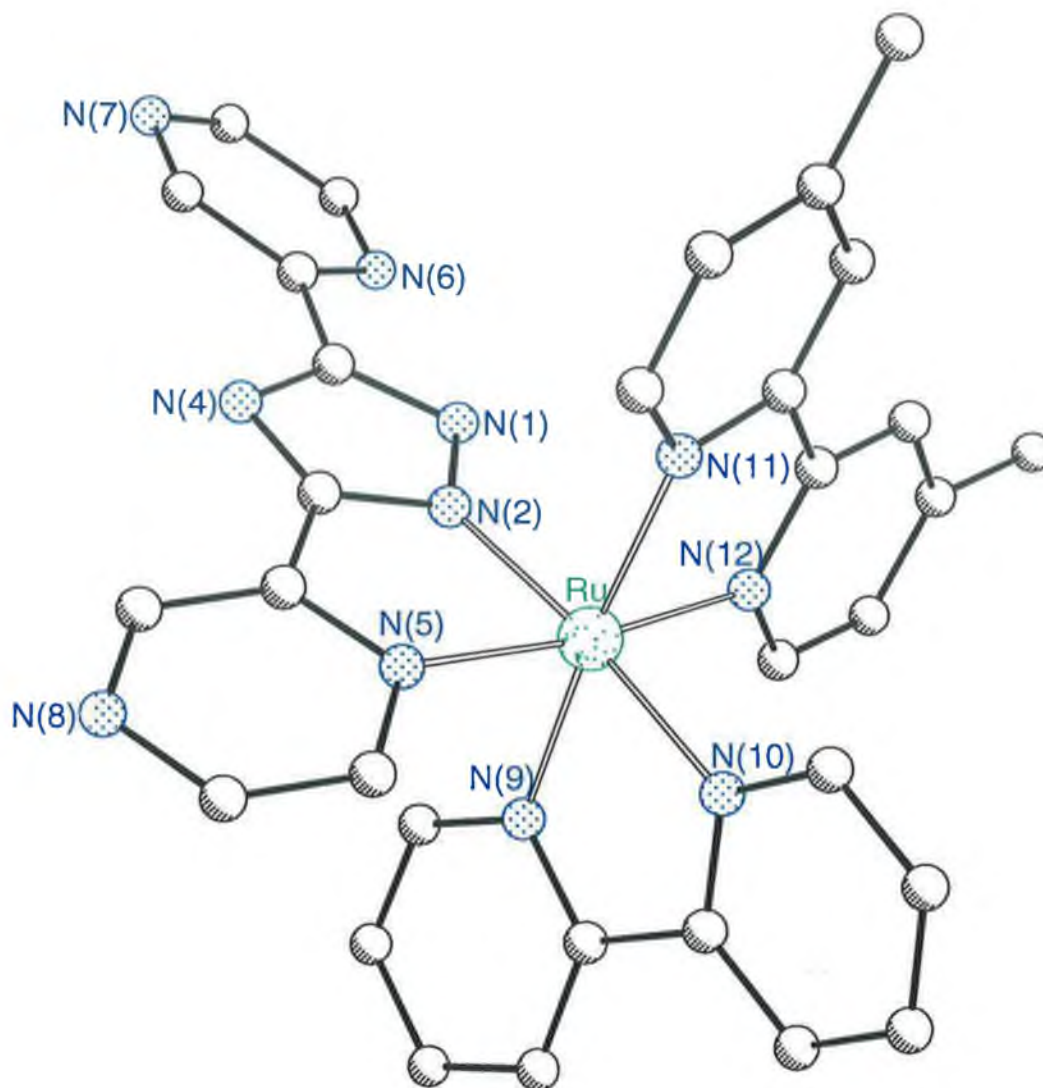
Figure 4.12. *Crystal structure for* $[Ru(bpy)(Me_2bpy)(bpzt)]^+$. *The PF_6^- group, diethyl ether molecule and hydrogen atoms are omitted for reasons of clarity.*

The biggest difference between the two complexes is in the metal–triazole bond lengths. Although the Ru–(N2) distances are pretty much equal, (2.048 Å for bpt⁻ and 2.046 Å for bpzt⁻) a large difference exists in the two Ru–(N5) bond lengths. In the case of $[Ru(bpy)(Me_2bpy)(bpt)]^+$ this distance is 2.105 Å. For the pyrazine analogue this distance is more in line with the other polypryidyl ligands at just 2.069 Å. This discrepancy is in accordance with the properties of the two types of triazole ligands as described in Chapter 1. Bpt⁻ is a ligand with strong σ-donating and weak π-accepting properties. This weak π-accepting property leads to an enlargement of the Ru–N(5) bond length. On the other hand, bpzt⁻ is a ligand that combines both the strong σ-donating capabilities of the triazole and the

strong π-accepting properties of the pyrazine. Therefore, as Ru–N(2) remains pretty much identical to that of [Ru(bpy)(Me$_2$bpy)(bpt)]$^+$, Ru–N(5) has shortened by as much as 0.036 Å.

Table 4.5. Crystallographic parameters for [Ru(bpy)(Me$_2$bpy)(bpt)]$^+$.

	[Ru(bpy)(Me$_2$bpy)(bpt)] (PF$_6$).½(C$_4$H$_{10}$O)
chemical formula	C$_{36}$H$_{33}$N$_9$RuPF$_6$O$_{½}$
fw	845.75
colour	red
crystal source	MeCN/ether
temperature (K)	200(2)
crystal size (mm)	0.42x0.24x0.20
a (Å)	13.95240(10)
b (Å)	12.24230(10)
c (Å)	23.4412(10)
α (deg.)	90
β (deg.)	95.9090(10)
γ (deg.)	90
V (Å^3)	3982.70(8)
$D_{calc.}$ (g.cm^{-3})	1.411
Z	4
F (000)	1716
radiation	Mo Kα
abs. coeff., μ (mm^{-1})	0.501
abs. corr., T (min, max)	0.40, 0.93
2θ limits, deg.	1.47-26.38
no. of reflections	22545
no. of parameters	509
R (F)	0.1060
R_w (F)	0.0599
goodness of fit	1.001

The differences in Ru–N(5) bond lengths does not affect the bite angle for the triazole ligands with N(2)–Ru–N(5) being 77.82° for [Ru(bpy)(Me$_2$bpy)(bpt)]$^+$ and 78.03° for [Ru(bpy)(Me$_2$bpy)(bpzt)]$^+$. Indeed, the bite angles for all the

ligands are very similar and fall between 77.82 and 79.01°. These acute bite angles result in the deviation from a perfect octahedral that is observed.

Table 4.6. Selected bond lengths and angles for $[Ru(bpy)(Me_2bpy)(bpt)]^+$ and $[Ru(bpy)(Me_2bpy)(bpzt)]^+$.

	[Ru(bpy)(Me₂bpy)(bpt)] (PF₆).½(C₄H₁₀O)	[Ru(bpy)(Me₂bpy)(bpzt)](PF)₆
	bond distances (Å)	
Ru-N(2)	2.048(4)	2.046(3)
Ru-N(5)	2.105(4)	2.069(3)
Ru-N(9)	2.065(4)	2.055(3)
Ru-N(10)	2.064(4)	2.070(3)
Ru-N(11)	2.059(4)	2.061(3)
Ru-N(12)	2.054(4)	2.050(3)
	bond angles (deg.)	
N(2)-Ru-N(10)	174.82(14)	173.99(12)
N(5)-Ru-N(12)	171.10(15)	171.61(11)
N(9)-Ru-N(11)	173.35(15)	175.05(11)
N(2)-Ru-N(5)	77.82(15)	78.03(11)
N(2)-Ru-N(9)	98.24(16)	97.68(11)
N(2)-Ru-N(11)	87.73(15)	86.40(11)
N(2)-Ru-N(12)	93.81(15)	93.65(11)
N(5)-Ru-N(9)	86.71(15)	84.23(12)
N(5)-Ru-N(10)	97.85(15)	96.75(11)
N(5)-Ru-N(11)	97.46(15)	99.39(12)
N(9)-Ru-N(10)	78.56(16)	78.69(12)
N(9)-Ru-N(12)	97.59(15)	98.11(11)
N(10)-Ru-N(11)	95.69(16)	97.46(12)
N(10)-Ru-N(12)	90.66(16)	91.61(11)
N(11)-Ru-N(12)	79.01(15)	78.78(11)

4.3.5 Resonance Raman studies of $[Ru(bpy)(dpp)(bpt)]^+$ and $[Ru(bpy)(dpp)(bpzt)]^+$

One of the great difficulties in characterising tris(heteroleptic) complexes containing a triazole ligand has been the fact that each mononuclear complex contains two structural isomers. As to be expected, the presence of isomers has not affected the mass spectrometry or CHN analysis as each isomer give identical results. HPLC studies proved ineffective in separating the isomers. As no attempt

136

to separate these isomers on a preparative scale was investigated, an alternative method of characterisation was required.

By comparing the ground-state resonance Raman spectra of known triazole complexes containing just bpy ($[Ru(bpy)_2(bpt)]^+$) or dpp ($[Ru(dpp)_2(pztrz)]^+$) peripheral ligands with the tris(heteroleptic) complexes being investigated in this chapter, the presence of both bpy and dpp ligands on the one metal centre can be verified.

Fig. 4.13 shows the four spectra obtained from samples of $[Ru(bpy)_2(bpt)]^+$ (a), $[Ru(bpy)(dpp)(bpt)]^+$ (b), $[Ru(bpy)(dpp)(bpzt)]^+$ (c) and $[Ru(dpp)_2(pztrz)]^+$ (d). The measurements were obtained in CD_2Cl_2 at room temperature and 457.9 nm excitation using a 350 mW laser source. The most immediate observation is that both $[Ru(bpy)(dpp)(bpt)]^+$ and $[Ru(bpy)(dpp)(bpzt)]^+$ give virtually identical spectra. Such similarity suggests that bpt$^-$ and bpzt$^-$ ligands give no resonances at the excitation wavelength studied. This has been verified by Hage *et al.* who showed that by exciting the complex $[Ru(bpy)_2(bpt)]^+$ at different wavelengths, it could be proved that the MLCT band for the complex was a Ru$\rightarrow\pi^*$(bpy) MLCT transition and that no transitions to bpt$^-$ were observed [8]. The purpose of these studies is to see whether or not both bpy and dpp vibrations could be observed. From Fig. 4.13a it can be seen that the vibrations of the bpy ligands are observed at 1605, 1560, 1487, 1319, 1275 and 1171 cm^{-1} [9]. Fig. 4.13d shows the spectra obtained from $[Ru(dpp)_2(pztrz)]^+$ and the dpp vibrations are visible at 1625, 1603, 1595, 1557, 1516, 1442, 1401, 1290 and 1263 cm^{-1} [10,11]. It can be seen that the spectra of the tris(heteroleptic) complexes contain vibrations from both bpy and dpp moieties. The peak observed at 1560 cm^{-1} for $[Ru(bpy)(dpp)(bpt)]^+$ and 1559 cm^{-1} for $[Ru(bpy)(dpp)(bpzt)]^+$ consists of two overlapping peaks from both bpy and dpp resonances. The appearance of both bpy and dpp vibrations in the same molecule is further evidence for the existence of these tris(heteroleptic) complexes. Further studies are required on the excited-state nature of these complexes. Excited-state resonance Raman would prove invaluable in determining which of the three ligands the excited state lies.
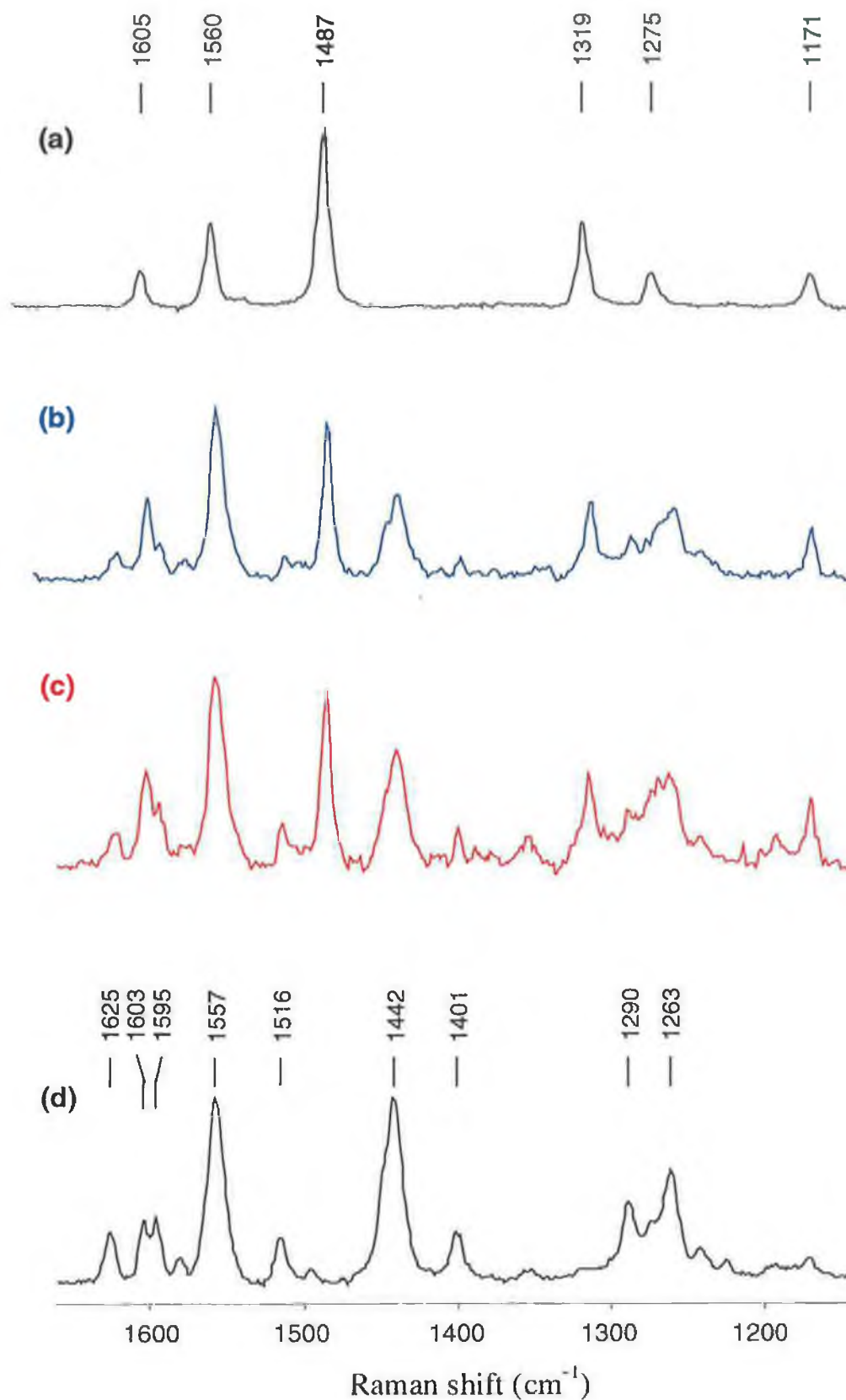
Figure 4.13. Resonance Raman spectra obtained in CD_2Cl_2 for (a) $[Ru(bpy)_2(bpt)]^+$, (b) $[Ru(bpy)(dpp)(bpt)]^+$, (c) $[Ru(bpy)(dpp)(bpzt)]^+$ and (d) $[Ru(dpp)_2(pztrz)]$.

4.4   Electrochemical properties of mononuclear complexes

Electrochemistry was carried out according to procedures in the literature [12]. Both differential pulse voltammetry (DPV) and cyclic voltammetry (CV) were used. The measurements were all obtained in dry MeCN and are reported versus the Fc/Fc^+ couple. Because earlier measurements on similar types of complexes were reported versus saturated calomel electrode (SCE), a conversion factor was applied to the literature values. This conversion factor was obtained from Pavlishchuk and Addisons publication on the conversion constants for redox potentials measured versus different electrodes in MeCN at room temperature [13].

As DPV and CV complement each other, both techniques were utilised in acquiring the redox potentials of the complexes. Using two different techniques also has the advantage of corroborating the results obtained. Fig. 4.14 illustrates how the different experiments carried out complement each other. Fig. 4.14a and b show the DPV and CV scan of $[Ru(bpy)(phen)(bpzt)](PF_6)$. Both scans have been referenced against Ag/Ag^+. DPV is a more sensitive technique and so is generally more accurate. Care must be taken when graphing DPV results, as certain factors must be considered. As well as standardising against the Fc/Fc^+ couple, the direction of the scan must be taken into consideration. The peak is observed 25 mV earlier than the actual peak. Thus, on an anodic scan, 25 mV is added to the observed peak. Conversely, 25 mV is subtracted from peaks observed during a cathodic scan. The results for all oxidations and reductions for both CV and DPV are shown in Table 4.7.
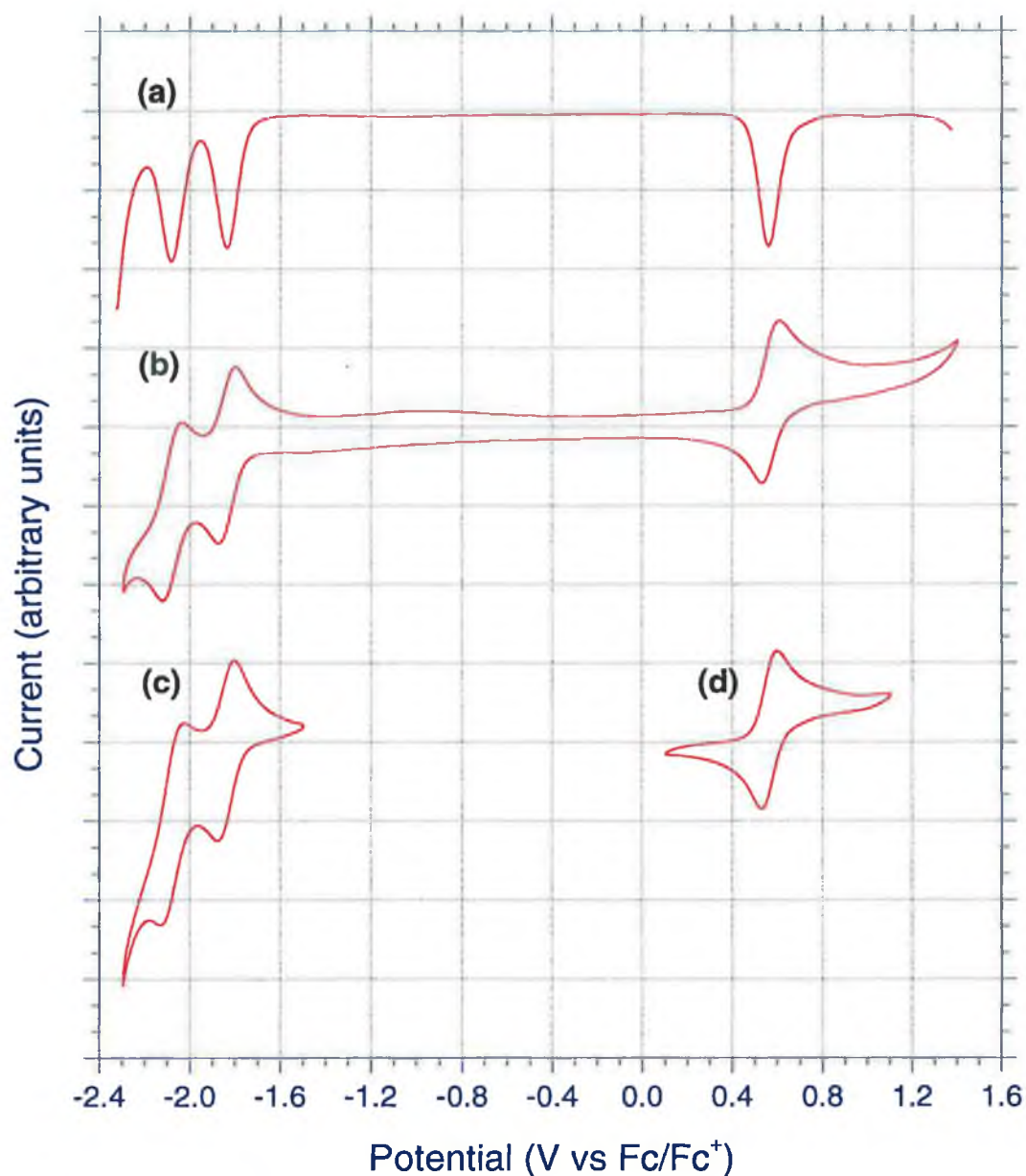
Figure 4.14. *Electrochemical data obtained from [Ru(bpy)(phen)(bpzt)]$^+$ in MeCN with 0.1 M TBABF$_4$; (a) cathodic DPV scan, (b) anodic CV scan from 0 V, (c) anodic CV scan from –2.3 V and (d) cathodic CV scan from 1.1 V.*

The CV in Fig 4.14b shows that the oxidation and reductions for [Ru(bpy)(phen)(bpzt)](PF$_6$) are reversible. In fact, all the mononuclear complexes showed similar results, i.e., one reversible oxidation wave and two reversible reduction waves. The area of each wave also indicates the number of electrons being transferred. In all cases each wave represented a one-electron transfer. For Ru(II) polypyridyl complexes, the oxidation is generally metal based and the

reductions are generally ligand based. For mixed ligand triazole complexes, the first two reduction waves are bpy based [1]. The triazoles are weak π-acceptors and so are more difficult to reduce than bpy.

Table 4.7. CV and DPV electrochemical results (vs Ag/Ag^+) in MeCN with 0.1 M $TBABF_4$ for the mononuclear complexes.

Complex	$E_{1/2}$ (V)			DPV (V)		
	ox	red		ox	red	
$[Ru(bpy)_2(bpt)]^+$	0.48	−1.85	−2.10	0.49	−1.85	−2.11
$[Ru(bpy)(Me_2bpy)(bpt)]^+$	0.43	−1.90	−2.17	0.42	−1.90	−2.16
$[Ru(bpy)(phen)(bpt)]^+$	0.49	−1.84	−2.11	0.50	−1.84	−2.11
$[Ru(bpy)(dpp)(bpt)]^+$	0.47	−1.81	−2.04	0.47	−1.82	−2.04
$[Ru(bpy)_2(bpzt)]^+$	0.60	−1.78	−2.00	0.60	−1.79	−2.02
$[Ru(bpy)(Me_2bpy)(bpzt)]^+$	0.63	−1.80	−2.01	0.64	−1.80	−2.02
$[Ru(bpy)(phen)(bpzt)]^+$	0.57	−1.84	−2.08	0.57	−1.84	−2.08
$[Ru(bpy)(dpp)(bpzt)]^+$	0.61	−1.78	−1.96	0.61	−1.77	−1.97

Separate oxidation and reduction CVs were also carried out to determine the reproducibility of the results when starting at different potentials. In Fig. 4.14a the DPV was scanned from 1.4 V to −2.3 V. Thus all peaks are negative indicating that a reduction took place. The CV on Fig. 4.14b was scanned from 0 V through the anodic switching potential (1.4 V) followed by the reduction switching potential (-2.3 V). In Figs. 4.14c and d the CV's were scanned from −2.3 V and 1.1 V respectively. All complexes were examined in this way and in each case identical sets of results were obtained for each complex.

However, in one particular set of experiments the complexes did not appear to be so stable. This was noticed when examining the oxidation wave after spending some time at low reduction potentials. If the sample is oxidised first, one

reversible oxidation wave is observed as was seen in Fig. 4.15a. If the sample is reduced first, two oxidation waves are then observed. An example of this is shown for $[Ru(bpy)(Me_2bpy)(bpzt)](PF_6)$ (Fig. 4.15b).
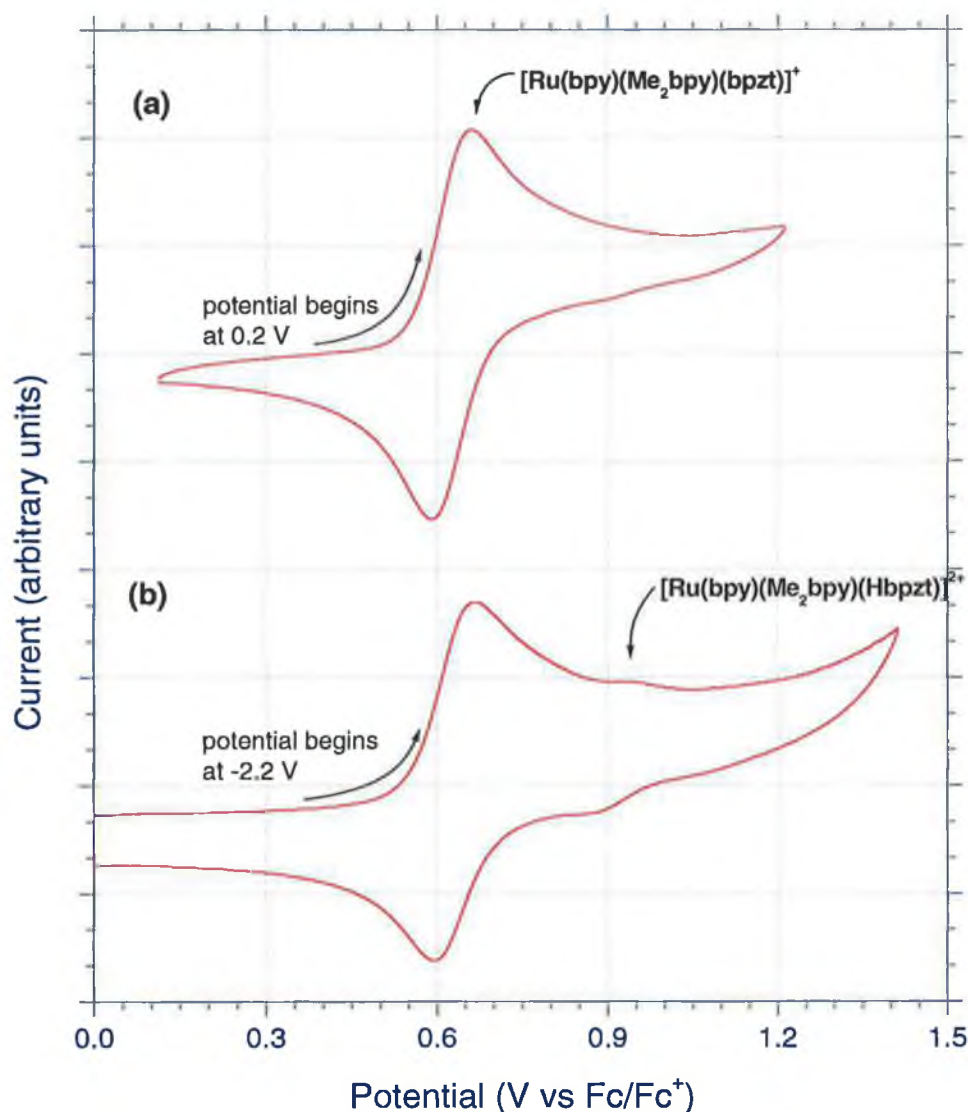
Figure 4.15. *Electrochemical data obtained from $[Ru(bpy)(Me_2bpy)(bpzt)]^+$ in MeCN with 0.1 M TBABF$_4$; (a) anodic CV scan from 0.1 V and (b) anodic CV scan from –2.2 V.*

When the complex is scanned from 0.1 V (Fig. 4.15a) only one wave is observed. When the starting potential is –2.2 V (Fig 4.15b) then a second oxidation wave appears. As this wave is at a higher oxidation potential, it must be attributable to a

species that is more difficult to oxidise. The oxidation potential suggests that the extra wave is that of the protonated complex, in this case $[Ru(bpy)(Me_2bpy)(Hbpzt)]^{2+}$. The appearance of this complex is accounted for by considering what happens during the reduction process.

When the complex is reduced, it first acquires one electron (–1.80 V) making the complex neutral, $[Ru(bpy^-)(Me_2bpy)(bpzt^-)]$. The addition of a second electron at a potential of –2.02 V gives the complex a negative charge. Some of the complex then compensates for this by acquiring a proton from solution to yield the protonated species $[Ru(bpy^-)(Me_2bpy^-)(Hbpzt)]$. It is this slight residue of protonated complex that leads to the second oxidation wave. Addition of a small amount of perchloric acid causes an increase in the higher potential peak.

The fact that the second oxidation wave occurs at a higher potential than the initial wave in all cases is in agreement with results found previously by Hage [1] and O'Connor [14]. They found that the oxidation wave for $[Ru(bpy)_2(bpt)]^+$ occurs at 0.49 V (Ag/Ag^+) [15]. The oxidation potential for the protonated $[Ru(bpy)_2(Hbpt)]^{2+}$ occurs at 0.68 V. When the triazole is protonated, it becomes a slightly lower sigma-donor than the deprotonated triazole making electron extraction more difficult, hence the increase in oxidation potential.

The extent of protonation was found to be dependent on the scan rate of the reduction process. The longer the complex was reduced the more protonation was observed. In some cases the second oxidation wave was quite small and difficult to spot but if a DPV scan was carried out, the wave was far more notable. This is due to the superior sensitivity of the DPV technique. Fig. 4.16 shows an example for the complex $[Ru(bpy)(dpp)(bpzt)]^+$. In Fig. 4.16a the second oxidation potential is difficult to determine. The DPV in Fig 4.16b solves this problem.
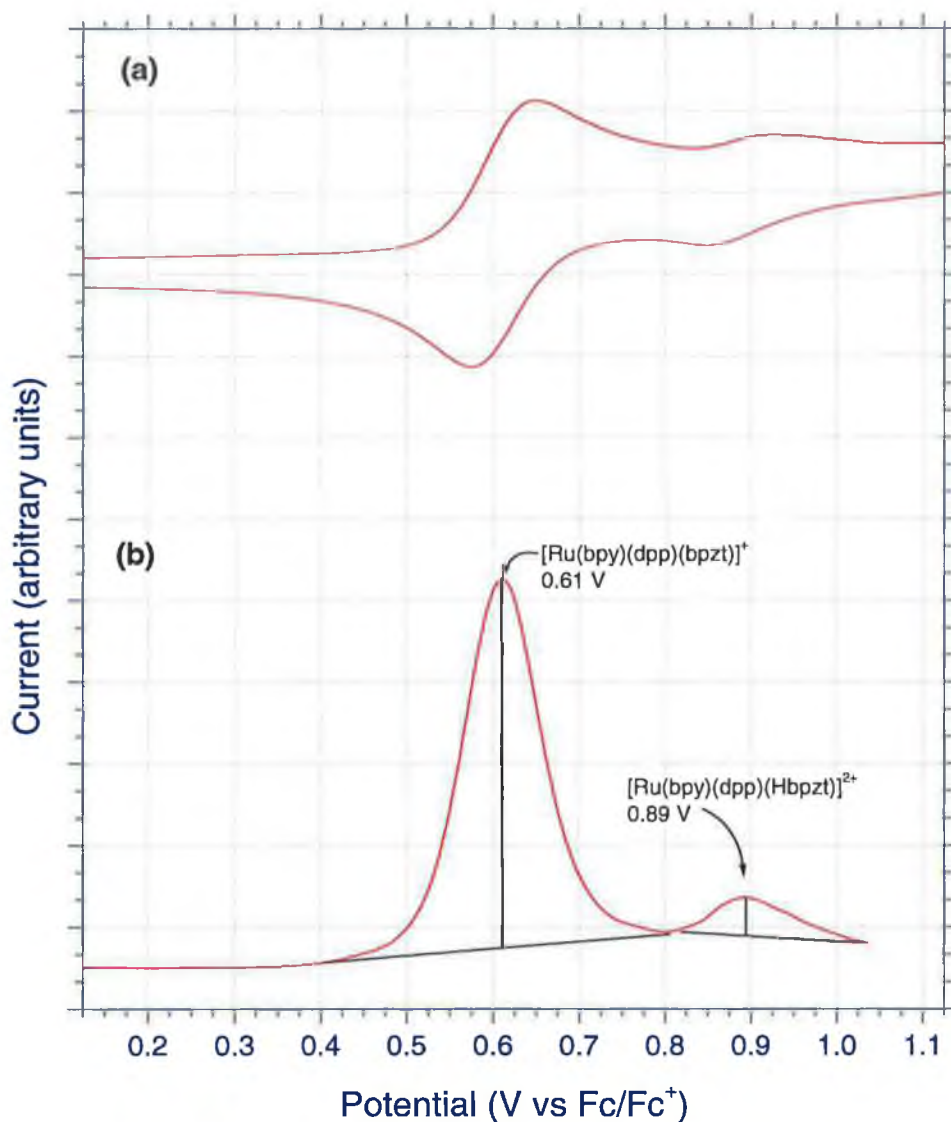
Figure 4.16. *Electrochemical data obtained from [Ru(bpy)(dpp)(bpzt)]$^+$ in MeCN with 0.1 M TBABF$_4$; (a) anodic CV scan from –2.1 V and (b) anodic DPV scan from –2.1 V.*

As none of the complexes were isolated in their protonated forms the oxidation potentials of the Ru(II) centres were not directly measured. However, as these peaks appeared when the scans began with the reduced complex, they can be estimated and are tabulated in Table 4.8.

Table 4.8. Oxidation potentials (vs Ag/Ag^+) in MeCN with 0.1 M $TBABF_4$ for the protonated mononuclear complexes.

Complex	DPV (V)
	ox
$[Ru(bpy)_2(Hbpt)]^{2+}$	0.68
$[Ru(bpy)(Me_2bpy)(Hbpt)]^{2+}$	0.57
$[Ru(bpy)(phen)(Hbpt)]^{2+}$	0.64
$[Ru(bpy)(dpp)(Hbpt)]^{2+}$	0.65
$[Ru(bpy)_2(Hbpzt)]^{2+}$	0.86
$[Ru(bpy)(Me_2bpy)(Hbpzt)]^{2+}$	0.92
$[Ru(bpy)(phen)(Hbpzt)]^{2+}$	0.65
$[Ru(bpy)(dpp)(Hbpzt)]^{2+}$	0.89

Huges and Hage both studied the triazole complexes containing bpy and phen ligands. In all cases only the bisheteroleptic complexes were studied [16,17,18]. Now that the synthesis of complexes containing mixtures of these ligands has been accomplished further studies can be carried out.

The results obtained from the bpt⁻ studies match the general patterns observed by Hage and Hughes for their triazole systems [16,18]. In all cases the oxidation of the ruthenium centre occurs at a much lower potential than that of $[Ru(bpy)_3]^{2+}$ due to the strong σ-donating capabilities of the triazole ligand. By adding electron density to the metal centre, it is easier to remove an electron, hence the lower oxidation potentials. It can be seen that substituting a bpy ligand in $[Ru(bpy)_2(bpt)]^+$ for another ligand (Me_2bpy, phen or dpp) does not have as drastic affect on the oxidation potentials as replacing a bpy ligand in $[Ru(bpy)_3]^{2+}$ with that of bpt⁻. This is due in part to the similar σ-donating properties of the

three ligands Me$_2$bpy, phen and dpp. It can be seen from Table 4.7 that there are some slight differences between the three ligands. The introduction of Me groups on the 4,4-position of a bipyridine reduces the oxidation potential by 70 mV. This suggests that the Me$_2$bpy ligand is a stronger σ-donor than bpy as the methyl groups donate electron density into the ring. Replacing bpy with phen has no significant effect, but introducing phenyl groups to the phenanthroline ring reduces the oxidation potential by 30 mV. The phenyl groups do not donate electron density to the ring as effectively as methyl groups. A similar pattern is observed for the protonated complexes except that the oxidation potentials have increased by up to 180 mV. When the triazole ring is protonated its σ-donating abilities decrease thus reducing electron density around the metal centre. This in turn makes it more difficult to remove an electron from the filled metal orbitals, resulting in the higher oxidation potentials.

Two reduction potentials were observed for each of the bpt$^-$ mononuclear complexes studied. A third reduction potential was observed by Hage at -2.28 V for $[Ru(bpy)_2(bpt)]^+$ and is attributed to the reduction of the triazole ligand [1]. The set up used did not allow for such negative potentials to be explored in this case, but as the main focus of these studies is the effect of replacing a bpy ligand, the results obtained were sufficient for our purposes. As bpt$^-$ is such a weak π^*-acceptor, the first two reductions are attributed to the reduction of the two bpy ligands in $[Ru(bpy)_2(bpt)]^+$. In these studies the two reductions are attributed to a bpy and either the Me$_2$bpy, phen or dpp ligand present. It is clear that no great differences exist between the four ligands as all are relatively good π^*-acceptors. The Me$_2$bpy shows a slightly more negative reduction potential due to the same reasons it showed a slightly less positive oxidation potential. It seems that replacing a bpy for a phen has no significant effect on the redox potentials of the complexes. Indeed, Hughes found that replacing both bpy ligands for phen ligands only affected the second reduction potential of $[Ru(phen)_2(bpt)]^+$, reducing it by 60 mV. As the protonated species were only observed *in situ* and were never isolated, their reduction potentials were not measured. Indeed, measuring reduction potentials in acid conditions is very difficult as the complexes tend to adsorb to the electrode surfaces.

Attaching a pyrazyl ring to a triazole ring has the advantage of combining a class A and class B ligand. As bpzt⁻ has a lower pKa than bpt⁻, it has a lower σ-donating capacity. This manifests itself in higher oxidation potentials as compared to the bpt⁻ analogues. As bpzt⁻ introduces less electron density to the coordinated metal, the metal d-orbitals are reduced in energy, thus making it more difficult to remove a proton. Conversely, the reduction potentials of the complexes are found at a less negative value. The [Ru(bpy)(phen)(bpzt)]⁺ complex did not show this behavior. As for the bpt⁻ analogues, the protonated mononuclear complexes were observed during electrochemical experiments and their oxidation potentials are given in Table 4.8. As for the bpt⁻ analogues, all waves were one-electron transfers and were all reversible. The reduction of bpzt⁻ was not observed as it occurs at a potential outside the range studied.

4.5   Absorption and emission spectra of mononuclear complexes

The mononuclear complexes synthesised in this chapter show intense absorption bands (extinction coefficients ca. 1.5×10^4 $M^{-1}cm^{-1}$) in the visible part of the spectrum. These bands have been assigned as singlet dπ–π* MLCT transition bands and their details are presented in Table 4.9.

[Ru(bpy)₃]²⁺ shows a MLCT band at 452 nm in MeCN. The bands for the bpt⁻ mononuclear complexes are red shifted compared to this, further evidence of the σ-donating abilities of the triazole ligand. As the triazole donates electron density to the metal centre, the energy of the HOMO is increased, thus lowering the gap between the HOMO and LUMO causing a red shift in the absorption spectrum. This is not the case with [Ru(bpy)(phen)(bpt)]⁺ whose λ_{max} is observed at 429 nm, very similar to that of [Ru(phen)₂(bpt)]⁺ (430 nm) studied by Hughes [19].

The bpzt⁻ mononuclear complexes exhibit a similar type of absorption spectrum to their bpt⁻ analogues. It is clear from Fig. 4.17 that the MLCT band for the bpzt⁻ mononuclear complexes has shifted to a lower energy and is observed *ca.* 450 nm, similar to that of [Ru(bpy)₃]²⁺. As described earlier in Section 1.4.3, the bpzt⁻

ligand consists of both a good σ-donor (triazole) and a good π*-acceptor (pyrazine). These properties lower the HOMO and LUMO respectively as compared to $[Ru(bpy)_3]^{2+}$ but the actual MLCT gap between the two energy levels remains much the same.

Table 4.9. Absorption maxima and luminescence properties of the bpt⁻ and bpzt⁻ containing complexes.

Complex	Absorption[a] (nm)/ ($\varepsilon \times 10^4$)	Emission[b] 298 K (nm)/ τ (μs)	Emission[c] 77K (nm)/ τ (μs)
$[Ru(bpy)_2(bpt)]^{+d}$	481 (1.14)	678 (0.35)	628 (2.8)
$[Ru(bpy)(Me_2bpy)(bpt)]^+$	475 (1.10)	686 (0.37)	612 (3.0)
$[Ru(bpy)(phen)(bpt)]^+$	429 (1.06)	653 (0.61)	598 (6.9)
$[Ru(bpy)(dpp)(bpt)]^+$	484 (1.72)	686 (0.38)	617 (9.4)
$[Ru(bpy)(Me_2bpy)(bpzt)]^+$	445 (1.45)	647 (0.51)	600 (8.1)
$[Ru(bpy)(phen)(bpzt)]^+$	453 (1.34)	660 (0.78)	607 (7.6)
$[Ru(bpy)(dpp)(bpzt)]^+$	455 (1.76)	619 (0.46)	604 (9.2)

[a] absorption spectra carried out in MeCN, [b] emission spectra in deaerated MeCN, [c] emission spectra in deaerated EtOH/MeOH (4:1) and [d] values from Ref. [1].

Emission from the ^{3}MLCT excited state is observed at room temperature for all the mononuclear complexes. Electrochemical measurements in Section 4.4 suggest that the LUMO is localised on the bpy or Me₂bpy/phen/dpp ligands and not on the triazole bpt⁻ ligand. A strong correlation exists between the photochemical and electrochemical properties of these complexes. Excitation of an electron by light from the HOMO to the LUMO is the equivalent to the first oxidation and reduction steps carried out using a potentiostat. From the electrochemistry, it can be concluded that the emission is bpy/Me₂bpy/phen/dpp based and not bpt⁻ based. A similar conclusion has been reached for similar systems involving triazole ligands [1,18].
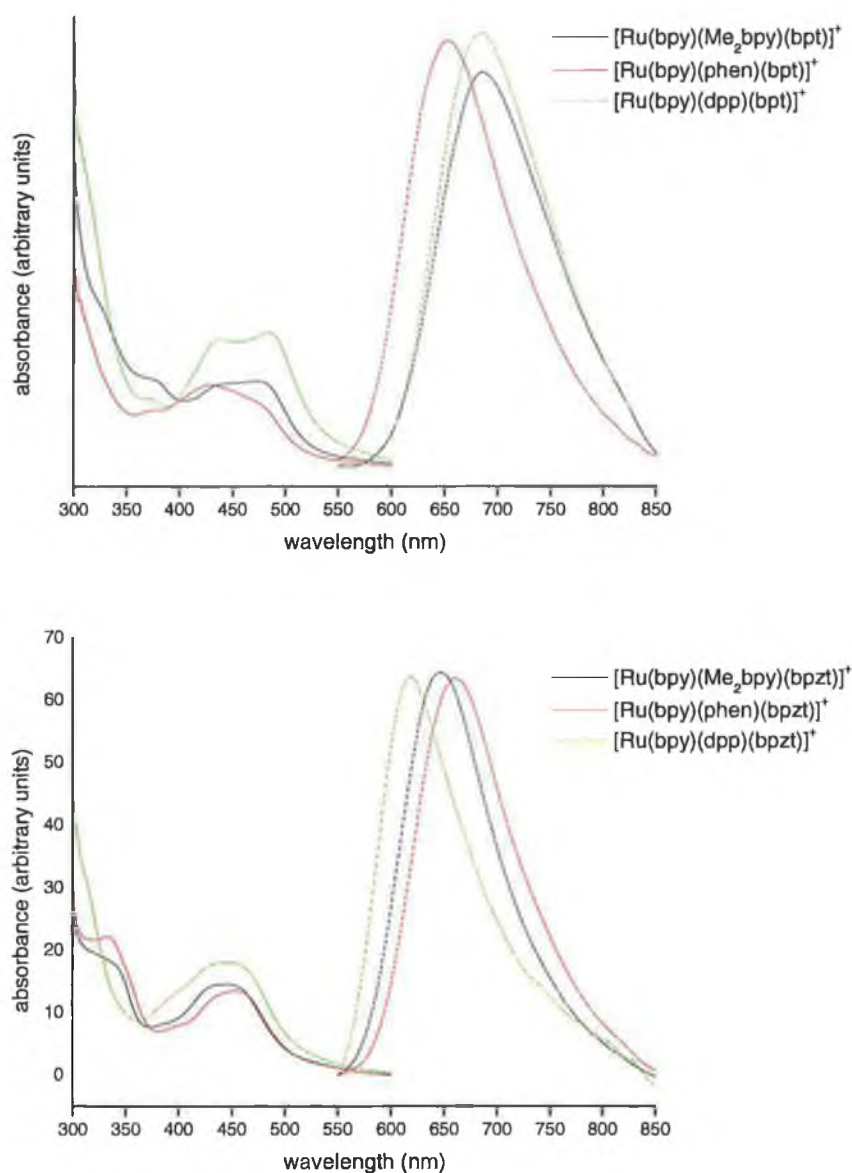
Figure 4.17. Absorption and emission spectra for the mononuclear complexes at 298 K in deaerated MeCN.

The emission observed for these complexes was found to be temperature dependent. At 77 K the emission of the bpt⁻ and bpzt⁻ complexes are blue shifted, a result of rigidchromism [20]. At 77 K the solvent dipoles are immobile on the timescale of the excited state and so cannot respond to the change in electronic configuration that accompanies an excitation. An increase in emission intensity is also observed which results from a number of factors. In a rigid glass, the Ru–N vibrations are greatly reduced, thus diminishing one mode of radiationless decay.

Secondly, even though the samples were deaerated with N_2, residual oxygen might still be present. At 77 K such oxygen will be unable to migrate to quench the excited state. Finally, Chapter 1 discussed the possibility of thermal ^{3}MC population of Ru(II) metal complexes. At 77 K such population is greatly diminished which results (in addition to the other factors mentioned) in a greatly enhanced emission spectrum. In addition to an enhanced emission, the shape of the spectrum changes to one exhibiting more vibrational structure. This vibrational structure has been attributed to relaxation *via* bpy-based vibrations [21].

Protonatation of the triazole ring results in a blue shift of the absorption and emission maxima for the bpt⁻ complexes. Protonating the triazole ring reduces its σ-donating abilities, thus decreasing electron density on the metal centre. The HOMO energy level is lowered, increasing the MLCT energy gap. This is best observed during pKa titrations of the mononuclear complexes as discussed in the next section.

4.6   Acid–Base properties of mononuclear complexes

The ability to protonate the coordinated triazole ring results in these type of complexes exhibiting an acid-base photochemistry as outlined in Scheme 4.1.

$$[Ru(bpy)(Me_2bpy)(Hbpt)]^{2+} \underset{H^+}{\overset{pK_a}{\rightleftharpoons}} [Ru(bpy)(Me_2bpy)(bpt)]^+$$

$$\downarrow h\nu \qquad\qquad \downarrow h\nu$$

$$[Ru(bpy)(Me_2bpy)(Hbpt)]^{*2+} \underset{H^+}{\overset{pK_a^*}{\rightleftharpoons}} [Ru(bpy)(Me_2bpy)(bpt)]^{*+}$$
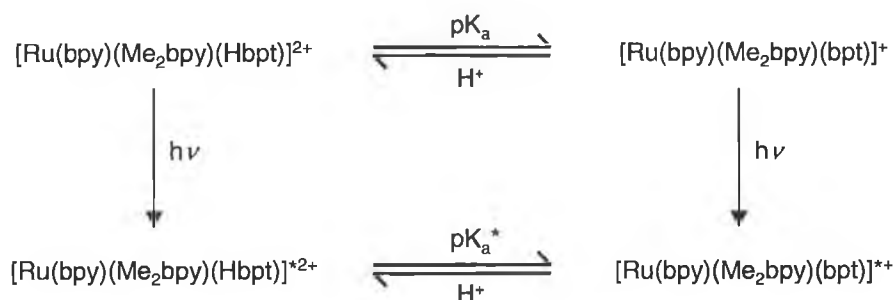
Scheme 4.1. *Acid–base processes for the complex [Ru(bpy)(Me₂bpy)(bpt)]⁺.*

This property allows one to determine whether the excited state is located on the triazole ring or not. If the excited state is located on the triazole ring, it will experience an increased negative charge due to the excited electron. This will decrease its ability to deprotonate thus yielding a higher pKa in the excited state (pK_a*) than in the ground state. Conversely, location of the excited state on any other ligand will encourage deprotonation which would result in a lower pK_a* compared to pK_a [22].

The pH dependence of the absorption spectra were monitored in a Britton-Robinson buffer. pH adjustments were made by adding conc. NaOH or H_2SO_4 to a large volume of the dissolved complex. Fig 4.18a shows the results for $[Ru(bpy)(Me_2bpy)(bpt)]^+$ which are representative of the other pyridyl-triazole mononuclear species. At a pH 5.25, the complex exhibits λ_{max} at 455 nm. This gradually shifts to higher energy upon increasing the acidity of the solution. At pH 1.00, λ_{max} is at 431 nm. Further decrease of the pH yields no further difference in the λ_{max} shift. Three isobestic points at 329, 356 and 476 nm are observed. These are useful when carrying out luminescence pKa studies, as both the protonated and deprotonated species have the same absorption coefficient at these wavelengths.

A plot of absorbance (monitored at 430 nm) against pH results in a curve (Fig. 4.18a inset) which allows the pH inflection point (pH_i) to be determined. For the ground state studies, the pH_i is also the pK_a of the complex.
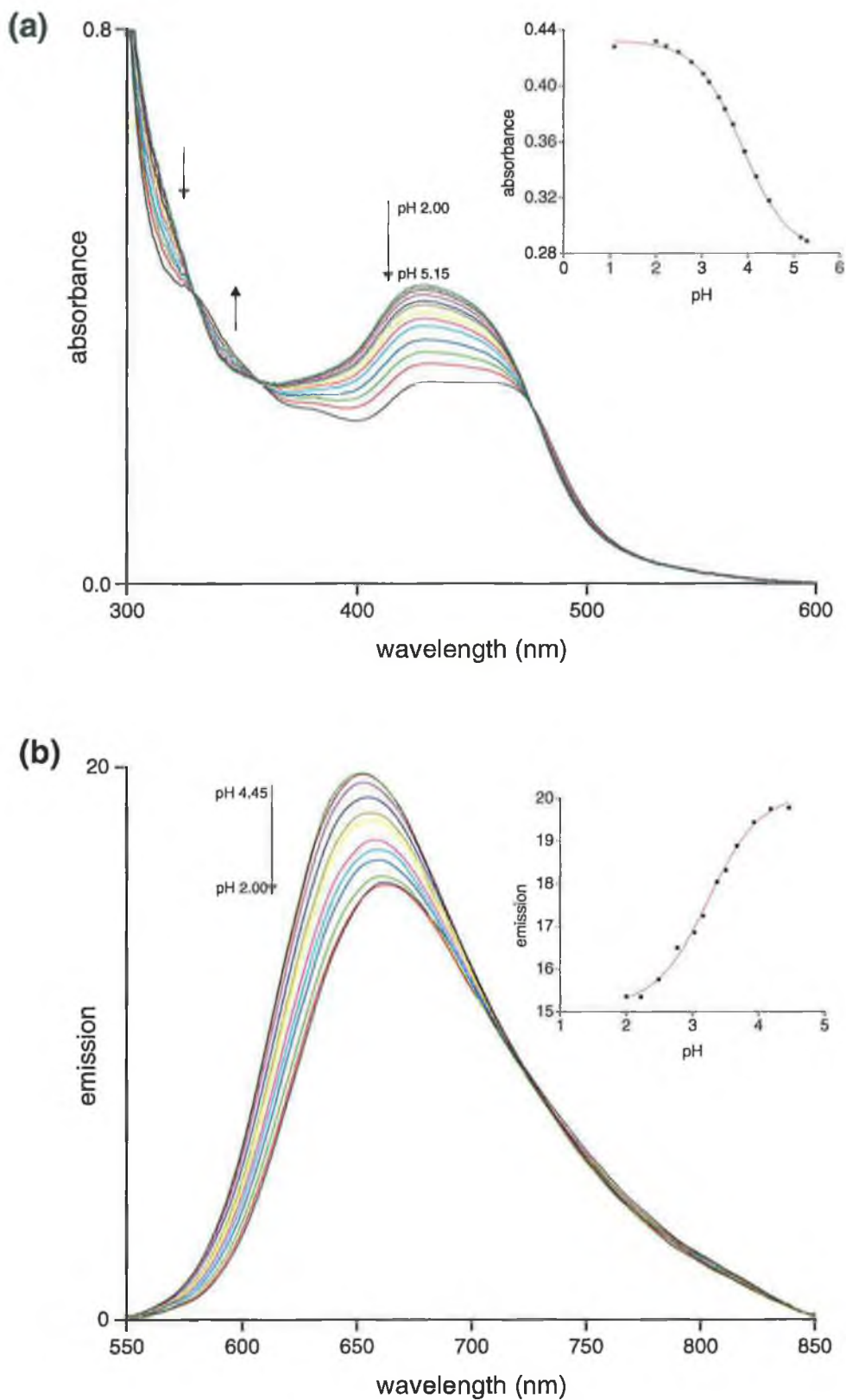
Figure 4.18. (a) pH dependence of the absorption spectra of [Ru(bpy)(Me₂bpy)(bpt)]⁺ in Britton–Robinson buffer. Inset shows a plot of intensity versus increasing pH, with fitted curve. (b) pH dependence of the emission spectra for the same species with inset showing a plot of intensity versus increasing pH.

The excited state acid-base properties of a complex can vary significantly to those of the ground state. This is due to the redistribution of electron density around the complex when excited. Fig. 4.18b shows the pH dependence of the emission spectra of $[Ru(bpy)(Me_2bpy)(bpt)]^+$. The spectra were obtained by exciting the complex at 476 nm. Exciting the complex at an isobestic point ensures that, in this case, both $[Ru(bpy)(Me_2bpy)(bpt)]^+$ and $[Ru(bpy)(Me_2bpy)(Hbpt)]^{2+}$ absorb light to the same extent. Thus, any difference in luminescence behaviour is determined solely by the pH of the solution. At pH 4.45, λ_{em} is at 663 nm. Incremental adjustments to the pH blue-shifts the λ_{em} and ends at 653 nm at pH 2.00. The emission intensity also increases upon protonation of the complex.

As for the groundstate pK_a values, a plot of emission (monitored at 653 nm) against pH results in a curve (Fig. 4.18b inset) which allows pH_i^* to be determined. However, unlike the ground-state titrations, pH_i^* does not equal pK_a^*. This is due to the fact that the protonated and deprotonated species have different luminescence lifetimes. By using Eq. (1), the pK_a^* can be calculated from pH_i^* and the lifetimes of the protonated (τ_a) and deprotonated (τ_b) species.

$$pK_a^* \quad = \quad pH_i^* \quad + \quad \log\left(\frac{\tau_a}{\tau_b}\right) \qquad \text{Eq. (1)}$$

Another method of calculating pK_a^* is by using Försters equation (Eq. (2)) which relates pK_a^* to the groundstate pK_a, pH_i^* and the emission maxima (in wavenumbers) of the protonated (ν_a) and deprotonated (ν_b) species for a given temperature, T;

$$pK_a^* \quad = \quad pK_a \quad + \quad \frac{0.625(\nu_b - \nu_a)}{T} \qquad \text{Eq. (2)}$$

The values of pK_a and pK_a^* are given in Table 4.10. Comparing pK_a and pK_a^* suggests that the excited state is not triazole-based for the bpt⁻ complexes. However, when the pyrazyl-triazole complexes are examined, a different outcome is realised. pK_a titrations of the pyrazyl-triazole complexes were carried out as for

153

the analogous pyridyl-triazoles [22]. The results obtained for [Ru(bpy)(phen)(bpzt)]$^+$ are shown in Fig.4.19.

Table 4.10. Ground-state and excited-state pK_a, values for the mononuclear complexes. pK_a* are calculated using Eq. (2).

Complex	pK_a	pH_i	pK_a*
[Ru(bpy)(Me$_2$bpy)(bpt)]$^+$	3.8	3.3	3.4
[Ru(bpy)(phen)(bpt)]$^+$	3.8	3.1	3.2
[Ru(bpy)(dpp)(bpt)]$^+$	3.7	2.9	2.9
[Ru(bpy)(Me$_2$bpy)(bpzt)]$^+$	2.0	4.0	3.3
[Ru(bpy)(phen)(bpzt)]$^+$	2.2	3.6	2.9
[Ru(bpy)(dpp)(bpzt)]$^+$	2.6	3.8	3.0

Unlike the pyridyl-triazole complexes, the emission of the pyrazyl-triazole complexes is quite weak in aqueous solution. This makes the monitoring of λ_{em} as a function of pH more difficult to measure. However, pK_a and pK_a* values were obtained (Table 4.10) and differ from the pyridyl-triazole results. As the pyrazyl-triazoles show a greater pK_a* than pK_a, they are more basic in their excited-state than in their ground-state. This suggests that the excited-state state is based on the pyrazyl-triazole unlike the pyridyl-triazoles where the excited state is bpy/Me$_2$bpy/phen/dpp based.

154
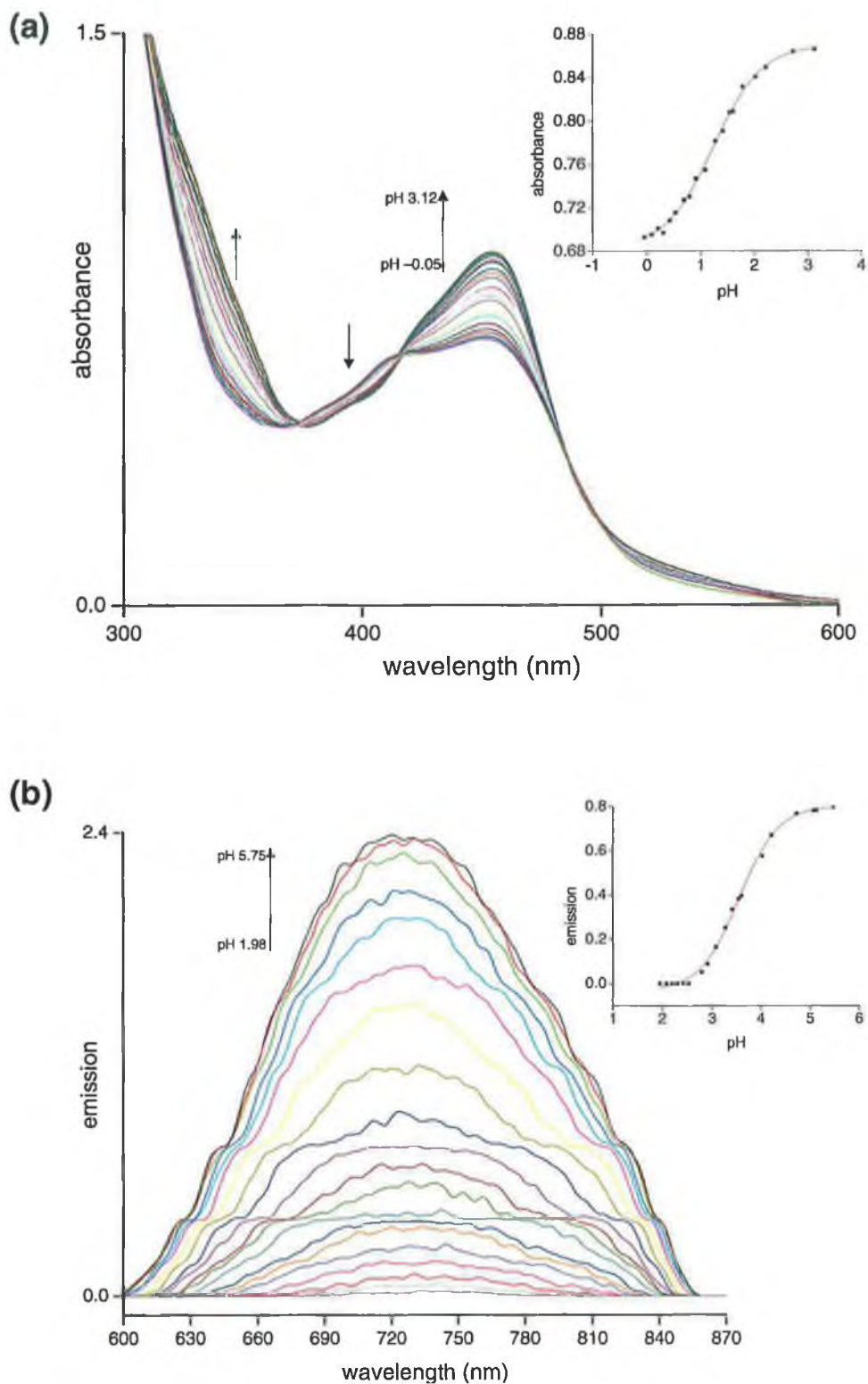
Figure 4.19. *(a) pH dependence of the absorption spectra of [Ru(bpy)(phen)bpzt]$^+$ in Britton–Robinson buffer. Inset shows a plot of intensity versus increasing pH, with fitted curve. (b) pH dependence of the emission spectra for the same species with inset showing a plot of intensity versus increasing pH.*

4.7 Experimental

[Ru(bpy)(Me₂bpy)Cl₂]

The synthesis of this complex is described in Chapter 3.

[Ru(bpy)(phen)Cl₂]

The mixture of [Ru(bpy)(MeCN)₄]Cl₂ and [Ru(bpy)(MeCN)₃Cl]Cl (0.4 g) was dissolved in dry acetone (30 ml). To this, phen (0.20 g, 1.1 mmol) was added, and the solution was heated at reflux under a CaCl₂ drying tube for 15 h. The solution was filtered hot. The purple precipitate collected was washed with cold acetone, water and finally diethyl ether. Yield 0.14 g. Elemental Analysis for C₂₂H₁₆Cl₂N₄Ru: Calc. C 51.98, H 3.17, N 11.02; Found C 51.50, H 3.14, N 10.89. Mass spectrometry: MH⁺ m/z 509.

[Ru(bpy)(dpp)Cl₂]

The mixture of [Ru(bpy)(MeCN)₄]Cl₂ and [Ru(bpy)(MeCN)₃Cl]Cl (0.4 g) was dissolved in dry acetone (50 ml). To this, dpp (0.37 g, 1.1 mmol) was added, and the solution was heated at reflux under a CaCl₂ drying tube for 24 h. The solution was filtered hot. The purple precipitate collected was washed with cold acetone, water and finally diethyl ether. Yield 0.19 g. Elemental Analysis for C₃₄H₂₄Cl₂N₄Ru: Calc. C 61.82, H 3.66, N 8.48; Found C 61.50, H 3.24, N 8.66. Mass spectrometry: MH⁺ m/z 661.

[Ru(bpy)(Me₂bpy)(bpt)](PF₆).H₂O

Hbpt (0.11 g, 0.5 mmol) was dissolved in hot EtOH/H₂O (80/20, 50 ml). The Hbpt solution was brought to reflux and [Ru(bpy)(Me₂bpy)Cl₂] (0.20 g, 0.4 mmol) was added in four portions over the course of 2 h. After adding the final portion, the solution was heated at reflux for a further 3 h. The reaction colour changed from purple to red over the duration of the experiment. The reaction solution was allowed cool, filtered and reduced on a rotary evaporator. After removal of the reaction solvent, the product was columned on a silica column using MeCN/H₂O (80:20) with 0.05 M KNO₃ mobile phase. The product eluted as the second band. The fraction containing the product was reduced to ~5

ml. After micro-filtering using a glass pipette, a drop of NH_3 was added. This solution was then transferred drop wise to a stirring aqueous solution of NH_4PF_6. The resulting orange precipitate was filtered, washed with H_2O, diethyl ether and then dried *in vacuo*. The product was further purified by column chromatography on an alumina column using MeCN as mobile phase. The product was obtained as the first band. Crystals were grown by allowing diethyl ether to slowly diffuse into a MeCN solution of the complex. A second set of crystals were obtained by allowing the slow evaporation of acetone from a acetone/H_2O solution of the complex. Both crystals gave identical ^1H NMR. Yield 0.24 g, 0.3 mmol, 75%. Elemental Analysis for $C_{34}H_{30}F_6N_9OPRu$: Calc. C 49.40, H 3.66, N 15.25; Found C 49.71, H 3.37, N 15.48. Mass spectrometry: $(M–PF_6)^+$ m/z 664.

[Ru(bpy)(phen)(bpt)](PF$_6$)

The procedure followed was similar to that for [Ru(bpy)(Me$_2$bpy)(bpt)](PF$_6$) with the following differences. Hbpt (0.11 g, 0.5 mmol) was dissolved in hot EtOH/H_2O (80/20, 50 ml). [Ru(bpy)(phen)Cl$_2$] (0.21 g, 0.4 mmol) was added in four portions over the course of 2 h and the reaction stopped after a further 3 h. After removal of the reaction solvent, the product was columned on a silica column using MeCN/H_2O (80:20) with 0.05 M KNO$_3$ mobile phase. The second main fraction was collected and reduced. A drop of NH_3 was added to the reduced solution and the desired complex was precipitated by adding to an aqueous solution of NH_4PF_6. The product was washed and dried *in vacuo* and was further purified by column chromatography on an alumina column using MeCN as mobile phase. The product was obtained as the first band. Yield 0.21 g, 0.26 mmol, 65%. Elemental Analysis for $C_{34}H_{24}F_6N_9PRu$: Calc. C 50.75, H 3.01, N 15.67; Found C 50.82, H 3.19, N 15.85. Mass spectrometry: $(M–PF_6)^+$ m/z 660.

[Ru(bpy)(dpp)(bpt)](PF$_6$).3H$_2$O

The procedure followed was similar to that for [Ru(bpy)(Me$_2$bpy)(bpt)](PF$_6$) with the following differences. Hbpt (1.1 g, 0.5 mmol) was dissolved in hot EtOH/H_2O (80/20, 50 ml). [Ru(bpy)(dpp)Cl$_2$] (0.28 g, 0.4 mmol) was added in four portions over the course of 2 h and the reaction stopped after a further 3 h. After reducing the second band collected on the silica column, a drop of NH_4 was added and the complex isolated as the PF_6^- salt. The red precipitate was washed with H_2O and

diethyl ether. The product was washed and dried *in vacuo* and further purified by column chromatography on an alumina column using MeCN as mobile phase. The product was obtained as the first band. Yield 0.20 g, 0.21 mmol, 53%. Elemental Analysis for $C_{46}H_{38}F_6N_9O_3PRu$: Calc. C 54.65, H 3.79, N 12.47; Found C 54.75, H 3.46, N 12.25. Mass spectrometry: $(M–PF_6)^+$ m/z 812.

[Ru(bpy)(Me₂bpy)(bpzt)](PF₆).2H₂O

Hbpzt (0.11 g, 0.5 mmol) was dissolved in hot $EtOH/H_2O$ (80/20, 50 ml). $[Ru(bpy)(Me_2bpy)Cl_2]$ (0.20 g, 0.4 mmol) was added over the course of 2 h in four portions. The reaction was heated at reflux for a further 3 h. As for the bpt⁻ analogues, the reaction colour changed from purple to red over the duration of the reaction. The reaction solution was allowed cool, filtered and reduced on a rotary evaporator. After removal of the reaction solvent, the product was columned on a silica column using $MeCN/H_2O$ (80:20) with 0.05 M KNO_3 mobile phase. The product eluted as the second band. The fraction containing the product was reduced to ~5 ml. After micro-filtering using a glass pipette, a drop of NH_3 was added. This solution was then transferred drop wise to a stirring aqueous solution of NH_4PF_6. The resulting orange precipitate was filtered, washed with H_2O, diethyl ether and then dried *in vacuo*. The product was further purified by column chromatography on an alumina column using MeCN as mobile phase. The product was obtained as the first band. Crystals were grown by allowing diethyl ether to slowly diffuse into a MeCN solution of the complex. Yield 0.19 g, 0.23 mmol, 58%. Elemental Analysis for $C_{32}H_{30}F_6N_{11}O_2PRu$: Calc. C 45.39, H 3.57, N 18.20; Found C 45.16, H 3.69, N 18.59. Mass spectrometry: $(M–PF_6)^+$ m/z 666.

[Ru(bpy)(phen)(bpzt)](PF₆).H₂O

The procedure followed was similar to that for $[Ru(bpy)(Me_2bpy)(bpzt)](PF_6)$ with the following differences. Hbpzt (0.11 g, 0.5 mmol) was dissolved in hot $EtOH/H_2O$ (80/20, 50 ml). $[Ru(bpy)(phen)Cl_2]$ (0.21 g, 0.4 mmol) was added in four portions over the course of 2 h and the reaction stopped after a further 3 h. After removal of the reaction solvent, the product was columned on a silica column using $MeCN/H_2O$ (80:20) with 0.05 M KNO_3 mobile phase. The second main fraction was collected and reduced. A drop of NH_3 was added to the reduced

158

solution and the desired complex was precipitated by adding to an aqueous solution of NH_4PF_6. The product was washed and dried *in vacuo* and was further purified by column chromatography on an alumina column using MeCN as mobile phase. The product was obtained as the first band. Yield 0.15 g, 0.19 mmol, 48%. Elemental Analysis for $C_{32}H_{24}F_6N_{11}OPRu$: Calc. C 46.61, H 2.93, N 18.68; Found C 46.48, H 3.05, N 18.95. Mass spectrometry: $(M–PF_6)^+$ m/z 662.

[Ru(bpy)(dpp)(bpzt)](PF$_6$)

The procedure followed was similar to that for $[Ru(bpy)(Me_2bpy)(bpzt)](PF_6)$ with the following differences. Hbpzt (0.11 g, 0.5 mmol) was dissolved in hot $EtOH/H_2O$ (80/20, 50 ml). $[Ru(bpy)(dpp)Cl_2]$ was added in four portions over the course of 2 h and the reaction stopped after a further 3 h. After reducing the second band collected on the silica column, a drop of NH_4 was added and the complex isolated as the PF_6^- salt. The red precipitate was washed with H_2O and diethyl ether. The product was washed and dried *in vacuo* and further purified by column chromatography on an alumina column using MeCN as mobile phase. The product was obtained as the first band. Yield 0.22 g, 0.23 mmol, 58%. Elemental Analysis for $C_{44}H_{30}F_6N_{11}PRu$: Calc. C 55.12, H 3.15, N 16.07; Found C 55.32, H 3.09, N 15.76. Mass spectrometry: $(M–PF_6)^+$ m/z 814.

4.8   Biliography

[1]   Hage R., Ruthenium and osmium complexes containing triazole ligands: syntheses, structures, electrochemical and photophysical properties, Ph.D. Dissertation, Leiden University, The Netherlands, **1991**.

[2]   Liang X., Suwanrumpha S., Freas R.B., *Inorg. Chem.*, **1991**, *30*, 652–658.

[3]   Cerny R.L., Sullivan B.P., Bursey M.M., Meyer T.J., *Inorg. Chem.*, **1985**, *24*, 397–401.

[4]   Bignozzi C.A., Bortolini O., Curcuruto O., Hamdan M., *Inorg. Chim. Acta*, **1995**, *233*, 113–118.

[5]   Juris A., Balzani V., Barigelletti F., Campagna S., Belser P., Von Zelewsky A., *Coord. Chem. Rev.*, **1988**, *84*, 85–277.

[6]   Hage R., de Graaff R.A.G., Haasnoot J.G., Turkenburg J.P., Reedijk J., Vos J.G., *Acta Cryst. (C)*, **1989**, *45*, 381–383.

[7]   Hage R., Haasnoot J.G., Nieuwenhuis H.A., Reedijk J., de Ridder D., Vos J.G., *J. Am. Chem. Soc.*, **1990**, *112*, 9245–9251.

[8]   Hage R., Haasnoot J.G., Stufkens D.J., SnoeckT.L., Vos J.G., Reedijk J., *Inorg. Chem.*, **1989**, *28*, 1413–1414.

[9]   Coates C.G., Keyes T.E., Hughes H.P., Jayaweera P.M., McGarvey J.J., Vos J.G., *J. Phys. Chem. A*, **1988**, *102*, 5013–5018.

[10]   Kumar C.V., Barton J.K., Turro N.J., Gould I.R., *Inorg. Chem.*, **1987**, *26*, 1455–1457.

[11]   Turro C., Bossman S.H., Leroi G.E., Barton J.K., Turro N.J., *Inorg. Chem.*, **1994**, *33*, 1344–1347.

[12]   Kaifer A.E., Gomez-Kaifer M., Supramolecular Electrochemistry, Wiley-VCH, Weinheim, Germany, **1999**.

[13]   Pavlishchuk V.V., Addison A.W., *Inorg. Chim. Acta*, **2000**, *298*, 97–102.

[14]   O'Connor C.M., Synthesis and characterisation of novel Ru(II) complexes with selective deuteration, Ph.D. Dissertation, Dublin City University, **1999**.

[15]   Hage R., Dijkhuis A.H.J., Haasnoot J.G., Prins R., Reedijk J., Buchanan B.E., Vos J.G., *Inorg. Chem.*, **1988**, *27*, 2185–2189.

[16]   Hughes H.P., Martin D., Bell S., McGarvey J.J., Vos J.G., *Inorg. Chem.*, **1993**, *32*, 4402–4408.

[17] Barigelletii F., DeCola L., Balzani V., Hage R., Haasnoot J.G., Reedijk J., Vos J.G., *Inorg. Chem.*, **1991**, *30*, 641–645.

[18] Hage R., Haasnoot J.G., Reedijk J., Vos J.G., *Chemtracts (Inorg. Chem.)*, **1992**, *4*, 75–93.

[19] Hughes H.P., The synthesis, characterisation, photochemical and photophysical properties of ruthenium(II) and osmium(II) polypyridyl complexes containing triazole ligands, Ph.D. Dissertation, Dublin City University, Ireland, **1993**.

[20] Wrighton M., Morse D.L., *J. Am. Chem. Soc.*, **1974**, *96*, 998–1003

[21] Lumpkin R.S., Kober E.M., Worl L., Murtaza Z., Meyer T.J., *J. Phys. Chem.*, **1990**, *94*, 239–243.

[22] Buchanan B.E., Vos J.G., Kaneko M., van der Putten W.J.M., Kelly J.M., Hage R., de Graaff R.A.G., Prins R., Haasnoot J.G., Reedijk J., *J. Chem. Soc., Dalton Trans.*, **1990**, 2425–2431.

Chapter 5.

Dinuclear Tris(heteroleptic) Complexes

Continuing on from the mononuclear complexes synthesised in the previous chapter, Chapter 5 examines the suitability of the new synthetic strategy in synthesising dinuclear complexes containing the pyridyl- and pyrazyl-triazole bridging ligands. In addition, a series of dinuclear complexes containing the dpp ligand are synthesised. All the complexes are characterised and examined for their photophysical and electrochemical properties. The different properties of bpt⁻ and bpzt⁻ Ru(II) complexes are examined.

Chapter 5.

Dinuclear Tris(heteroleptic) Complexes

Continuing on from the mononuclear complexes synthesised in the previous chapter, Chapter 5 examines the suitability of the new synthetic strategy in synthesising dinuclear complexes containing the pyridyl- and pyrazyl-triazole bridging ligands. In addition, a series of dinuclear complexes containing the dpp ligand are synthesised. All the complexes are characterised and examined for their photophysical and electrochemical properties. The different properties of bpt⁻ and bpzt⁻ Ru(II) complexes are examined.

Chapter 5.

Dinuclear Tris(heteroleptic) Complexes

Continuing on from the mononuclear complexes synthesised in the previous chapter, Chapter 5 examines the suitability of the new synthetic strategy in synthesising dinuclear complexes containing the pyridyl- and pyrazyl-triazole bridging ligands. In addition, a series of dinuclear complexes containing the dpp ligand are synthesised. All the complexes are characterised and examined for their photophysical and electrochemical properties. The different properties of bpt and bpzt* Ru(II) complexes are examined.*

5.1 Introduction

The synthesis of dinuclear triazole complexes can be carried out by either one of two methods and is depicted in Scheme 5.1; reacting excess metal chloride with the free ligand (Method A) or first preparing the mononuclear species and reacting that with the metal dichloride (Method B). In the first case, typically 2.5 molar equivalent of [Ru(L)(L')Cl$_2$] was added to Hbpt or Hbpzt. The reaction was heated at reflux in EtOH/H$_2$O (80:20) for approximately 24 h. The solution was reduced and the product columned on silica using a 0.5 M KNO$_3$ solution in MeCN/H$_2$O (80:20). After removing the mobile phase the product was precipitated by addition of concentrated aqueous NH$_4$PF$_6$ salt. If required, the complex was further purified by passing down an alumina column with MeCN/MeOH (95:5) mobile phase. The second method was to react *circa* 1.2 molar equivalent of [Ru(L)(L')Cl$_2$] with the desired mononuclear complex [Ru(L)(L')bpt]$^+$ in EtOH/H$_2$O (80:20) for 24 h. The isolation of the dinuclear complexes was identical for both methods. The complexes prepared by both methods are illustrated in Scheme 5.1.

Method B requires the isolation of the monomer *en route* to the dinuclear complex. Overall yields tend to be lower by this method. This is expected as each step of isolation and purification leads to inevitable loss in yield. However, a distinct advantage of Method B over Method A is that the monomer is indeed isolated. The choice can then be made whether to react the monomer with the same metal chloride to form the dinuclear complex as in Method A, or use a different dichloride, thus creating a complex with different ligand systems around each metal centre. This method opens up a route to vast numbers of possible complexes. For the purpose of these studies, only the [Ru(bpy)(dpp)-bpt-Ru(bpy)$_2$]$^{3+}$ and [Ru(bpy)$_2$-bpt-Ru(bpy)(dpp)]$^{3+}$ dinuclear complexes were synthesised in this manner.
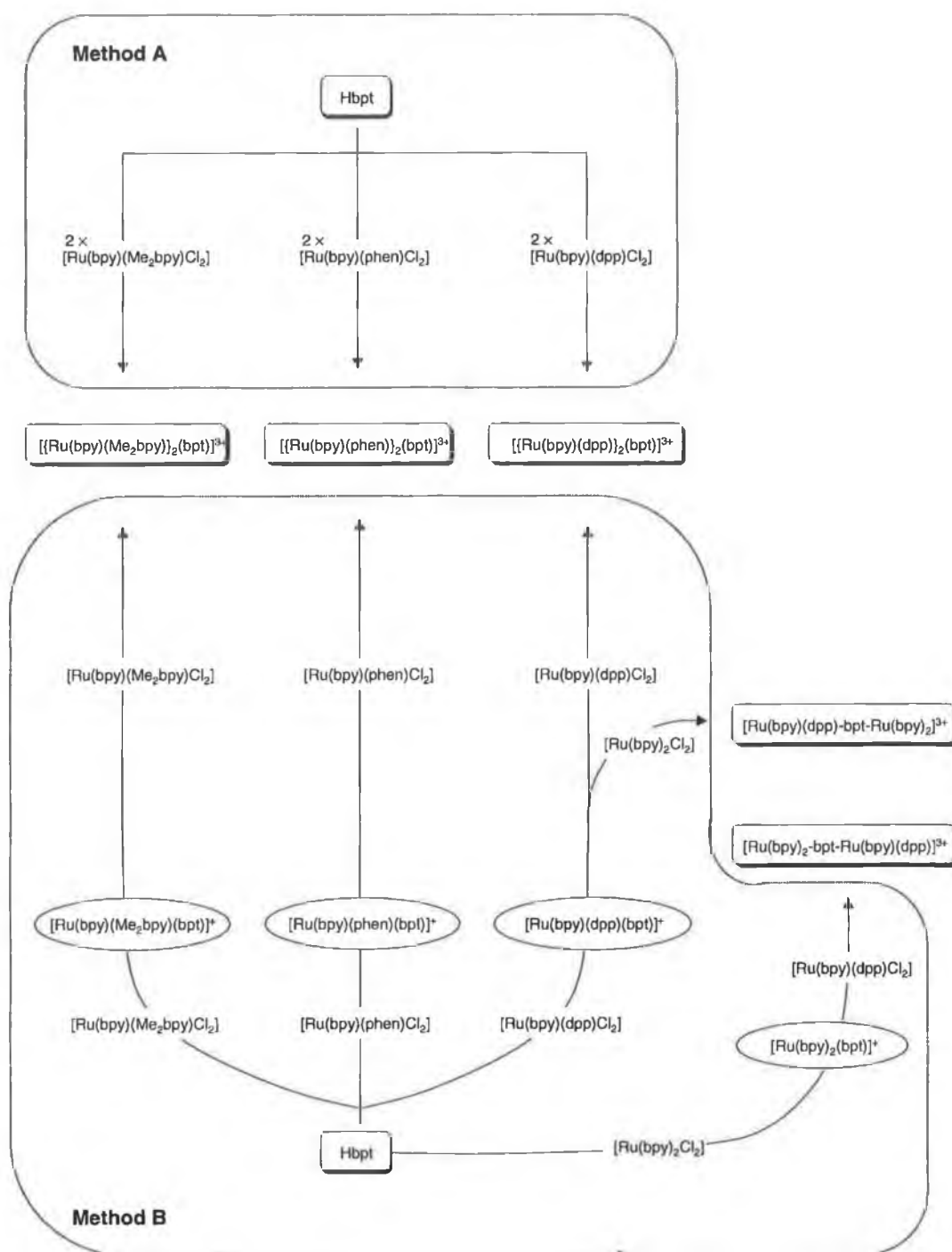
Scheme 5.1. *The two possible routes to the dinuclear complexes. Method B is used to introduce different metal centres to the bridging ligand.*

When synthesising the dinuclear complexes by method A, the order in which the metal chlorides are added is insignificant, although the N2 of the triazole will bind first. The reaction is refluxed for 24 h to ensure that the second metal centre binds to the N4 site. When a metal centre is bound to N2, the triazole ring deprotonates

and thus stabilises the complex by sharing electron density with the metal centre. The addition of a second metal centre requires that the triazole further shares this electron density and so binding of the second metal centre is more difficult, hence the longer reaction times. When creating dinuclear complexes by method B the order in which the reaction is carried out is very significant. As the triazole has preferential N2 binding, the metal centre that is to be complexed to N2 should be reacted first. The second metal centre is then added which binds to N4 [1].

The notation used throughout this chapter for the dinuclear complexes with two different metal centres is as follows; The metal centre bound through N2 of the triazole is written first, followed by the metal centre bound through N4. For example, in the complex $[Ru(bpy)(dpp)-bpt-Ru(bpy)_2]^{3+}$, the tris(heteroleptic) centre is bound through N2 whereas the bis(heteroleptic) is bound through N4. See Appendix C for additional information on the naming of such complexes. As was the case with the mononuclear complexes in Chapter 4, each metal centre has two positional isomers. Therefore, in the dinuclear complexes where both metal centres are tris(heteroleptic) in nature, there are four positional isomers, each having four further optical isomers. These isomers will be addressed later in the nuclear magnetic studies.

5.2   Characterisation of dinuclear complexes

5.2.1   HPLC of dinuclear complexes

In the previous chapter it was shown how HPLC could be used as a powerful tool in the analysis of the complexes prepared. Although this technique cannot be used as a definitive tool in establishing the structure of a complex, it can provide useful information on purity and the absorption properties of the species being studied. The complexes were analysed at comparable flow rates to those of their analogous mononuclear counterparts and the results are shown in Fig. 5.1.
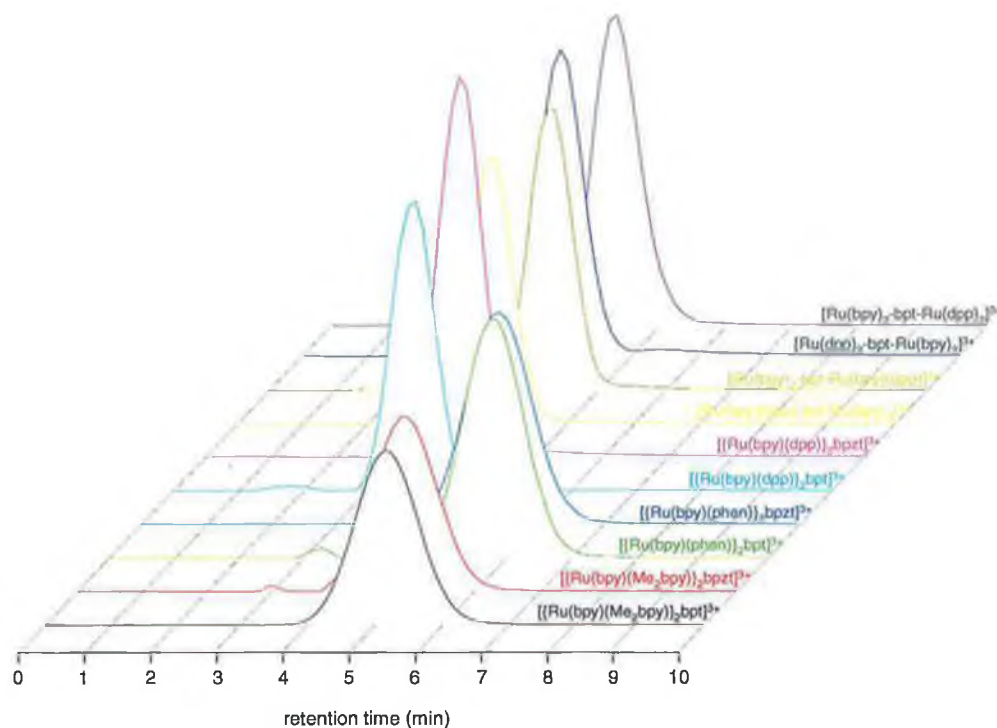
Figure 5.1. Comparison of the chromatograms obtained for the different dinuclear complexes. Mobile phase: 0.08 M LiClO$_4$ in 80/20 MeCN/H$_2$O using P10SCX-3095 cation exchange column and flow rate 1.5 ml min^{-1}.

As explained in Section 4.3.1, the column used separates species according to charge, with higher charged species being retained longer on the column. The +3 charge on the dinuclear complexes results in their having longer retention times than the mononuclear complexes. A secondary feature of the longer retention time is the peak width of each eluting species. As each species spends longer on the column, the band broadens slightly thus eluting over a greater time period. The retention times and λ_{max} of each complex are tabulated in Table 5.1.

166

Table 5.1. Retention times and λ_{max} of eluting peak for the dinuclear complexes.

Complex	Retention time (min)	λ_{max} of peak (nm)
$[\{Ru(bpy)(Me_2bpy)\}_2(bpt)]^{3+}$	4.96	455
$[\{Ru(bpy)(Me_2bpy)\}_2(bpzt)]^{3+}$	5.17	452
$[\{Ru(bpy)(phen)\}_2(bpt)]^{3+}$	5.43	424
$[\{Ru(bpy)(phen)\}_2(bpzt)]^{3+}$	5.82	448
$[\{Ru(bpy)(dpp)\}_2(bpt)]^{3+}$	3.78	434
$[\{Ru(bpy)(dpp)\}_2(bpzt)]^{3+}$	3.90	450
$[Ru(bpy)(dpp)\text{-}bpt\text{-}Ru(bpy)_2]^{3+}$	3.89	447
$[Ru(bpy)_2\text{-}bpt\text{-}Ru(bpy)(dpp)]^{3+}$	3.91	446
$[Ru(bpy)_2\text{-}bpt\text{-}Ru(dpp)_2]^{3+}$	4.31	436
$[Ru(dpp)_2\text{-}bpt\text{-}Ru(bpy)_2]^{3+}$	4.27	437

In some cases a slight impurity is observed prior to the main peak but generally remains small at < 2%. By comparing its retention time with those complexes studied in Chapter 4 it is likely that the impurity is a result of trace amounts of mononuclear complex. A common feature observed when carrying out HPLC measurements was the appearance of this impurity in samples that had been left out on the bench for some time. This phenomena is probably due to the slightly unstable nature of these complexes in light and is observed in other analytical techniques such as electrochemistry and emission studies.

Another feature observed is the earlier elution of the dpp dinuclear complexes as was observed in Chapter 4. This is once again attributed to the bulky nature of these complexes and the shielding effect that the dpp ligands have on the metal centre. Other than this effect, the dinuclear complexes have similar retention times with no discernable difference between the bpt and bpzt analogues.

5.2.2   Mass spectrometry of dinuclear complexes

The dinuclear complexes were studied by electrospray mass spectrometry, primarily to confirm that a particular complex was synthesised by the appearance of its molecular ion. The molecular ions observed and their theoretical values are given in Table 5.2. In each case (M^+ –PF_6) was observed at the correct m/z with the only exception being [Ru(bpy)$_2$-bpt-Ru(bpy)(dpp)](PF$_6$)$^+$ which appeared approximately one unit lower than calculated. As for the mononuclear complexes, M^+ was never observed which was also the case for Bignozzi *et al.* using electrospray [2] and Liang *et al.* [3] using FAB mass spectrometry.

Table 5.2. Observed and theoretical m/z values for the (M–PF_6)$^+$ species.

Complex	Observed (m/z)	Theoretical (m/z)
[{Ru(bpy)(Me$_2$bpy)}$_2$(bpt)](PF$_6$)$_2$$^+$	1396.2	1396.2
[{Ru(bpy)(Me$_2$bpy)}$_2$(bpzt)](PF$_6$)$_2$$^+$	1398.2	1398.1
[{Ru(bpy)(phen)}$_2$(bpt)](PF$_6$)$_2$$^+$	1388.0	1388.1
[{Ru(bpy)(phen)}$_2$(bpzt)](PF$_6$)$_2$$^+$	1390.0	1390.1
[{Ru(bpy)(dpp)}$_2$(bpt)](PF$_6$)$_2$$^+$	1692.3	1692.2
[{Ru(bpy)(dpp)}$_2$(bpzt)](PF$_6$)$_2$$^+$	1694.2	1694.2
[Ru(bpy)(dpp)-bpt-Ru(bpy)$_2$](PF$_6$)$_2$$^+$	1516.1	1516.2
[Ru(bpy)$_2$-bpt-Ru(bpy)(dpp)](PF$_6$)$_2$$^+$	1515.2	1516.2
[Ru(bpy)$_2$-bpt-Ru(dpp)$_2$](PF$_6$)$_2$$^+$	1692.1	1692.2
[Ru(dpp)$_2$-bpt-Ru(bpy)$_2$](PF$_6$)$_2$$^+$	1692.0	1692.2

In contrast to the mononuclear complexes studied in Chapter 4, the molecular ion was not always the base ion. Two examples of the mass spectra are shown in Fig. 5.2. The top figure (a) shows the spectrum produced by [{Ru(bpy)(dpp)}$_2$(bpt)](PF$_6$)$_3$ where the molecular ion [{Ru(bpy)(dpp)}$_2$(bpt)](PF$_6$)$_2$$^+$ appears at m/z 1692. In this case it is also the most abundant ion formed.
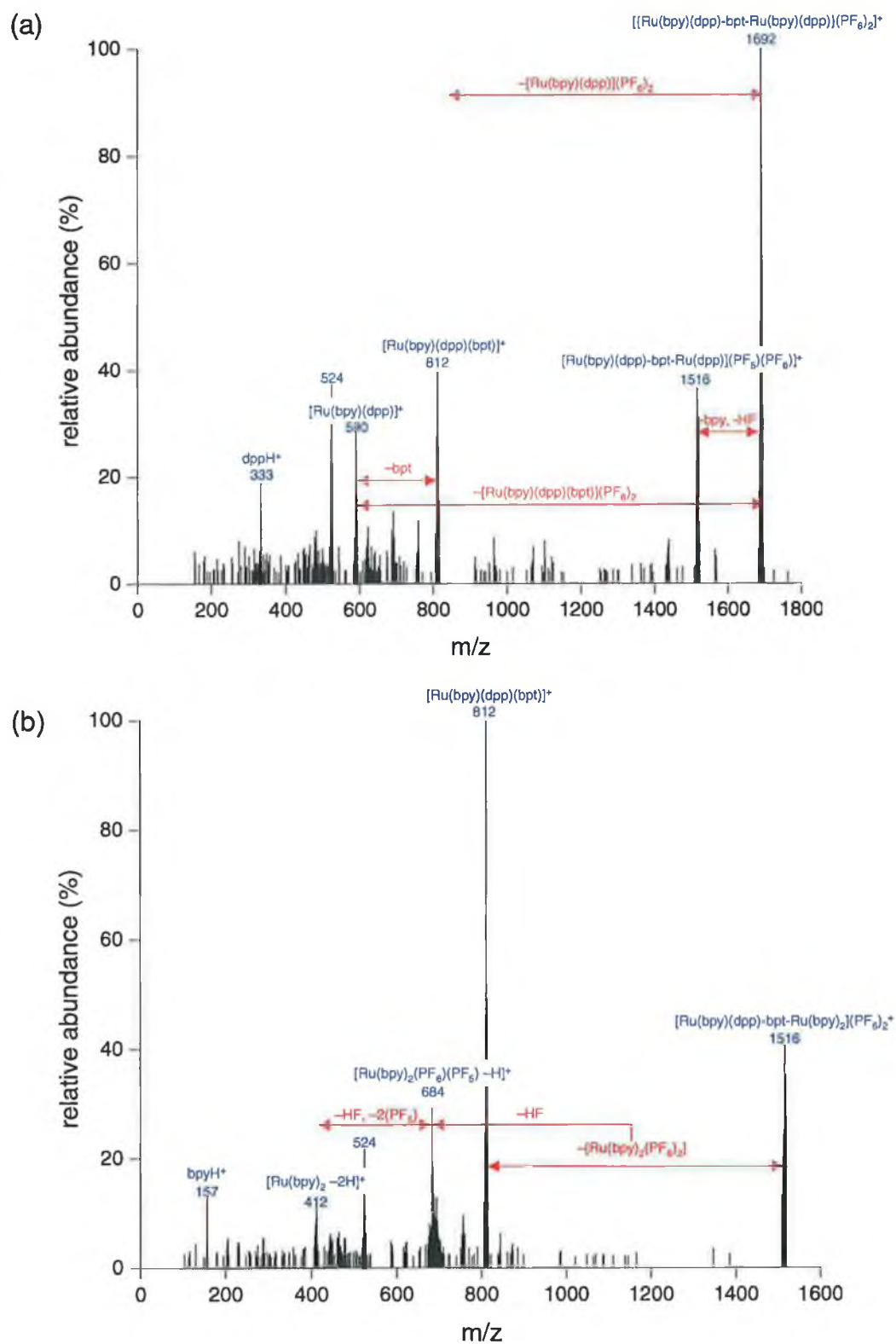
Figure 5.2. *Mass spectra for [{Ru(bpy)(dpp)}₂(bpt)](PF₆)₃ (a) and [Ru(bpy)(dpp)-bpt-Ru(bpy)₂](PF₆)₃ (b) in MeCN.*

Fig. 5.2b shows the spectrum obtained from $[Ru(bpy)(dpp)-bpt-Ru(bpy)_2](PF_6)_3$. In this case the molecular ion, $[Ru(bpy)(dpp)-bpt-Ru(bpy)_2](PF_6)_2{}^+$, is not the base ion as the most abundant ion present is $[Ru(bpy)(dpp)(bpt)]^+$. In each spectrum there are a number of peaks present suggesting that the dinuclear complexes are not as stable as their mononuclear analogues (which showed very few defragmentation pathways). Some of the possible ions are labelled in Fig. 5.2 and the possible pathways marked in red. However, it must be stressed that in order to confirm these fragmentation pathways, MS/MS experiments are required. For example, in Fig.5.2a, $[Ru(bpy)(dpp)]^+$ (m/z 590) might be formed by the loss of bpt from $[Ru(bpy)(dpp)(bpt)]^+$ (m/z 812) or by the loss of $[Ru(bpy)(dpp)(bpt)](PF_6)_2$ from the molecular ion $[\{Ru(bpy)(dpp)\}_2(bpt)](PF_6)_2{}^+$ (m/z 1692). Only MS/MS studies can verify which process actually takes place.

In some spectra the protonated bpy or dpp free ligand was observed confirming that they had dissociated from the Ru atom altogether. A familiar defragmentation, that of HF loss was observed for most samples. Before disassociating, the F atom aquires a proton from one of the organic ligands, leaving behind the neutral PF_5 atom. This phenomena has also been observed by Liang *et al.* in their studies using electrospray mass spectrometry in the analysis of Ru complexes [3].

The dpp dinuclear complexes show a peak at m/z 524 (Fig 5.2a and b) which is not readily identifiable. A possible structure (i.e. one with the correct mass) is $[Ru(dpp)Cl_2HF]^+$. As the samples were introduced in a CH_2Cl_2 solution, the possibility of the complexes gaining Cl atoms is present, however it is unclear how likely this might be, particularly under the soft ionisation conditions used.

5.2.3 ^{1}H NMR of dinuclear complexes

The existence of isomers for the mononuclear complexes was discussed in Chapter 4, as was the difficulty in distinguishing between them using analytical techniques such as MS, CHN or even HPLC. The same problem arises for the dinuclear complexes except that each metal centre adds to the total number of

isomers, thus creating four possible structures. The possible arrangements of the ligands around the metal centres for $[\{Ru(bpy)(Me_2bpy)\}_2(bpt)]^{3+}$ are shown in Fig. 5.3 where the bpy ligands are coloured yellow and the Me_2bpy ligands coloured cyan. Appendix C gives further insight into the naming of these complexes.

N2 *trans*(trz, bpy); N4 *trans*(trz, bpy)

N2 *trans*(trz, bpy); N4 *trans*(trz, Me$_2$bpy)

N2 *trans*(trz, Me$_2$bpy); N4 *trans*(trz, bpy)

N2 *trans*(trz, Me$_2$bpy); N4 *trans*(trz, Me$_2$bpy)
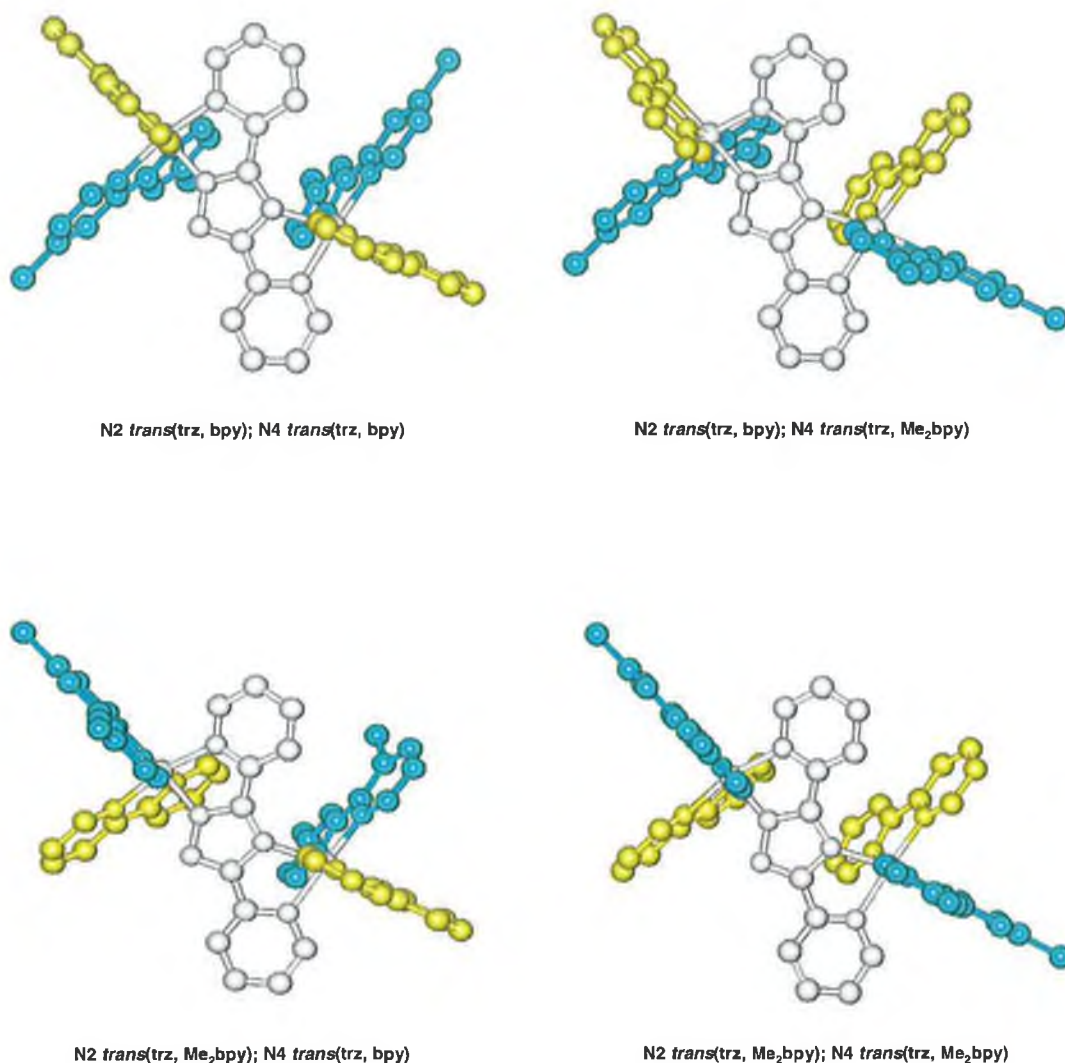
Figure 5.3. Structures of the four possible geometrical isomers for $[\{Ru(bpy)(Me_2bpy)\}_2(bpt)]^{3+}$ showing the relative orientations of the Me$_2$bpy (cyan) and bpy (yellow) ligands. Each isomer is represented as its $\Lambda\Lambda$ optical isomer.

Each of the isomers in Fig. 5.3 has an additional four optical isomers, ΛΛ, ΛΔ, ΔΔ and ΔΛ (it should be noted that because of the triazoles inherent asymmetry, the ΛΔ and ΔΛ isomers are not the same). As the current interest of these studies is in the synthesis of these complexes and not their optical isomer resolution, no further remarks on Λ and Δ optical isomers will be made.

So, in total there are a possible 16 isomers giving at least four different ^{1}H NMR spectra. The complexity of the spectra obtained for most of the dinuclear complexes demonstrates this case. As such, none of the spectra could be fully interpreted. However, as was observed for the mononuclear complexes, differences between the bpt⁻ and bpzt⁻ complexes were evident. This is shown in Fig. 5.4 where the ^{1}H NMR spectra of $[\{Ru(bpy)(dpp)\}_2(bpt)]^{3+}$ and $[\{Ru(bpy)(dpp)\}_2(bpzt)]^{3+}$ can be compared. Both show the characteristic broad peak of a phenyl group at 7.61 and 7.65 ppm respectively indicating the presence of dpp.

The mononuclear $[Ru(bpy)(phen)(bpzt)]^+$ in the previous chapter showed two peaks above 9 ppm in its ^{1}H NMR spectrum, Fig. 4.10. These peaks are characteristic of the bpzt⁻ H3 protons for mononuclear complexes. However, when the bridging ligand is bound to two centres, H3 of ring A sits over a bipyridyl ligand as shown in Fig. 5.5. This causes a shift towards higher field (Hage found it shifted to 7.71 ppm for $[\{Ru(bpy)_2\}_2(bpt)]^{3+}$ [1,12]) whereas H3 of ring B remains relatively undisturbed. This accounts for the appearance of only one peak at 8.98 ppm in Fig. 5.4b, confirming that a dinuclear bpzt⁻ complex has been successfully isolated. The absence of other peaks at around 9 ppm suggests that the sample used to produce this spectra is a single isomer, or that the nature of the bipyridyl ligand over which H3 sits does not have much bearing on its shift.

(a)

(b)
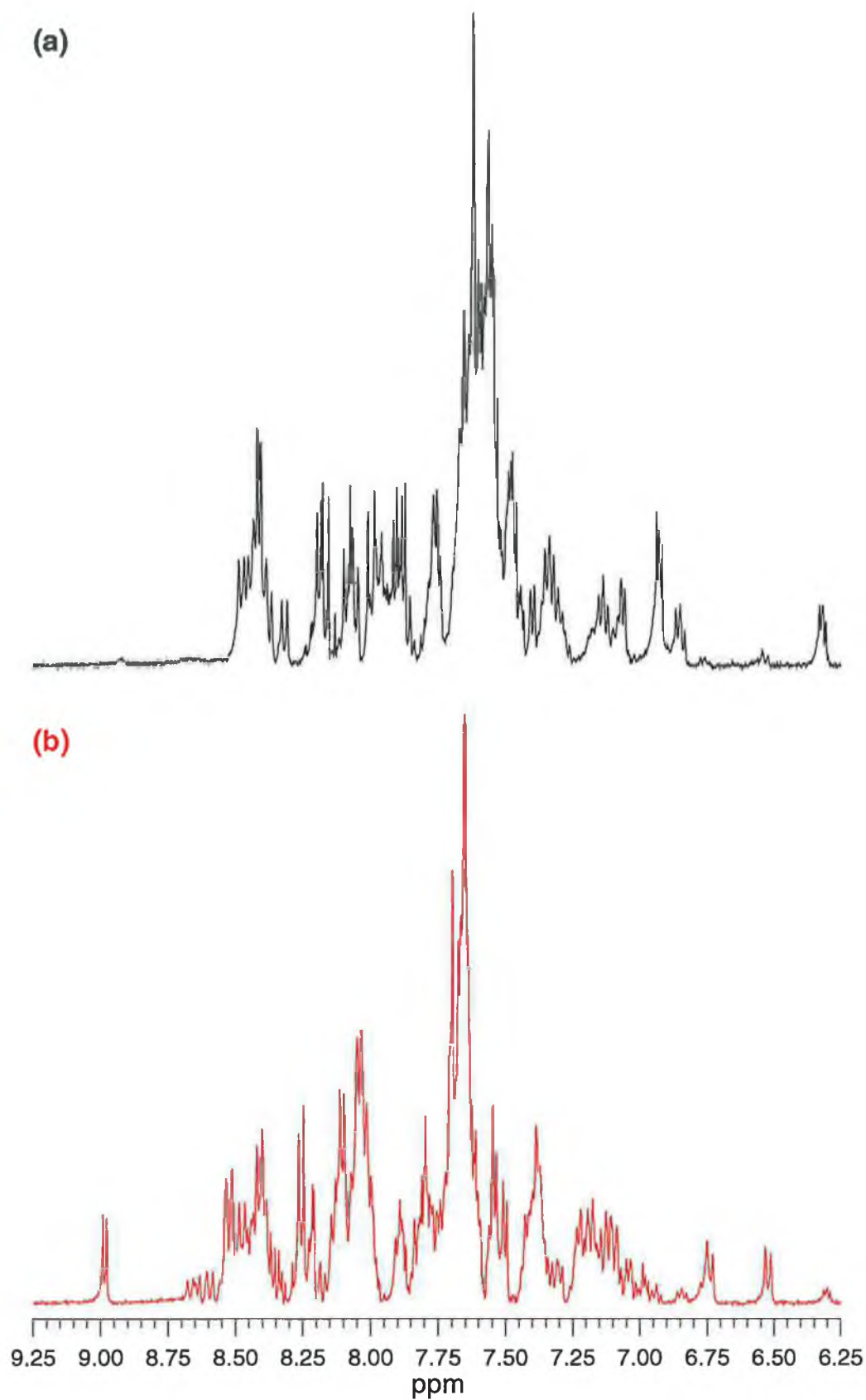
Figure 5.4. ^1H NMR of aromatic region of $[\{Ru(bpy)(dpp)\}_2(bpt)]^{3+}$ (a) and $[\{Ru(bpy)(dpp)\}_2(bpzt)]^{3+}$ (b) in d_3-MeCN.
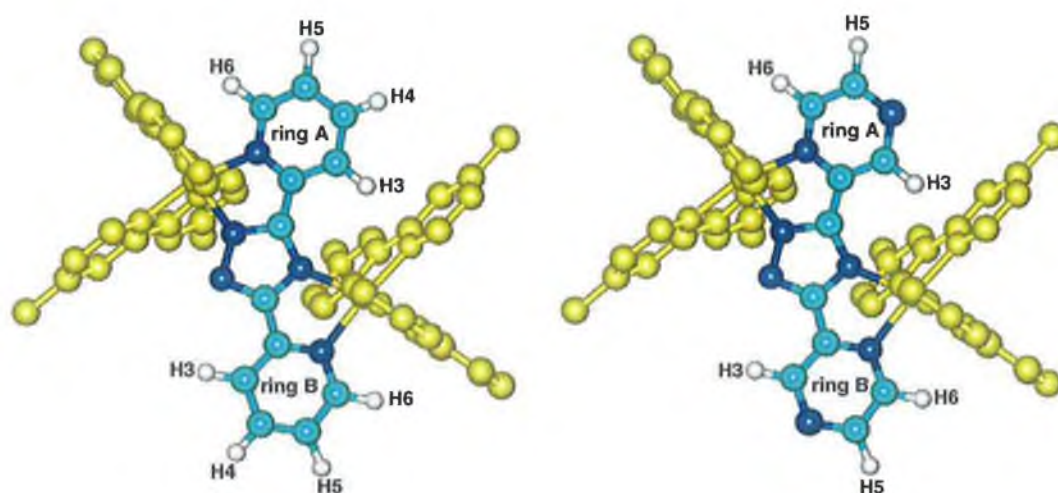
Figure 5.5. Orientation of the bridging ligand protons for dinuclear complexes. The bpt⁻ bridge is shown on the left and the bpzt⁻ bridge on the right.

The anisotropic shift experienced by H3 in the bpzt⁻ dinuclear complex is also experienced by H3 in the bpt⁻ complex. As the mononuclear complex, H3 sits in free space. With the introduction of a second metal centre, H3 on ring A sits over a pyridyl ring. This causes it to shift to a higher field and is found at 6.32 ppm for $[\{Ru(bpy)(dpp)\}_2(bpt)]^{3+}$ in Fig. 5.4a. The presence of at least two overlapping peaks suggests the presence of isomers. Although both of the complexes $[\{Ru(bpy)(dpp)\}_2(bpt)]^{3+}$ and $[\{Ru(bpy)(dpp)\}_2(bpzt)]^{3+}$ were prepared and purified in a similar fashion, ^{1}H NMR studies suggest that one isomer of the $[\{Ru(bpy)(dpp)\}_2(bpzt)]^{3+}$ complex was isolated. Although no attempts were made to isolate the isomers, it is possible that the recrystallisation procedure from acetone/H$_2$O favoured one isomer over the others. Without further HPLC studies it is impossible to predict accurately which isomer produces the spectra in Fig. 5.4b.

5.2.4 Resonance Raman studies of $[\{\mathbf{Ru(bpy)(dpp)}\}_2(\mathbf{bpt})]^{3+}$ and $[\{\mathbf{Ru(bpy)(dpp)}\}_2(\mathbf{bpzt})]^{3+}$

The difficulties in characterising the mononuclear complexes was explained in Chapter 4. These difficulties, namely that of ^{1}H NMR interpretation, are further increased when dealing with dinuclear complexes. Thus, resonance Raman was

used once again to confirm the presence of both bpy and dpp ligands in the dinuclear complex. Fig. 5.6 shows the spectra obtained from two examples, both the bpt$^-$ and bpzt$^-$ analogues, [{Ru(bpy)(dpp)}$_2$(bpt)]$^{3+}$ (b) and [{Ru(bpy)(dpp)}$_2$(bpzt)]$^{3+}$ (d). The measurements were obtained in CD$_2$Cl$_2$ at room temperature and 457.9 nm excitation using a 350 mW laser source. The mononuclear analogues from Chapter 4, [Ru(bpy)(dpp)(bpt)]$^+$ (a) and [Ru(bpy)(dpp)(bpzt)]$^+$ (c), are included for comparison. Once again both spectra show bpy and dpp vibrations [4]. In the case of the bpt$^-$ bridging ligand, both mononuclear and dinuclear complexes give virtually identical results with the exception that the peaks at 1261 and 1269 cm^{-1} are more resolved in the dinuclear case. The lack of bpt$^-$ vibrations indicates that the MLCT for the dinuclear complexes is still Ru→bpy and Ru→dpp based.

The bpzt$^-$ dinculear complex is interesting in that there are a few new vibrations that are not associated with either bpt or dpp. Comparing Fig. 5.6b and d, it can be seen that some of the bpy and dpp vibrations bands have been reduced. The peak at 1627 cm^{-1} is one such example. It is present in the mononuclear complex but not in the dinuclear complex. On the other hand, new peaks at 1507 and 1195 cm^{-1} are not characteristic of either bpy or dpp ligand vibrations [5,6]. Comparison with bpzt$^-$ complexes in the literature suggests that these new vibrations are bpzt$^-$ based [7]. This suggests that for the bpzt dinuclear complexes, the MLCT band has gained some Ru→bpzt character. The resonance Raman studies presented here are primarily for structural characterisation. Further studies have to be carried out in order to determine the nature of the electronic transitions occurring within these complexes.

The presence of the different electronic transitions under any one absorption band can be probed by comparing the dependence on wavelength of the resonance Raman spectra. These studies should determine whether the π* level sits primarily on the bpy or the dpp ligand or in the case of bpzt$^-$ dinuclear complexes, the bpzt$^-$ ligand itself. Previous work by Hughes suggests that the π* level of a mixed ligand complex [Ru(bpy)$_2$-bpt-Ru(phen)$_2$]$^{3+}$ sits on the bpy ligands, regardless of whether that bipyridyl metal centre is N2 or N4 bound [8,9].
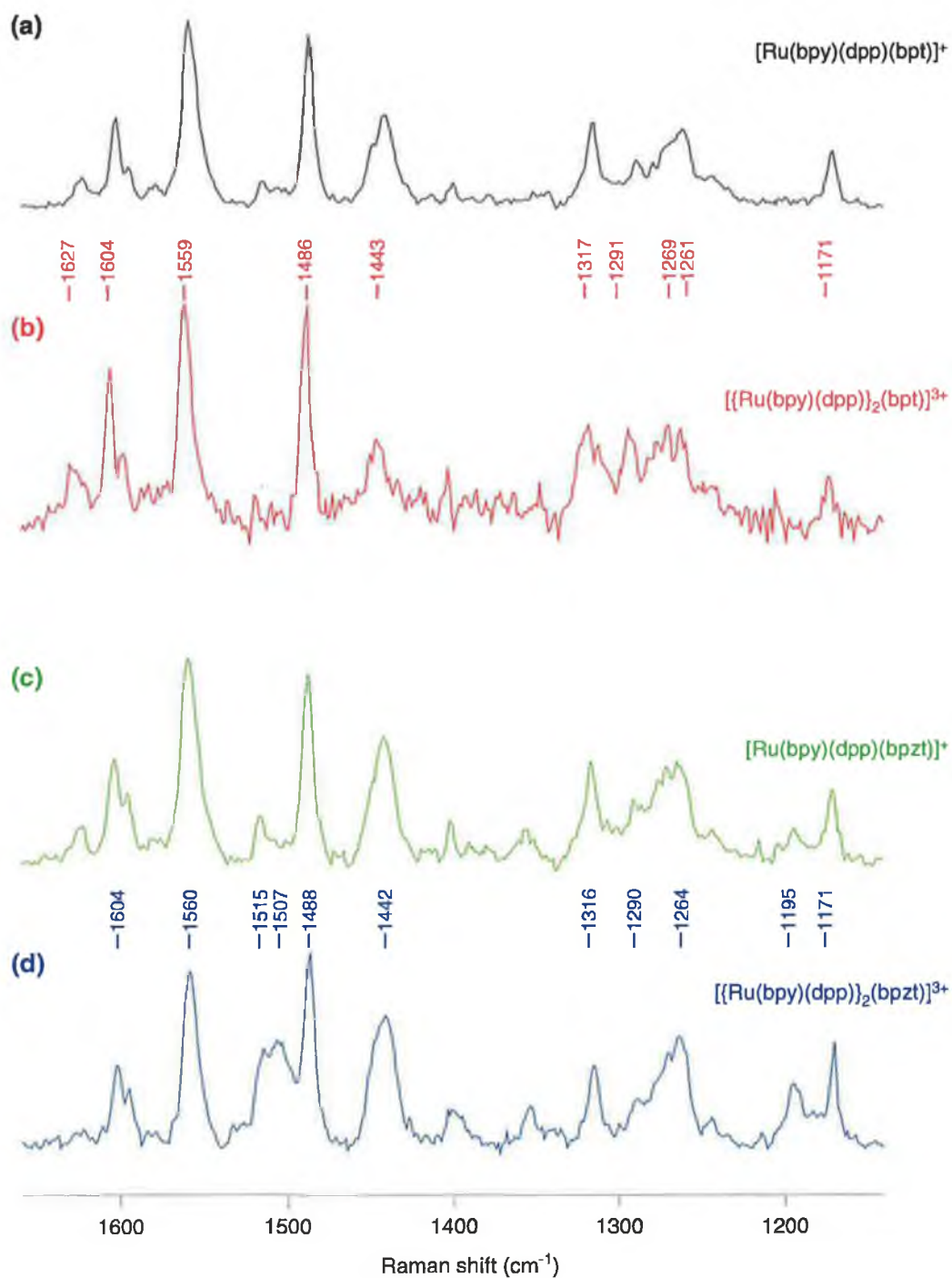
Figure 5.6. *Resonance Raman spectra obtained in CD$_2$Cl$_2$ for (a) [Ru(bpy)(dpp)(bpt)]$^+$, (b) [{Ru(bpy)(dpp)}$_2$(bpt)]$^{3+}$, (c) [Ru(bpy)(dpp)(bpzt)]$^+$ and (d) [{Ru(bpy)(dpp)}$_2$(bpzt)]$^{3+}$.*

5.3 Electrochemical properties of dinuclear complexes

Electrochemical measurements were carried out on the dinuclear species in a similar manner to that described in Chapter 4 [10,11]. Both differential pulse voltammetry (DPV) and cyclic voltammetry (CV) were used and the measurements were all obtained in dry MeCN and reported versus the Ag/Ag^+ couple. Table 5.3 gives the oxidation and reduction potentials obtained from all the dinuclear complexes as measured by DPV. As reduction waves were not always reversible it was sometimes impossible to determine a reduction $E_{1/2}$. Fig. 5.7 shows the typical set of results obtained from these complexes. Both CV and DPV were carried out to verify the results obtained from each technique. The example shown in Fig. 5.7 is that of $[\{Ru(bpy)(Me_2bpy)\}_2(bpt)]^{3+}$.

Table 5.3. DPV electrochemical results in MeCN with 0.1 M $TBABF_4$ for the dinuclear complexes.

Dinuclear complex	DPV[a] (V)		
	Oxidation		Reduction
$[\{Ru(bpy)_2\}_2bpt]^{3+b}$	0.66	0.96	-1.78, -2.00, -2.05
$[\{Ru(bpy)(Me_2bpy)\}_2bpt]^{3+}$	0.62	0.92	-1.81, -2.11
$[\{Ru(bpy)(phen)\}_2bpt]^{3+}$	0.70	1.01	-1.78, -1.97
$[\{Ru(bpy)(dpp)\}_2bpt]^{3+}$	0.69	0.99	-1.71, -1.85, -2.08
$[\{Ru(bpy)_2\}_2bpzt]^{3+}$	0.78	1.08	-1.64, -1.77, -1.93, -2.01, -2.23
$[\{Ru(bpy)(Me_2bpy)\}_2bpzt]^{3+}$	0.79	1.05	-1.66, -1.79, -1.91, -2.25
$[\{Ru(bpy)(phen)\}_2bpzt]^{3+}$	0.75	1.09	-1.67, -1.76, -1.94, -2.24
$[\{Ru(bpy)(dpp)\}_2bpzt]^{3+}$	0.79	1.07	-1.70, -1.94, -2.24
$[Ru(bpy)_2-bpt-Ru(bpy)(dpp)]^{3+}$	0.70	0.98	-1.70, -1.76, -1.92, -2.07
$[Ru(bpy)(dpp)-bpt-Ru(bpy)_2]^{3+}$	0.69	1.00	-1.73, -1.94, -2.03
$[Ru(bpy)_2-bpt-Ru(dpp)_2]^{3+}$	0.69	0.97	-1.67, -1.77, -1.84, -2.08
$[Ru(dpp)_2-bpt-Ru(bpy)_2]^{3+}$	0.68	0.98	-1.72, -1.89, -1.99, -2.04

[a] measurements carried out in dry MeCN with 0.1 M $TBABF_4$ and referenced against the Ag/Ag^+ redox couple. [b] values from Ref. [12].
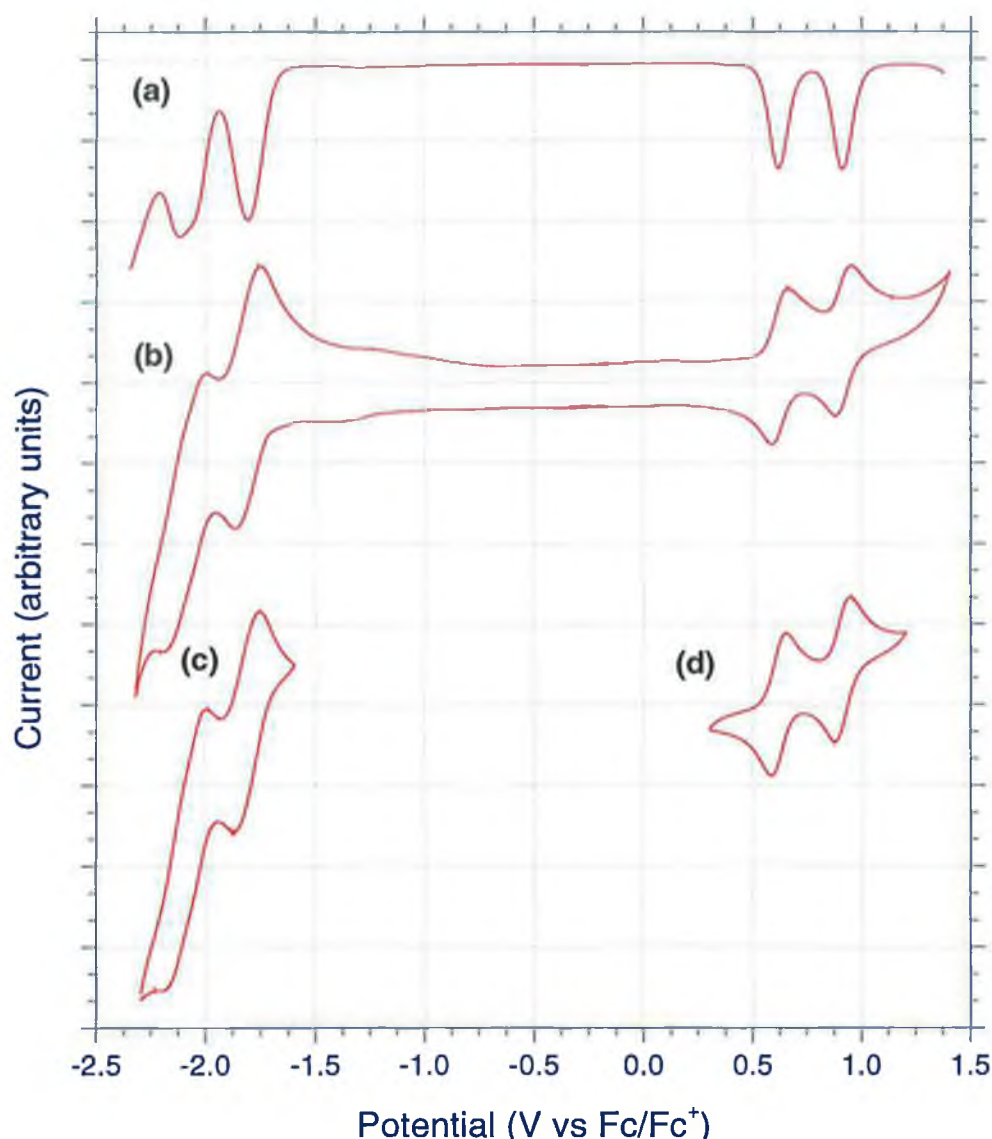
Figure 5.7. *Electrochemical data obtained from [{Ru(bpy)(Me$_2$bpy)}$_2$(bpt)]$^{3+}$ in MeCN with 0.1 M TBABF$_4$; (a) cathodic DPV scan, (b) anodic CV scan from 0 V, (c) anodic CV scan from –2.3 V and (d) cathodic CV scan from 1.2 V.*

The first point of note is the presence of two oxidation peaks, corresponding to the oxidation of the two metal centres present. The difference in oxidation potentials is approximately 300 mV in all cases. The unusual difference between the two metal centres has been attributed to several factors [13];

-      As oxidation of the first metal centre raises the overall charge of the complex, removal of a second electron

178

requires greater energy and so occurs at a greater potential.

- After the first oxidation step, the unpaired electron delocalises over the Ru(III) centre and so removal requires greater energy than would be expected for a totally localised system.

- The oxidation potentials of N2 and N4 bound mononuclear complexes have been shown to differ by up to 60 mV, with the N4 bound complex requiring the greater oxidation potential.

It can been seen straight away that there is metal–metal interaction across the bpt⁻ and bpzt⁻ bridges. Were there no interaction one would expect only a slight difference in the two oxidation potentials, primarily due to their N2/N4 coordination modes. Another characteristic of the dinuclear complexes is the higher first oxidation potential with respect to the mononuclear analogue. Upon complexation of the Hbpt or Hbpzt, the bridging ligand deprotonates and acquires a negative charge. This charge is somewhat delocalised onto the metal centre of a mononuclear complex through N2 of the triazole ring. Addition of a second metal centre results in a delocalisation over two metal centres thus reducing the electron density over both and increasing the first oxidation potential.

The oxidation potentails for the dpp series show that the presence of a coordinated dpp ligand has no real affect on the oxidation results. Whether one, two or indeed no dpp ligands are coordinated to each centre, the results are the same within experimental error. In Chapter 4 the bpzt⁻ mononuclear complexes were discovered to have higher oxidation potentials than their bpt⁻ analogues due to the poorer σ-donating abilities of bpzt⁻ compared with bpt⁻. The results for the dinuclear complexes are in agreement with those observed in Chapter 4 as each bpzt⁻ dinuclear complex has higher first and second oxidation potentials than their bpt⁻ counterparts.

All of the complexes exhibit reduction waves as tabulated in Table 5.3. In all cases the reduction waves appear at a less negative potential than their mononuclear analogues. This is expected as the negatively charged bpt⁻/bpzt⁻ bridging ligand is now sharing that electron density over two metal centres, resulting in a lower electron density around each dinuclear centre as compared to the mononuclear centre. The overall 3+ charge of the complex also contributes to the easier reduction of the peripheral ligands. However, in the case of the bpzt⁻ complexes, the first reduction wave has been shifted to a less negative potential than the bpt⁻ dinuclear complexes. The lower first reduction potential of these complexes suggests that first reduction is not bpy/Me₂bpy/phen/dpp based but indeed bpzt⁻ based. Further remarks on the position of the excited state for the bpzt⁻ complexes will be made in the next section.

Fig. 5.7c shows the reversible reduction waves for $[\{Ru(bpy)(Me_2bpy)\}_2(bpt)]^{3+}$. Each wave corresponds to a two-electron reduction. An interesting characteristic of the $[\{Ru(bpy)_2\}_2(bpt)]^{3+}$ complex is the splitting of the second reduction peak into two peaks at –2.00 and –2.05 V. A similar result was obtained for $[\{Ru(bpy)(Me_2bpy)\}_2(bpt)]^{3+}$. The second DPV reduction potential in Fig. 5.7a. at –2.11 V is not as fully resolved as that observed by Hage but a definite broadening is apparent [12]. This broadening was not observed for any of the other dinuclear complexes.

In the example shown in Fig. 5.7, two reversible reduction waves are observed. This was not always the case as the dpp series in Fig. 5.8 illustrates. For these complexes, the CV did not always prove useful in determining the nature of the reduction potentials. Separate DPV measurements were carried out as shown in Fig. 5.9 and give a more accurate representation of the reduction waves. In each case a two-electron wave is observed at approximately –1.70 V. This wave is reversible if the reduction potential is not lowered beyond –2.1 V. Returning from a more negative potential results in a spike in both the CV and DPV and loss of reversibility for the reduction peak at –1.70 V.
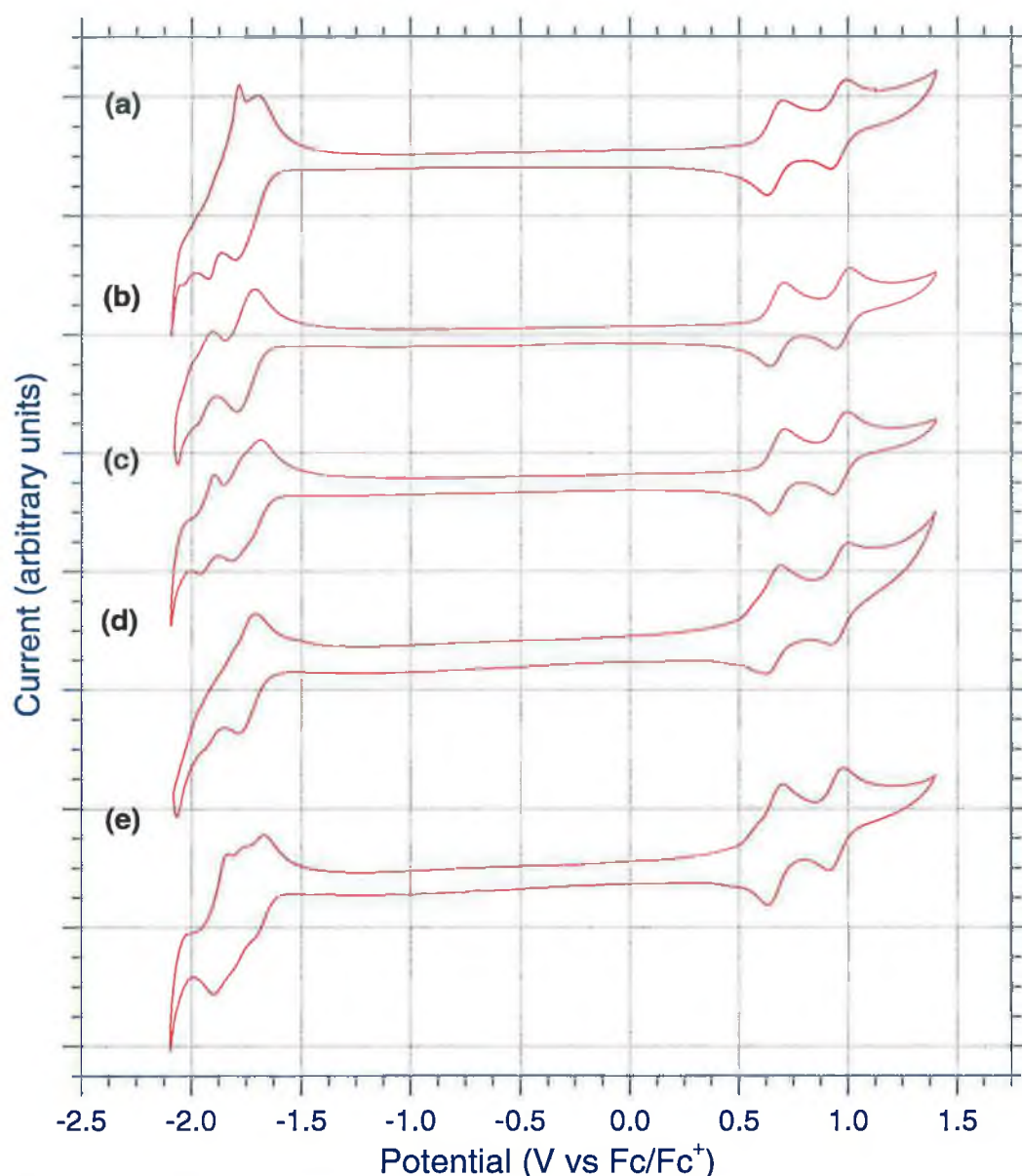
Figure 5.8. *Electrochemical data (initial anodic CV scan from 0 V) obtained from [{Ru(bpy)(dpp)}₂(bpt)]³⁺ (a), [Ru(bpy)(dpp)-bpt-Ru(bpy)₂]³⁺ (b), [Ru(bpy)₂-bpt-Ru(bpy)(dpp)]³⁺ (c), [Ru(dpp)₂-bpt-Ru(bpy)₂]³⁺ (d) and [Ru(bpy)₂-bpt-Ru(dpp)₂]³⁺ (e) in MeCN with 0.1 M TBABF₄.*

The second and third reductions observed by DPV are more complicated as the peaks are not clearly defined. The peak observed at approximately –2.05 V must be treated with caution. Although it may be a reduction peak, the sharpness of its return to the base line suggests that it may be a current overload.

181
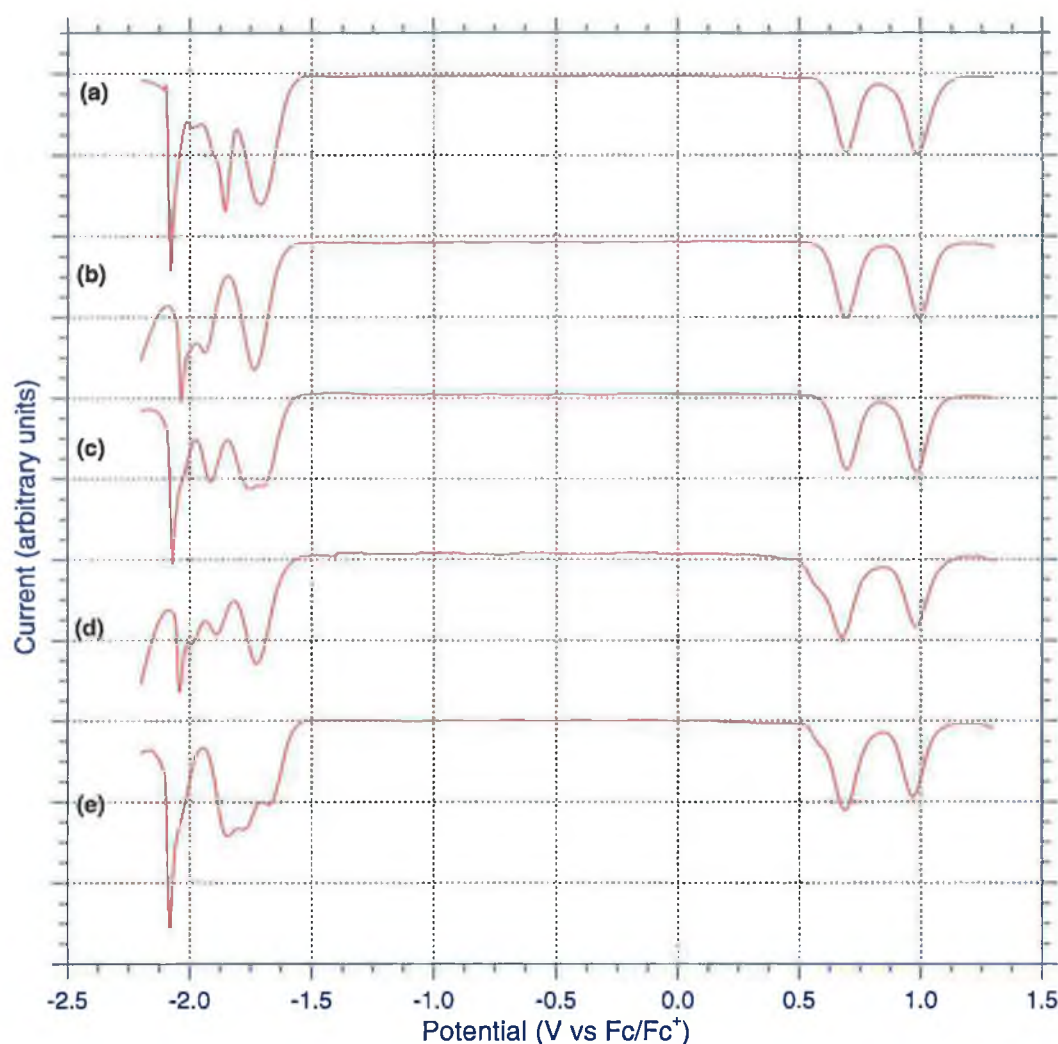
Figure 5.9. *DPV spectra obtained for [{Ru(bpy)(dpp)}$_2$(bpt)]$^{3+}$ (a), [Ru(bpy)(dpp)-bpt-Ru(bpy)$_2$]$^{3+}$ (b), [Ru(bpy)$_2$-bpt-Ru(bpy)(dpp)]$^{3+}$ (c), [Ru(dpp)$_2$-bpt-Ru(bpy)$_2$]$^{3+}$ (d) and [Ru(bpy)$_2$-bpt-Ru(dpp)$_2$]$^{3+}$ (e) in MeCN with 0.1 M TBABF$_4$.*

5.4   Absorption and emission spectra of dinuclear complexes

As for the mononuclear complexes in Chapter 4, the dinuclear complexes exhibit intense absorption bands in the visible part of the spectrum. Like the mononuclear analogues, these bands are assigned as singlet dπ–π* MLCT transitions. Table 5.4 gives λ_{max} for each of the dinuclear complexes. Comparing Tables 4.9 and 5.4, it can be seen that λ_{max} of the bpt$^-$ dinuclear complexes has shifted to a higher energy as when compared with their mononuclear analogues. This can be

182

explained by the sharing of the triazole negative charge between two metal centres as opposed to one. As outlined in Chapter 4, the triazole group is a good electron donor and raises the HOMO of the mononuclear complex. However, upon complexation of a second metal centre, the electron donating ability of the triazole is shared causing a relative lowering of the HOMO energy level. The larger energy gap between the HOMO and LUMO manifests itself as a higher energy λ_{max}. The same principle leads to the higher emission energy exhibited by these complexes.

Table 5.4. Absorption and emission properties for the dinuclear complexes.

Complex	Absorption[a] (nm)/ ($\varepsilon \times 10^4$)	Emission[b] 298 K (nm)/ τ (μs)	Emission[c] 77K (nm)/ τ (μs)
$[\{Ru(bpy)_2\}_2(bpt)]^{3+d}$	453 (2.26)	648 (0.08)	608 (3.6)
$[\{Ru(bpy)(Me_2bpy)\}_2(bpt)]^{3+}$	452 (2.18)	645 (0.08)	606 (3.8)
$[\{Ru(bpy)(phen)\}_2(bpt)]^{3+}$	423 (1.40)	631 (0.24)	601 (7.0)
$[\{Ru(bpy)(dpp)\}_2(bpt)]^{3+}$	436 (3.09)	639 (0.32)	613 (8.2)
$[\{Ru(bpy)(Me_2bpy)\}_2(bpzt)]^{3+}$	451 (2.32)	666 (0.09)	602 (7.8)
$[\{Ru(bpy)(phen)\}_2(bpzt)]^{3+}$	450 (2.87)	679 (0.28)	604 (8.0)
$[\{Ru(bpy)(dpp)\}_2(bpzt)]^{3+}$	452 (3.58)	665 (0.44)	605 (8.5)
$[Ru(bpy)_2-bpt-Ru(dpp)_2]^{3+}$	438 (3.08) 464 (2.98)	638 (0.29)	609 (6.1)
$[Ru(dpp)_2-bpt-Ru(bpy)_2]^{3+}$	439 (3.34)	640 (0.37)	617 (9.1)
$Ru(bpy)_2-bpt-Ru(bpy)(dpp)]^{3+}$	436 (2.67) 457 (2.67)	633 (0.27)	604 (5.5)
$Ru(bpy)(dpp)-bpt-Ru(bpy)_2]^{3+}$	447 (3.02)	641 (0.31)	615 (8.5)

[a] absorption spectra carried out in MeCN, [b] emission spectra in deaerated MeCN, [c] emission spectra in deaerated EtOH/MeOH (4:1) and [d] values from Ref. [12].

The behaviour of the bpzt⁻ dinuclear complexes is somewhat different. Comparisons of λ_{max} with their mononuclear analogues shows that the complexes

absorb at similar wavelength but emit at a lower energy. As discussed for the bpzt⁻ mononuclear complexes, the ligand bpzt⁻ is both a good σ-donor (triazole ring) and π-acceptor (pyrazine ring). Thus, as the σ-donating ability of the triazole ligand causes the HOMO of the metal ion to rise, the pyrazine ring causes the LUMO to fall. A red shift in energy would be expected in this case due to the narrowing of the MLCT band gap. As this is not the case a different process must be taking place. The electrochemical results in Section 5.3 suggest that the first reduction of the dinuclear bpzt⁻ complexes is bpzt⁻ based rather than bpy/Me₂bpy/phen/dpp based. Since this reduction occurs at a lower potential, the energy level of the LUMO (bpzt⁻ based) is slightly lower than that of the mononuclear complex (bpy/Me₂bpy/phen/dpp based). Since sharing the negative triazole bridge reduces its σ-donating capabilities, the HOMO energy is also reduced. The lowering of both the HOMO and LUMO cancel each other out and so the energy gap between them remains the same, hence similar λ_{max} and emission values.

It is interesting to note that the shape and λ_{max} of the dinuclear complexes is similar to that for the mononuclear complexes at low pH as studied in Section 4.6. Protonation of the mononuclear triazole ring reduces its σ-donating abilities. In the same manner, addition of a second metal centre causes the ring to share its negative charge with two metal centres as discussed above. Both effects produce similar results hence the similar spectra observed.

Fig. 5.11 shows the absorption and emission spectra for the dpp series. In each case λ_{max} is found at values typical for bpt⁻ dinuclear complexes. Two of the complexes, $[Ru(bpy)_2\text{-}bpt\text{-}Ru(dpp)_2]^{3+}$ and $[Ru(bpy)_2\text{-}bpt\text{-}Ru(bpy)(dpp)]^{3+}$ show more fine structure in their absorption spectra and exhibit two λ_{max} in the visible spectrum, Table 5.4. The emission maxima for these complexes are similar (~640 nm) with the exception of $[Ru(bpy)_2\text{-}bpt\text{-}Ru(bpy)(dpp)]^{3+}$ which shows an emission maxima at slightly higher energy (633 nm). The reason for this exception is unclear but a look at their 77 K emission maxima shows a clearer pattern.
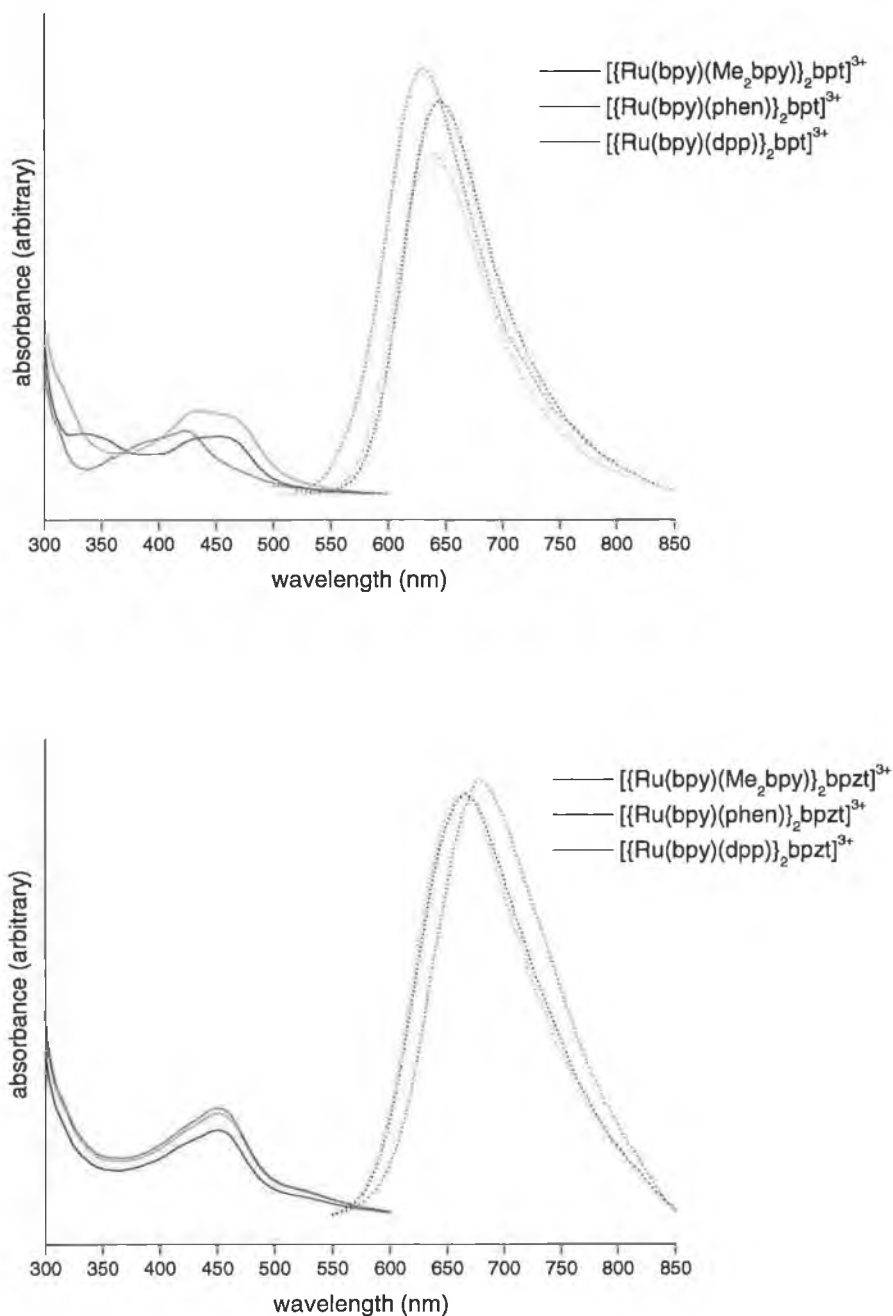
Figure 5.10. Absorption and emission spectra for the bpt⁻ (top) and bpzt⁻ (bottom) dinuclear complexes in MeCN.

As with the mononuclear complexes of Chapter 4, the dinuclear complexes show vibrational structure in their emission at 77 K [14]. This can be seen in the spectra for the dpp series in Fig. 5.12. In addition, their emission maxima are blue-shifted with respect to the room temperature emissions, a result of rigidchromism which is explained in Section 4.5 [15].

185
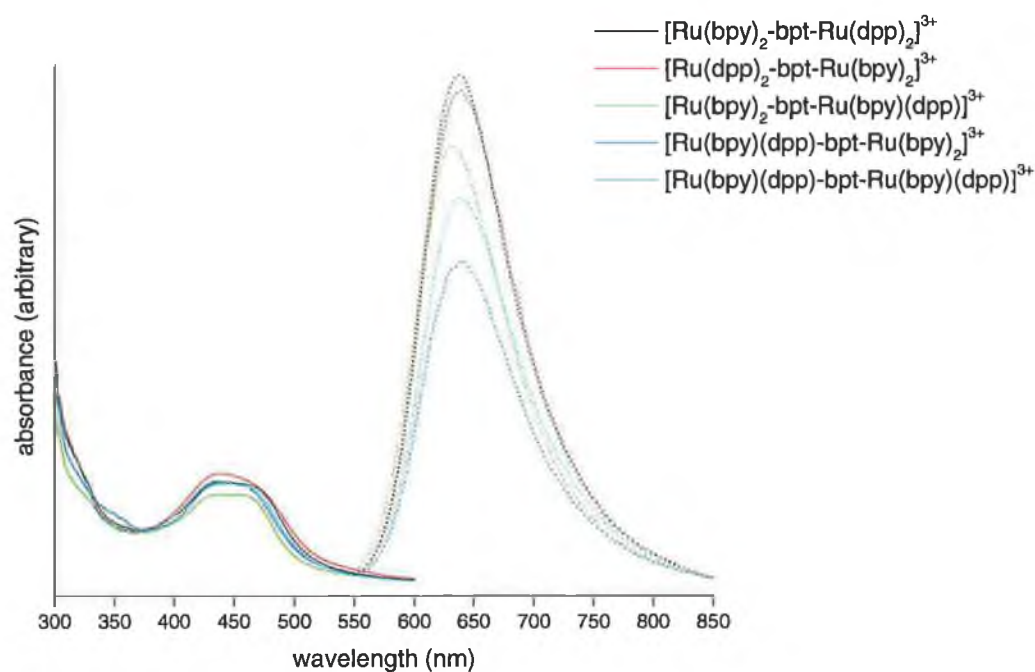
Figure 5.11. *Absorption and emission spectra for the dpp series of bpt⁻ dinuclear complexes in MeCN.*
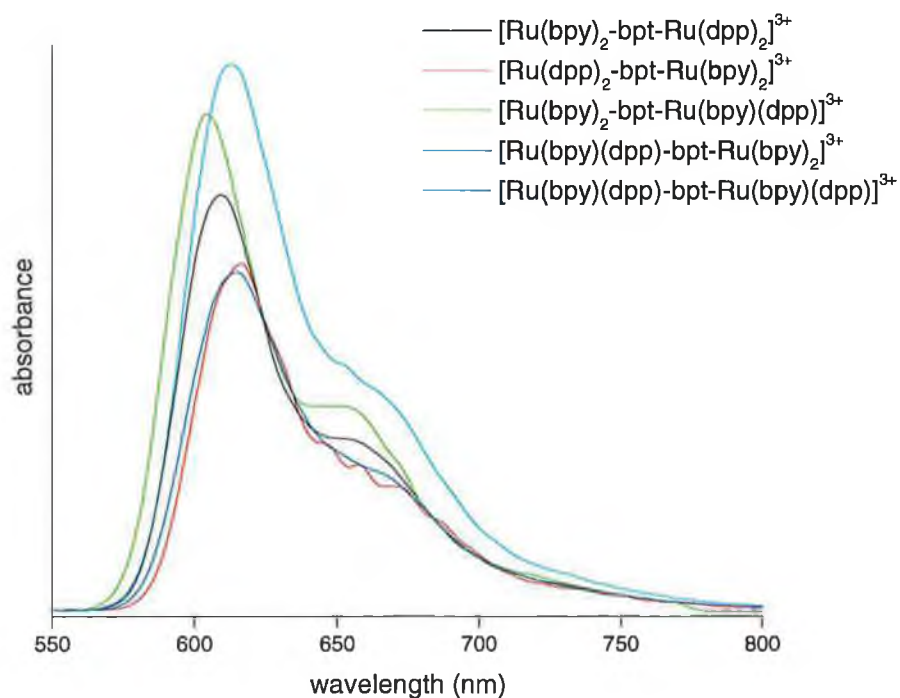
Figure 5.12. *Emission spectra for the dpp series of bpt⁻ dinuclear complexes in deaerated EtOH/MeOH (4:1) at 77 K.*

Comparing the emission maxima for the dpp series shows some interesting results. They suggest that the position of the dpp ligand in the dinuclear complex has some effect on the emission energy. The emission maxima of $[\{Ru(bpy)_2\}_2(bpt)]^{3+}$ at 77 K is 608 nm [1]. Replacing a bpy with dpp on the N2-bound centre, $[Ru(bpy)(dpp)\text{-}bpt\text{-}Ru(bpy)_2]^{3+}$, shifts the maxima to 615 nm. Correspondingly, the lifetime rises from 3.6 to 8.5 μs respectively. Alternatively, replacing an N4-bound bpy blue-shifts the maxima to 604 nm for $[Ru(bpy)_2\text{-}bpt\text{-}Ru(bpy)(dpp)]^{3+}$ with just a slight increase in lifetime (5.5 μs). Replacing both, as is the case for $[\{Ru(bpy)(dpp)\}_2(bpt)]^{3+}$ (613 nm, 8.2 μs), gives similar results to just replacing an N2-bound bpy. Thus, it seems that dpp has more effect when N2-bound than N4 bound. This agrees with previous studies that shows N2 to be a better σ-donor than N4. As part of an N2-bound centre, dpp aids electron donation to the metal centre which raises the HOMO level as is observed by the slight red-shift on going from $[\{Ru(bpy)_2\}_2(bpt)]^{3+} \rightarrow [Ru(bpy)(dpp)\text{-}bpt\text{-}Ru(bpy)_2]^{3+}$ (608 → 615 nm). Addition of a second dpp to N2 has only a slight effect as can be seen by the emission and lifetime of $[Ru(dpp)_2\text{-}bpt\text{-}Ru(bpy)_2]^{3+}$ (617 nm, 9.1 μs).

5.5 Experimental

[{Ru(bpy)(Me₂bpy)}₂bpt](PF₆)₃.2H₂O

Hbpt (0.08 g, 0.36 mmol) was dissolved in EtOH/H_2O (80/20, 20 ml) and heated at reflux. [Ru(bpy)(Me₂bpy)Cl₂] (0.41 g, 0.81 mmol) was added in one portion and the reaction continued for 24 h. The solution was reduced and purified by column chromatography on silica using a 0.1 M KNO_3 in MeCN/H_2O mobile phase. The second band (main band) was collected, reduced to dryness and redissolved in H_2O. A conc. aqueous NH₄PF₆ solution (1 ml) was added. The precipitate was filtered and dried *in vacuo*. The compound was further purified by column chromatography on alumina with MeCN as mobile phase. The first band was collected and the compound isolated by evaporating the solvent. This product was dissolved in a minimum of acetone, to which H_2O was added dropwise until a precipitate began to form. One or two drops of acetone were added to redissolve the precipitate and the solution allowed to slowly evaporate in darkness. The resulting precipitate was collected by vacuum filtration. Yield 0.29 g, 0.19 mmol, 53%. Elemental Analysis for $C_{56}H_{48}F_{18}N_{13}P_3Ru_2$: Calc. C 43.67, H 3.14, N 11.82, Found C 43.52, H 3.08, N 11.52. Mass spectrometry: $(M–PF_6)^+$ m/z 1396.

[{Ru(bpy)(phen)}₂bpt](PF₆)₃.2H₂O

As for [{Ru(bpy)(Me₂bpy)}₂bpt](PF₆)₃ except Hbpt (0.09 g, 0.40 mmol) and [Ru(bpy)(phen)Cl₂] (0.44 g, 0.87 mmol) in EtOH/H_2O (80/20, 20 ml) for 20 h. Yield 0.26 g, 0.17 mmol, 43%. Elemental Analysis for $C_{56}H_{44}F_{18}N_{13}O_2P_3Ru_2$: Calc. C 42.89, H 2.83, N 11.61, Found C 43.11, H 2.68, N 11.52. Mass spectrometry: $(M–PF_6)^+$ m/z 1388.

[{Ru(bpy)(dpp)}₂bpt](PF₆)₃.3H₂O

As for [{Ru(bpy)(Me₂bpy)}₂bpt](PF₆)₃ except Hbpt (0.05 g, 0.22 mmol) and [Ru(bpy)(dpp)Cl₂] (0.36 g, 0.54 mmol) in EtOH/H_2O (80/20, 20 ml) for 24 h. Yield 0.24 g, 0.13 mmol, 59%. Elemental Analysis for $C_{80}H_{62}F_{18}N_{13}O_3P_3Ru_2$: Calc. C 50.83, H 3.31, N 9.63, Found C 50.41, H 3.09, N 10.04. Mass spectrometry: $(M–PF_6)^+$ m/z 1692.

[{Ru(bpy)(Me₂bpy)}₂bpzt](PF₆)₃

As for [{Ru(bpy)(Me₂bpy)}₂bpt](PF₆)₃ except Hbpzt (0.08 g, 0.36 mmol) and [Ru(bpy)(Me₂bpy)Cl₂] (0.42 g, 0.83 mmol) in EtOH/H₂O (80/20, 20 ml) for 24 h. Yield 0.29 g, 0.19 mmol, 53%. Elemental Analysis for $C_{54}H_{46}F_{18}N_{15}P_3Ru_2$: Calc. C 42.06, H 3.01, N 13.62, Found C 42.52, H 3.08, N 13.32. Mass spectrometry: $(M-PF_6)^+$ m/z 1398.

[{Ru(bpy)(phen)}₂bpzt](PF₆)₃.H₂O

As for [{Ru(bpy)(Me₂bpy)}₂bpt](PF₆)₃ except Hbpzt (0.08 g, 0.36 mmol) and [Ru(bpy)(phen)Cl₂] (0.40 g, 0.79 mmol) in EtOH/H₂O (80/20, 20 ml) for 20 h. Yield 0.29 g, 0.19 mmol, 52%. Elemental Analysis for $C_{54}H_{40}F_{18}N_{15}OP_3Ru_2$: Calc. C 41.79, H 2.60, N 13.54, Found C 41.51, H 2.88, N 13.52. Mass spectrometry:$(M-PF_6)^+$ m/z 1390.

[{Ru(bpy)(dpp)}₂bpzt](PF₆)₃.3H₂O

As for [{Ru(bpy)(Me₂bpy)}₂bpt](PF₆)₃ except Hbpzt (0.07 g, 0.31 mmol) and [Ru(bpy)(dpp)Cl₂] (0.47 g, 0.71 mmol) in EtOH/H₂O (80/20, 20 ml) for 24 h. Yield 0.24 g, 0.13 mmol, 43%. Elemental Analysis for $C_{78}H_{60}F_{18}N_{15}O_3P_3Ru_2$: Calc. C 49.50, H 3.20, N 11.10, Found C 49.58, H 2.94, N 11.11. Mass spectrometry: $(M-PF_6)^+$ m/z 1694.

[Ru(bpy)₂(bpt)](PF₆)

Hbpt (1.02 g, 4.57 mmol) was dissolved in EtOH/H₂O (80/20, 100 ml) at reflux, to which [Ru(bpy)₂Cl₂].2H₂O (1.83 g, 3.51 mmol) was added in four portions over a one hour period. The solution was allowed to reflux for a further 4 h. The solution was reduced and purified by column chromatography on silica using a 0.1 M KNO₃ in MeCN/H₂O mobile phase. The second band was collected, reduced to dryness and redissolved in H₂O. A few drops of NH₃ were added followed by a conc. aqueous NH₄PF₆ solution (2 ml). The precipitate was filtered and dried *in vacuo*. The compound was further purified by column chromatography on alumina with MeCN as mobile phase. The first band was collected and the compound isolated by evaporating the solvent. This product was then dissolved in a minimum of acetone, to which H₂O was added dropwise until a precipitate began to form. One or two drops of acetone and one drop of

ammonium solution were added to redissolve the precipitate and the solution allowed to slowly evaporate in darkness. The resulting precipitate was collected by vacuum filtration. Yield 1.65 g, 2.11 mmol, 60%. Mass spectrometry: $(M-PF_6)^+$ m/z 636.

$[Ru(dpp)_2(bpt)](PF_6).H_2O$

As for $[Ru(bpy)_2(bpt)](PF_6)$ except Hbpt (0.88 g, 3.95 mmol) and $[Ru(dpp)_2Cl_2].2H_2O$ (1.67 g, 1.91 mmol) in $EtOH/H_2O$ (80/20, 50 ml). Yield 1.40 g, 1.24 mmol, 65%. Elemental Analysis for $C_{60}H_{42}F_6N_9OPRu$: Calc. C 62.61, H 3.68, N 10.95, Found C 62.48, H 3.31, N 10.68. Mass spectrometry: $(M-PF_6)^+$ m/z 988.

$[Ru(bpy)(dpp)-bpt-Ru(bpy)_2](PF_6)_3$

$[Ru(bpy)(dpp)(bpt)](PF_6)$ (0.24 g, 0.25 mmol) was refluxed in $EtOH/H_2O$ (80/20, 40 ml) with $[Ru(bpy)_2Cl_2].2H_2O$ (0.15 g, 0.29 mmol) for 22 h. The solution was reduced to 10 ml and aqueous NH_4PF_6 was added. The precipitate was collected, washed with H_2O, diethyl ether and then purified on an alumina column using $MeCN\backslash H_2O$ mobile phase. The solution was evaporated and the product obtained recrystallised from an acetone/H_2O solution as described for $[\{Ru(bpy)(Me_2bpy)\}_2bpt](PF_6)_3$. Yield 0.25 g, 0.15 mmol, 61%. Elemental Analysis for $C_{66}H_{48}F_{18}N_{13}P_3Ru_2$: Calc. C 47.75, H 2.91, N 10.97, Found C 47.78, H 2.66, N 10.56. Mass spectrometry: $(M-PF_6)^+$ m/z 1516.

$[Ru(bpy)_2-bpt-Ru(bpy)(dpp)](PF_6)_3$

$[Ru(bpy)_2(bpt)](PF_6)$ (0.21 g, 0.27 mmol) was refluxed in $EtOH/H_2O$ (80/20, 40 ml) with $[Ru(dpp)_2Cl_2].2H_2O$ (0.20 g, 0.30 mmol) for 22 h. The solution was reduced to 10 ml and aqueous NH_4PF_6 was added. The precipitate was collected, washed with H_2O, diethyl ether and then purified on an alumina column using $MeCN\backslash H_2O$ mobile phase. The solution was evaporated and the product obtained recrystallised from an acetone/H_2O solution as described for $[\{Ru(bpy)(Me_2bpy)\}_2bpt](PF_6)_3$. Yield 0.30 g, 0.18 mmol, 67%. Elemental Analysis for $C_{66}H_{48}F_{18}N_{13}P_3Ru_2$: Calc. C 47.75, H 2.91, N 10.97, Found C 47.97, H 2.53, N 10.77. Mass spectrometry: $(M-PF_6)^+$ m/z 1515.

[Ru(bpy)₂-bpt-Ru(dpp)₂](PF₆)₃.3H₂O

[Ru(bpy)$_2$(bpt)](PF$_6$) (0.20 g, 0.26 mmol) was refluxed with [Ru(dpp)$_2$Cl$_2$].2H$_2$O (0.25 g, 0.29 mmol) in EtOH\H$_2$O (80/20, 40 ml) for 21 h. The solution was reduced to 10 ml and aqueous NH$_4$PF$_6$ was added. The precipitate was collected, washed with H$_2$O, diethyl ether and then purified on an alumina column using MeCN\H$_2$O mobile phase. The solution was evaporated and the product obtained recrystallised from an acetone/H$_2$O solution as described for [{Ru(bpy)(Me$_2$bpy)}$_2$bpt](PF$_6$)$_3$. Yield 0.28 g, 0.15 mmol, 58%. Elemental Analysis for C$_{80}$H$_{62}$F$_{18}$N$_{13}$O$_3$P$_3$Ru$_2$: Calc. C 50.83, H 3.31, N 9.63, Found C 50.82, H 3.17, N 10.14. Mass spectrometry: (M–PF$_6$)$^+$ m/z 1692.

[Ru(dpp)₂-bpt-Ru(bpy)₂](PF₆)₃.2H₂O

[Ru(dpp)$_2$(bpt)](PF$_6$) (0.22 g, 0.19 mmol) was refluxed with [Ru(bpy)$_2$Cl$_2$].2H$_2$O (0.11 g, 0.22 mmol) in EtOH\H$_2$O (80/20, 40 ml) for 20 h. The solution was reduced to 10 ml and aqueous NH$_4$PF$_6$ was added. The precipitate was collected, washed with H$_2$O, diethyl ether and then purified on an alumina column using MeCN\H$_2$O mobile phase. The solution was evaporated and the product obtained recrystallised from an acetone/H$_2$O solution as described for [{Ru(bpy)(Me$_2$bpy)}$_2$bpt](PF$_6$)$_3$. Yield 0.18 g, 0.10 mmol, 53%. Elemental Analysis for C$_{80}$H$_{60}$F$_{18}$N$_{13}$O$_2$P$_3$Ru$_2$: Calc. C 51.32, H 3.23, N 9.72, Found C 51.48, H 2.86, N 10.20. Mass spectrometry: (M–PF$_6$)$^+$ m/z 1692.

5.6   Bibliography

[1] Hage R., Dijkhuis A.H.J., Haasnoot J.G., Prins R., Reedijk J., Buchanan B.E., Vos J.G., *Inorg. Chem.*, **1988**, *27*, 2185–2189.

[2] Bignozzi C.A., Bortolini O., Curcuruto O., Hamdan M., *Inorg. Chim. Acta*, **1995**, *233*, 113–118.

[3] Liang X., Suwanrumpha S., Freas R.B., *Inorg. Chem.*, **1991**, *30*, 652–658.

[4] Hage R., Haasnoot J.G., Stufkens D.J., SnoeckT.L., Vos J.G., Reedijk J., *Inorg. Chem.*, **1989**, *28*, 1413–1414.

[5] Kumar C.V., Barton J.K., Turro N.J., Gould I.R., *Inorg. Chem.*, **1987**, *26*, 1455–1457.

[6] Turro C., Bossman S.H., Leroi G.E., Barton J.K., Turro N.J., *Inorg. Chem.*, **1994**, *33*, 1344–1347.

[7] Coates C.G., Keyes T.E., Hughes H.P., Jayaweera P.M., McGarvey J.J., Vos J.G., *J. Phys. Chem. A*, **1988**, *102*, 5013–5018.

[8] Hughes H.P., Martin D., Bell S., McGarvey J.J., Vos J.G., *Inorg. Chem.*, **1993**, *32*, 4402–4408.

[9] Hughes H.P., The synthesis, characterisation, photochemical and photophysical properties of ruthenium(II) and osmium(II) polypyridyl complexes containing triazole ligands, Ph.D. Dissertation, Dublin City University, Ireland, **1993**.

[10] Kaifer A.E., Gomez-Kaifer M., Supramolecular Electrochemistry, Wiley-VCH, Weinheim, Germany, **1999**.

[11] Pavlishchuk V.V., Addison A.W., *Inorg. Chim. Acta*, **2000**, *298*, 97–102.

[12] Hage R., Ruthenium and osmium complexes containing triazole ligands: syntheses, structures, electrochemical and photophysical properties, Ph.D. Dissertation, Leiden University, The Netherlands, **1991**.

[13] Hage R., Haasnoot J.G., Reedijk J., Vos J.G., *Chemtracts (Inorg. Chem.)*, **1992**, *4*, 75–93.

[14] Lumpkin R.S., Kober E.M., Worl L., Murtaza Z., Meyer T.J., *J. Phys. Chem.*, **1990**, *94*, 239–243.

[15] Wrighton M., Morse D.L., *J. Am. Chem. Soc.*, **1974**, *96*, 998–1003.

Chapter 6.

Conclusions and Future Work

This chapter summarises the synthetic work presented in this thesis, concentrating on the successful route to a tris(heteroleptic) complex containing a triazole ligand. The properties of the subsequent mononuclear and dinuclear complexes are reviewed with suggestions of future studies which might answer queries arising from this work.

A number of mononuclear and dinuclear Ru(II) tris(heteroleptic) complexes have been successfully synthesised as outlined in the previous chapters. The synthetic route employed is one which should prove generic enough to allow the design and synthesis of a wide range of complexes. A number of alternative routes are available but were found to be inadequate for our purposes.

At the beginning of Chapter 3 a number of requirements for a successful synthetic route were posed. These included mild reaction conditions, isolation of a dichloride precursor and relatively high yields. With these points in mind a number of synthetic routes were explored. Two of these routes began with the starting materials [Ru(bpy)Cl$_3$] and [Ru(DMSO)$_4$Cl$_2$]. The ready availability of such materials showed promise but as outlined in Chapter 3, no dichloride precursor was isolated. Numerous attempts in various solvents under different conditions proved futile. Even bypassing the dichloride isolation with a one-pot synthesis proved ineffective at introducing a triazole to the metal coordination sphere.

The synthesis of a tris(heteroleptic) complex was achieved using [Ru(bpy)(CO)$_2$Cl$_2$] as starting material. In this case Me$_2$bpy was added to form [Ru(bpy)(Me$_2$bpy)(CO)$_2$]$^{2+}$ which when photolysed in MeCN yielded the useful precursor [Ru(bpy)(Me$_2$bpy)(MeCN)$_2$]$^{2+}$. It is likely that this precursor will react with any bidentate ligand but in this case was only reacted with Hpytrz. The drawback of this method is that the carbonyl complex [Ru(L)(L')(CO)$_2$]$^+$ was only readily synthesised for a few examples of L such as bpy, Me$_2$bpy and phen. Removing the Cl ligands with triflic acid was attempted. Replacing Cl with triflate groups to form [Ru(bpy)(CO)$_2$(CF$_3$SO$_3$)$_2$] proved troublesome and so this method was set aside.

Attempts to remove the carbonyl ligands a stage earlier were undertaken and so the photolysis of [Ru(bpy)(CO)$_2$Cl$_2$] in MeCN was performed. This resulted in a mixture of two complexes, the characterisation of which suggests a 1:4 ratio of [Ru(bpy)(MeCN)$_2$Cl$_2$] and [Ru(bpy)(MeCN)$_3$Cl]Cl. Preparative separation of the two species is an area which should be further explored. This would identify whether one species reacts with the second bidentate ligand more favourably than

the other to create the dichloride. Such information would allow the tailoring of the photolysis reaction to maximise the yield of the desired acetonitrile complex.

Even without preparative separation the mixture was successfully reacted with a second bidentate polypyridyl ligand (bpy/Me$_2$bpy/phen/dpp) to create a number of dichlorides in sufficient yield and purity. The isolation of [Ru(bpy)(Me$_2$bpy)(pytrz)]$^+$ in Chapter 3 preceded the synthesis of a number of mononuclear and dinuclear complexes containing different triazole ligands, namely bpt$^-$ and bpzt$^-$. CHN, MS, HPLC and X-ray crystallography measurements corroborated each other which suggests that these complexes were successfully synthesised and isolated. Several peaks remain unaccounted for in the mass spectra of the dinuclear complexes. Further MS/MS studies should shed light on the fragmentation patterns observed.

The characterisation of these complexes were complicated by the fact that a number of potential isomers may form. Thus, ^{1}H NMR spectra were difficult to assess. A number of examples of how ^{1}H NMR proved useful are given. In the case of mononuclear complexes, ^{1}H NMR studies suggest that one of the two possible isomers might be synthetically favourable over the other. However, without resolution of the isomers it is difficult to assess which orientation is favoured. Semi-preparative HPLC studies have been carried out in our laboratory to isolate species which did not separate readily on a preparative column. Further studies with these complexes might prove adequate at separating the isomers.

Electrochemical and luminescence studies show that the bpt$^-$ and bpzt$^-$ complexes behave quite differently. In the case of the bpt$^-$ and bpzt$^-$ mononuclear complexes, the excited state lies on an auxiliary ligand and not on the triazole bridge. In the case of the dinuclear complexes, the excited state remains on the auxiliary ligands for the bpt$^-$ complexes but switches to the bridge for the bpzt$^-$ dinuclear compounds.

The results of the dpp series of bpt$^-$ dinuclear complexes suggest that the effect of ligand substitution around the N2-bound centre has more of an effect on emission properties than that of N4-bound. These studies are only preliminary and further

investigation is required. Although resonance Raman studies were carried out in the course of this thesis, they were primarily used for confirmation of dpp ligands around the metal centre. Excited-state resonance Raman studies are an obvious next step, the results of which should confirm which auxiliary ligand the excited-state lies.

Now that a suitable method for synthesising tris(heteroleptic) complexes is available, a great number of specially designed complexes are possible. One such idea would be to use this method to introduce deuterated ligands to the metal sphere. One could synthesise complexes where one, two or all three ligands are deuterated. In addition to simplifying the NMR spectra of such a complex, the excited state could also be located.

Although the method is new and needs fine-tuning (maximise yields and lower reaction times), it is hoped that it will prove useful in the future for building larger and more complicated structures based on Ru(II) polypyridyl systems.

Appendix A.   Ru(II) Triazole-Carbonyl Intermediates

As an alternative possible route to Ru(II) tris(heteroleptic) complexes a range of triazole $[Ru(L)(CO)_2Cl_2]$ complexes were synthesised and characterised. Scheme 3.1 shows where these synthetic intermediates might fit into an overall strategy in producing Ru(II) tris(heteroleptic) triazole complexes. The complexes prepared are outlined in Table A1 below.

In a typical experiment 1 mmol of $[Ru(CO)_2Cl_2]_n$ was refluxed with 1.3 mmol of L in MeOH (40 ml) for 2 h. If a precipitate appeared it was filtered hot and washed with MeOH and dried *in vacuo*. If a precipitate did not appear, the solution was reduced to 5 ml, filtered, and 2 drops conc. HCl added. The solution was placed in a freezer overnight and the resulting precipitate filtered. Crystals were obtained by dissolving $[Ru(CO)_2Cl_2]_n$ and L in separate aliquots of boiling MeOH, filtering, mixing and letting stand over night. The resultant crystals were collected by filtration, washed with cold MeOH and dried under vacuum.

The synthetic method followed was similar to that of Rheingold *et al.* who reported the synthesis of an amino-triazole complex with ruthenium [1]. They also reported crystal structures of the two coordination isomers of this complex as shown in Fig. A1.

Figure A1. Crystal structures of the amine-bpt (apt) used by Rheingold et al [1]. Data for crystals was supplied by Cambridge Crystallographic Data Centre and modelled using CCDC supplied Mercury 1.1.2 software. H atoms are omitted for clarity.

[1] Rheingold A.L., Saisuwan P., Thomas N.C., *Inorg. Chim. Acta*, **1993**, *214*, 41–45.
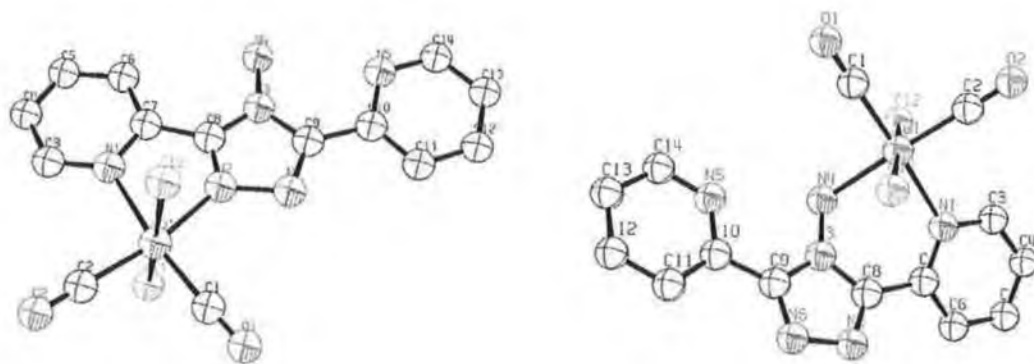
Table A1. Yield and spectroscopic IR data for $[Ru(L)(CO)_2Cl_2]$ complexes where L is a triazole ligand.
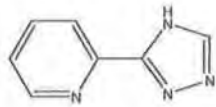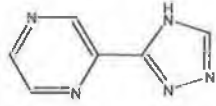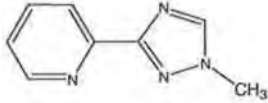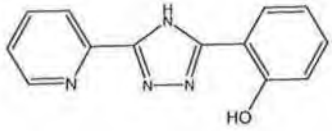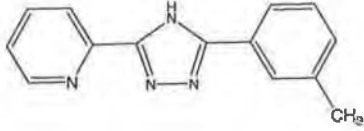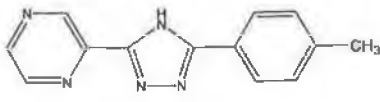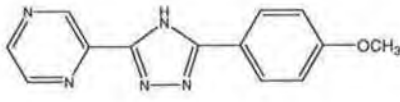
Triazole ligand	Yield (%)	$\nu_{(CO)}$ of $[Ru(L)(CO)_2Cl_2]$ in $CHCl_3$ (cm^{-1})
L1	26	2075, 2000
L2	40	2072, 2011
L3	59	2072, 2012
L4	31	2072, 2019
L5	56	2078, 2021
L6	24	2074, 2012
L7	32	2077, 2020

Table A1 shows the yield and spectroscopic data for the ligands used in these studies. CHN analysis indicate that the triazole ring remains protonated when complexed to the metal centre. This is unusual because normally the triazole deprotonates to yield the anion upon complexation to a metal centre. ^{1}H NMR and IR studies show only one set of resonances for each ligand and carbonyl group

respectively. The absence of any new resonances suggests that the complexes take on a *trans*-(Cl),*cis*-(CO) configuration with the carbonyl ligands *trans* to the binding nitrogens. As previously mentioned in Chapter 2 regarding the structure of [Ru(bpy)(CO)$_2$Cl$_2$], the carbonyl ligands would be expected to favour a *cis*-formation due to competition for π-backbonding from the metal orbitals. Indeed, the structures obtained from crystals of [Ru(CO)$_2$Cl$_2$]$_n$ complexed with ligands **(1)**, **(6)** and **(7)** show similar arrangements of the ligands around the metal centre. Table A2 lists the crystallographic data for [Ru(L6)(CO)$_2$Cl$_2$] and [Ru(L7)(CO)$_2$Cl$_2$] with the structures represented in Fig. A2.

Table A2. Crystallographic data for [Ru(L)(CO)$_2$Cl$_2$] where L is triazole ligand (L6) and (L7).

	[Ru(L6)(CO)$_2$Cl$_2$]	[Ru(L7)(CO)$_2$Cl$_2$]
chemical formula	C$_{16}$H$_{15}$Cl$_2$N$_5$O$_3$Ru	C$_{15}$H$_{11}$Cl$_2$N$_5$O$_3$Ru
fw	497.30	481.26
colour	yellow	yellow
crystal source	methanol	methanol
temperature (K)	296 (2)	294 (2)
crystal size (mm)	0.48×0.18×0.16	0.45×0.20×0.08
a (Å)	11.0433 (6)	14.2089 (11)
b (Å)	10.6963 (6)	9.5634 (5)
c (Å)	16.7567 (10)	14.5834 (9)
α (deg.)	90	90
β (deg.)	97.842 (2)	115.618 (5)
γ (deg.)	90	90
V (Å^3)	1960.83 (19)	1786.9 (2)
$D_{calc.}$ (g.cm^{-3})	1.685	1.789
Z	4	4
F (000)	992	952
radiation	Mo Kα	Mo Kα
abs. coeff., μ (mm^{-1})	1.098	1.202
abs. corr., T (min, max)	0.621, 0.844	0.6137, 0.9099
2θ limits, deg.	1.9–26.0	2.13–28.05
no. of reflections	3858	4314
no. of parameters	254	240
R (F)	0.0387	0.0487
R_w (F)	0.0286	0.0322
goodness of fit	1.050	1.044
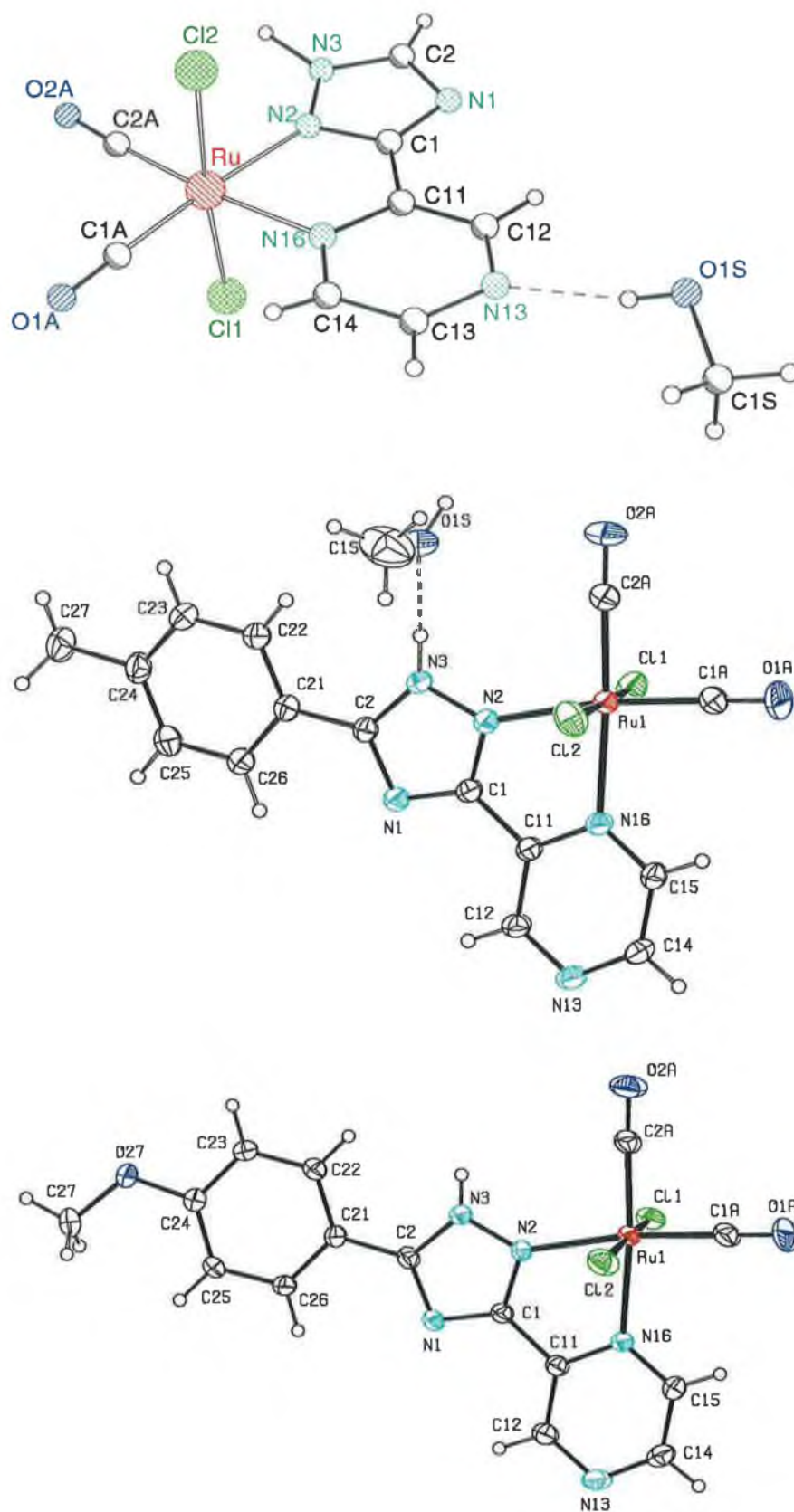
Figure A2. *Crystal structures for [Ru(L1)(CO)₂Cl₂] (top), [Ru(L6)(CO)₂Cl₂] (middle) and [Ru(L7)(CO)₂Cl₂] (bottom).*

The crystal structures obtained corroborate the CHN results in that the triazole ring is protonated on N(3) in each case. It is interesting that only the pyrazine triazoles yielded crystals suitable for study.

The similarity of these complexes and those of Rheingold *et al.* is apparent from Table A3. The Ru–CO and Ru–Cl distances are comparable in all cases. In both triazole complexes the Ru–CO distance opposite the triazole is slightly shorter. Strangely, Haukka et al. report different bond distances for the two Ru–CO ligands although both are opposite a pyridine ring and thus inhabit a similar chemical environment. Their two C–O bonds also show different lengths. They do not include the CH_2Cl_2 molecule, which was part of their crystal structure, and this might be having some kind of interaction with the molecule. The "bite" angle for both triazole complexes is expected to be similar and this is indeed found to be true.

Table A3. Selected bond lengths and angles for the crystals [Ru(L1)(CO)$_2$Cl$_2$], [Ru(L6)(CO)$_2$Cl$_2$], [Ru(L7)(CO)$_2$Cl$_2$] and [Ru(apt)(CO)$_2$Cl$_2$].

	[Ru(L1)(CO)$_2$Cl$_2$]	[Ru(L6)(CO)$_2$Cl$_2$]	[Ru(L7)(CO)$_2$Cl$_2$]	[Ru(apt)(CO)$_2$Cl$_2$]*
	Bond distances (Å)			
Ru–Cl(1)	2.3999(10)	2.387 (8)	2.4064(8)	2.387 (1)
Ru–Cl(2)	2.3749(10)	2.381 (9)	2.3818(9)	2.386 (1)
Ru–C(1A)	1.875(4)	1.862 (3)	1.876(3)	1.851 (6)
Ru–C(2A)	1.882(4)	1.871 (3)	1.888(3)	1.881 (6)
Ru–N(2)	2.106(3)	2.115 (2)	2.109(2)	2.070 (4)
Ru–N(16)	2.150(3)	2.163 (2)	2.143(2)	2.150 (4)
C(1A)–O(1A)	1.140(5)	1.126 (4)	1.127(4)	1.131 (8)
C(2A)–O(2A)	1.130(5)	1.135 (4)	1.125(3)	1.135 (8)
	Bond angles (deg.)			
Cl(1)–Ru–Cl(2)	175.12(4)	175.81 (3)	174.44(2)	173.4 (1)
Cl(1)–Ru–C(1A)	91.95(13)	91.45 (11)	92.11(12)	94.3 (2)
Cl(1)–Ru–C(2A)	91.74(13)	90.88 (11)	93.51(10)	92.8 (2)
Cl(1)–Ru–N(16)	89.10(8)	89.30 (6)	88.57(6)	85.5 (1)
Cl(1)–Ru–N(2)	89.33(9)	86.07 (7)	87.24(7)	89.7 (1)
Cl(2)–Ru–C(1A)	92.02(13)	92.59 (11)	90.66(12)	89.8 (2)
Cl(2)–Ru–C(2A)	91.09(13)	90.35 (11)	91.38(10)	92.2 (2)
Cl(2)–Ru–N(16)	87.67(8)	89.22 (6)	86.36(6)	88.9 (1)
Cl(2)–Ru–N(2)	86.39(9)	89.77 (7)	89.33(7)	85.7 (1)
C(1A)–Ru–C(2A)	89.91(18)	88.48 (13)	88.46(13)	91.2 (3)
C(1A)–Ru–N(16)	89.10(8)	95.19 (11)	95.82(11)	97.6 (2)
C(1A)–Ru–N(2)	173.03(15)	171.02 (11)	171.89(11)	172.6 (2)
C(2A)–Ru–N(16)	173.94(14)	176.32 (10)	175.18(11)	171.1 (2)
C(2A)–Ru–N(2)	96.90(15)	100.18 (11)	99.65(10)	94.9 (2)
N(16)–Ru–N(2)	77.11(12)	76.17 (8)	76.09(8)	76.4 (1)

* Data for [Ru(apt)(CO)$_2$Cl$_2$] obtained from Ref 1.

As part of the triazole carbonyl studies, the ligand L8 (a gift from Prof. Sally Brooker) was complexed to a ruthenium centre. The reaction was carried out in a similar fashion to that described previously for the triazole ligands with the exception that some CHCl$_3$ was added to aid solubility of the ligand. With L8, two binding sites exist. Although the mononuclear complex was successfully isolated, attempts to add a second nucleus failed, even when large excess of [Ru(CO)$_2$Cl$_2$]$_n$ was used.

L8
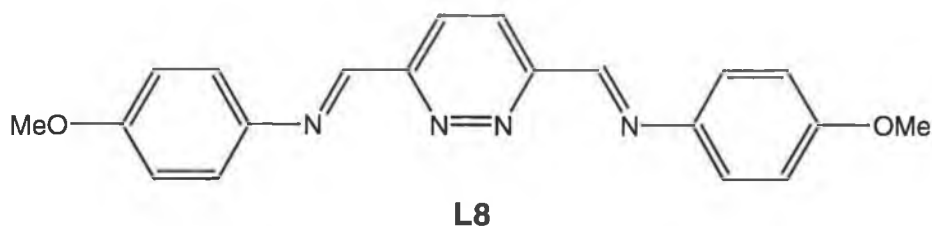
Figure A3. *Structure of the ligand L8 used, courtesy of Prof. Sally Brooker.*

^{1}H NMR of the isolated complex suggests the formation of a mononuclear species. Complexation of a metal to one of the binding sites would introduce an inequivalency to the proton spectrum. This is observed as shown in the spectrum in Fig. A4. The appearance of two IR $v_{(CO)}$ stretching bands at 2066 and 1999 cm^{-1} (KBr) is also indicative of asymmetry and suggests that the CO ligands take up a *cis*-orientation as was found for the triazole complexes earlier.
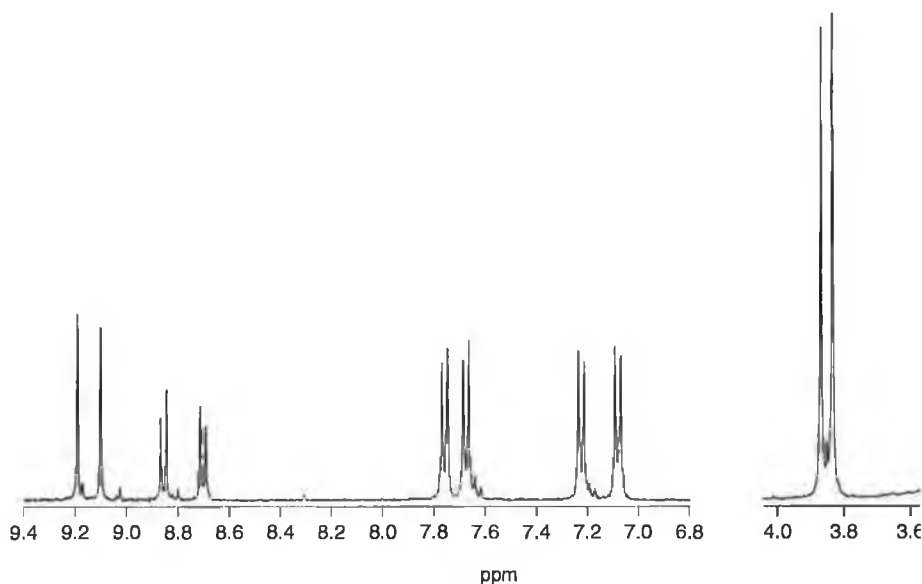
Figure A.4. *^{1}H NMR spectra of [Ru(L8)(CO)$_2$Cl$_2$] in d$_6$-DMSO.*

Crystals were successfully grown by allowing a dilute solution of L8 and $[Ru(CO)_2Cl_2]_n$ in MeOH react slowly at room temperature. These studies confirm the results obtained by ^{1}H NMR, IR and CHN. The results are tabulated in Tables A4 and A5 and the structure shown in Fig. A5. The bond lengths found are

similar to those of the triazole complexes. In fact, [Ru(L8)(CO)$_2$Cl$_2$] most closely matches [Ru(L7)(CO)$_2$Cl$_2$] which both have a methoxy phenyl group in common.

Table A4. Crystallographic data for [Ru(L8)(CO)$_2$Cl$_2$].

	[Ru(L8)(CO)$_2$Cl$_2$]
chemical formula	C$_{22}$H$_{18}$Cl$_2$N$_4$O$_4$Ru
fw	574.37
colour	red
crystal source	methanol
temperature (K)	168(2)
crystal size (mm)	0.35 x 0.11 x 0.06
a (Å)	9.303(3)
b (Å)	10.354(3)
c (Å)	13.072(4)
α (deg.)	70.746(4)
β (deg.)	72.006(4)
γ (deg.)	80.088
V (Å^3)	1127.2(6)
$D_{calc.}$ (g.cm^{-3})	1.692
Z	2
F (000)	576
radiation	
abs. coeff., μ (mm^{-1})	0.970
abs. corr., T (min, max)	0.91, 1.00
2θ limits, deg.	2.09–26.48
no. of reflections	14761
no. of parameters	300
R (F)	0.0439
R_w (F)	0.0266
goodness of fit	0.957
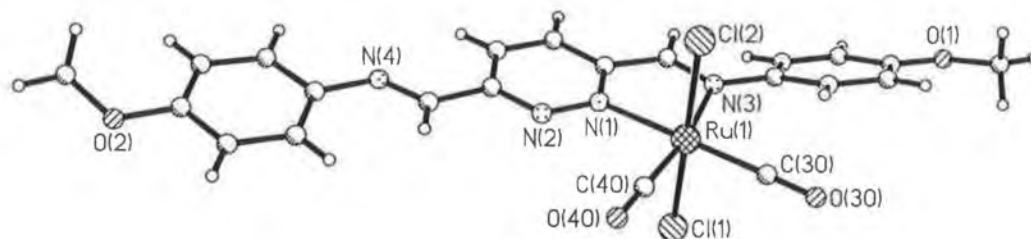
Figure A5. Crystal structure for [Ru(L8)(CO)$_2$Cl$_2$].

Table A5. Selected bond lengths and angles for [Ru(L8)(CO)$_2$Cl$_2$]

[Ru(L8)(CO)$_2$Cl$_2$]	
	Bond distances (Å)
Ru(1)-C(40)	1.873(3)
Ru(1)-C(30)	1.886(3)
Ru(1)-N(1)	2.092(2)
Ru(1)-N(3)	2.176(2)
Ru(1)-Cl(1)	2.3882(10)
Ru(1)-Cl(2)	2.4058(9)
	Bond angles (deg.)
C(40)-Ru(1)-C(30)	87.53(11)
C(40)-Ru(1)-N(1)	92.90(10)
C(30)-Ru(1)-N(1)	179.06(10)
C(40)-Ru(1)-N(3)	169.48(9)
C(30)-Ru(1)-N(3)	102.84(9)
N(1)-Ru(1)-N(3)	76.71(8)
C(40)-Ru(1)-Cl(1)	89.12(9)
C(30)-Ru(1)-Cl(1)	88.97(8)
N(1)-Ru(1)-Cl(1)	90.21(6)
N(3)-Ru(1)-Cl(1)	89.29(6)
C(40)-Ru(1)-Cl(2)	94.02(9)
C(30)-Ru(1)-Cl(2)	92.44(8)
N(1)-Ru(1)-Cl(2)	88.37(6)
N(3)-Ru(1)-Cl(2)	87.39(6)
Cl(1)-Ru(1)-Cl(2)	176.62(3)

It was thought that these carbonyl complexes might provide an alternative route towards tris(heteroleptic) complexes. However, failure of the carbonyl complex to react further with bpy or Me$_2$bpy resulted in this synthetic avenue being discarded. A fuller description of subsequent attempted reactions is given in Chapter 3.

Synthesis of Complexes

[Ru(L1)(CO)₂Cl₂].H₂O

[Ru(CO)₂Cl₂]$_n$ (0.31 g, 1.4 mmol) was dissolved in hot MeOH (30 ml). A methanolic solution of L1 (0.20 g, 1.4 mmol in 10 ml) was added and the solution heated at reflux for 2.5 h. The solution was reduced to 5 ml, 2 drops conc. HCl added and cooled at –4°C overnight. The resultant feathery yellow precipitate was filtered, washed with cold MeOH (5 ml) and dried *in vacuo*. Yield 0.13 g, 0.36 mmol, 26%. ^{1}H NMR (d₆-DMSO, 298 K) δ 9.91 (s), 9.17 (d), 8.41 (d), 8.34 (t), 7.85 (t) ppm. IR (CHCl₃) $\nu_{(CO)}$ 2075, 2000 cm^{-1}. Elemental Analysis for C₉H₈Cl₂N₄O₃Ru: Calc. C 27.56, H 2.06, N 14.29; Found C 27.88, H 1.80, N 14.29.

[Ru(L2)(CO)₂Cl₂].MeOH

[Ru(CO)₂Cl₂]$_n$ (0.30 g, 1.3 mmol) was dissolved in hot MeOH (30 ml). A methanolic solution of L2 (0.20 g, 1.35 mmol in 10 ml) was added and the solution heated at reflux for 1.5 h. The resultant red precipitate was filtered hot, washed with MeOH (10 ml) and dried *in vacuo*. Yield 0.20 g, 0.52 mmol, 40%. ^{1}H NMR (d₆-DMSO, 298 K) δ 10.01 (s), 9.71 (d), 9.34 (dd), 9.10 (d) ppm. IR (CHCl₃) $\nu_{(CO)}$ 2072, 2011 cm^{-1}. Elemental Analysis for C₉H₉Cl₂N₅O₃Ru: Calc. C 26.55, H 2.23, N 17.20; Found C 26.42, H 2.09, N 16.94.

[Ru(L3)(CO)₂Cl₂]

[Ru(CO)₂Cl₂]$_n$ (0.23 g, 1.0 mmol) was dissolved in hot MeOH (30 ml). A methanolic solution of L3 (0.20 g, 1.3 mmol in 10 ml) was added and the solution heated at reflux for 1 h. The resultant feathery yellow precipitate was filtered hot, washed with MeOH (10 ml) and dried *in vacuo*. Yield 0.23 g, 0.6 mmol, 59%. ^{1}H NMR (d₆-DMSO, 298 K) δ 9.72 (s), 9.05 (d), 8.22 (t), 8.21 (d), 7.73 (t), 4.03 (s) ppm. IR (CHCl₃) $\nu_{(CO)}$ 2072, 2012 cm^{-1}. Elemental Analysis for C₁₀H₈Cl₂N₄O₂Ru: Calc. C 30.94, H 2.08, N 14.43; Found C 30.94, H 1.96, N 14.18.

[Ru(L4)(CO)₂Cl₂].H₂O

[Ru(CO)₂Cl₂]$_n$ (0.19 g, 0.83 mmol) was dissolved in hot MeOH (30 ml). A methanolic solution of L4 (0.20 g, 0.83 mmol in 10 ml) was added and the solution heated at reflux for 3 h. The resultant precipitate was filtered hot, washed with MeOH (5 ml) and dried *in vacuo*. Yield 0.12 g, 0.25 mmol, 31%. ^{1}H NMR (d₆-DMSO, 298 K) δ 9.18 (d), 8.53 (d), 8.39 (t), 8.02 (d), 7.81 (t), 7.44 (t), 7.12 (d), 7.04 (t) ppm. IR (CHCl₃) ν$_{(CO)}$ 2072, 2019 cm^{-1}. Elemental Analysis for C₁₅H₁₂Cl₂N₄O₄Ru: Calc. C 37.20, H 2.50, N 11.57; Found C 37.43, H 2.36, N 11.10.

[Ru(L5)(CO)₂Cl₂].H₂O

[Ru(CO)₂Cl₂]$_n$ (0.19 g, 0.83 mmol) was dissolved in hot MeOH (30 ml). A methanolic solution of L5 (0.2 g, 0.85 mmol in 10 ml) was added and the solution heated at reflux for 2 h. The solution was reduced to 5 ml, 2 drops conc. HCl added and cooled at –4°C overnight. The resultant yellow precipitate was filtered, washed with cold MeOH (5 ml) and dried *in vacuo*. Yield 0.21 g, 0.46 mmol, 56%. ^{1}H NMR (d₆-DMSO, 298 K) δ 9.03 (d), 8.27 (d), 8.23 (t), 7.81 (s), 7.78 (d), 7.67 (t), 7.37 (t), 7.27 (d), 2.28 (s) ppm. IR (CHCl₃) ν$_{(CO)}$ 2078, 2021 cm^{-1}. Elemental Analysis for C₁₆H₁₄Cl₂N₄O₃Ru: Calc. C 39.85, H 2.93, N 11.62; Found C 40.13, H 2.99, N 11.51.

[Ru(L6)(CO)₂Cl₂].MeOH

[Ru(CO)₂Cl₂]$_n$ (0.19 g, 0.83 mmol) was dissolved in hot MeOH (30 ml). A methanolic solution of L6 (0.2 g, 0.85 mmol in 10 ml) was added and the solution heated at reflux for 2 h. After cooling, 1 ml conc. HCl was added and the solution stored at –4°C overnight. The resultant yellow precipitate was filtered, washed with cold MeOH (5 ml) and dried *in vacuo*. Yield 0.09 g, 0.20 mmol, 24%. ^{1}H NMR (d₆-DMSO, 298 K) δ 9.48 (s), 9.22 (d), 8.93 (d), 7.96 (d), 7.35 (d), 3.07 (s) ppm. IR (CHCl₃) ν$_{(CO)}$ 2074, 2012 cm^{-1}. Elemental Analysis for C₁₆H₁₅Cl₂N₅O₃Ru: Calc. C 38.64, H 3.04, N 14.08; Found C 38.41, H 3.06, N 13.79.

[Ru(L7)(CO)₂Cl₂].MeOH

[Ru(CO)₂Cl₂]$_n$ (0.20 g, 0.88 mmol) was dissolved in hot MeOH (30 ml). A methanolic solution of L7 (0.23 g, 0.90 mmol in 10 ml) was added and the solution heated at reflux for 2 h. HCl was added and the solution stored at –4°C overnight. The resultant yellow precipitate was filtered, washed with cold MeOH (5 ml) and dried *in vacuo*. Yield 0.13 g, 0.28 mmol, 32%. ^{1}H NMR (d$_6$-DMSO, 298 K) δ 9.52 (s), 9.32 (d), 9.01 (d), 8.14 (d, 2H), 7.16 (d, 2H), 3.95 (s, 3H) ppm. Elemental Analysis for $C_{16}H_{15}Cl_2N_5O_4Ru$: Calc. C 37.44, H 2.95, N 13.64; Found C 37.32, H 2.80, N 13.39.

[Ru(L8)(CO)₂Cl₂]

L8 (104 mg, 0.3 mmol) was dissolved in 30 ml of MeOH/CHCl₃ (2:1) with a little heating. [Ru(CO)₂Cl₂]$_n$ (160 mg, 0.7 mmol) was dissolved in 15 ml MeOH and added in one portion. The solution was allowed reflux for 3 h, cooled and the resulting precipitate filtered. The precipitate was washed with hot MeOH (2 × 10 ml) and finally CHCl₃ (3 × 5 ml). Yield 90 mg, 0.16 mmol, (53%).^{1}H NMR (d$_6$-DMSO, 298 K) δ 9.20 (s), 9.11 (s), 8.86 (d), 8.71 (d), 7.76 (d), 7.68 (d), 7.23 (d), 7.08 (d), 3.87 (s), 3.84 (s) ppm. IR (KBr) $v_{(CO)}$ 2066, 1999 cm^{-1}. Elemental Analysis for $C_{22}H_{18}Cl_2N_4O_4Ru$: Calc. C 46.00, H 3.16, N 9.75; Found C 45.76, H 3.07, N 9.62.

Appendix B.   Assigning Protons of Dichloride Precursors

Dichlorides of the form [Ru(L)(L')Cl$_2$] where L and L' are different polypyridyl ligands have been prepared as described in Chapters 3 and 4. The four ligands used in preparing the dichloride precursors are shown in Fig. B1 with their protons labelled.

2,2'-bipyridine

4,4'-dimethyl-2,2'-bipyridine

1,10'-phenanthroline

4,7'-diphenyl-1,10'-phenanthroline
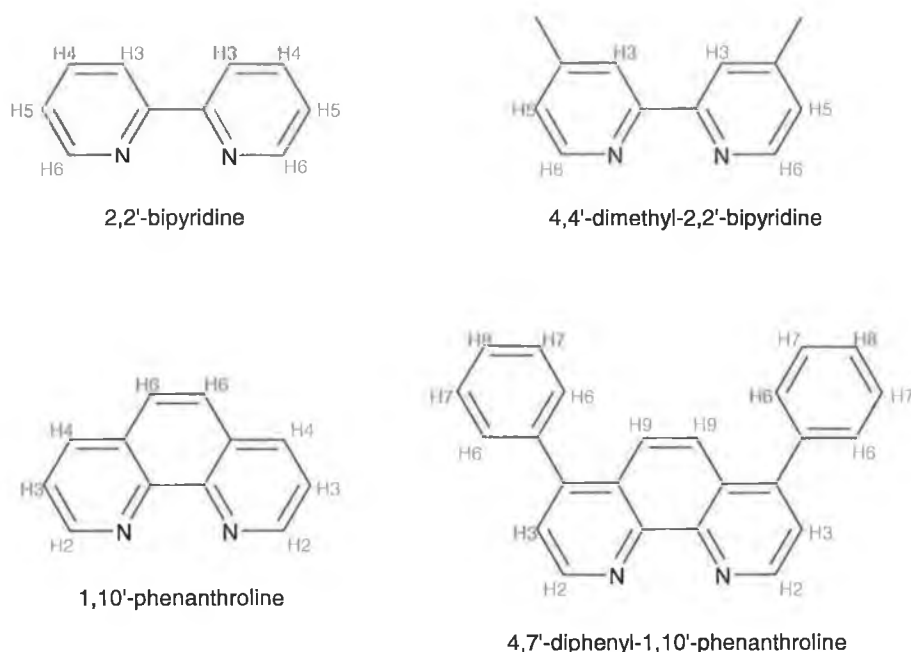
Figure B1. *The four ligands used in preparing the Ru(II) dichloride complexes.*

When they are used in the preparation of a dichloride species of the form [Ru(L)(L')Cl$_2$], the chlorines take on a *cis-* configuration. Thus, each ring is in a different chemical environment and each proton will produce its own unique ^{1}H NMR resonance. It is important to distinguish between the rings for the purpose of characterisation. Thus in all cases, the ring that sits directly over a chlorine atom has its protons assigned as H2, H3, H4 etc. The ring not sitting over a chlorine has its protons assigned as H2', H3', H4' etc. Fig. B2 below demonstrates the numbering scheme used.
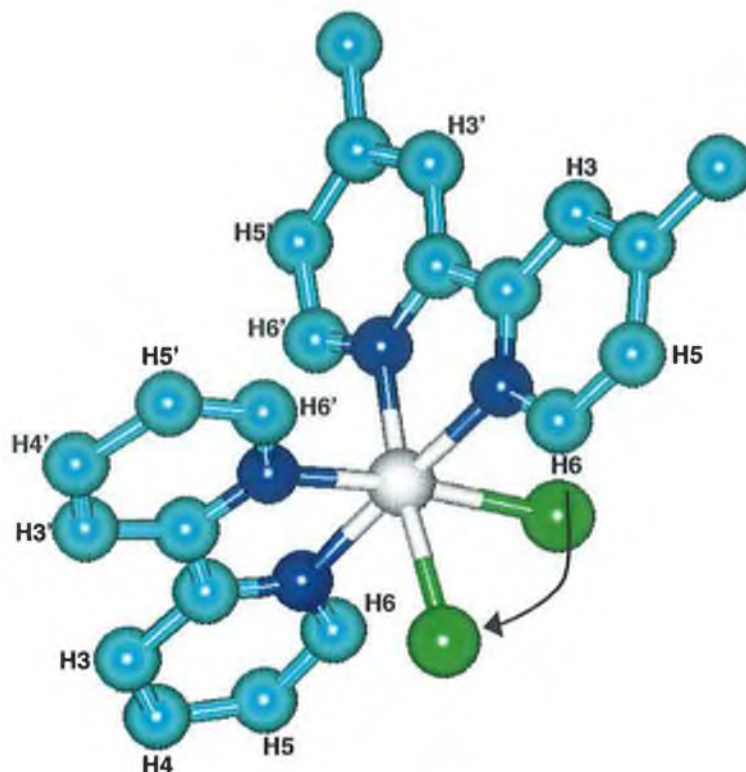
Figure B2. *Molecular model of [Ru(bpy)(Me₂bpy)Cl₂] showing the numbering system used to assign the protons for this molecule.*

Using the system described above, the proton resonances for [Ru(bpy)(Me₂bpy)Cl₂] can be assigned using the ¹H NMR (Fig. 3.19b) and the 2D COSY (Fig. 3.20). Fig. A3 below shows the ¹H NMR of [Ru(bpy)(Me₂bpy)Cl₂] with assigned peaks.
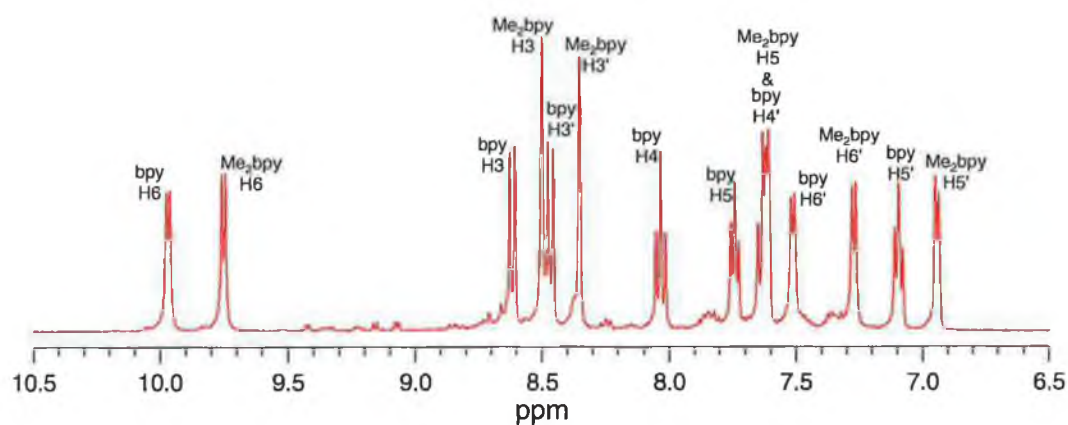
Figure B3. *¹H NMR of [Ru(bpy)(Me₂bpy)Cl₂] in d₆-DMSO with assigned peaks.*
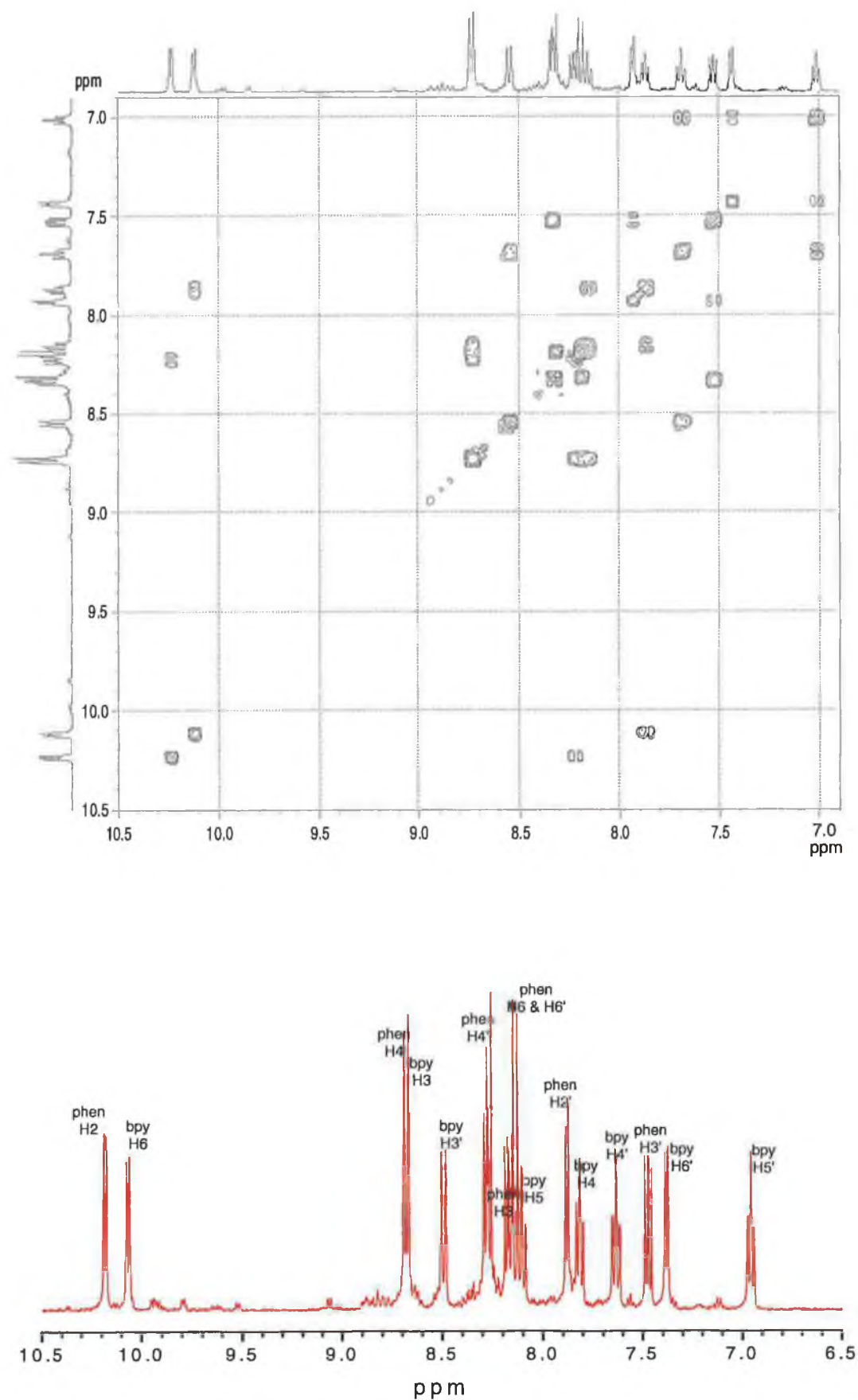
Figure B.4. 2D COSY ^{1}H NMR of the [Ru(bpy)(phen)Cl$_2$] complex in d_6-DMSO (top) and assigned protons (bottom).
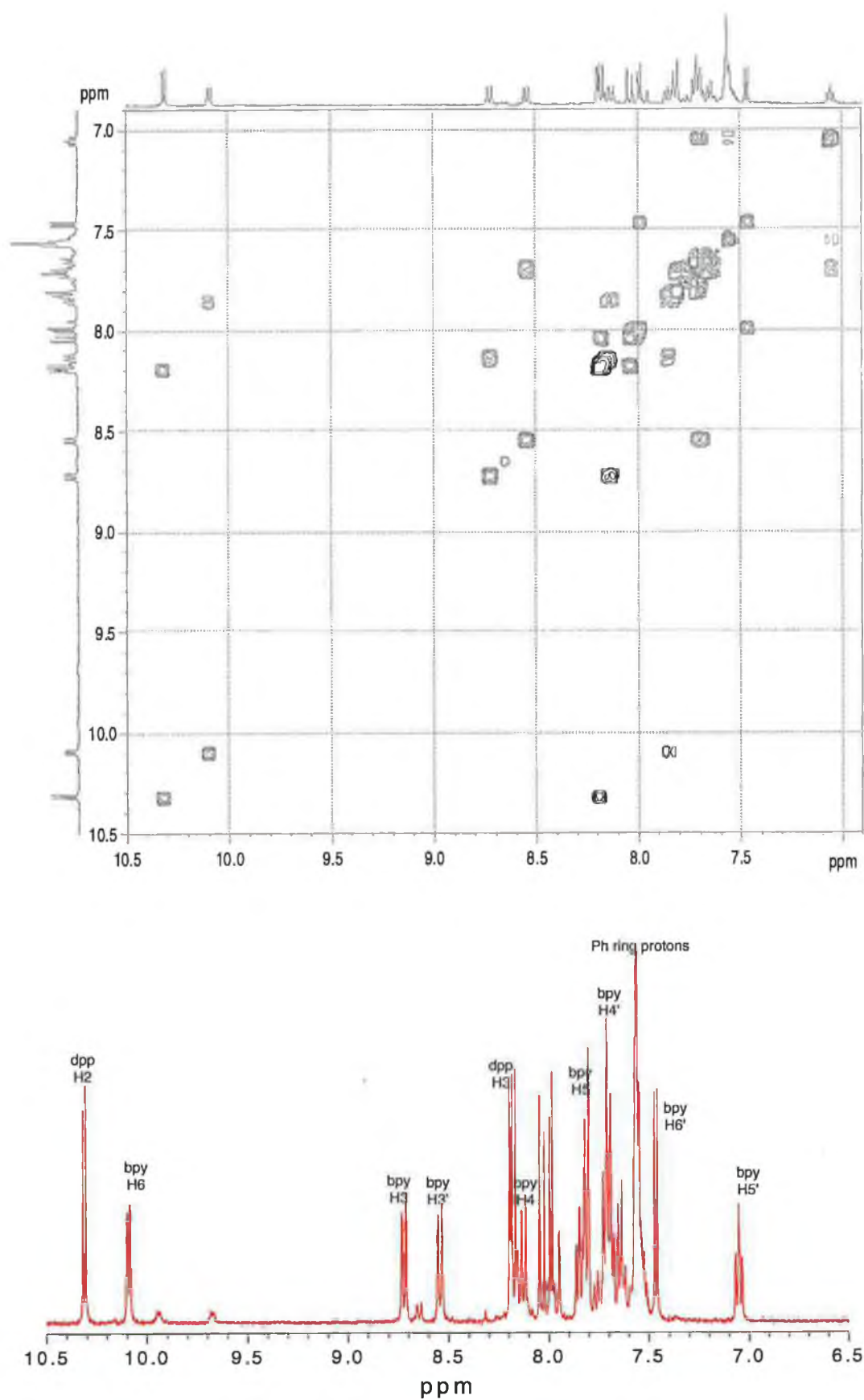
Figure B.5. 2D COSY ^1H NMR of the [Ru(bpy)(dpp)Cl$_2$] complex in d$_6$-DMSO (top) and some assigned protons.

Appendix C.　　　Assigning Names to Tris(heteroleptic) Complexes

As the triazole ligands featured throughout this thesis are asymmetrical, a variety of isomers are present upon complexation. In addition to the N2/N4 coordination modes, the triazole can complex to the metal centre by two further means. These additional binding modes are discussed below.

The triazole ligand used throughout Chapter 3 in the synthetic method development does not include a substituent on the triazole 5-position and so both N2 and N4 isomers are possible. Thus, the names include the N2 or N4 binding mode as well as the ligand *trans-* to the triazole. Two of the four possible isomers are illustrated in Fig. B1.

N2 bound *trans*(trz, bpy)　　　　　N4 bound *trans*(trz, Me₂bpy)
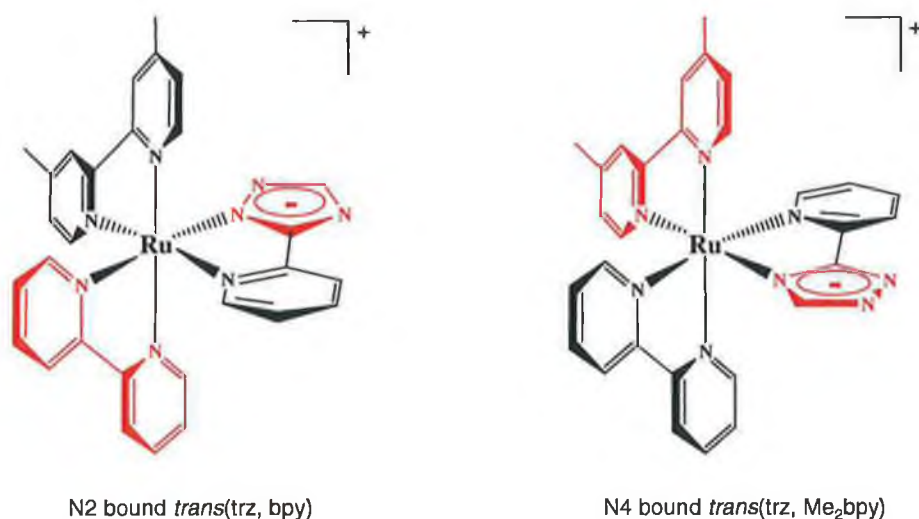
Figure C1. *Two of the isomers for the complex [Ru(bpy)(Me₂bpy)(pytrz)]⁺.*

As discussed in Chapters 1 and 4, a 3,5-substituted triazole binds predominantly through its N2 atom As such, it is not necessary to state that the triazole is N2 bound. The mononuclear complexes in Chapter 4 are named according to the ligand that is *trans-* to the triazole ring. Fig. C2 shows two different mononuclear complexes and the names assigned to each.

1

trans(trz, bpy)   trans(trz, phen)
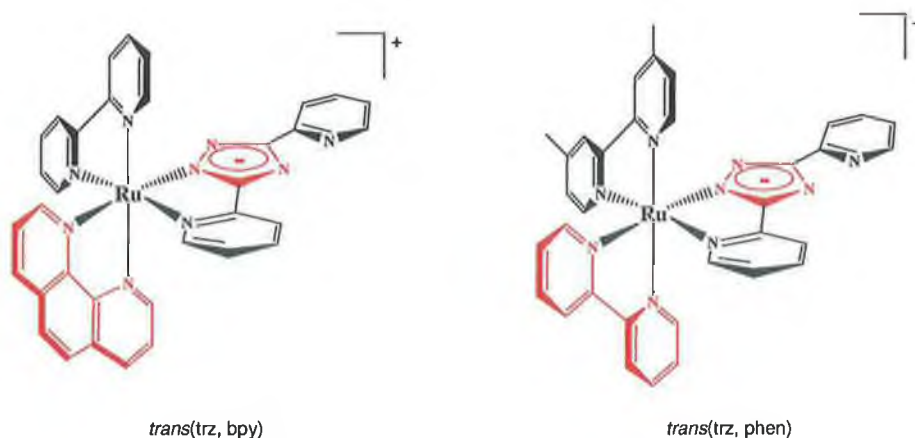
Figure C2. *Isomers of two different tris(heteroleptic) mononuclear complexes and the names used to describe the particular isomers shown.*

The dinuclear complexes of Chapter 5 are bound through N2 and N4 and so four different isomers are possible. As for the monomers, they are named according to the ligand *trans-* to the triazole ring but this time the N2 or N4 binding mode is also included. See Fig. C3 for examples.

N2 *trans*(trz, phen); N4 *trans*(trz,phen)   N2 *trans*(trz, bpy); N4 *trans*(trz,Me$_2$bpy)
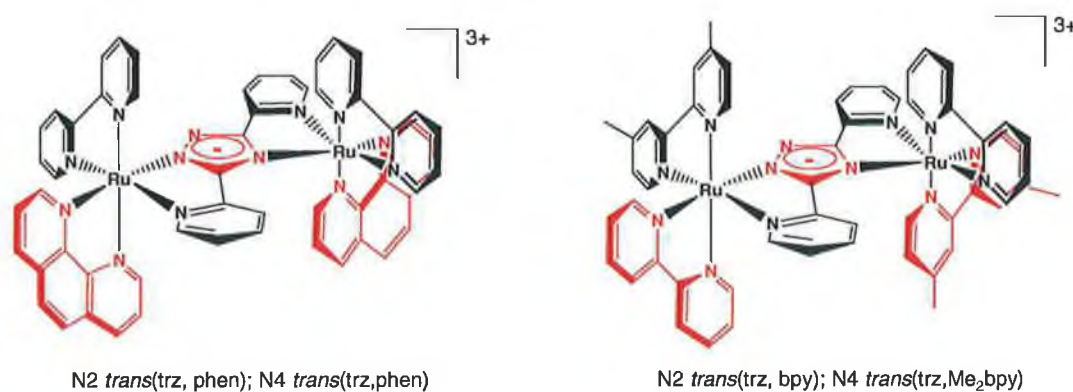
Figure C3. *Isomers of two different tris(heteroleptic) dinuclear complexes and the names used to describe the particular isomers shown.*

2

Appendix D.   Crystallographic Structures and Data

Crystal Data for [Ru(bpy)(Me$_2$bpy)(bpt)](PF$_6$)
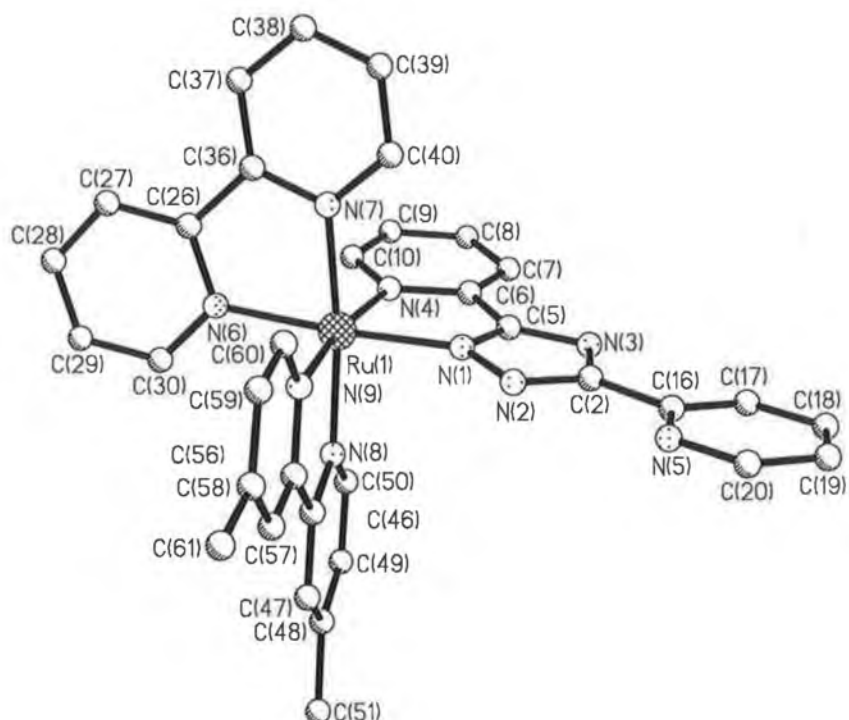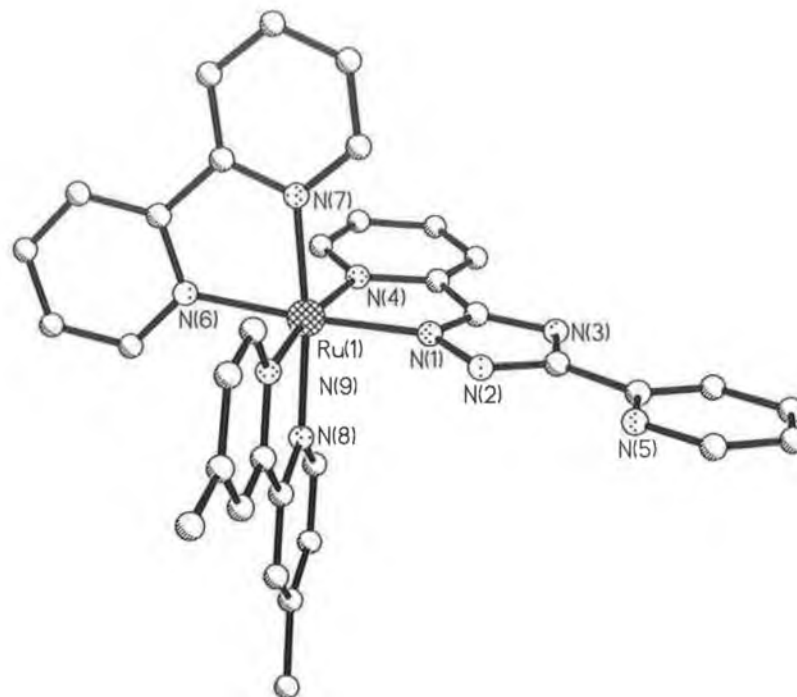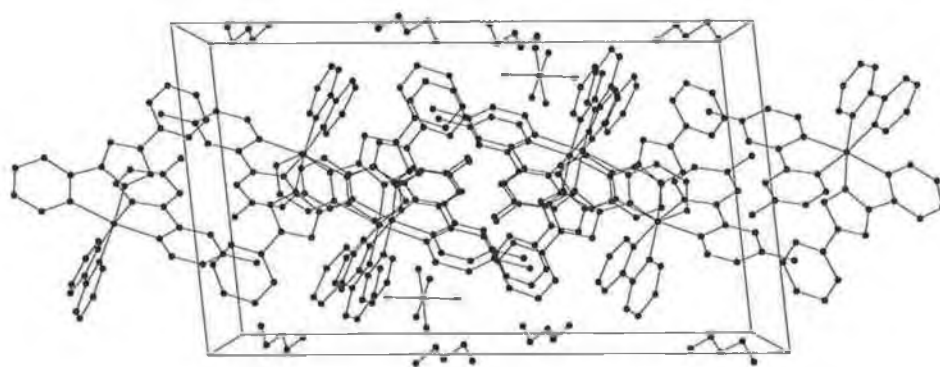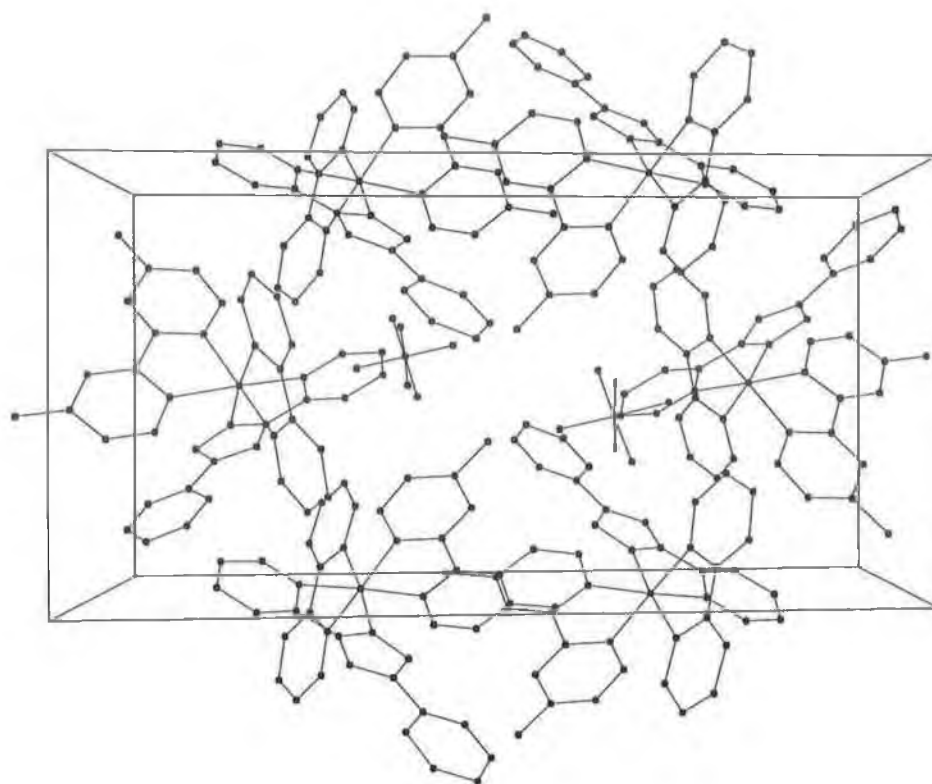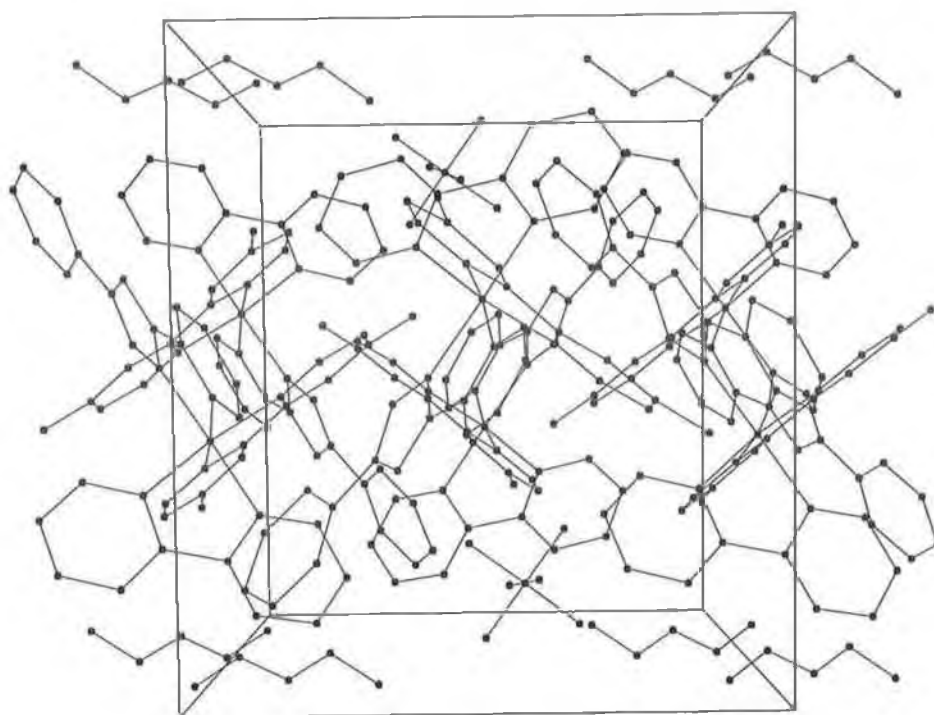
Table D1. Crystal data and structure refinement for Ru(bpy)(Me$_2$bpy)(bpt)](PF$_6$).

Empirical formula	C$_{36}$ H$_{33}$ F$_6$ N$_9$ O$_{0.5}$ P Ru
Formula weight	845.75
Temperature	200(2) K
Wavelength	0.71073 Å
Crystal system	Monoclinic
Space group	P2(1)/c
Unit cell dimensions	a = 13.95240(10) Å α = 90°.
	b = 12.24230(10) Å β = 95.91(10)°.
	c = 23.4412(4) Å γ = 90°.
Volume	3982.70(8) Å^3
Z	4
Density (calculated)	1.411 mg/m^3
Absorption coefficient	0.501 mm^{-1}
F(000)	1716
Crystal size	0.42×0.24×0.20 mm^3
Theta range for data collection	1.47 to 26.38°.
Index ranges	-15 ≤ h ≤ 17, -15 ≤ k ≤ 15, -26 ≤ l ≤ 29
Reflections collected	22545
Independent reflections	8079 [R(int) = 0.0787]
Completeness to theta = 26.38°	99.1 %
Absorption correction	Semi-empirical (SADABS)
Max. and min. transmission	0.93 and 0.40
Refinement method	Full-matrix least-squares on F^2
Data / restraints / parameters	8079 / 0 / 509
Goodness-of-fit on F^2	1.001
Final R indices [I>2sigma(I)]	R1 = 0.0599, wR2 = 0.1587
R indices (all data)	R1 = 0.1060, wR2 = 0.1872
Largest diff. peak and hole	1.248 and -1.133 e.Å^{-3}

Table D2. Atomic coordinates $(\times 10^4)$ and equivalent isotropic displacement parameters $(\text{Å}^2 \times 10^3)$ for $[Ru(bpy)(Me_2bpy)(bpt)](PF_6)$. U(eq) is defined as one third of the trace of the orthogonalized U^{ij} tensor.

	x	y	z	U(eq)
Ru(1)	3902(1)	8(1)	3187(1)	33(1)
N(1)	5106(3)	950(3)	3375(2)	35(1)
N(2)	5496(3)	1540(3)	3833(2)	36(1)
C(2)	6350(4)	1861(4)	3672(2)	37(1)
N(3)	6545(3)	1516(3)	3149(2)	40(1)
C(5)	5736(4)	945(4)	2984(2)	36(1)
C(6)	5477(4)	354(4)	2454(2)	35(1)
C(7)	6040(4)	321(4)	2006(2)	41(1)
C(8)	5703(4)	-242(4)	1509(2)	47(1)
C(9)	4836(4)	-775(4)	1493(2)	48(1)
C(10)	4315(4)	-732(4)	1965(2)	44(1)
N(4)	4623(3)	-185(3)	2448(2)	36(1)
C(16)	7027(4)	2564(4)	4038(2)	41(1)
C(17)	7901(4)	2869(6)	3855(3)	65(2)
C(18)	8495(5)	3587(7)	4186(3)	90(2)
C(19)	8185(5)	3958(6)	4689(3)	80(2)
C(20)	7321(5)	3592(5)	4846(3)	66(2)
N(5)	6732(3)	2920(4)	4528(2)	53(1)
N(6)	2692(3)	-902(3)	2922(2)	39(1)
C(26)	1988(4)	-370(4)	2587(2)	42(1)
C(27)	1125(4)	-893(5)	2404(3)	61(2)
C(28)	964(5)	-1946(5)	2562(3)	65(2)
C(29)	1661(5)	-2470(5)	2894(3)	66(2)
C(30)	2522(4)	-1938(4)	3071(3)	55(2)
N(7)	3054(3)	1152(3)	2727(2)	36(1)
C(36)	2202(4)	772(4)	2462(2)	40(1)
C(37)	1607(4)	1435(5)	2099(3)	60(2)
C(38)	1853(4)	2519(5)	2030(3)	61(2)
C(39)	2699(4)	2904(5)	2310(2)	55(2)
C(40)	3283(4)	2218(4)	2654(2)	45(1)
N(8)	4601(3)	-1216(3)	3668(2)	38(1)
C(46)	4445(4)	-1246(4)	4231(2)	40(1)
C(47)	4871(4)	-2014(4)	4603(2)	49(1)
C(48)	5466(4)	-2815(4)	4402(3)	53(1)
C(49)	5612(4)	-2777(5)	3832(3)	56(2)
C(50)	5178(4)	-1974(4)	3481(2)	49(1)
C(51)	5949(5)	-3646(6)	4814(3)	83(2)
N(9)	3403(3)	269(3)	3970(2)	36(1)
C(56)	3776(4)	-392(4)	4404(2)	37(1)
C(57)	3533(4)	-264(4)	4950(2)	47(1)

C(58)	2889(4)	541(5)	5085(2)	48(1)
C(59)	2536(4)	1202(4)	4639(2)	50(1)
C(60)	2804(4)	1057(4)	4095(2)	47(1)
C(61)	2600(5)	675(6)	5680(3)	75(2)
P(1)	8578(1)	5728(1)	6298(1)	56(1)
F(11)	8521(5)	5425(5)	6943(2)	130(2)
F(12)	7658(3)	6460(4)	6339(3)	116(2)
F(13)	7916(3)	4690(4)	6124(2)	91(1)
F(14)	9245(4)	6728(4)	6484(3)	126(2)
F(15)	8605(6)	6011(5)	5663(2)	160(3)
F(16)	9499(4)	4988(4)	6289(4)	153(3)
C(80)	419(11)	2097(14)	500(6)	90(5)
C(81)	-160(11)	3014(19)	612(8)	102(6)
O(82)	228(6)	3785(8)	986(4)	60(2)
C(83)	-195(14)	4690(20)	1084(9)	129(9)
C(84)	236(14)	5466(12)	1442(10)	118(8)

Table D3. Selected bond lengths [Å] and angles [°] for [Ru(bpy)(Me$_2$bpy)(bpt)](PF$_6$).

Ru(1)-N(1)	2.048(4)
Ru(1)-N(9)	2.054(4)
Ru(1)-N(8)	2.059(4)
Ru(1)-N(6)	2.064(4)
Ru(1)-N(7)	2.065(4)
Ru(1)-N(4)	2.105(4)
N(1)-Ru(1)-N(9)	93.81(15)
N(1)-Ru(1)-N(8)	87.73(15)
N(9)-Ru(1)-N(8)	79.01(15)
N(1)-Ru(1)-N(6)	174.82(14)
N(9)-Ru(1)-N(6)	90.66(16)
N(8)-Ru(1)-N(6)	95.69(16)
N(1)-Ru(1)-N(7)	98.24(16)
N(9)-Ru(1)-N(7)	97.59(15)
N(8)-Ru(1)-N(7)	173.35(15)
N(6)-Ru(1)-N(7)	78.56(16)
N(1)-Ru(1)-N(4)	77.82(15)
N(9)-Ru(1)-N(4)	171.10(15)
N(8)-Ru(1)-N(4)	97.46(15)
N(6)-Ru(1)-N(4)	97.85(15)
N(7)-Ru(1)-N(4)	86.71(15)

Table D4. Bond lengths [Å] and angles [°] for [Ru(bpy)(Me$_2$bpy)(bpt)](PF$_6$).

Bond lengths:

Ru(1)-N(1)	2.048(4)	N(7)-C(40)	1.359(6)
Ru(1)-N(9)	2.054(4)	N(7)-C(36)	1.365(6)
Ru(1)-N(8)	2.059(4)	C(36)-C(37)	1.387(7)
Ru(1)-N(6)	2.064(4)	C(37)-C(38)	1.385(8)
Ru(1)-N(7)	2.065(4)	C(38)-C(39)	1.373(8)
Ru(1)-N(4)	2.105(4)	C(39)-C(40)	1.373(7)
N(1)-C(5)	1.333(6)	N(8)-C(50)	1.332(6)
N(1)-N(2)	1.360(5)	N(8)-C(46)	1.361(6)
N(2)-C(2)	1.345(6)	C(46)-C(47)	1.374(7)
C(2)-N(3)	1.352(6)	C(46)-C(56)	1.485(7)
C(2)-C(16)	1.484(7)	C(47)-C(48)	1.398(8)
N(3)-C(5)	1.350(6)	C(48)-C(49)	1.373(8)
C(5)-C(6)	1.450(6)	C(48)-C(51)	1.513(8)
C(6)-N(4)	1.361(6)	C(49)-C(50)	1.380(8)
C(6)-C(7)	1.377(7)	N(9)-C(60)	1.328(6)
C(7)-C(8)	1.393(8)	N(9)-C(56)	1.361(6)
C(8)-C(9)	1.371(7)	C(56)-C(57)	1.365(7)
C(9)-C(10)	1.386(7)	C(57)-C(58)	1.391(8)
C(10)-N(4)	1.346(6)	C(58)-C(59)	1.373(7)
C(16)-N(5)	1.332(6)	C(58)-C(61)	1.502(7)
C(16)-C(17)	1.385(8)	C(59)-C(60)	1.376(7)
C(17)-C(18)	1.390(9)	P(1)-F(15)	1.533(5)
C(18)-C(19)	1.374(10)	P(1)-F(11)	1.567(5)
C(19)-C(20)	1.371(9)	P(1)-F(14)	1.572(5)
C(20)-N(5)	1.335(7)	P(1)-F(16)	1.574(5)
N(6)-C(30)	1.343(6)	P(1)-F(12)	1.576(5)
N(6)-C(26)	1.359(7)	P(1)-F(13)	1.599(4)
C(26)-C(27)	1.392(7)	C(80)-C(81)	1.42(2)
C(26)-C(36)	1.465(7)	C(81)-O(82)	1.36(2)
C(27)-C(28)	1.366(8)	O(82)-C(83)	1.29(2)
C(28)-C(29)	1.344(9)	C(83)-C(84)	1.36(3)
C(29)-C(30)	1.390(8)		

Bond angles

N(1)-Ru(1)-N(9)	93.81(15)	N(6)-C(26)-C(36)	115.0(4)
N(1)-Ru(1)-N(8)	87.73(15)	C(27)-C(26)-C(36)	124.4(5)
N(9)-Ru(1)-N(8)	79.01(15)	C(28)-C(27)-C(26)	120.8(6)
N(1)-Ru(1)-N(6)	174.82(14)	C(29)-C(28)-C(27)	118.6(6)
N(9)-Ru(1)-N(6)	90.66(16)	C(28)-C(29)-C(30)	120.0(6)
N(8)-Ru(1)-N(6)	95.69(16)	N(6)-C(30)-C(29)	122.3(6)
N(1)-Ru(1)-N(7)	98.24(16)	C(40)-N(7)-C(36)	118.4(4)
N(9)-Ru(1)-N(7)	97.59(15)	C(40)-N(7)-Ru(1)	126.0(4)
N(8)-Ru(1)-N(7)	173.35(15)	C(36)-N(7)-Ru(1)	115.6(3)
N(6)-Ru(1)-N(7)	78.56(16)	N(7)-C(36)-C(37)	121.2(5)
N(1)-Ru(1)-N(4)	77.82(15)	N(7)-C(36)-C(26)	114.8(4)
N(9)-Ru(1)-N(4)	171.10(15)	C(37)-C(36)-C(26)	124.0(5)
N(8)-Ru(1)-N(4)	97.46(15)	C(38)-C(37)-C(36)	119.5(6)
N(6)-Ru(1)-N(4)	97.85(15)	C(39)-C(38)-C(37)	118.9(5)
N(7)-Ru(1)-N(4)	86.71(15)	C(38)-C(39)-C(40)	120.0(5)
C(5)-N(1)-N(2)	107.8(4)	N(7)-C(40)-C(39)	121.8(5)
C(5)-N(1)-Ru(1)	115.7(3)	C(50)-N(8)-C(46)	117.6(4)
N(2)-N(1)-Ru(1)	136.1(3)	C(50)-N(8)-Ru(1)	126.5(3)
C(2)-N(2)-N(1)	103.2(4)	C(46)-N(8)-Ru(1)	115.9(3)
N(2)-C(2)-N(3)	115.5(4)	N(8)-C(46)-C(47)	122.1(5)
N(2)-C(2)-C(16)	122.5(4)	N(8)-C(46)-C(56)	114.4(4)
N(3)-C(2)-C(16)	122.0(4)	C(47)-C(46)-C(56)	123.5(5)
C(5)-N(3)-C(2)	100.4(4)	C(46)-C(47)-C(48)	120.0(5)
N(1)-C(5)-N(3)	113.1(4)	C(49)-C(48)-C(47)	117.2(5)
N(1)-C(5)-C(6)	117.8(4)	C(49)-C(48)-C(51)	122.9(6)
N(3)-C(5)-C(6)	129.1(4)	C(47)-C(48)-C(51)	119.9(5)
N(4)-C(6)-C(7)	123.0(4)	C(48)-C(49)-C(50)	120.2(5)
N(4)-C(6)-C(5)	113.1(4)	N(8)-C(50)-C(49)	122.9(5)
C(7)-C(6)-C(5)	123.9(5)	C(60)-N(9)-C(56)	117.9(4)
C(6)-C(7)-C(8)	118.9(5)	C(60)-N(9)-Ru(1)	126.1(3)
C(9)-C(8)-C(7)	118.6(5)	C(56)-N(9)-Ru(1)	115.9(3)
C(8)-C(9)-C(10)	119.6(5)	N(9)-C(56)-C(57)	121.3(5)
N(4)-C(10)-C(9)	122.8(5)	N(9)-C(56)-C(46)	114.7(4)
C(10)-N(4)-C(6)	117.0(4)	C(57)-C(56)-C(46)	124.1(5)
C(10)-N(4)-Ru(1)	127.5(3)	C(56)-C(57)-C(58)	121.5(5)
C(6)-N(4)-Ru(1)	115.4(3)	C(59)-C(58)-C(57)	115.7(5)
N(5)-C(16)-C(17)	122.7(5)	C(59)-C(58)-C(61)	122.3(5)
N(5)-C(16)-C(2)	116.9(5)	C(57)-C(58)-C(61)	122.0(5)
C(17)-C(16)-C(2)	120.3(5)	C(58)-C(59)-C(60)	121.2(5)
C(16)-C(17)-C(18)	119.3(6)	N(9)-C(60)-C(59)	122.3(5)
C(19)-C(18)-C(17)	117.8(7)	F(15)-P(1)-F(11)	178.4(4)
C(20)-C(19)-C(18)	119.1(6)	F(15)-P(1)-F(14)	91.2(3)
N(5)-C(20)-C(19)	124.0(6)	F(11)-P(1)-F(14)	90.2(3)
C(16)-N(5)-C(20)	117.1(5)	F(15)-P(1)-F(16)	90.8(4)
C(30)-N(6)-C(26)	117.8(5)	F(11)-P(1)-F(16)	90.0(4)
C(30)-N(6)-Ru(1)	126.3(4)	F(14)-P(1)-F(16)	89.5(3)
C(26)-N(6)-Ru(1)	115.8(3)	F(15)-P(1)-F(12)	91.8(4)
N(6)-C(26)-C(27)	120.5(5)	F(11)-P(1)-F(12)	87.4(3)

F(14)-P(1)-F(12)	90.1(3)	F(16)-P(1)-F(13)	89.4(3)
F(16)-P(1)-F(12)	177.3(4)	F(12)-P(1)-F(13)	90.8(3)
F(15)-P(1)-F(13)	90.2(3)	O(82)-C(81)-C(80)	118.0(13)
F(11)-P(1)-F(13)	88.4(3)	C(83)-O(82)-C(81)	123.5(15)
F(14)-P(1)-F(13)	178.3(3)	O(82)-C(83)-C(84)	121.9(17)

Table D5. Anisotropic displacement parameters ($\text{Å}^2 \times 10^3$) for [Ru(bpy)(Me$_2$bpy)(bpt)](PF$_6$). The anisotropic displacement factor exponent takes the form: $-2\text{p}^2[\,\text{h}^2\,\text{a}^{*2}\text{U}^{11} + ... + 2\,\text{h}\,\text{k}\,\text{a}^*\,\text{b}^*\,\text{U}^{12}\,]$.

	U^{11}	U^{22}	U^{33}	U^{23}	U^{13}	U^{12}
Ru(1)	39(1)	30(1)	31(1)	1(1)	3(1)	-2(1)
N(1)	41(2)	36(2)	26(2)	1(2)	2(2)	-3(2)
N(2)	41(2)	34(2)	32(2)	2(2)	-5(2)	-1(2)
C(2)	46(3)	33(2)	30(3)	4(2)	-4(2)	1(2)
N(3)	43(2)	43(2)	34(2)	-2(2)	2(2)	-2(2)
C(5)	45(3)	33(3)	29(2)	-1(2)	2(2)	-6(2)
C(6)	42(3)	34(2)	29(3)	2(2)	-1(2)	-1(2)
C(7)	44(3)	42(3)	38(3)	-1(2)	4(2)	-2(2)
C(8)	60(3)	44(3)	38(3)	-1(2)	15(3)	1(3)
C(9)	60(3)	45(3)	39(3)	-8(2)	1(2)	-10(3)
C(10)	50(3)	39(3)	41(3)	-6(2)	1(2)	-11(2)
N(4)	42(2)	34(2)	31(2)	0(2)	1(2)	-1(2)
C(16)	45(3)	41(3)	35(3)	0(2)	-5(2)	-2(2)
C(17)	55(4)	83(5)	56(4)	-18(3)	6(3)	-20(3)
C(18)	72(5)	114(7)	84(5)	-22(5)	2(4)	-43(5)
C(19)	74(5)	86(5)	76(5)	-25(4)	-14(4)	-27(4)
C(20)	78(5)	69(4)	46(3)	-18(3)	-12(3)	-4(4)
N(5)	61(3)	59(3)	38(3)	-8(2)	-6(2)	-7(3)
N(6)	45(2)	32(2)	40(2)	-3(2)	7(2)	-3(2)
C(26)	45(3)	38(3)	42(3)	-3(2)	5(2)	-2(2)
C(27)	51(3)	56(4)	73(4)	4(3)	-11(3)	-7(3)
C(28)	56(4)	61(4)	75(4)	4(3)	-7(3)	-23(3)
C(29)	69(4)	43(3)	88(5)	2(3)	12(4)	-21(3)
C(30)	55(4)	35(3)	73(4)	3(3)	4(3)	-4(3)
N(7)	46(2)	32(2)	31(2)	1(2)	3(2)	0(2)
C(36)	42(3)	39(3)	38(3)	-1(2)	-1(2)	-1(2)
C(37)	55(4)	60(4)	60(4)	9(3)	-16(3)	-3(3)
C(38)	63(4)	58(4)	59(4)	16(3)	-9(3)	15(3)
C(39)	69(4)	40(3)	55(4)	8(3)	6(3)	0(3)
C(40)	54(3)	41(3)	38(3)	3(2)	2(2)	-3(3)
N(8)	42(2)	31(2)	40(2)	1(2)	5(2)	-2(2)

C(46)	40(3)	38(3)	41(3)	4(2)	5(2)	-2(2)
C(47)	54(3)	46(3)	46(3)	15(2)	2(3)	7(3)
C(48)	54(3)	36(3)	69(4)	13(3)	1(3)	5(3)
C(49)	60(4)	44(3)	66(4)	3(3)	16(3)	13(3)
C(50)	52(3)	46(3)	48(3)	3(3)	7(3)	7(3)
C(51)	92(5)	67(5)	89(5)	26(4)	3(4)	34(4)
N(9)	36(2)	37(2)	34(2)	2(2)	7(2)	2(2)
C(56)	42(3)	35(2)	35(3)	5(2)	5(2)	-1(2)
C(57)	51(3)	51(3)	39(3)	8(2)	4(2)	4(3)
C(58)	56(3)	49(3)	41(3)	-1(3)	10(3)	4(3)
C(59)	56(3)	46(3)	48(3)	3(2)	10(3)	10(3)
C(60)	55(3)	41(3)	44(3)	5(2)	5(3)	9(3)
C(61)	90(5)	85(5)	52(4)	7(4)	19(4)	18(4)
P(1)	53(1)	56(1)	59(1)	-5(1)	2(1)	-5(1)
F(11)	215(6)	111(4)	65(3)	0(3)	15(3)	-4(4)
F(12)	81(3)	78(3)	189(5)	-3(3)	12(3)	14(3)
F(13)	89(3)	73(3)	106(3)	-14(2)	-12(3)	-21(2)
F(14)	111(4)	79(3)	183(5)	-26(3)	-17(4)	-39(3)
F(15)	276(8)	140(5)	66(3)	5(3)	27(4)	-42(5)
F(16)	63(3)	116(5)	281(9)	-46(4)	18(4)	18(3)
C(80)	90(11)	114(13)	67(9)	-23(9)	9(8)	-64(11)
C(81)	57(9)	157(18)	90(12)	-2(12)	-3(8)	18(11)
O(82)	34(4)	62(5)	83(6)	20(5)	-1(4)	6(4)
C(83)	71(12)	200(30)	118(17)	87(17)	17(11)	32(15)
C(84)	109(15)	38(8)	220(20)	16(11)	99(16)	18(9)

Table D6. Hydrogen coordinates ($\times 10^4$) and isotropic displacement parameters ($\text{Å}^2 \times 10^3$) for [Ru(bpy)(Me$_2$bpy)(bpt)](PF$_6$).

	x	y	z	U(eq)
H(7)	6649	677	2034	49
H(8)	6066	-257	1187	56
H(9)	4594	-1171	1161	58
H(10)	3716	-1106	1948	52
H(17)	8092	2590	3506	78
H(18)	9096	3814	4069	108
H(19)	8563	4461	4925	96
H(20)	7130	3831	5203	79
H(27)	643	-513	2166	73
H(28)	373	-2300	2440	78
H(29)	1566	-3203	3007	79
H(30)	3006	-2322	3305	66

H(37)	1035	1147	1900	72
H(38)	1443	2990	1793	73
H(39)	2881	3644	2265	66
H(40)	3864	2497	2847	53
H(47)	4760	-2000	4996	59
H(49)	6014	-3304	3678	67
H(50)	5296	-1962	3089	58
H(51A)	5758	-4384	4685	100
H(51B)	5751	-3522	5198	100
H(51C)	6650	-3572	4826	100
H(57)	3809	-736	5244	56
H(59)	2098	1770	4707	60
H(60)	2551	1536	3798	56
H(61A)	2398	1431	5735	90
H(61B)	3149	501	5961	90
H(61C)	2064	180	5734	90
H(80A)	318	1913	92	108
H(80B)	239	1472	728	108
H(80C)	1100	2274	605	108
H(81A)	-356	3380	242	122
H(81B)	-755	2738	759	122
H(83A)	-811	4499	1234	155
H(83B)	-363	5047	708	155
H(84A)	413	5146	1821	142
H(84B)	-212	6074	1475	142
H(84C)	816	5736	1285	142

Table D7. Torsion angles [°] for [Ru(bpy)(Me$_2$bpy)(bpt)](PF$_6$).

N(9)-Ru(1)-N(1)-C(5)	174.0(3)	N(5)-C(16)-C(17)-C(18)	-1.0(10)
N(8)-Ru(1)-N(1)-C(5)	95.2(3)	C(2)-C(16)-C(17)-C(18)	175.7(6)
N(6)-Ru(1)-N(1)-C(5)	-36.3(18)	C(16)-C(17)-C(18)-C(19)	0.5(11)
N(7)-Ru(1)-N(1)-C(5)	-87.7(3)	C(17)-C(18)-C(19)-C(20)	1.2(12)
N(4)-Ru(1)-N(1)-C(5)	-2.9(3)	C(18)-C(19)-C(20)-N(5)	-2.7(12)
N(9)-Ru(1)-N(1)-N(2)	1.0(4)	C(17)-C(16)-N(5)-C(20)	-0.3(8)
N(8)-Ru(1)-N(1)-N(2)	-77.8(4)	C(2)-C(16)-N(5)-C(20)	-177.1(5)
N(6)-Ru(1)-N(1)-N(2)	150.7(15)	C(19)-C(20)-N(5)-C(16)	2.2(9)
N(7)-Ru(1)-N(1)-N(2)	99.2(4)	N(1)-Ru(1)-N(6)-C(30)	132.9(16)
N(4)-Ru(1)-N(1)-N(2)	-176.0(4)	N(9)-Ru(1)-N(6)-C(30)	-77.3(4)
C(5)-N(1)-N(2)-C(2)	0.7(5)	N(8)-Ru(1)-N(6)-C(30)	1.7(4)
Ru(1)-N(1)-N(2)-C(2)	174.1(3)	N(7)-Ru(1)-N(6)-C(30)	-174.9(5)
N(1)-N(2)-C(2)-N(3)	-0.6(5)	N(4)-Ru(1)-N(6)-C(30)	100.1(4)
N(1)-N(2)-C(2)-C(16)	178.3(4)	N(1)-Ru(1)-N(6)-C(26)	-50.5(18)
N(2)-C(2)-N(3)-C(5)	0.3(5)	N(9)-Ru(1)-N(6)-C(26)	99.3(4)
C(16)-C(2)-N(3)-C(5)	-178.6(4)	N(8)-Ru(1)-N(6)-C(26)	178.3(3)
N(2)-N(1)-C(5)-N(3)	-0.6(5)	N(7)-Ru(1)-N(6)-C(26)	1.7(3)
Ru(1)-N(1)-C(5)-N(3)	-175.5(3)	N(4)-Ru(1)-N(6)-C(26)	-83.3(4)
N(2)-N(1)-C(5)-C(6)	179.6(4)	C(30)-N(6)-C(26)-C(27)	-0.4(7)
Ru(1)-N(1)-C(5)-C(6)	4.7(5)	Ru(1)-N(6)-C(26)-C(27)	-177.3(4)
C(2)-N(3)-C(5)-N(1)	0.2(5)	C(30)-N(6)-C(26)-C(36)	177.4(4)
C(2)-N(3)-C(5)-C(6)	180.0(5)	Ru(1)-N(6)-C(26)-C(36)	0.5(5)
N(1)-C(5)-C(6)-N(4)	-3.9(6)	N(6)-C(26)-C(27)-C(28)	0.7(9)
N(3)-C(5)-C(6)-N(4)	176.3(5)	C(36)-C(26)-C(27)-C(28)	-176.9(6)
N(1)-C(5)-C(6)-C(7)	177.1(5)	C(26)-C(27)-C(28)-C(29)	-0.6(10)
N(3)-C(5)-C(6)-C(7)	-2.7(8)	C(27)-C(28)-C(29)-C(30)	0.3(10)
N(4)-C(6)-C(7)-C(8)	3.4(8)	C(26)-N(6)-C(30)-C(29)	0.1(8)
C(5)-C(6)-C(7)-C(8)	-177.8(5)	Ru(1)-N(6)-C(30)-C(29)	176.6(4)
C(6)-C(7)-C(8)-C(9)	-2.2(8)	C(28)-C(29)-C(30)-N(6)	0.0(10)
C(7)-C(8)-C(9)-C(10)	0.6(8)	N(1)-Ru(1)-N(7)-C(40)	-5.7(4)
C(8)-C(9)-C(10)-N(4)	0.0(8)	N(9)-Ru(1)-N(7)-C(40)	89.3(4)
C(9)-C(10)-N(4)-C(6)	1.0(7)	N(8)-Ru(1)-N(7)-C(40)	148.1(12)
C(9)-C(10)-N(4)-Ru(1)	177.6(4)	N(6)-Ru(1)-N(7)-C(40)	178.5(4)
C(7)-C(6)-N(4)-C(10)	-2.7(7)	N(4)-Ru(1)-N(7)-C(40)	-82.9(4)
C(5)-C(6)-N(4)-C(10)	178.3(4)	N(1)-Ru(1)-N(7)-C(36)	172.2(3)
C(7)-C(6)-N(4)-Ru(1)	-179.7(4)	N(9)-Ru(1)-N(7)-C(36)	-92.8(3)
C(5)-C(6)-N(4)-Ru(1)	1.3(5)	N(8)-Ru(1)-N(7)-C(36)	-34.1(14)
N(1)-Ru(1)-N(4)-C(10)	-175.9(4)	N(6)-Ru(1)-N(7)-C(36)	-3.7(3)
N(9)-Ru(1)-N(4)-C(10)	164.1(8)	N(4)-Ru(1)-N(7)-C(36)	95.0(3)
N(8)-Ru(1)-N(4)-C(10)	98.1(4)	C(40)-N(7)-C(36)-C(37)	3.7(7)
N(6)-Ru(1)-N(4)-C(10)	1.3(4)	Ru(1)-N(7)-C(36)-C(37)	-174.3(4)
N(7)-Ru(1)-N(4)-C(10)	-76.7(4)	C(40)-N(7)-C(36)-C(26)	-176.9(4)
N(1)-Ru(1)-N(4)-C(6)	0.8(3)	Ru(1)-N(7)-C(36)-C(26)	5.1(5)
N(9)-Ru(1)-N(4)-C(6)	-19.3(11)	N(6)-C(26)-C(36)-N(7)	-3.6(6)
N(8)-Ru(1)-N(4)-C(6)	-85.3(3)	C(27)-C(26)-C(36)-N(7)	174.0(5)
N(6)-Ru(1)-N(4)-C(6)	177.9(3)	N(6)-C(26)-C(36)-C(37)	175.7(5)
N(7)-Ru(1)-N(4)-C(6)	99.9(3)	C(27)-C(26)-C(36)-C(37)	-6.6(8)
N(2)-C(2)-C(16)-N(5)	-3.5(7)	N(7)-C(36)-C(37)-C(38)	-3.7(9)
N(3)-C(2)-C(16)-N(5)	175.4(5)	C(26)-C(36)-C(37)-C(38)	177.0(5)
N(2)-C(2)-C(16)-C(17)	179.7(5)	C(36)-C(37)-C(38)-C(39)	2.0(9)
N(3)-C(2)-C(16)-C(17)	-1.5(8)	C(37)-C(38)-C(39)-C(40)	-0.5(9)

C(36)-N(7)-C(40)-C(39)	-2.1(7)	N(6)-Ru(1)-N(9)-C(60)	-85.5(4)
Ru(1)-N(7)-C(40)-C(39)	175.7(4)	N(7)-Ru(1)-N(9)-C(60)	-7.0(4)
C(38)-C(39)-C(40)-N(7)	0.5(8)	N(4)-Ru(1)-N(9)-C(60)	111.5(10)
N(1)-Ru(1)-N(8)-C(50)	-88.3(4)	N(1)-Ru(1)-N(9)-C(56)	-83.8(4)
N(9)-Ru(1)-N(8)-C(50)	177.4(5)	N(8)-Ru(1)-N(9)-C(56)	3.1(3)
N(6)-Ru(1)-N(8)-C(50)	87.8(4)	N(6)-Ru(1)-N(9)-C(56)	98.8(4)
N(7)-Ru(1)-N(8)-C(50)	117.7(12)	N(7)-Ru(1)-N(9)-C(56)	177.3(3)
N(4)-Ru(1)-N(8)-C(50)	-10.9(4)	N(4)-Ru(1)-N(9)-C(56)	-64.2(10)
N(1)-Ru(1)-N(8)-C(46)	92.2(3)	C(60)-N(9)-C(56)-C(57)	1.0(7)
N(9)-Ru(1)-N(8)-C(46)	-2.2(3)	Ru(1)-N(9)-C(56)-C(57)	177.0(4)
N(6)-Ru(1)-N(8)-C(46)	-91.7(3)	C(60)-N(9)-C(56)-C(46)	-179.5(4)
N(7)-Ru(1)-N(8)-C(46)	-61.8(14)	Ru(1)-N(9)-C(56)-C(46)	-3.5(5)
N(4)-Ru(1)-N(8)-C(46)	169.5(3)	N(8)-C(46)-C(56)-N(9)	1.6(6)
C(50)-N(8)-C(46)-C(47)	0.9(7)	C(47)-C(46)-C(56)-N(9)	-177.8(5)
Ru(1)-N(8)-C(46)-C(47)	-179.6(4)	N(8)-C(46)-C(56)-C(57)	-178.9(5)
C(50)-N(8)-C(46)-C(56)	-178.6(4)	C(47)-C(46)-C(56)-C(57)	1.7(8)
Ru(1)-N(8)-C(46)-C(56)	1.0(5)	N(9)-C(56)-C(57)-C(58)	0.4(8)
N(8)-C(46)-C(47)-C(48)	-1.7(8)	C(46)-C(56)-C(57)-C(58)	-179.0(5)
C(56)-C(46)-C(47)-C(48)	177.7(5)	C(56)-C(57)-C(58)-C(59)	-1.2(9)
C(46)-C(47)-C(48)-C(49)	1.3(8)	C(56)-C(57)-C(58)-C(61)	178.7(6)
C(46)-C(47)-C(48)-C(51)	178.8(6)	C(57)-C(58)-C(59)-C(60)	0.6(9)
C(47)-C(48)-C(49)-C(50)	-0.2(9)	C(61)-C(58)-C(59)-C(60)	-179.3(6)
C(51)-C(48)-C(49)-C(50)	-177.6(6)	C(56)-N(9)-C(60)-C(59)	-1.6(8)
C(46)-N(8)-C(50)-C(49)	0.3(8)	Ru(1)-N(9)-C(60)-C(59)	-177.2(4)
Ru(1)-N(8)-C(50)-C(49)	-179.2(4)	C(58)-C(59)-C(60)-N(9)	0.8(9)
C(48)-C(49)-C(50)-N(8)	-0.6(9)	C(80)-C(81)-O(82)-C(83)	174.0(16)
N(1)-Ru(1)-N(9)-C(60)	91.8(4)	C(81)-O(82)-C(83)-C(84)	176.9(17)
N(8)-Ru(1)-N(9)-C(60)	178.8(4)		

Crystal Data for [Ru(bpy)(Me₂bpy)(bpzt)](PF₆)

Table D8. Bond lengths [Å] and angles [°] for [Ru(bpy)(Me$_2$bpy)(bpzt)](PF$_6$).

Bond length:

Ru-N(3)	2.046(3)	C(25)-C(24)	1.379(5)
Ru-N(11)	2.050(3)	C(25)-C(26)	1.473(5)
Ru-N(9)	2.055(3)	C(23)-C(24)	1.394(5)
Ru-N(10)	2.061(3)	C(23)-C(22)	1.401(6)
Ru-N(1)	2.069(3)	C(27)-C(28)	1.382(5)
Ru-N(8)	2.070(3)	C(27)-C(26)	1.386(5)
C(32)-C(28)	1.508(5)	N(7)-C(8)	1.326(5)
N(11)-C(30)	1.348(4)	N(7)-C(9)	1.337(6)
N(11)-C(26)	1.360(4)	C(15)-C(14)	1.385(5)
N(3)-C(5)	1.340(4)	C(15)-C(16)	1.469(6)
N(3)-N(4)	1.357(4)	C(16)-C(17)	1.389(6)
N(5)-C(5)	1.334(4)	C(21)-C(22)	1.374(6)
N(5)-C(6)	1.357(4)	C(19)-C(18)	1.375(7)
N(8)-C(11)	1.355(5)	C(19)-C(20)	1.374(6)
N(8)-C(15)	1.362(5)	C(18)-C(17)	1.380(7)
C(31)-C(23)	1.480(6)	C(3)-N(2)	1.342(5)
N(4)-C(6)	1.349(4)	C(3)-C(4)	1.382(5)
N(1)-C(4)	1.357(4)	N(2)-C(2)	1.336(6)
N(1)-C(1)	1.355(4)	C(11)-C(12)	1.374(6)
C(6)-C(7)	1.464(5)	C(1)-C(2)	1.371(6)
N(6)-C(10)	1.326(5)	C(12)-C(13)	1.371(8)
N(6)-C(7)	1.340(5)	C(10)-C(9)	1.380(7)
N(9)-C(20)	1.342(5)	C(14)-C(13)	1.380(8)
N(9)-C(16)	1.358(4)	P(1)-F(1)	1.539(5)
C(5)-C(4)	1.455(5)	P(1)-F(4)	1.539(4)
C(30)-C(29)	1.380(5)	P(1)-F(2)	1.543(5)
N(10)-C(21)	1.353(5)	P(1)-F(5)	1.570(4)
N(10)-C(25)	1.359(4)	P(1)-F(3)	1.582(4)
C(29)-C(28)	1.390(5)	P(1)-F(6)	1.601(4)
C(7)-C(8)	1.399(5)		

Bond angle:

N(3)-Ru-N(11)	93.65(11)	N(3)-Ru-N(8)	173.99(12)
N(3)-Ru-N(9)	97.68(11)	N(11)-Ru-N(8)	91.61(11)
N(11)-Ru-N(9)	98.11(11)	N(9)-Ru-N(8)	78.69(12)
N(3)-Ru-N(10)	86.40(11)	N(10)-Ru-N(8)	97.46(12)
N(11)-Ru-N(10)	78.78(11)	N(1)-Ru-N(8)	96.75(11)
N(9)-Ru-N(10)	175.05(11)	C(30)-N(11)-C(26)	118.1(3)
N(3)-Ru-N(1)	78.03(11)	C(30)-N(11)-Ru	126.1(2)
N(11)-Ru-N(1)	171.61(11)	C(26)-N(11)-Ru	115.6(2)
N(9)-Ru-N(1)	84.23(12)	C(5)-N(3)-N(4)	108.2(3)
N(10)-Ru-N(1)	99.39(12)	C(5)-N(3)-Ru	116.2(2)

N(4)-N(3)-Ru	135.4(2)	N(9)-C(16)-C(17)	121.6(4)
C(5)-N(5)-C(6)	100.7(3)	N(9)-C(16)-C(15)	114.9(3)
C(11)-N(8)-C(15)	119.0(3)	C(17)-C(16)-C(15)	123.3(4)
C(11)-N(8)-Ru	125.6(3)	N(10)-C(21)-C(22)	122.5(4)
C(15)-N(8)-Ru	115.3(2)	C(27)-C(28)-C(29)	117.3(3)
C(6)-N(4)-N(3)	102.7(3)	C(27)-C(28)-C(32)	121.3(3)
C(4)-N(1)-C(1)	116.0(3)	C(29)-C(28)-C(32)	121.4(3)
C(4)-N(1)-Ru	115.7(2)	C(18)-C(19)-C(20)	119.0(4)
C(1)-N(1)-Ru	127.6(3)	N(7)-C(8)-C(7)	122.5(4)
N(4)-C(6)-N(5)	115.3(3)	C(19)-C(18)-C(17)	119.5(4)
N(4)-C(6)-C(7)	122.4(3)	C(21)-C(22)-C(23)	120.3(4)
N(5)-C(6)-C(7)	122.2(3)	N(2)-C(3)-C(4)	122.4(4)
C(10)-N(6)-C(7)	116.3(4)	C(3)-N(2)-C(2)	115.8(3)
C(20)-N(9)-C(16)	118.2(3)	C(16)-C(17)-C(18)	118.9(4)
C(20)-N(9)-Ru	125.4(3)	N(1)-C(4)-C(3)	121.3(3)
C(16)-N(9)-Ru	115.9(2)	N(1)-C(4)-C(5)	114.0(3)
N(3)-C(5)-N(5)	113.0(3)	C(3)-C(4)-C(5)	124.5(3)
N(3)-C(5)-C(4)	115.6(3)	N(9)-C(20)-C(19)	122.7(4)
N(5)-C(5)-C(4)	131.3(3)	N(8)-C(11)-C(12)	121.2(5)
N(11)-C(30)-C(29)	122.4(3)	N(1)-C(1)-C(2)	121.4(4)
C(21)-N(10)-C(25)	117.9(3)	C(13)-C(12)-C(11)	120.5(5)
C(21)-N(10)-Ru	126.5(3)	N(6)-C(10)-C(9)	122.3(4)
C(25)-N(10)-Ru	115.6(2)	N(7)-C(9)-C(10)	122.1(4)
C(30)-C(29)-C(28)	120.1(3)	C(15)-C(14)-C(13)	120.1(5)
N(6)-C(7)-C(8)	120.9(3)	N(2)-C(2)-C(1)	123.1(4)
N(6)-C(7)-C(6)	117.6(3)	C(12)-C(13)-C(14)	118.4(4)
C(8)-C(7)-C(6)	121.5(3)	F(1)-P(1)-F(4)	177.2(4)
N(10)-C(25)-C(24)	122.0(3)	F(1)-P(1)-F(2)	89.4(5)
N(10)-C(25)-C(26)	114.5(3)	F(4)-P(1)-F(2)	93.2(4)
C(24)-C(25)-C(26)	123.5(3)	F(1)-P(1)-F(5)	90.3(3)
C(24)-C(23)-C(22)	116.8(4)	F(4)-P(1)-F(5)	88.9(3)
C(24)-C(23)-C(31)	121.0(4)	F(2)-P(1)-F(5)	88.4(3)
C(22)-C(23)-C(31)	122.3(4)	F(1)-P(1)-F(3)	91.9(4)
C(28)-C(27)-C(26)	120.7(3)	F(4)-P(1)-F(3)	89.0(3)
N(11)-C(26)-C(27)	121.4(3)	F(2)-P(1)-F(3)	92.0(3)
N(11)-C(26)-C(25)	114.9(3)	F(5)-P(1)-F(3)	177.9(3)
C(27)-C(26)-C(25)	123.7(3)	F(1)-P(1)-F(6)	89.2(4)
C(8)-N(7)-C(9)	115.8(4)	F(4)-P(1)-F(6)	88.1(3)
N(8)-C(15)-C(14)	120.7(4)	F(2)-P(1)-F(6)	178.4(4)
N(8)-C(15)-C(16)	114.7(3)	F(5)-P(1)-F(6)	90.7(2)
C(14)-C(15)-C(16)	124.6(4)	F(3)-P(1)-F(6)	89.0(2)
C(25)-C(24)-C(23)	120.6(4)		

Crystal Data for [Ru(bpy)(Me₂bpy)(MeCN)₂](PF₆)₂
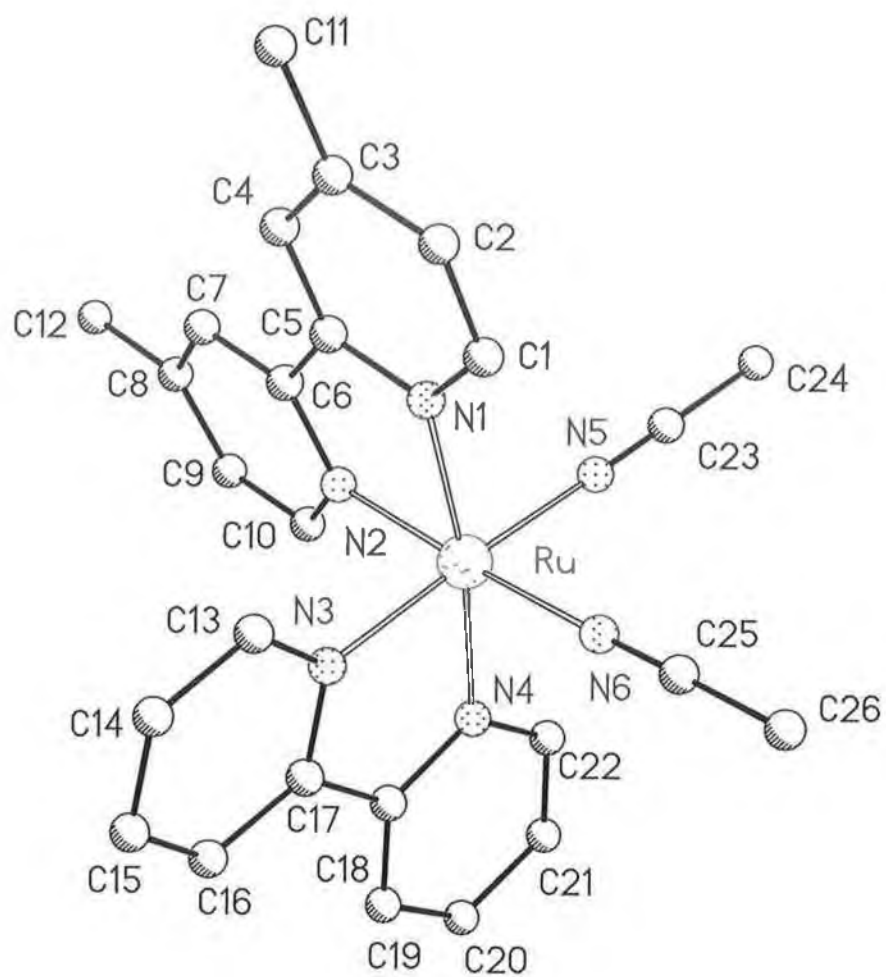
Table D9. Bond lengths [Å] and angles [°] for [Ru(bpy)(Me$_2$bpy)(MeCN)$_2$](PF$_6$)$_2$

<u>Bond length:</u>

Ru-N(5)	2.032(4)	C(13)-C(14)	1.388(6)
Ru-N(6)	2.037(4)	C(14)-C(15)	1.371(6)
Ru-N(3)	2.043(3)	C(15)-C(16)	1.379(6)
Ru-N(2)	2.046(3)	C(16)-C(17)	1.384(6)
Ru-N(1)	2.067(3)	C(17)-C(18)	1.471(6)
Ru-N(4)	2.067(3)	C(18)-C(19)	1.375(6)
N(1)-C(5)	1.356(5)	C(19)-C(20)	1.374(6)
N(1)-C(1)	1.348(5)	C(20)-C(21)	1.382(6)
N(2)-C(10)	1.346(5)	C(21)-C(22)	1.381(6)
N(2)-C(6)	1.361(5)	C(23)-C(24)	1.468(6)
N(3)-C(13)	1.350(5)	C(25)-C(26)	1.451(6)
N(3)-C(17)	1.360(5)	P(1)-F(12)	1.582(3)
N(4)-C(22)	1.341(5)	P(1)-F(16)	1.587(3)
N(4)-C(18)	1.356(5)	P(1)-F(13)	1.589(3)
N(5)-C(23)	1.134(5)	P(1)-F(15)	1.598(3)
N(6)-C(25)	1.145(5)	P(1)-F(14)	1.596(3)
C(1)-C(2)	1.379(6)	P(1)-F(11)	1.596(3)
C(2)-C(3)	1.374(6)	P(2)-F(21)	1.568(3)
C(3)-C(4)	1.390(6)	P(2)-F(22)	1.572(4)
C(3)-C(11)	1.506(6)	P(2)-F(26)	1.575(3)
C(4)-C(5)	1.379(6)	P(2)-F(24)	1.575(3)
C(5)-C(6)	1.479(6)	P(2)-F(23)	1.578(4)
C(6)-C(7)	1.384(6)	P(2)-F(25)	1.600(3)
C(7)-C(8)	1.387(6)	O(1E)-C(3E)	1.406(6)
C(8)-C(9)	1.374(6)	O(1E)-C(2E)	1.425(6)
C(8)-C(12)	1.514(6)	C(1E)-C(2E)	1.480(8)
C(9)-C(10)	1.378(6)	C(3E)-C(4E)	1.499(7)

<u>Bond angle:</u>

N(5)-Ru-N(6)	90.35(13)	N(2)-Ru-N(4)	95.79(14)
N(5)-Ru-N(3)	176.04(14)	N(1)-Ru-N(4)	171.14(13)
N(6)-Ru-N(3)	89.66(13)	C(5)-N(1)-C(1)	118.3(4)
N(5)-Ru-N(2)	89.88(13)	C(5)-N(1)-Ru	115.5(3)
N(6)-Ru-N(2)	175.34(14)	C(1)-N(1)-Ru	126.0(3)
N(3)-Ru-N(2)	90.43(13)	C(10)-N(2)-C(6)	117.9(4)
N(5)-Ru-N(1)	89.67(13)	C(10)-N(2)-Ru	126.0(3)
N(6)-Ru-N(1)	96.65(14)	C(6)-N(2)-Ru	116.1(3)
N(3)-Ru-N(1)	94.26(13)	C(13)-N(3)-C(17)	118.3(4)
N(2)-Ru-N(1)	78.70(14)	C(13)-N(3)-Ru	125.6(3)
N(5)-Ru-N(4)	97.30(14)	C(17)-N(3)-Ru	116.1(3)
N(6)-Ru-N(4)	88.80(13)	C(22)-N(4)-C(18)	118.5(4)
N(3)-Ru-N(4)	78.74(14)	C(22)-N(4)-Ru	126.0(3)

C(18)-N(4)-Ru	115.4(3)		N(5)-C(23)-C(24)	178.4(5)
C(23)-N(5)-Ru	177.4(4)		N(6)-C(25)-C(26)	179.3(5)
C(25)-N(6)-Ru	177.8(4)		F(12)-P(1)-F(16)	90.69(18)
N(1)-C(1)-C(2)	122.1(4)		F(12)-P(1)-F(13)	90.21(19)
C(3)-C(2)-C(1)	120.5(4)		F(16)-P(1)-F(13)	90.61(18)
C(2)-C(3)-C(4)	117.0(4)		F(12)-P(1)-F(15)	178.87(19)
C(4)-C(3)-C(11)	121.7(4)		F(16)-P(1)-F(15)	89.93(17)
C(2)-C(3)-C(11)	121.3(4)		F(13)-P(1)-F(15)	90.33(18)
C(5)-C(4)-C(3)	121.0(4)		F(12)-P(1)-F(14)	179.5(2)
N(1)-C(5)-C(4)	121.0(4)		F(16)-P(1)-F(14)	89.58(16)
N(1)-C(5)-C(6)	114.4(4)		F(13)-P(1)-F(14)	89.35(17)
C(4)-C(5)-C(6)	124.6(4)		F(15)-P(1)-F(14)	89.80(15)
N(2)-C(6)-C(7)	121.3(4)		F(12)-P(1)-F(11)	90.27(19)
N(2)-C(6)-C(5)	114.6(4)		F(16)-P(1)-F(11)	89.78(17)
C(7)-C(6)-C(5)	124.1(4)		F(13)-P(1)-F(11)	179.4(2)
C(6)-C(7)-C(8)	120.3(4)		F(15)-P(1)-F(11)	89.27(17)
C(9)-C(8)-C(7)	117.8(4)		F(14)-P(1)-F(11)	90.17(17)
C(9)-C(8)-C(12)	121.2(4)		F(21)-P(2)-F(22)	90.6(2)
C(7)-C(8)-C(12)	120.9(4)		F(21)-P(2)-F(26)	90.2(2)
C(8)-C(9)-C(10)	119.9(4)		F(22)-P(2)-F(26)	89.4(2)
N(2)-C(10)-C(9)	122.7(4)		F(21)-P(2)-F(24)	179.6(2)
N(3)-C(13)-C(14)	122.4(4)		F(22)-P(2)-F(24)	89.4(2)
C(15)-C(14)-C(13)	119.3(4)		F(26)-P(2)-F(24)	90.2(2)
C(14)-C(15)-C(16)	118.6(4)		F(21)-P(2)-F(23)	90.3(3)
C(15)-C(16)-C(17)	120.4(4)		F(22)-P(2)-F(23)	178.9(3)
N(3)-C(17)-C(16)	120.9(4)		F(26)-P(2)-F(23)	91.3(2)
N(3)-C(17)-C(18)	114.8(4)		F(24)-P(2)-F(23)	89.7(2)
C(16)-C(17)-C(18)	124.3(4)		F(21)-P(2)-F(25)	89.35(19)
N(4)-C(18)-C(19)	121.6(4)		F(22)-P(2)-F(25)	90.5(2)
N(4)-C(18)-C(17)	114.7(4)		F(26)-P(2)-F(25)	179.5(2)
C(19)-C(18)-C(17)	123.7(4)		F(24)-P(2)-F(25)	90.3(2)
C(20)-C(19)-C(18)	119.3(4)		F(23)-P(2)-F(25)	88.77(19)
C(19)-C(20)-C(21)	119.8(4)		C(3E)-O(1E)-C(2E)	112.1(4)
C(22)-C(21)-C(20)	118.2(4)		O(1E)-C(2E)-C(1E)	107.8(5)
N(4)-C(22)-C(21)	122.6(4)		O(1E)-C(3E)-C(4E)	109.3(4)

Crystal Data for [Ru(pytrz)(CO)$_2$Cl$_2$]
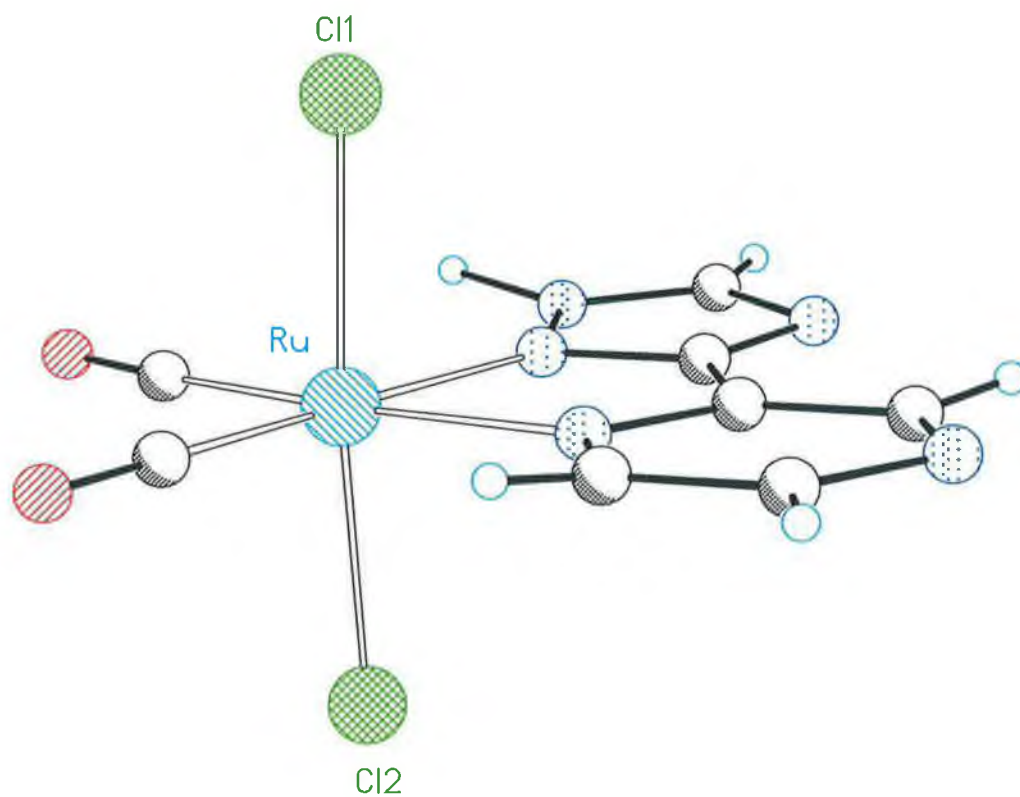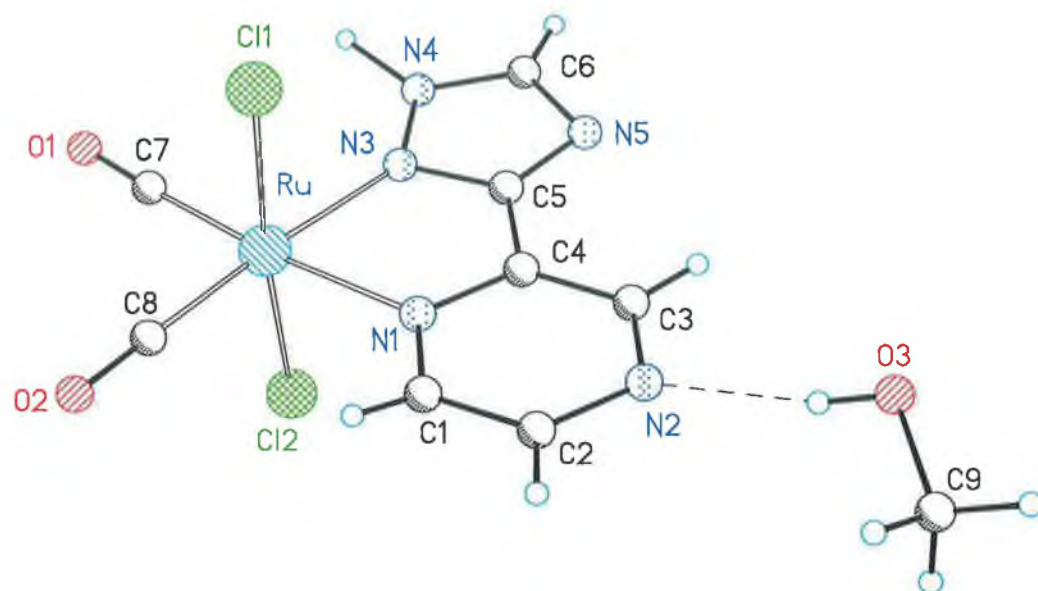
Table D10. Bond lengths [Å] and angles [°] for [Ru(pytrz)(CO)₂Cl₂]

Bond length:

Ru-C(8)	1.875(4)	N(2)-C(2)	1.344(5)
Ru-C(7)	1.882(4)	N(3)-N(4)	1.344(5)
Ru-N(3)	2.106(3)	N(3)-C(5)	1.357(5)
Ru-N(1)	2.150(3)	N(4)-C(6)	1.325(5)
Ru-Cl(1)	2.3749(10)	N(5)-C(5)	1.316(5)
Ru-Cl(2)	2.3999(10)	N(5)-C(6)	1.354(5)
O(1)-C(7)	1.130(5)	C(1)-C(2)	1.375(6)
O(2)-C(8)	1.140(5)	C(3)-C(4)	1.386(6)
N(1)-C(1)	1.339(5)	C(4)-C(5)	1.456(5)
N(1)-C(4)	1.354(5)	O(3)-C(9)	1.408(5)
N(2)-C(3)	1.331(5)		

Bond angle:

C(8)-Ru-C(7)	89.91(18)	C(3)-N(2)-C(2)	116.5(4)
C(8)-Ru-N(3)	173.03(15)	N(4)-N(3)-C(5)	103.6(3)
C(7)-Ru-N(3)	96.90(15)	N(4)-N(3)-Ru	141.5(3)
C(8)-Ru-N(1)	96.06(15)	C(5)-N(3)-Ru	114.8(2)
C(7)-Ru-N(1)	173.94(14)	C(6)-N(4)-N(3)	108.5(4)
N(3)-Ru-N(1)	77.11(12)	C(5)-N(5)-C(6)	102.5(3)
C(8)-Ru-Cl(1)	92.02(13)	N(1)-C(1)-C(2)	121.9(4)
C(7)-Ru-Cl(1)	91.09(13)	N(2)-C(2)-C(1)	121.8(4)
N(3)-Ru-Cl(1)	86.39(9)	N(2)-C(3)-C(4)	122.5(4)
N(1)-Ru-Cl(1)	87.67(8)	N(1)-C(4)-C(3)	120.6(3)
C(8)-Ru-Cl(2)	91.95(13)	N(1)-C(4)-C(5)	114.1(3)
C(7)-Ru-Cl(2)	91.74(13)	C(3)-C(4)-C(5)	125.3(4)
N(3)-Ru-Cl(2)	89.33(9)	N(5)-C(5)-N(3)	114.1(3)
N(1)-Ru-Cl(2)	89.10(8)	N(5)-C(5)-C(4)	127.6(4)
Cl(1)-Ru-Cl(2)	175.12(4)	N(3)-C(5)-C(4)	118.3(3)
C(1)-N(1)-C(4)	116.8(3)	N(4)-C(6)-N(5)	111.3(3)
C(1)-N(1)-Ru	127.5(3)	O(1)-C(7)-Ru	177.8(4)
C(4)-N(1)-Ru	115.7(2)	O(2)-C(8)-Ru	178.9(4)

Crystal Data for [Ru(L6)(CO)$_2$Cl$_2$]
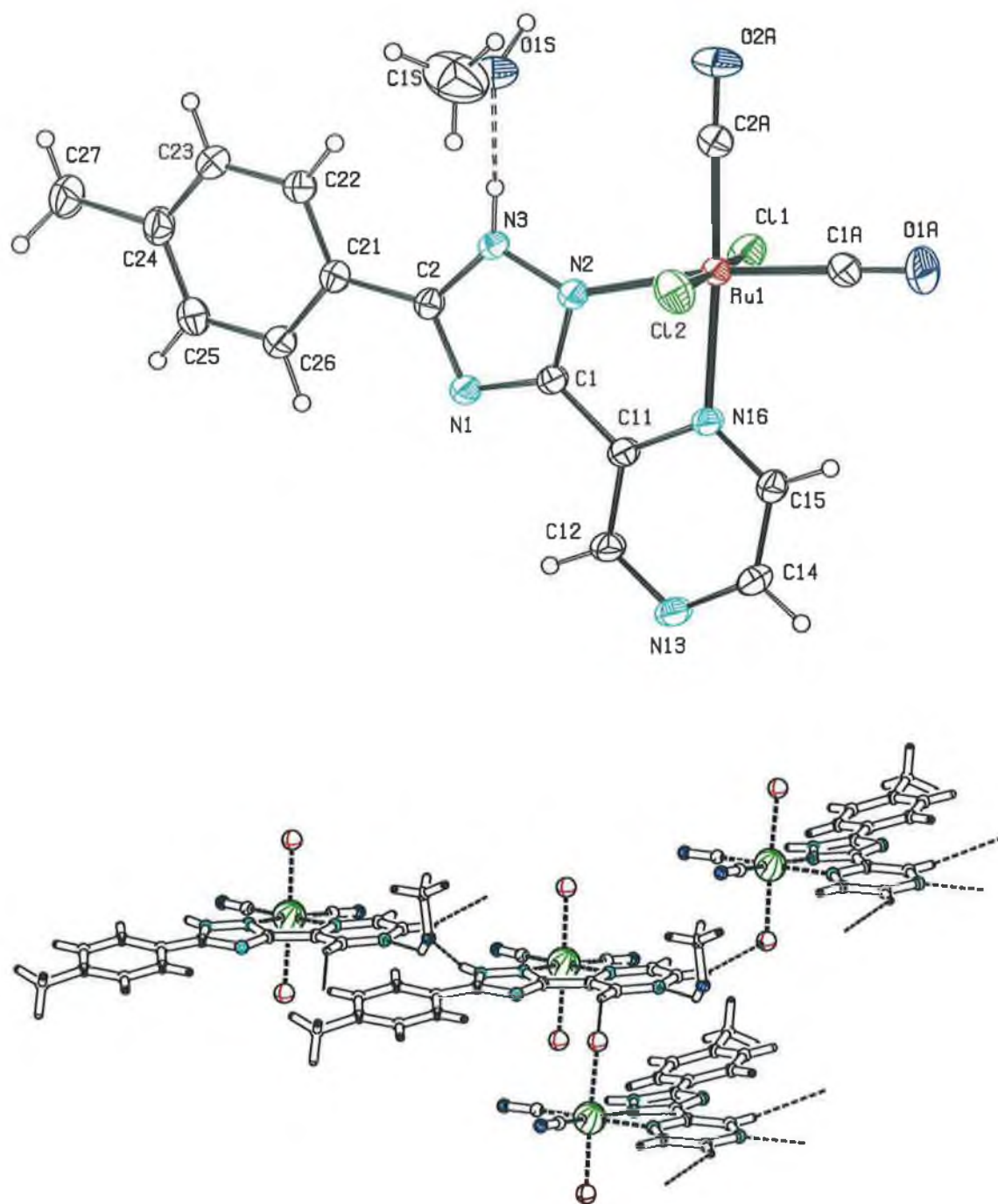
Table D11. Crystal data and structure refinement for [Ru(L6)(CO)$_2$Cl$_2$].

Empirical formula	C$_{16}$H$_{15}$Cl$_2$N$_5$O$_3$Ru
Formula weight	497.30
Temperature	296(2) K
Wavelength	0.71073 Å
Crystal system, space group	
Unit cell dimensions	a = 11.0433(6) Å α = 90°
	b = 10.6963(6) Å β = 97.842° (4)
	c = 16.7567(10) Å γ = 90°
Volume	1960.83(19) Å^3
Z	4
Calculated density	1.685 mg/m^3
Absorption coefficient	1.098 mm^{-1}
F(000)	992
Crystal size	0.48 × 0.18 × 0.16 mm
Theta range for data collection	1.86 to 26.04 deg.
Index ranges	-1 ≤ h ≤ 13, -1 ≤ k ≤ 13, -20 ≤ l ≤20
Reflections collected / unique	4982 / 3858 [R(int) = 0.0147]
Completeness to theta = 26.04°	94.1%
Max. and min. transmission	0.8438 and 0.6207
Refinement method	Full-matrix least-squares on F^2
Data / restraints / parameters	3858 / 0 / 254
Goodness-of-fit on F^2	1.050
Final R indices [I>2sigma(I)]	R1 = 0.0286, wR2 = 0.0698
R indices (all data)	R1 = 0.0387, wR2 = 0.0750
Largest diff. peak and hole	0.552 and -0.294 e. Å^{-3}

Table D12. Atomic coordinates ($\times 10^4$) and equivalent isotropic displacement parameters ($\text{Å}^2 \times 10^3$) for $[Ru(L6)(CO)_2Cl_2]$. U(eq) is defined as one third of the trace of the orthogonalized U^{ij} tensor.

	x	y	z	U(eq)
Ru(1)	2837(1)	405(1)	2305(1)	36(1)
Cl(1)	1144(1)	355(1)	1255(1)	53(1)
Cl(2)	4422(1)	429(1)	3420(1)	57(1)
O(1A)	4593(3)	48(3)	1115(2)	80(1)
C(1A)	3939(3)	194(3)	1568(2)	49(1)
O(2A)	3121(3)	3177(2)	2110(2)	90(1)
C(2A)	2988(3)	2134(3)	2186(2)	54(1)
N(1)	122(2)	-776(2)	3655(1)	36(1)
C(1)	1077(2)	-772(2)	3238(2)	34(1)
C(2)	-24(2)	440(2)	3804(2)	34(1)
N(2)	1520(2)	345(2)	3110(1)	36(1)
N(3)	802(2)	1128(2)	3475(1)	36(1)
C(11)	1679(2)	-1850(2)	2940(2)	34(1)
C(12)	1399(2)	-3081(2)	3106(2)	40(1)
N(13)	2025(2)	-4039(2)	2862(1)	43(1)
C(14)	2935(3)	-3743(3)	2444(2)	43(1)
C(15)	3217(2)	-2533(3)	2260(2)	40(1)
N(16)	2589(2)	-1572(2)	2501(1)	35(1)
C(21)	-977(2)	946(3)	4236(2)	36(1)
C(22)	-1060(3)	2210(3)	4396(2)	44(1)
C(23)	-2033(3)	2658(3)	4753(2)	50(1)
C(24)	-2927(3)	1872(3)	4964(2)	45(1)
C(25)	-2818(3)	601(3)	4823(2)	46(1)
C(26)	-1855(3)	138(3)	4466(2)	41(1)
C(27)	-4023(3)	2387(3)	5312(2)	61(1)
O(1S)	1636(3)	3482(2)	3582(2)	68(1)
C(1S)	2447(6)	3614(5)	4296(3)	120(2)

Table D13. Bond lengths [Å] and angles [deg] for [Ru(L6)(CO)$_2$Cl$_2$].

Bond length:

Ru(1)-C(1A)	1.862(3)	C(14)-H(14)	0.9300
Ru(1)-C(2A)	1.871(3)	C(15)-N(16)	1.333(3)
Ru(1)-N(2)	2.115(2)	C(15)-H(15)	0.9300
Ru(1)-N(16)	2.163(2)	C(21)-C(22)	1.384(4)
Ru(1)-Cl(2)	2.3803(9)	C(21)-C(26)	1.393(4)
Ru(1)-Cl(1)	2.3869(8)	C(22)-C(23)	1.385(4)
O(1A)-C(1A)	1.126(4)	C(22)-H(22)	0.9300
O(2A)-C(2A)	1.135(4)	C(23)-C(24)	1.379(4)
N(1)-C(2)	1.339(3)	C(23)-H(23)	0.9300
N(1)-C(1)	1.343(3)	C(24)-C(25)	1.389(4)
C(1)-N(2)	1.320(3)	C(24)-C(27)	1.516(4)
C(1)-C(11)	1.453(3)	C(25)-C(26)	1.380(4)
C(2)-N(3)	1.347(3)	C(25)-H(25)	0.9300
C(2)-C(21)	1.460(3)	C(26)-H(26)	0.9300
N(2)-N(3)	1.355(3)	C(27)-H(27A)	0.9600
N(3)-H(3)	0.85(4)	C(27)-H(27B)	0.9600
C(11)-N(16)	1.356(3)	C(27)-H(27C)	0.9600
C(11)-C(12)	1.389(3)	O(1S)-C(1S)	1.399(5)
C(12)-N(13)	1.332(3)	O(1S)-H(1S)	0.91(3)
C(12)-H(12)	0.9300	C(1S)-H(1S1)	0.9600
N(13)-C(14)	1.338(3)	C(1S)-H(1S2)	0.9600
C(14)-C(15)	1.376(4)	C(1S)-H(1S3)	0.9600

Bond angle:

C(1A)-Ru(1)-C(2A)	88.48(13)	C(2)-N(1)-C(1)	102.6(2)
C(1A)-Ru(1)-N(2)	171.02(11)	N(2)-C(1)-N(1)	115.0(2)
C(2A)-Ru(1)-N(2)	100.18(11)	N(2)-C(1)-C(11)	117.8(2)
C(1A)-Ru(1)-N(16)	95.19(11)	N(1)-C(1)-C(11)	127.3(2)
C(2A)-Ru(1)-N(16)	176.32(10)	N(1)-C(2)-N(3)	110.4(2)
N(2)-Ru(1)-N(16)	76.17(8)	N(1)-C(2)-C(21)	124.5(2)
C(1A)-Ru(1)-Cl(2)	92.59(11)	N(3)-C(2)-C(21)	125.1(2)
C(2A)-Ru(1)-Cl(2)	90.35(11)	C(1)-N(2)-N(3)	103.5(2)
N(2)-Ru(1)-Cl(2)	89.77(7)	C(1)-N(2)-Ru(1)	115.68(16)
N(16)-Ru(1)-Cl(2)	89.22(6)	N(3)-N(2)-Ru(1)	139.88(17)
C(1A)-Ru(1)-Cl(1)	91.45(11)	C(2)-N(3)-N(2)	108.6(2)
C(2A)-Ru(1)-Cl(1)	90.88(11)	C(2)-N(3)-H(3)	136(2)
N(2)-Ru(1)-Cl(1)	86.07(7)	N(2)-N(3)-H(3)	116(2)
N(16)-Ru(1)-Cl(1)	89.30(6)	N(16)-C(11)-C(12)	121.2(2)
Cl(2)-Ru(1)-Cl(1)	175.81(3)	N(16)-C(11)-C(1)	114.8(2)
O(1A)-C(1A)-Ru(1)	178.7(3)	C(12)-C(11)-C(1)	123.9(2)
O(2A)-C(2A)-Ru(1)	177.6(3)	N(13)-C(12)-C(11)	121.9(2)

N(13)-C(12)-H(12)	119.0	C(23)-C(24)-C(27)	120.9(3)
C(11)-C(12)-H(12)	119.0	C(25)-C(24)-C(27)	120.9(3)
C(12)-N(13)-C(14)	115.9(2)	C(26)-C(25)-C(24)	121.0(3)
N(13)-C(14)-C(15)	123.3(2)	C(26)-C(25)-H(25)	119.5
N(13)-C(14)-H(14)	118.3	C(24)-C(25)-H(25)	119.5
C(15)-C(14)-H(14)	118.3	C(25)-C(26)-C(21)	120.3(3)
N(16)-C(15)-C(14)	120.9(2)	C(25)-C(26)-H(26)	119.9
N(16)-C(15)-H(15)	119.5	C(21)-C(26)-H(26)	119.9
C(14)-C(15)-H(15)	119.5	C(24)-C(27)-H(27A)	109.5
C(15)-N(16)-C(11)	116.7(2)	C(24)-C(27)-H(27B)	109.5
C(15)-N(16)-Ru(1)	128.71(18)	H(27A)-C(27)-H(27B)	109.5
C(11)-N(16)-Ru(1)	114.56(16)	C(24)-C(27)-H(27C)	109.5
C(22)-C(21)-C(26)	119.0(2)	H(27A)-C(27)-H(27C)	109.5
C(22)-C(21)-C(2)	122.0(2)	H(27B)-C(27)-H(27C)	109.5
C(26)-C(21)-C(2)	118.9(2)	C(1S)-O(1S)-H(1S)	125.2(17)
C(21)-C(22)-C(23)	119.9(3)	O(1S)-C(1S)-H(1S1)	109.5
C(21)-C(22)-H(22)	120.1	O(1S)-C(1S)-H(1S2)	109.5
C(23)-C(22)-H(22)	120.1	H(1S1)-C(1S)-H(1S2)	109.5
C(24)-C(23)-C(22)	121.7(3)	O(1S)-C(1S)-H(1S3)	109.5
C(24)-C(23)-H(23)	119.2	H(1S1)-C(1S)-H(1S3)	109.5
C(22)-C(23)-H(23)	119.2	H(1S2)-C(1S)-H(1S3)	109.5
C(23)-C(24)-C(25)	118.1(3)		

Table D14.   Anisotropic   displacement   parameters   ($Å^2 \times 10^3$)   for [Ru(L6)(CO)$_2$Cl$_2$]. The anisotropic displacement factor exponent takes the form: -2 pi^2 [h^2 a*^2 U11 + ... + 2 h k a* b* U12]

	U11	U22	U33	U23	U13	U12
Ru(1)	38(1)	27(1)	46(1)	1(1)	18(1)	-1(1)
Cl(1)	53(1)	52(1)	54(1)	-6(1)	7(1)	13(1)
Cl(2)	45(1)	70(1)	58(1)	4(1)	9(1)	-12(1)
O(1A)	83(2)	78(2)	94(2)	-5(2)	61(2)	-6(2)
C(1A)	50(2)	40(2)	61(2)	1(1)	25(2)	-6(1)
O(2A)	129(3)	31(1)	122(2)	10(1)	53(2)	-10(1)
C(2A)	64(2)	38(2)	63(2)	2(1)	28(2)	-5(2)
N(1)	35(1)	29(1)	46(1)	1(1)	15(1)	0(1)
C(1)	35(1)	28(1)	42(1)	-2(1)	10(1)	0(1)
C(2)	31(1)	34(1)	39(1)	0(1)	9(1)	3(1)
N(2)	37(1)	29(1)	43(1)	-2(1)	14(1)	-1(1)
N(3)	41(1)	25(1)	45(1)	-2(1)	16(1)	1(1)
C(11)	33(1)	28(1)	43(1)	-2(1)	10(1)	1(1)
C(12)	40(1)	28(1)	55(2)	-2(1)	14(1)	-4(1)
N(13)	47(1)	27(1)	56(1)	-2(1)	11(1)	0(1)
C(14)	48(2)	30(1)	50(2)	-7(1)	9(1)	6(1)
C(15)	37(1)	37(1)	48(2)	-2(1)	14(1)	4(1)
N(16)	33(1)	27(1)	46(1)	-1(1)	12(1)	-1(1)
C(21)	35(1)	36(1)	38(1)	0(1)	10(1)	4(1)
C(22)	46(2)	36(2)	53(2)	2(1)	19(1)	2(1)
C(23)	60(2)	38(2)	56(2)	1(1)	23(2)	11(1)
C(24)	43(2)	54(2)	41(1)	3(1)	13(1)	12(1)
C(25)	40(2)	51(2)	49(2)	2(1)	16(1)	-2(1)
C(26)	43(2)	35(1)	48(2)	-2(1)	15(1)	-1(1)
C(27)	56(2)	65(2)	67(2)	2(2)	26(2)	17(2)
O(1S)	86(2)	35(1)	84(2)	-1(1)	16(2)	-8(1)
C(1S)	163(5)	94(4)	95(4)	1(3)	-7(4)	-52(4)

Table D15. Hydrogen coordinates ($\times 10^4$) and isotropic displacement parameters ($\text{Å}^2 \times 10^3$) for [Ru(L6)(CO)$_2$Cl$_2$].

	x	y	z	U(eq)
H(3)	970(3)	1900(4)	3450(2)	68(11)
H(12)	755	-3240	3396	48
H(14)	3399	-4387	2269	51
H(15)	3855	-2383	1964	48
H(22)	-464	2758	4264	53
H(23)	-2085	3510	4854	60
H(25)	-3402	53	4971	55
H(26)	-1793	-717	4380	50
H(27A)	-3849	3221	5505	91
H(27B)	-4193	1866	5750	91
H(27C)	-4720	2398	4902	91
H(1S)	1550(2)	4040(3)	3163(16)	29(7)
H(1S1)	3164	4054	4185	179
H(1S2)	2675	2803	4510	179
H(1S3)	2058	4077	4681	179

Table D16. Torsion angles [deg] for [Ru(L6)(CO)₂Cl₂].

C(2A)-Ru(1)-C(1A)-O(1A)	-141(13)	N(16)-C(11)-C(12)-N(13)	1.7(4)
N(2)-Ru(1)-C(1A)-O(1A)	24(14)	C(1)-C(11)-C(12)-N(13)	-175.7(3)
N(16)-Ru(1)-C(1A)-O(1A)	39(13)	C(11)-C(12)-N(13)-C(14)	-0.3(4)
Cl(2)-Ru(1)-C(1A)-O(1A)	129(13)	C(12)-N(13)-C(14)-C(15)	-0.8(4)
Cl(1)-Ru(1)-C(1A)-O(1A)	-50(13)	N(13)-C(14)-C(15)-N(16)	0.6(5)
C(1A)-Ru(1)-C(2A)-O(2A)	-33(8)	C(14)-C(15)-N(16)-C(11)	0.8(4)
N(2)-Ru(1)-C(2A)-O(2A)	149(8)	C(14)-C(15)-N(16)-Ru(1)	179.7(2)
N(16)-Ru(1)-C(2A)-O(2A)	143(7)	C(12)-C(11)-N(16)-C(15)	-1.8(4)
Cl(2)-Ru(1)-C(2A)-O(2A)	60(8)	C(1)-C(11)-N(16)-C(15)	175.8(2)
Cl(1)-Ru(1)-C(2A)-O(2A)	-124(8)	C(12)-C(11)-N(16)-Ru(1)	179.1(2)
C(2)-N(1)-C(1)-N(2)	-0.8(3)	C(1)-C(11)-N(16)-Ru(1)	-3.3(3)
C(2)-N(1)-C(1)-C(11)	177.5(3)	C(1A)-Ru(1)-N(16)-C(15)	10.1(3)
C(1)-N(1)-C(2)-N(3)	0.9(3)	C(2A)-Ru(1)-N(16)-C(15)	-165.8(18)
C(1)-N(1)-C(2)-C(21)	178.8(2)	N(2)-Ru(1)-N(16)-C(15)	-172.4(3)
N(1)-C(1)-N(2)-N(3)	0.4(3)	Cl(2)-Ru(1)-N(16)-C(15)	-82.5(2)
C(11)-C(1)-N(2)-N(3)	-178.1(2)	Cl(1)-Ru(1)-N(16)-C(15)	101.5(2)
N(1)-C(1)-N(2)-Ru(1)	-170.9(18)	C(1A)-Ru(1)-N(16)-C(11)	-171.0(2)
C(11)-C(1)-N(2)-Ru(1)	10.7(3)	C(2A)-Ru(1)-N(16)-C(11)	13(2)
C(1A)-Ru(1)-N(2)-C(1)	6.8(9)	N(2)-Ru(1)-N(16)-C(11)	6.53(18)
C(2A)-Ru(1)-N(2)-C(1)	171.2(2)	Cl(2)-Ru(1)-N(16)-C(11)	96.48(18)
N(16)-Ru(1)-N(2)-C(1)	-9.21(19)	Cl(1)-Ru(1)-N(16)-C(11)	-79.60(18)
Cl(2)-Ru(1)-N(2)-C(1)	-98.46(19)	N(1)-C(2)-C(21)-C(22)	177.8(3)
Cl(1)-Ru(1)-N(2)-C(1)	81.03(19)	N(3)-C(2)-C(21)-C(22)	-4.7(4)
C(1A)-Ru(1)-N(2)-N(3)	-159.8(7)	N(1)-C(2)-C(21)-C(26)	-4.7(4)
C(2A)-Ru(1)-N(2)-N(3)	4.5(3)	N(3)-C(2)-C(21)-C(26)	172.9(3)
N(16)-Ru(1)-N(2)-N(3)	-175.9(3)	C(26)-C(21)-C(22)-C(23)	-2.4(4)
Cl(2)-Ru(1)-N(2)-N(3)	94.9(3)	C(2)-C(21)-C(22)-C(23)	175.1(3)
Cl(1)-Ru(1)-N(2)-N(3)	-85.7(3)	C(21)-C(22)-C(23)-C(24)	0.6(5)
N(1)-C(2)-N(3)-N(2)	-0.8(3)	C(22)-C(23)-C(24)-C(25)	1.2(5)
C(21)-C(2)-N(3)-N(2)	-178.6(2)	C(22)-C(23)-C(24)-C(27)	-176.6(3)
C(1)-N(2)-N(3)-C(2)	0.3(3)	C(23)-C(24)-C(25)-C(26)	-1.3(5)
Ru(1)-N(2)-N(3)-C(2)	167.9(2)	C(27)-C(24)-C(25)-C(26)	176.5(3)
N(2)-C(1)-C(11)-N(16)	-4.8(4)	C(24)-C(25)-C(26)-C(21)	-0.5(5)
N(1)-C(1)-C(11)-N(16)	177.0(3)	C(22)-C(21)-C(26)-C(25)	2.3(4)
N(2)-C(1)-C(11)-C(12)	172.7(3)	C(2)-C(21)-C(26)-C(25)	-175.3(3)
N(1)-C(1)-C(11)-C(12)	-5.5(5)		

Table D17. Hydrogen-bonds for [Ru(L6)(CO)₂Cl₂]. [Å and deg.].

D-H	A		d(D-H)	d(H...A)	d(D...A)	<(DHA)
N(3)-H(3)	O(1S)		0.85(4)	1.85(4)	2.679(3)	166(3)
O(1S)-H(1S)	N(13)	#1	0.91(3)	2.20(3)	2.969(3)	141(2)
C(12)-H(12)	Cl(1)	#2	0.93	2.71	3.557(3)	152.2
C(14)-H(14)	Cl(2)	#3	0.93	2.81	3.543(3)	136.1
C(26)-H(26)	N(1)		0.93	2.58	2.895(3)	100.4

#1   x, y+1, z   #2   -x, y-1/2, -z+1/2   #3   -x+1, y-1/2, -z+1/2

Crystal Data for [Ru(L7)(CO)₂Cl₂]
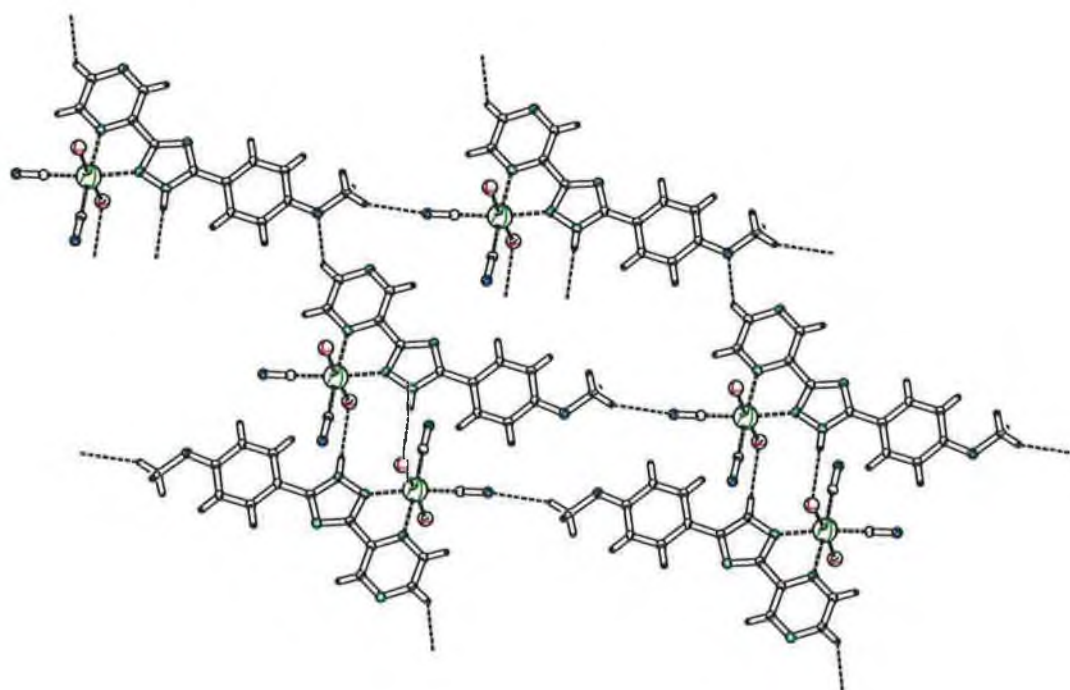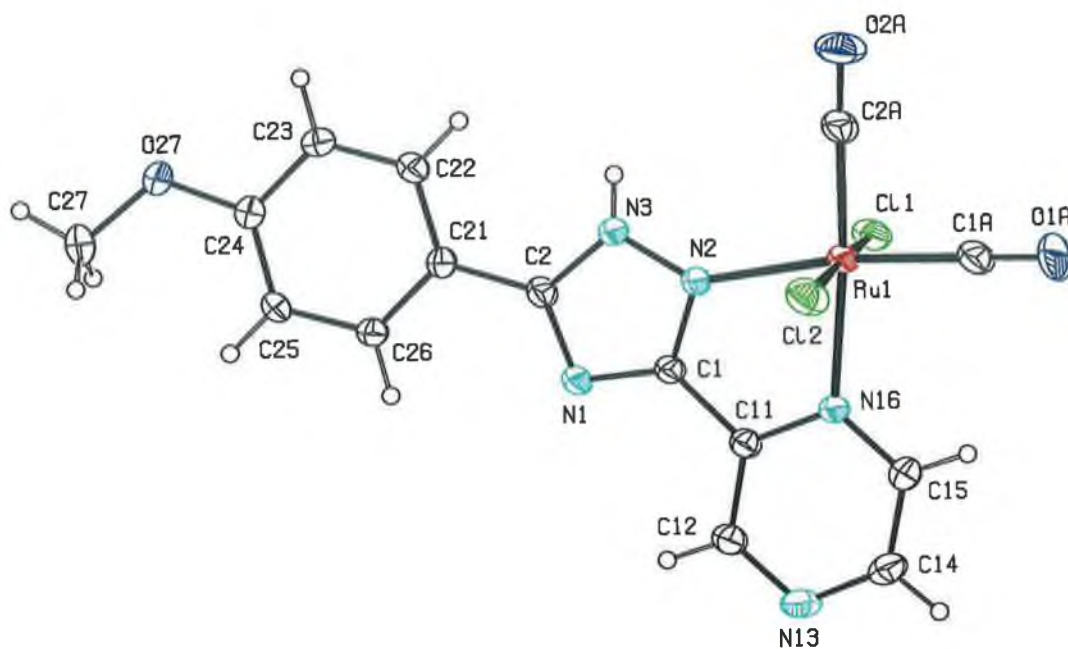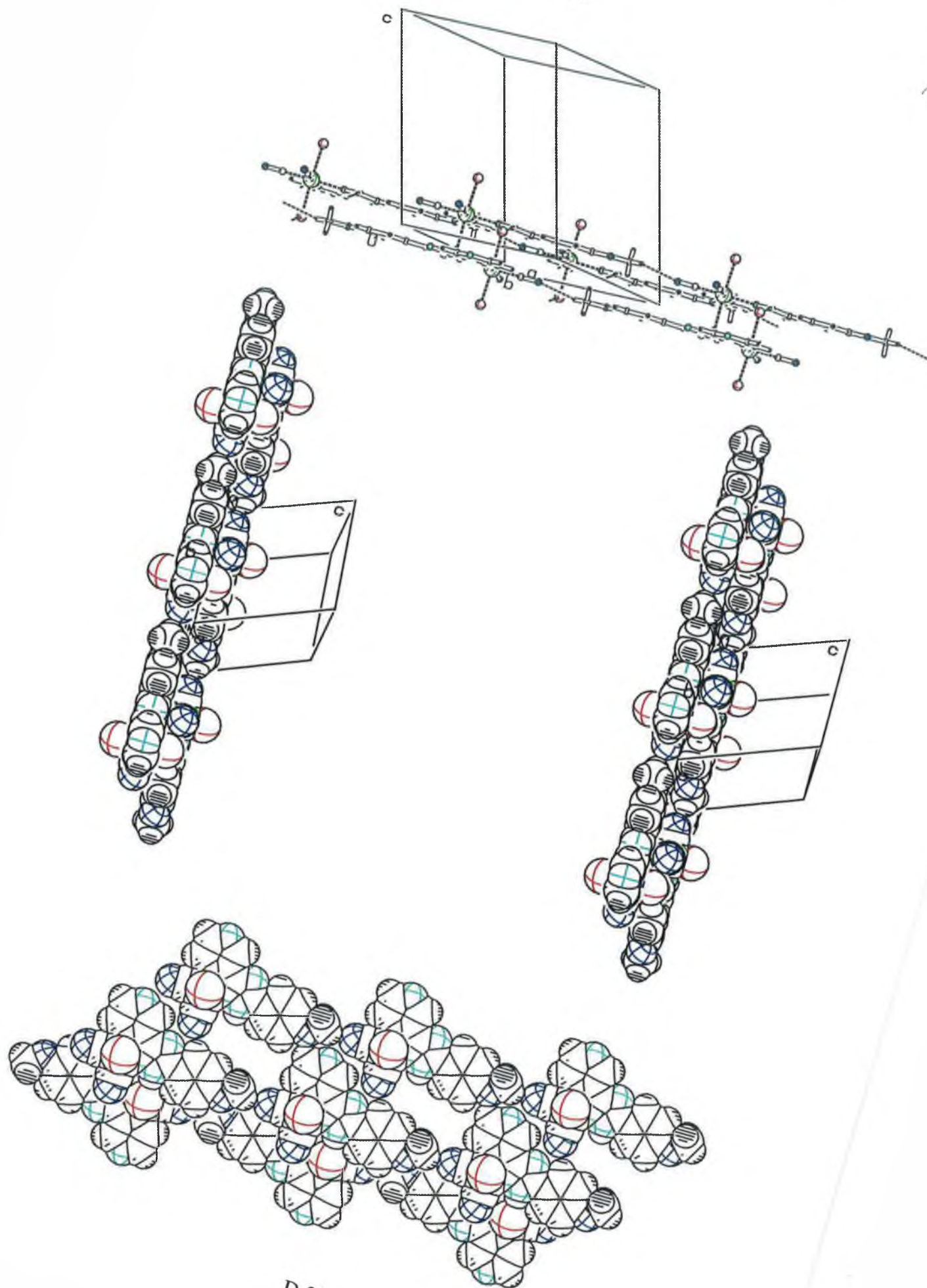
Table D18. Crystal data and structure refinement for [Ru(L7)(CO)$_2$Cl$_2$].

Empirical formula	C$_{15}$H$_{11}$Cl$_2$N$_5$O$_3$Ru
Formula weight	481.26
Temperature	294(2) K
Wavelength	0.71073 A
Crystal system, space group	
Unit cell dimensions	a = 14.2089(11) Å α = 90°
	b = 9.5634(5) Å β = 115.61(5)°
	c = 14.5834(9) Å γ = 90°
Volume	1786.9(2) Å^3
Z	4
Calculated density	1.789 Mg/m^3
Absorption coefficient	1.202 mm^{-1}
F(000)	952
Crystal size	0.45 × 0.20 × 0.08 mm
Theta range for data collection	2.13 to 28.05 deg.
Index ranges	-18 ≤ h ≤ 1, -12 ≤ k ≤ 1, -17 ≤ l ≤ 19
Reflections collected / unique	5367 / 4314 [R(int) = 0.0143]
Completeness to theta = 28.05°	93.9%
Max. and min. transmission	0.9099 and 0.6137
Refinement method	Full-matrix least-squares on F^2
Data / restraints / parameters	4314 / 0 / 240
Goodness-of-fit on F^2	1.044
Final R indices [I>2sigma(I)]	R1 = 0.0322, wR2 = 0.0708
R indices (all data)	R1 = 0.0487, wR2 = 0.0774
Largest diff. peak and hole	0.578 and -0.397 e.Å^{-3}

Table D19. Atomic coordinates ($\times 10^4$) and equivalent isotropic displacement parameters ($A^2 \times 10^3$) for [Ru(L7)(CO)$_2$Cl$_2$]. U(eq) is defined as one third of the trace of the orthogonalized U^{ij} tensor.

	x	y	z	U(eq)
Ru(1)	3881(1)	422(1)	1191(1)	37(1)
Cl(1)	3141(1)	566(1)	-635(1)	48(1)
Cl(2)	4594(1)	519(1)	2998(1)	55(1)
O(1A)	2161(2)	-1465(3	1120(3)	94(1)
C(1A)	2809(3)	-761(3)	1147(3)	55(1)
O(2A)	5134(2)	-2167(2)	1300(2)	71(1)
C(2A)	4677(2)	-1185(3)	1246(2)	47(1)
C(1)	4653(2)	3292(3)	1234(2)	33(1)
N(1)	5331(2)	4256(2)	1219(2)	34(1)
C(2)	6105(2)	3491(3)	1205(2)	33(1)
N(2)	4943(2)	1986(2)	1225(2)	35(1)
N(3)	5884(2)	2116(2)	1213(2)	36(1)
C(11)	3633(2)	3521(3)	1240(2)	34(1)
C(12)	3231(2)	4822(3)	1284(2)	40(1)
N(13)	2297(2)	4978(3)	1279(2)	46(1)
C(14)	1775(2)	3801(3)	1227(2)	47(1)
C(15)	2162(2)	2497(3)	1188(2)	43(1)
N(16)	3100(2)	2337(2)	1194(2)	36(1)
C(21)	7065(2)	4017(3)	1192(2)	32(1)
C(22)	7819(2)	3126(3)	1155(2)	39(1)
C(23)	8728(2)	3645(3)	1175(2)	42(1)
C(24)	8903(2)	5082(3)	1244(2)	38(1)
C(25)	8167(2)	5993(3)	1282(2)	35(1)
C(26)	7245(2)	5455(3)	1254(2)	34(1)
O(27)	9836(2)	5472(2)	1268(2)	56(1)
C(27)	10113(2)	6922(3)	1378(3)	56(1)

Table D20.   Bond lengths [Å] and angles [deg] for [Ru(L7)(CO)$_2$Cl$_2$].

Bond lengths:

Ru(1)-C(1A)	1.876(3)	N(13)-C(14)	1.332(4)
Ru(1)-C(2A)	1.888(3)	C(14)-C(15)	1.374(4)
Ru(1)-N(2)	2.109(2)	C(14)-H(14)	0.9300
Ru(1)-N(16)	2.143(2)	C(15)-N(16)	1.337(3)
Ru(1)-Cl(2)	2.3818(9)	C(15)-H(15)	0.9300
Ru(1)-Cl(1)	2.4064(8)	C(21)-C(22)	1.387(3)
O(1A)-C(1A)	1.127(4)	C(21)-C(26)	1.395(3)
O(2A)-C(2A)	1.125(3)	C(22)-C(23)	1.374(4)
C(1)-N(2)	1.317(3)	C(22)-H(22)	0.9300
C(1)-N(1)	1.339(3)	C(23)-C(24)	1.393(4)
C(1)-C(11)	1.470(3)	C(23)-H(23)	0.9300
N(1)-C(2)	1.329(3)	C(24)-O(27)	1.364(3)
C(2)-N(3)	1.353(3)	C(24)-C(25)	1.380(4)
C(2)-C(21)	1.461(3)	C(25)-C(26)	1.391(3)
N(2)-N(3)	1.351(3)	C(25)-H(25)	0.9300
N(3)-H(3)	0.80(3)	C(26)-H(26)	0.9300
C(11)-N(16)	1.347(3)	O(27)-C(27)	1.431(3)
C(11)-C(12)	1.382(3)	C(27)-H(27A)	0.9600
C(12)-N(13)	1.334(4)	C(27)-H(27B)	0.9600
C(12)-H(12)	0.9300	C(27)-H(27C)	0.9600

Bond angles:

C(1A)-Ru(1)-C(2A)	88.46(13)	N(1)-C(1)-C(11)	128.0(2)
C(1A)-Ru(1)-N(2)	171.89(11)	C(2)-N(1)-C(1)	103.2(2)
C(2A)-Ru(1)-N(2)	99.65(10)	N(1)-C(2)-N(3)	109.7(2)
C(1A)-Ru(1)-N(16)	95.82(11)	N(1)-C(2)-C(21)	126.5(2)
C(2A)-Ru(1)-N(16)	175.18(11)	N(3)-C(2)-C(21)	123.8(2)
N(2)-Ru(1)-N(16)	76.09(8)	C(1)-N(2)-N(3)	103.2(2)
C(1A)-Ru(1)-Cl(2)	90.66(12)	C(1)-N(2)-Ru(1)	116.75(16)
C(2A)-Ru(1)-Cl(2)	91.38(10)	N(3)-N(2)-Ru(1)	140.05(17)
N(2)-Ru(1)-Cl(2)	89.33(7)	N(2)-N(3)-C(2)	108.9(2)
N(16)-Ru(1)-Cl(2)	86.36(6)	N(2)-N(3)-H(3)	121(2)
C(1A)-Ru(1)-Cl(1)	92.11(12)	C(2)-N(3)-H(3)	129(2)
C(2A)-Ru(1)-Cl(1)	93.51(10)	N(16)-C(11)-C(12)	121.6(2)
N(2)-Ru(1)-Cl(1)	87.24(7)	N(16)-C(11)-C(1)	114.2(2)
N(16)-Ru(1)-Cl(1)	88.57(6)	C(12)-C(11)-C(1)	124.2(2)
Cl(2)-Ru(1)-Cl(1)	174.44(2)	N(13)-C(12)-C(11)	122.1(3)
O(1A)-C(1A)-Ru(1)	179.6(3)	N(13)-C(12)-H(12)	119.0
O(2A)-C(2A)-Ru(1)	177.4(3)	C(11)-C(12)-H(12)	119.0
N(2)-C(1)-N(1)	115.0(2)	C(14)-N(13)-C(12)	115.7(2)
N(2)-C(1)-C(11)	117.0(2)	N(13)-C(14)-C(15)	123.2(3)

N(13)-C(14)-H(14)	118.4	O(27)-C(24)-C(25)	124.9(2)
C(15)-C(14)-H(14)	118.4	O(27)-C(24)-C(23)	114.3(2)
N(16)-C(15)-C(14)	121.3(3)	C(25)-C(24)-C(23)	120.8(2)
N(16)-C(15)-H(15)	119.4	C(24)-C(25)-C(26)	119.0(2)
C(14)-C(15)-H(15)	119.4	C(24)-C(25)-H(25)	120.5
C(15)-N(16)-C(11)	116.2(2)	C(26)-C(25)-H(25)	120.5
C(15)-N(16)-Ru(1)	127.85(19)	C(25)-C(26)-C(21)	120.7(2)
C(11)-N(16)-Ru(1)	115.95(15)	C(25)-C(26)-H(26)	119.7
C(22)-C(21)-C(26)	119.0(2)	C(21)-C(26)-H(26)	119.7
C(22)-C(21)-C(2)	122.0(2)	C(24)-O(27)-C(27)	119.0(2)
C(26)-C(21)-C(2)	119.0(2)	O(27)-C(27)-H(27A)	109.5
C(23)-C(22)-C(21)	120.9(2)	O(27)-C(27)-H(27B)	109.5
C(23)-C(22)-H(22)	119.6	H(27A)-C(27)-H(27B)	109.5
C(21)-C(22)-H(22)	119.6	O(27)-C(27)-H(27C)	109.5
C(22)-C(23)-C(24)	119.6(2)	H(27A)-C(27)-H(27C)	109.5
C(22)-C(23)-H(23)	120.2	H(27B)-C(27)-H(27C)	109.5
C(24)-C(23)-H(23)	120.2		

Table D21. Anisotropic displacement parameters ($A^2 \times 10^3$) for [Ru(L7)(CO)$_2$Cl$_2$]. The anisotropic displacement factor exponent takes the form:
-2 pi^2 [h^2 a*^2 U11 + ... + 2 h k a* b* U12]

	U11	U22	U33	U23	U13	U12
Ru(1)	44(1)	21(1)	61(1)	0(1)	35(1)	-2(1)
Cl(1)	58(1)	31(1)	63(1)	-3(1)	32(1)	4(1)
Cl(2)	73(1)	39(1)	62(1)	4(1)	39(1)	2(1)
O(1A)	99(2)	56(2)	169(3)	-22(2)	98(2)	-37(2)
C(1A)	69(2)	30(1)	87(2)	-7(2)	55(2)	-7(1)
O(2A)	96(2)	35(1)	108(2)	12(1)	69(2)	20(1)
C(2A)	61(2)	30(1)	68(2)	2(1)	45(2)	-2(1)
C(1)	37(1)	24(1)	44(1)	1(1)	25(1)	0(1)
N(1)	39(1)	23(1)	45(1)	0(1)	24(1)	-2(1)
C(2)	37(1)	27(1)	38(1)	0(1)	19(1)	-3(1)
N(2)	38(1)	24(1)	55(1)	0(1)	31(1)	-2(1)
N(3)	37(1)	26(1)	57(1)	-1(1)	30(1)	0(1)
C(11)	40(1)	27(1)	41(1)	-1(1)	24(1)	0(1)
C(12)	47(2)	29(1)	48(2)	-2(1)	25(1)	1(1)
N(13)	51(1)	38(1)	55(1)	-2(1)	29(1)	12(1)
C(14)	45(2)	48(2)	61(2)	-1(2)	33(1)	7(1)
C(15)	41(1)	39(2)	58(2)	-4(1)	31(1)	-3(1)
N(16)	39(1)	26(1)	54(1)	-2(1)	30(1)	0(1)

C(21)	33(1)	30(1)	38(1)	1(1)	19(1)	-1(1)
C(22)	43(1)	27(1)	55(2)	-2(1)	27(1)	-2(1)
C(23)	37(2)	33(1)	62(2)	-2(1)	27(1)	4(1)
C(24)	34(1)	35(1)	49(2)	-2(1)	21(1)	-3(1)
C(25)	38(1)	23(1)	49(2)	-2(1)	21(1)	-4(1)
C(26)	35(1)	27(1)	44(1)	1(1)	21(1)	3(1)
O(27)	40(1)	39(1)	102(2)	-10(1)	43(1)	-8(1)
C(27)	49(2)	43(2)	85(2)	-8(2)	36(2)	-17(1)

Table D22. Hydrogen coordinates ($\times 10^4$) and isotropic displacement parameters ($A^2 \times 10^3$) for $[Ru(L7)(CO)_2Cl_2]$.

	x	y	z	U(eq)
H(3)	6170(2)	1450(3)	1120(2)	39(8)
H(12)	3626	5613	1318	48
H(14)	1118	3864	1218	57
H(15)	1764	1711	1155	51
H(22)	7706	2165	1118	47
H(23)	9225	3040	1141	50
H(25)	8285	6952	1324	43
H(26)	6744	6061	1278	41
H(27A)	9618	7432	805	84
H(27B)	10798	7029	1409	84
H(27C)	10108	7276	1991	84

Table D23. Torsion angles [deg] for [Ru(L7)(CO)$_2$Cl$_2$].

C(2A)-Ru(1)-C(1A)-O(1A)	-175(100)	C(1)-C(11)-C(12)-N(13)	179.4(3)
N(2)-Ru(1)-C(1A)-O(1A)	4(48)	C(11)-C(12)-N(13)-C(14)	0.0(4)
N(16)-Ru(1)-C(1A)-O(1A)	7(47)	C(12)-N(13)-C(14)-C(15)	0.3(4)
Cl(2)-Ru(1)-C(1A)-O(1A)	94(47)	N(13)-C(14)-C(15)-N(16)	-0.3(5)
Cl(1)-Ru(1)-C(1A)-O(1A)	-82(47)	C(14)-C(15)-N(16)-C(11)	-0.1(4)
C(1A)-Ru(1)-C(2A)-O(2A)	-34(7)	C(14)-C(15)-N(16)-Ru(1)	177.7(2)
N(2)-Ru(1)-C(2A)-O(2A)	146(7)	C(12)-C(11)-N(16)-C(15)	0.4(4)
N(16)-Ru(1)-C(2A)-O(2A)	119(7)	C(1)-C(11)-N(16)-C(15)	-179.4(2)
Cl(2)-Ru(1)-C(2A)-O(2A)	57(7)	C(12)-C(11)-N(16)-Ru(1)	-177.7(2)
Cl(1)-Ru(1)-C(2A)-O(2A)	-126(7)	C(1)-C(11)-N(16)-Ru(1)	2.6(3)
N(2)-C(1)-N(1)-C(2)	-0.3(3)	C(1A)-Ru(1)-N(16)-C(15)	1.2(3)
C(11)-C(1)-N(1)-C(2)	-179.1(3)	C(2A)-Ru(1)-N(16)-C(15)	-151.2(12)
C(1)-N(1)-C(2)-N(3)	-0.1(3)	N(2)-Ru(1)-N(16)-C(15)	-179.3(3)
C(1)-N(1)-C(2)-C(21)	-179.6(3)	Cl(2)-Ru(1)-N(16)-C(15)	-89.1(2)
N(1)-C(1)-N(2)-N(3)	0.6(3)	Cl(1)-Ru(1)-N(16)-C(15)	93.2(2)
C(11)-C(1)-N(2)-N(3)	179.5(2)	C(1A)-Ru(1)-N(16)-C(11)	179.0(2)
N(1)-C(1)-N(2)-Ru(1)	-177.7(17)	C(2A)-Ru(1)-N(16)-C(11)	26.6(13)
C(11)-C(1)-N(2)-Ru(1)	1.2(3)	N(2)-Ru(1)-N(16)-C(11)	-1.53(18)
C(1A)-Ru(1)-N(2)-C(1)	3.7(10)	Cl(2)-Ru(1)-N(16)-C(11)	88.68(19)
C(2A)-Ru(1)-N(2)-C(1)	-177.6(2)	Cl(1)-Ru(1)-N(16)-C(11)	-89.04(19)
N(16)-Ru(1)-N(2)-C(1)	0.1(2)	N(1)-C(2)-C(21)-C(22)	-178.6(3)
Cl(2)-Ru(1)-N(2)-C(1)	-86.3(2)	N(3)-C(2)-C(21)-C(22)	2.0(4)
Cl(1)-Ru(1)-N(2)-C(1)	89.3(2)	N(1)-C(2)-C(21)-C(26)	3.7(4)
C(1A)-Ru(1)-N(2)-N(3)	-173.6(8)	N(3)-C(2)-C(21)-C(26)	-175.7(3)
C(2A)-Ru(1)-N(2)-N(3)	5.0(3)	C(26)-C(21)-C(22)-C(23)	-0.4(4)
N(16)-Ru(1)-N(2)-N(3)	-177.3(3)	C(2)-C(21)-C(22)-C(23)	-178.0(3)
Cl(2)-Ru(1)-N(2)-N(3)	96.3(3)	C(21)-C(22)-C(23)-C(24)	0.8(5)
Cl(1)-Ru(1)-N(2)-N(3)	-88.1(3)	C(22)-C(23)-C(24)-O(27)	179.3(3)
C(1)-N(2)-N(3)-C(2)	-0.6(3)	C(22)-C(23)-C(24)-C(25)	-0.8(5)
Ru(1)-N(2)-N(3)-C(2)	177.0(2)	O(27)-C(24)-C(25)-C(26)	-179.8(3)
N(1)-C(2)-N(3)-N(2)	0.5(3)	C(23)-C(24)-C(25)-C(26)	0.4(4)
C(21)-C(2)-N(3)-N(2)	179.9(2)	C(24)-C(25)-C(26)-C(21)	0.1(4)
N(2)-C(1)-C(11)-N(16)	-2.5(4)	C(22)-C(21)-C(26)-C(25)	-0.1(4)
N(1)-C(1)-C(11)-N(16)	176.2(3)	C(2)-C(21)-C(26)-C(25)	177.6(2)
N(2)-C(1)-C(11)-C(12)	177.7(3)	C(25)-C(24)-O(27)-C(27)	2.5(5)
N(1)-C(1)-C(11)-C(12)	-3.5(5)	C(23)-C(24)-O(27)-C(27)	-177.7(3)
N(16)-C(11)-C(12)-N(13)	-0.3(4)		

Table D24. Hydrogen-bonds for [Ru(L7)(CO)$_2$Cl$_2$] [Å and deg.].

D-H	A		d(D-H)	d(H...A)	d(D...A)	<(DHA)
N(3)-H(3)	Cl(1)	#1	0.80(3)	2.40(3)	3.196(2)	173(3)
C(14)-H(14)	O(27)	#2	0.93	2.41	3.208(3)	144.0
C(26)-H(26)	N(1)		0.93	2.62	2.932(3)	100.2
C(27)-H(27B)	O(1A)	#3	0.96	2.59	3.455(4)	150.0

#1 -x+1,-y,-z   #2 x-1,y,z   #3 x+1,y+1,z

Crystal Data for [Ru(L8)(CO)₂Cl₂]
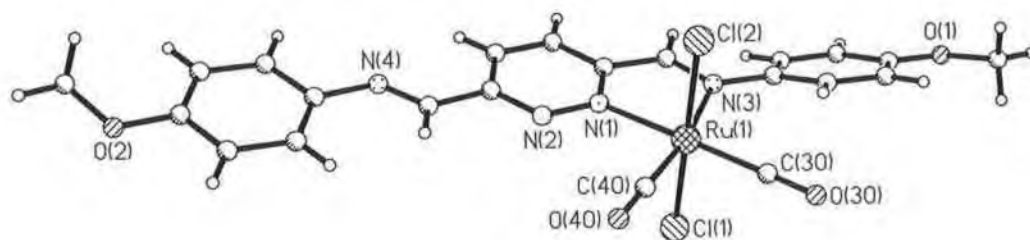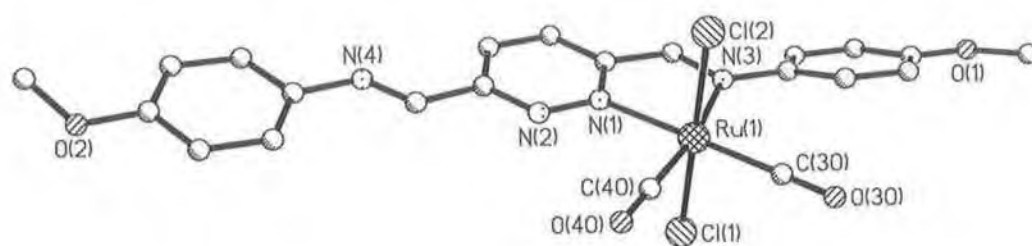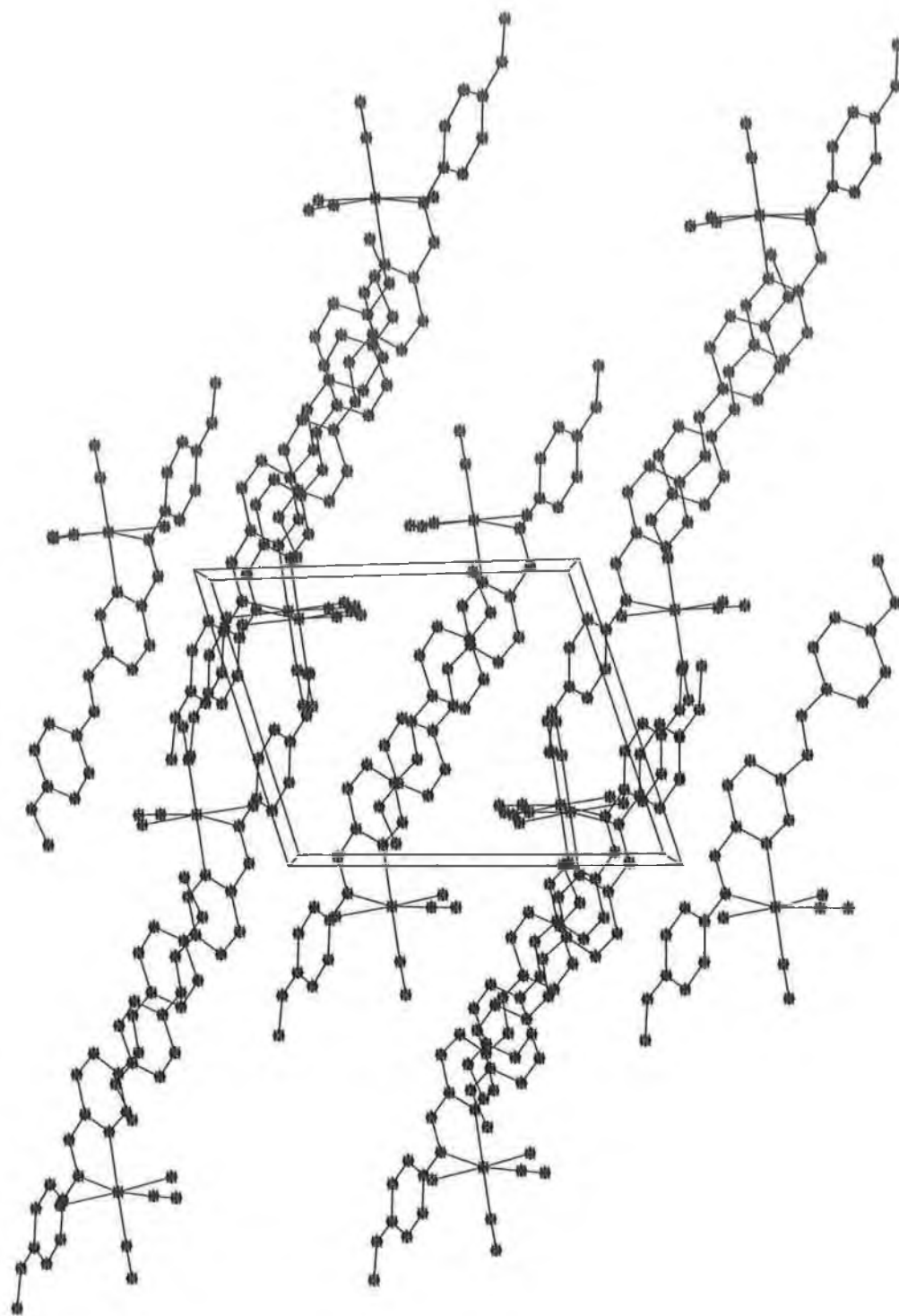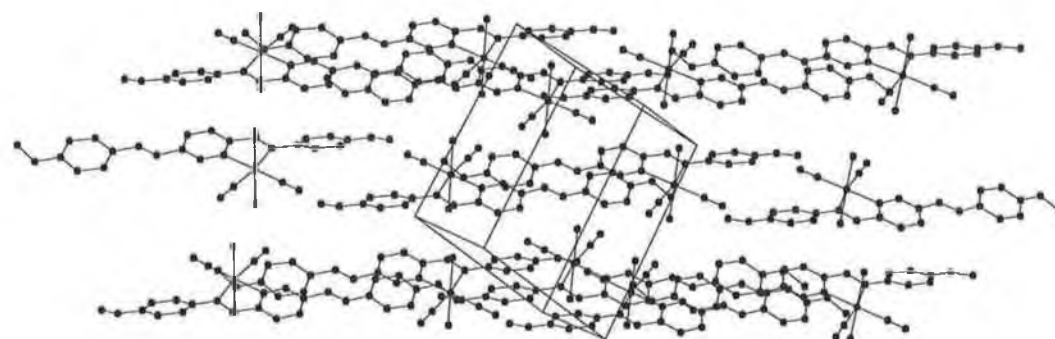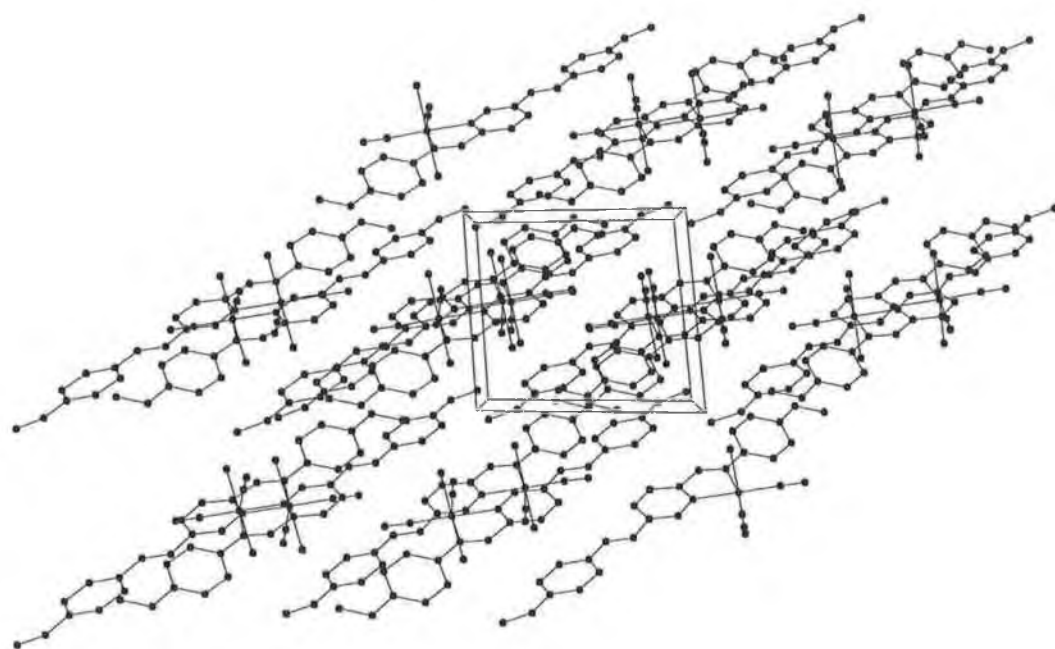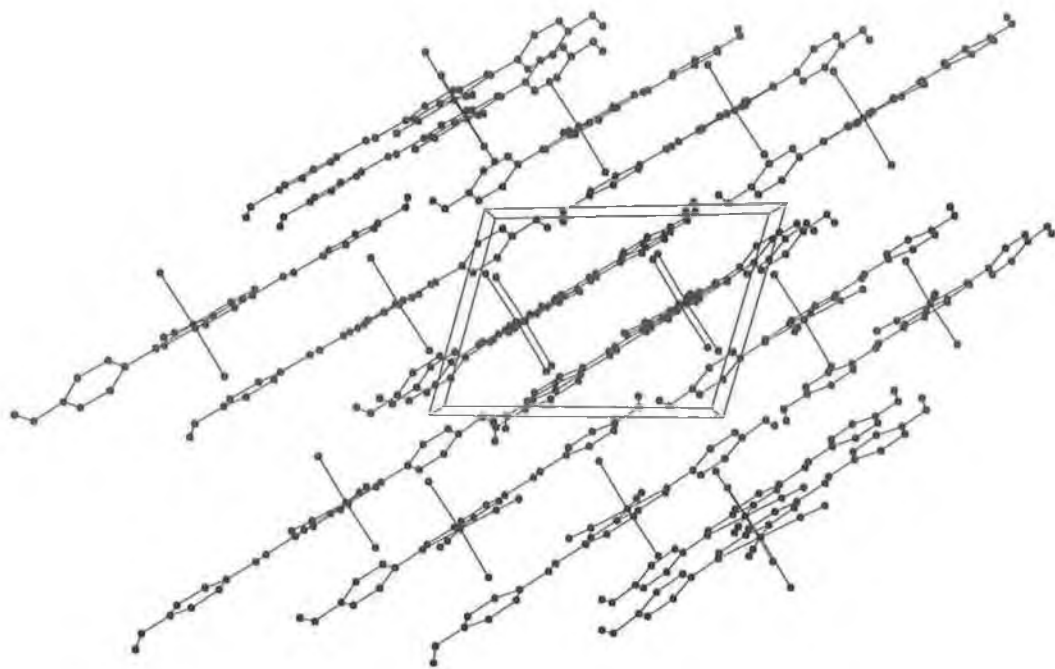
Table D25. Crystal data and structure refinement for [Ru(L8)(CO)$_2$Cl$_2$].

Empirical formula	C$_{22}$H$_{18}$Cl$_2$N$_4$O$_4$Ru
Formula weight	574.37
Temperature	168(2) K
Wavelength	0.71073 Å
Crystal system	Triclinic
Space group	P-1
Unit cell dimensions	a = 9.303(3) Å $\quad$ α = 70.746(4)°.
	b = 10.354(3) Å $\quad$ β = 72.006(4)°.
	c = 13.072(4) Å $\quad$ γ = 80.088(4)°.
Volume	1127.2(6) Å^3
Z	2
Density (calculated)	1.692 mg/m^3
Absorption coefficient	0.970 mm^{-1}
F(000)	576
Crystal size	0.35 × 0.11 × 0.06 mm^3
Theta range for data collection	2.09 to 26.48°.
Index ranges	-11 ≤ h ≤ 11, -12 ≤ k ≤ 12, -14 ≤ l ≤ 16
Reflections collected	14761
Independent reflections	4526 [R(int) = 0.0285]
Completeness to theta = 26.48°	97.4 %
Absorption correction	Semi-empirical (SADABS)
Max. and min. transmission	1.00 and 0.91
Refinement method	Full-matrix least-squares on F^2
Data / restraints / parameters	4526 / 0 / 300
Goodness-of-fit on F^2	0.957
Final R indices [I>2sigma(I)]	R1 = 0.0266, wR2 = 0.0556
R indices (all data)	R1 = 0.0439, wR2 = 0.0577
Largest diff. peak and hole	0.358 and -0.441 e.Å^{-3}

Table D26. Atomic coordinates $(\times 10^4)$ and equivalent isotropic displacement parameters $(\text{Å}^2 \times 10^3)$ for $[Ru(L8)(CO)_2Cl_2]$. U(eq) is defined as one third of the trace of the orthogonalized U^{ij} tensor.

	x	y	z	U(eq)
Ru(1)	5435(1)	8387(1)	7770(1)	22(1)
Cl(1)	7774(1)	8672(1)	6326(1)	33(1)
Cl(2)	3141(1)	8155(1)	9286(1)	33(1)
N(1)	5066(2)	10516(2)	7467(2)	22(1)
N(2)	4299(2)	11301(2)	6744(2)	26(1)
C(2)	4120(3)	12651(2)	6614(2)	23(1)
C(3)	4694(3)	13270(3)	7196(2)	26(1)
C(4)	5468(3)	12451(2)	7934(2)	24(1)
C(5)	5630(3)	11049(2)	8062(2)	22(1)
C(6)	6417(3)	10057(2)	8822(2)	24(1)
N(3)	6526(2)	8775(2)	8881(2)	21(1)
C(8)	7334(3)	7810(2)	9622(2)	23(1)
C(9)	7019(3)	6450(2)	10001(2)	25(1)
C(10)	7778(3)	5467(3)	10704(2)	27(1)
C(11)	8852(3)	5871(3)	11047(2)	28(1)
C(12)	9165(3)	7235(3)	10688(2)	34(1)
C(13)	8426(3)	8202(3)	9978(2)	32(1)
O(1)	9680(2)	4991(2)	11722(2)	36(1)
C(14)	9341(3)	3596(3)	12154(2)	39(1)
C(16)	3266(3)	13457(3)	5799(2)	29(1)
N(4)	3053(2)	14747(2)	5629(2)	26(1)
C(18)	2253(3)	15591(3)	4855(2)	25(1)
C(19)	1760(3)	15159(3)	4122(2)	29(1)
C(20)	991(3)	16104(3)	3394(2)	32(1)
C(21)	695(3)	17455(3)	3419(2)	30(1)
C(22)	1168(3)	17894(3)	4143(2)	30(1)
C(23)	1955(3)	16963(2)	4847(2)	27(1)
O(2)	-88(2)	18296(2)	2676(2)	43(1)
C(24)	-633(3)	19639(3)	2798(3)	42(1)
C(30)	5801(3)	6472(3)	8035(2)	27(1)
O(30)	5978(2)	5325(2)	8175(2)	42(1)
C(40)	4462(3)	8405(3)	6706(2)	29(1)
O(40)	3907(2)	8430(2)	6049(2)	48(1)

Table D27. Selected bond lengths [Å] and angles [°] for [Ru(L8)(CO)$_2$Cl$_2$].

Ru(1)-C(40)	1.873(3)
Ru(1)-C(30)	1.886(3)
Ru(1)-N(1)	2.092(2)
Ru(1)-N(3)	2.176(2)
Ru(1)-Cl(1)	2.3882(10)
Ru(1)-Cl(2)	2.4058(9)
C(40)-Ru(1)-C(30)	87.53(11)
C(40)-Ru(1)-N(1)	92.90(10)
C(30)-Ru(1)-N(1)	179.06(10)
C(40)-Ru(1)-N(3)	169.48(9)
C(30)-Ru(1)-N(3)	102.84(9)
N(1)-Ru(1)-N(3)	76.71(8)
C(40)-Ru(1)-Cl(1)	89.12(9)
C(30)-Ru(1)-Cl(1)	88.97(8)
N(1)-Ru(1)-Cl(1)	90.21(6)
N(3)-Ru(1)-Cl(1)	89.29(6)
C(40)-Ru(1)-Cl(2)	94.02(9)
C(30)-Ru(1)-Cl(2)	92.44(8)
N(1)-Ru(1)-Cl(2)	88.37(6)
N(3)-Ru(1)-Cl(2)	87.39(6)
Cl(1)-Ru(1)-Cl(2)	176.62(3)

Table D28. Bond lengths [Å] and angles [°] for [Ru(L8)(CO)$_2$Cl$_2$].

Bond lengths:

Ru(1)-C(40)	1.873(3)	C(6)-N(3)	1.292(3)
Ru(1)-C(30)	1.886(3)	N(3)-C(8)	1.433(3)
Ru(1)-N(1)	2.092(2)	C(8)-C(9)	1.380(3)
Ru(1)-N(3)	2.176(2)	C(8)-C(13)	1.405(3)
Ru(1)-Cl(1)	2.3882(10)	C(9)-C(10)	1.384(3)
Ru(1)-Cl(2)	2.4058(9)	C(10)-C(11)	1.384(3)
N(1)-N(2)	1.331(3)	C(11)-O(1)	1.360(3)
N(1)-C(5)	1.349(3)	C(11)-C(12)	1.386(4)
N(2)-C(2)	1.339(3)	C(12)-C(13)	1.371(3)
C(2)-C(3)	1.402(3)	O(1)-C(14)	1.420(3)
C(2)-C(16)	1.474(3)	C(16)-N(4)	1.270(3)
C(3)-C(4)	1.359(3)	N(4)-C(18)	1.414(3)
C(4)-C(5)	1.392(3)	C(18)-C(19)	1.397(3)
C(5)-C(6)	1.448(3)	C(18)-C(23)	1.397(3)

C(19)-C(20)	1.393(3)
C(20)-C(21)	1.388(4)
C(21)-O(2)	1.376(3)
C(21)-C(22)	1.381(4)

C(22)-C(23)	1.378(3)
O(2)-C(24)	1.439(3)
C(30)-O(30)	1.132(3)
C(40)-O(40)	1.122(3)

Bond angles:

C(40)-Ru(1)-C(30)	87.53(11)		C(6)-N(3)-Ru(1)	113.01(16)
C(40)-Ru(1)-N(1)	92.90(10)		C(8)-N(3)-Ru(1)	128.39(15)
C(30)-Ru(1)-N(1)	179.06(10)		C(9)-C(8)-C(13)	119.0(2)
C(40)-Ru(1)-N(3)	169.48(9)		C(9)-C(8)-N(3)	118.7(2)
C(30)-Ru(1)-N(3)	102.84(9)		C(13)-C(8)-N(3)	122.3(2)
N(1)-Ru(1)-N(3)	76.71(8)		C(8)-C(9)-C(10)	121.4(2)
C(40)-Ru(1)-Cl(1)	89.12(9)		C(9)-C(10)-C(11)	118.9(2)
C(30)-Ru(1)-Cl(1)	88.97(8)		O(1)-C(11)-C(10)	123.9(2)
N(1)-Ru(1)-Cl(1)	90.21(6)		O(1)-C(11)-C(12)	115.6(2)
N(3)-Ru(1)-Cl(1)	89.29(6)		C(10)-C(11)-C(12)	120.5(2)
C(40)-Ru(1)-Cl(2)	94.02(9)		C(13)-C(12)-C(11)	120.4(2)
C(30)-Ru(1)-Cl(2)	92.44(8)		C(12)-C(13)-C(8)	119.9(2)
N(1)-Ru(1)-Cl(2)	88.37(6)		C(11)-O(1)-C(14)	117.3(2)
N(3)-Ru(1)-Cl(2)	87.39(6)		N(4)-C(16)-C(2)	118.3(2)
Cl(1)-Ru(1)-Cl(2)	176.62(3)		C(16)-N(4)-C(18)	121.6(2)
N(2)-N(1)-C(5)	121.6(2)		C(19)-C(18)-C(23)	119.2(2)
N(2)-N(1)-Ru(1)	122.25(15)		C(19)-C(18)-N(4)	125.4(2)
C(5)-N(1)-Ru(1)	116.11(16)		C(23)-C(18)-N(4)	115.3(2)
N(1)-N(2)-C(2)	117.6(2)		C(20)-C(19)-C(18)	119.5(2)
N(2)-C(2)-C(3)	123.5(2)		C(21)-C(20)-C(19)	119.8(2)
N(2)-C(2)-C(16)	114.7(2)		O(2)-C(21)-C(22)	123.7(2)
C(3)-C(2)-C(16)	121.8(2)		O(2)-C(21)-C(20)	115.0(2)
C(4)-C(3)-C(2)	118.0(2)		C(22)-C(21)-C(20)	121.3(2)
C(3)-C(4)-C(5)	117.4(2)		C(23)-C(22)-C(21)	118.7(2)
N(1)-C(5)-C(4)	121.8(2)		C(22)-C(23)-C(18)	121.4(2)
N(1)-C(5)-C(6)	114.8(2)		C(21)-O(2)-C(24)	116.8(2)
C(4)-C(5)-C(6)	123.4(2)		O(30)-C(30)-Ru(1)	177.4(2)
N(3)-C(6)-C(5)	119.3(2)		O(40)-C(40)-Ru(1)	178.4(3)
C(6)-N(3)-C(8)	118.6(2)			

Table D29. Anisotropic displacement parameters $(\text{Å}^2 \times 10^3)$ for $[\text{Ru(L8)(CO)}_2\text{Cl}_2]$. The anisotropic displacement factor exponent takes the form: $-2p^2[\ h^2\ a^{*2}U^{11} + \dots + 2\ h\ k\ a^*\ b^*\ U^{12}\ ]$

	U^{11}	U^{22}	U^{33}	U^{23}	U^{13}	U^{12}
Ru(1)	27(1)	17(1)	27(1)	-8(1)	-11(1)	-2(1)
Cl(1)	34(1)	30(1)	33(1)	-9(1)	-6(1)	-3(1)
Cl(2)	30(1)	35(1)	37(1)	-14(1)	-7(1)	-7(1)
N(1)	26(1)	17(1)	26(1)	-7(1)	-10(1)	-1(1)
N(2)	30(1)	19(1)	31(1)	-5(1)	-14(1)	-1(1)
C(2)	24(2)	21(1)	24(1)	-5(1)	-6(1)	-2(1)
C(3)	29(2)	18(1)	30(2)	-8(1)	-5(1)	-3(1)
C(4)	25(2)	24(1)	28(2)	-12(1)	-8(1)	-4(1)
C(5)	22(1)	22(1)	23(1)	-7(1)	-6(1)	-3(1)
C(6)	26(2)	24(1)	25(1)	-10(1)	-8(1)	-4(1)
N(3)	23(1)	19(1)	23(1)	-6(1)	-7(1)	-3(1)
C(8)	24(2)	23(1)	23(1)	-8(1)	-10(1)	1(1)
C(9)	28(2)	24(1)	27(2)	-10(1)	-12(1)	0(1)
C(10)	35(2)	23(1)	27(2)	-8(1)	-12(1)	0(1)
C(11)	28(2)	31(2)	22(2)	-6(1)	-9(1)	5(1)
C(12)	32(2)	39(2)	35(2)	-8(1)	-17(1)	-8(1)
C(13)	35(2)	28(2)	35(2)	-4(1)	-16(1)	-8(1)
O(1)	38(1)	36(1)	34(1)	-5(1)	-20(1)	2(1)
C(14)	49(2)	30(2)	34(2)	-3(1)	-19(2)	9(1)
C(16)	32(2)	25(2)	31(2)	-7(1)	-11(1)	-3(1)
N(4)	26(1)	22(1)	27(1)	-4(1)	-9(1)	0(1)
C(18)	23(2)	25(1)	26(2)	-5(1)	-6(1)	-4(1)
C(19)	35(2)	23(1)	29(2)	-7(1)	-10(1)	-4(1)
C(20)	38(2)	34(2)	29(2)	-9(1)	-13(1)	-6(1)
C(21)	31(2)	28(2)	28(2)	-2(1)	-11(1)	-1(1)
C(22)	32(2)	23(1)	33(2)	-8(1)	-9(1)	-2(1)
C(23)	33(2)	26(2)	24(2)	-7(1)	-11(1)	-4(1)
O(2)	54(1)	37(1)	43(1)	-8(1)	-30(1)	4(1)
C(24)	40(2)	33(2)	47(2)	-2(1)	-21(2)	5(1)
C(30)	33(2)	22(2)	25(2)	-5(1)	-9(1)	-4(1)
O(30)	59(2)	24(1)	47(1)	-14(1)	-16(1)	-4(1)
C(40)	34(2)	25(2)	35(2)	-11(1)	-13(1)	-4(1)
O(40)	61(2)	49(1)	50(1)	-17(1)	-31(1)	-9(1)

Table D30. Hydrogen coordinates ($\times 10^4$) and isotropic displacement parameters ($\text{Å}^2 \times 10^3$) for $[Ru(L8)(CO)_2Cl_2]$.

	x	y	z	U(eq)
H(3)	4548	14234	7077	31
H(4)	5882	12821	8348	29
H(6)	6848	10346	9273	28
H(9)	6267	6184	9774	30
H(10)	7566	4532	10948	33
H(12)	9897	7502	10934	40
H(13)	8652	9134	9728	38
H(14A)	8276	3535	12593	47
H(14B)	9993	3076	12639	47
H(14C)	9518	3213	11529	47
H(16)	2885	13022	5411	35
H(19)	1949	14228	4120	34
H(20)	670	15824	2882	39
H(22)	956	18820	4156	35
H(23)	2301	17260	5338	33
H(24A)	-1267	19552	3568	50
H(24B)	-1233	20116	2265	50
H(24C)	231	20165	2645	50

Table D31. Torsion angles [°] for [Ru(L8)(CO)₂Cl₂].

C(40)-Ru(1)-N(1)-N(2)	2.4(2)	Ru(1)-N(3)-C(8)-C(13)	156.4(2)
C(30)-Ru(1)-N(1)-N(2)	120(6)	C(13)-C(8)-C(9)-C(10)	-1.3(4)
N(3)-Ru(1)-N(1)-N(2)	-179.2(2)	N(3)-C(8)-C(9)-C(10)	179.0(2)
Cl(1)-Ru(1)-N(1)-N(2)	91.56(18)	C(8)-C(9)-C(10)-C(11)	1.2(4)
Cl(2)-Ru(1)-N(1)-N(2)	-91.51(18)	C(9)-C(10)-C(11)-O(1)	-179.0(2)
C(40)-Ru(1)-N(1)-C(5)	-178.67(19)	C(9)-C(10)-C(11)-C(12)	-0.2(4)
C(30)-Ru(1)-N(1)-C(5)	-61(6)	O(1)-C(11)-C(12)-C(13)	178.2(2)
N(3)-Ru(1)-N(1)-C(5)	-0.31(17)	C(10)-C(11)-C(12)-C(13)	-0.7(4)
Cl(1)-Ru(1)-N(1)-C(5)	-89.54(18)	C(11)-C(12)-C(13)-C(8)	0.6(4)
Cl(2)-Ru(1)-N(1)-C(5)	87.39(18)	C(9)-C(8)-C(13)-C(12)	0.3(4)
C(5)-N(1)-N(2)-C(2)	0.9(3)	N(3)-C(8)-C(13)-C(12)	-180.0(2)
Ru(1)-N(1)-N(2)-C(2)	179.73(17)	C(10)-C(11)-O(1)-C(14)	-4.3(4)
N(1)-N(2)-C(2)-C(3)	-0.1(4)	C(12)-C(11)-O(1)-C(14)	176.9(2)
N(1)-N(2)-C(2)-C(16)	179.8(2)	N(2)-C(2)-C(16)-N(4)	-179.9(2)
N(2)-C(2)-C(3)-C(4)	-0.3(4)	C(3)-C(2)-C(16)-N(4)	-0.1(4)
C(16)-C(2)-C(3)-C(4)	179.9(2)	C(2)-C(16)-N(4)-C(18)	179.6(2)
C(2)-C(3)-C(4)-C(5)	-0.2(4)	C(16)-N(4)-C(18)-C(19)	-7.0(4)
N(2)-N(1)-C(5)-C(4)	-1.4(4)	C(16)-N(4)-C(18)-C(23)	173.0(2)
Ru(1)-N(1)-C(5)-C(4)	179.70(19)	C(23)-C(18)-C(19)-C(20)	0.4(4)
N(2)-N(1)-C(5)-C(6)	179.2(2)	N(4)-C(18)-C(19)-C(20)	-179.5(2)
Ru(1)-N(1)-C(5)-C(6)	0.3(3)	C(18)-C(19)-C(20)-C(21)	-1.3(4)
C(3)-C(4)-C(5)-N(1)	1.0(4)	C(19)-C(20)-C(21)-O(2)	-179.2(2)
C(3)-C(4)-C(5)-C(6)	-179.6(2)	C(19)-C(20)-C(21)-C(22)	1.0(4)
N(1)-C(5)-C(6)-N(3)	0.0(3)	O(2)-C(21)-C(22)-C(23)	-179.6(2)
C(4)-C(5)-C(6)-N(3)	-179.4(2)	C(20)-C(21)-C(22)-C(23)	0.2(4)
C(5)-C(6)-N(3)-C(8)	178.8(2)	C(21)-C(22)-C(23)-C(18)	-1.2(4)
C(5)-C(6)-N(3)-Ru(1)	-0.3(3)	C(19)-C(18)-C(23)-C(22)	0.9(4)
C(40)-Ru(1)-N(3)-C(6)	9.4(6)	N(4)-C(18)-C(23)-C(22)	-179.2(2)
C(30)-Ru(1)-N(3)-C(6)	179.48(18)	C(22)-C(21)-O(2)-C(24)	-10.0(4)
N(1)-Ru(1)-N(3)-C(6)	0.32(17)	C(20)-C(21)-O(2)-C(24)	170.2(2)
Cl(1)-Ru(1)-N(3)-C(6)	90.70(17)	C(40)-Ru(1)-C(30)-O(30)	-19(5)
Cl(2)-Ru(1)-N(3)-C(6)	-88.62(17)	N(1)-Ru(1)-C(30)-O(30)	-137(6)
C(40)-Ru(1)-N(3)-C(8)	-169.6(5)	N(3)-Ru(1)-C(30)-O(30)	162(5)
C(30)-Ru(1)-N(3)-C(8)	0.5(2)	Cl(1)-Ru(1)-C(30)-O(30)	-109(6)
N(1)-Ru(1)-N(3)-C(8)	-178.7(2)	Cl(2)-Ru(1)-C(30)-O(30)	75(6)
Cl(1)-Ru(1)-N(3)-C(8)	-88.30(19)	C(30)-Ru(1)-C(40)-O(40)	-109(9)
Cl(2)-Ru(1)-N(3)-C(8)	92.38(19)	N(1)-Ru(1)-C(40)-O(40)	70(9)
C(6)-N(3)-C(8)-C(9)	157.1(2)	N(3)-Ru(1)-C(40)-O(40)	61(9)
Ru(1)-N(3)-C(8)-C(9)	-23.9(3)	Cl(1)-Ru(1)-C(40)-O(40)	-20(9)
C(6)-N(3)-C(8)-C(13)	-22.6(4)	Cl(2)-Ru(1)-C(40)-O(40)	159(9)